

https://dspace.org/

Unravelling the Connection Between Hypercholesterolemia and Alzheimer's Disease: Insights into Oxidative Stress and Signalling Pathways

Tshipamba, Ester Keeyanda

2025-05

University of the Witwatersrand, Johannesburg

https://hdl.handle.net/10539/48326

Tshipamba, Ester Keeyanda. (2025). Unravelling the Connection Between Hypercholesterolemia and Alzheimer's Disease: Insights into Oxidative Stress and Signalling Pathways. [Master's dissertation, University of the Witwatersrand, Johannesburg]. WIReDSpace. https://hdl.handle.net/10539/48326

Downloaded from a DSpace repository. https://dspace.org/



UNIVERSITY OF THE
WITWATERSRAND,
JOHANNESBURG

Unravelling the Connection Between Hypercholesterolemia and Alzheimer's Disease: Insights into Oxidative Stress and Signalling Pathways

by

Ester Tshipamba

(2151946)

Dissertation

Submitted in fulfilment of the requirements for the degree

Master of Science

in

Molecular and Cell Biology

in the Faculty of Science, University of the Witwatersrand, Johannesburg, South Africa

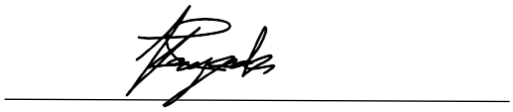
Supervisor: Dr. Eloise van der Merwe

May 2025

Declaration

I, Ester Tshipamba (2151946), am a student registered for the degree of Master of Science by dissertation (MSc) in the academic year 2025.

I declare that this dissertation is my own, unaided work. It is being submitted for the Degree of Master of Science at the University of the Witwatersrand, Johannesburg. It has not been submitted before for any degree or examination at any other University.



(Signature of candidate)

23rd day of May 2025 at Johannesburg

Abstract

Alzheimer's disease (AD) is a progressive neurodegenerative disorder and the leading cause of dementia worldwide, characterised by amyloid beta (Aβ) plaques, neurofibrillary tau tangles and overall cognitive decline. Despite extensive research, the complex and multifactorial nature of AD has left its aetiology largely unknown, but emerging evidence identified hypercholesterolemia as a potential risk factor for AD. Hypercholesterolemia is characterised by elevated levels of low-density lipoprotein (LDL) in patients, commonly due to mutations in the LDL receptor (LDLR) gene and treated using statin therapy. Common cellular markers between these diseases, such as mitochondrial dysfunction, and the influence of cholesterol levels on Aβ pathogenesis, highlight a possible link between them. However, the exact cellular mechanisms constituting this link remain unclear, hence, this study aimed to assess the effects of hypercholesterolemia on Alzheimer's disease hallmarks and signalling pathways. Proteomic analysis of SWATH-MS data from familial hypercholesterolemia (FH) patient plasma samples revealed 28 differentially expressed proteins (DEPs) involved in cytoskeletal dynamics and regulation, oxidative stress, antioxidant defence, inflammation, immune regulation, and metabolism, with most of these processes also being associated with AD pathogenesis. Furthermore, proteomic analysis of the plasma samples of FH patients on statin therapy indicated a reversible effect of statin therapy on 13 of the DEPs. Based on the proteomic analysis, an *in vitro* investigation was done whereby a squalene synthase inhibitor (SSI) was employed to upregulate LDLR expression and inhibit cholesterol biosynthesis in HEK293 and SH-SY5Y cell lines, which were treated with Aβ, LDL, and hydrogen peroxide (H_2O_2) to create an early-stage hypercholesterolemic-AD cell model. After validating SSI-induced LDLR upregulation via western blot analysis, the MTT and Alamar Blue® assays revealed that SSI had limited effects on rescuing metabolic activity in the cell model. In contrast, a fluorescence-based assay measuring reactive oxygen species (ROS) production indicated an antioxidant effect of SSI against the excess ROS produced by H_2O_2 treatment. Additionally, quantitative PCR analysis of mitochondrial DNA copy number (mtDNA-CN) found distinct effects of the hypercholesterolemic-AD conditions on mtDNA-CN levels where SSI treatment increased the levels across all conditions. Overall, the results of this study provided both *in vitro* and systemic insights into the complexity of cholesterol modulation and the potential molecular pathways that may link hypercholesterolemia and AD.

Acknowledgements

I would like to express my deepest gratitude to my supervisor, Dr Eloise van der Merwe, for the invaluable opportunity to conduct my research in her lab and for her continuous guidance, patience and support throughout my Master's journey.

A special thank you to my seniors, Dr Tyrone Otgaar, Dr Martin Bernert and Dr Monique Bignoux, for their insightful advice, knowledge and mentorship since my Honour's year. Your guidance has been instrumental in my growth as a researcher.

To my fellow lab members at the Cell Biology and Signalling Research Laboratory, thank you for your encouragement, support and friendship that made this experience all the more fulfilling.

Lastly, I am profoundly grateful to my family and friends for their unconditional love and belief in me every step of the way.

Collaborations:

Prof. Derick Raal – Head of the Division of Endocrinology at the School of Clinical Medicine at the University of the Witwatersrand

The Council for Scientific and Industrial Research (CSIR)

Financial aid:

National Research Foundation (NRF) – Postgraduate Master's Study Bursary (2023 – 2024)

University of the Witwatersrand – Postgraduate Merit Award (2023 – 2024)

Table of Contents

Declaration **2**

Abstract **3**

Acknowledgements **4**

List of Abbreviations **8**

List of Figures **11**

List of Tables **13**

1. Introduction **14**

1.1 – Alzheimer's Disease 14

1.1.1 – Overview: Prevalence, symptoms, diagnosis & treatment *14*

1.1.2 – Histopathological Hallmarks of AD: Neurofibrillary Tau Tangle Formation & Cytoskeletal Dysregulation *16*

1.1.3 – Histopathological Hallmarks of AD: Amyloid Beta Plaque Formation *19*

1.2 – Familial Hypercholesterolemia 22

1.3 – Associations between AD and FH 25

1.3.1 – Altered cholesterol homeostasis in the AD brain *25*

1.3.2 – Influence of high cholesterol on APP processing *27*

1.3.3 – The role of LDLR in neurogenesis and Aβ clearance *28*

1.3.4 – Mitochondrial Dysfunction and Oxidative Stress *29*

1.3.5 – Inflammation *32*

1.4 – Induced LDLR upregulation through drug treatment 34

1.4.1 – Conventional Statin Treatment *34*

1.4.2 – Squalene Synthase Inhibitors: Novel compound SSI *35*

1.5 – Rationale of the study 37

1.6 – Scope of the study 37

2. Aims and Objectives **39**

2.1 - Main aim 39

2.2 – Objectives 39

3. Methodology **40**

3.1 - Proteomic Analysis: SWATH-MS 40

3.2 - Cell Culture 42

3.2.1 - Harvesting and Passage *43*

3.2.2 - Cell Quantification and Seeding *44*

3.3 – Treatment 44
3.3.1 - Compound SSI *45*
3.3.2 - Amyloid-beta Protein (Aβ42) *45*
3.3.3 – Low-density lipoprotein (LDL) cholesterol *46*
3.3.4 – Hydrogen Peroxide (H_2O_2) *46*
3.4 - Cell Morphology 46
3.5 – Metabolic Activity Assays 47
3.5.1 - 3-(4, 5-Dimethylthiazol-2-yl)-2, 5-Diphenyltetrazolium Bromide (MTT) assay *47*
3.5.2 - Alamar Blue® Cell Viability Assay *48*
3.6 - Western Blot Analysis 48
3.6.1 - Protein Extraction *49*
3.6.2 - Protein Quantification: Bicinchoninic acid (BCA) assay *49*
3.6.3 - SDS-PAGE and Western Blotting *50*
3.7 - Total Reactive Oxygen Species (ROS) Assay 52
3.8 - Mitochondrial DNA Copy Number (mtDNA-CN) Analysis 53
3.8.1 – DNA Extraction *53*
3.8.2 – Agarose Gel Electrophoresis *55*
3.8.3 – Quantitative Polymerase Chain Reaction (qPCR) *55*
3.9 - Statistical analysis 57
4. Results 58
4.1 – Proteomic Analysis 58
4.2 – *In vitro* Results 73
4.2.1 – Dose- and time-dependent effect of SSI on cell viability in HEK293 and SH-SY5Y cells *73*
4.2.2 - Treatment with SSI causes a significant increase in LDLR protein levels in HEK293 and SH-SY5Y cells *78*
4.2.3 - SSI treatment and the hypercholesterolemic-AD conditions decrease mitochondrial activity but do not significantly affect overall cell metabolic activity *82*
4.2.4 - Treatment with SSI shows a promising trend of decreasing total ROS production in the hypercholesterolemic-AD cell model *89*
4.2.5 - Treatment with SSI increases mtDNA-CN in the hypercholesterolemic-AD cell model *93*
5. Discussion 95
5.1 – Proteomics Discussion 95
5.1.1 - Dysregulated proteins in cytoskeletal dynamics and regulation *96*
5.1.1.2 - Intermediate Filaments: Structural Stability and Cellular Integrity *97*
5.1.1.3 - Microtubules: Intracellular Transport and Dynamics *98*

5.1.1.4 - Microfilaments and Actin-Binding Proteins: Cytoskeletal Remodelling and Cell-Cell Interactions *100*

5.1.1.5 - Pathway Enrichment Analysis of Cytoskeletal Dysregulation *104*

5.1.2 - Dysregulated proteins in oxidative stress and antioxidant defence *108*

5.1.3 - Dysregulated proteins in inflammation and immune regulation *112*

5.1.4 - Dysregulated proteins in metabolism and energy regulation *120*

5.1.5 - Statin therapy mitigates hypercholesterolemic-induced changes in proteomic expression .. *122*

5.2 – *In vitro* Investigation Discussion 126

5.2.1 - Treatment with SSI is non-toxic and causes significant upregulation of LDLR in HEK293 and SH-SY5Y cells *126*

5.2.2 - SSI treatment and the hypercholesterolemic-AD conditions decrease mitochondrial activity but do not significantly affect overall cellular metabolic activity *128*

5.2.3 - Treatment with SSI shows a promising trend of decreasing total ROS production in the hypercholesterolemic-AD cell model *134*

5.2.4 - Treatment with SSI increases mitochondrial DNA copy number in the hypercholesterolemic-AD cell model (HEK293 cells) *141*

6. Conclusion **146**

7. Future studies **148**

8. Study limitations **150**

9. References **151**

10. Appendix **183**

10.1 - Supplementary Results 183

10.2 - Recipes 186

10.3 - Ethics Clearance Form 188

List of Abbreviations

Abbreviation	Meaning
24-HC	24 (S) hydroxycholesterol
ABCA1	ATP-binding cassette transporter A1
ACAT	Acyl-CoA cholesterol acyltransferase
AD	Alzheimer's Disease
ADF	Actin depolymerising factor
AICD	APP intracellular domain
AMPK	Adenosine monophosphate-activated protein kinase
ANOVA	Analysis of variance
ApoB	Apolipoprotein B
APOE	Apolipoprotein E
APP	Amyloid precursor protein
APP-CTF83/αCTF	APP C-terminal fragment
ATP	Adenosine triphosphate
Aβ42	Amyloid beta 42
BBB	Blood-brain barrier
BCA	Bicinchoninic acid
BRSK1/2	brain-specific kinases
BSA	Bovine serum albumin
CAD	Coronary heart disease
CAD	Cath.a-differentiated
CaMKK	Calcium/calmodulin-dependent protein kinase kinase
CDK5	Cyclin-dependent kinase 5
CE	Cholesterol esters
CNS	Central nervous system
CoQ10	Coenzyme Q10/ubiquinone
CSIR	Council for Scientific and Industrial Research
DAMP	Damage-associated molecular pattern
DDA	Data-dependent acquisition
DEPs	Differentially expressed proteins
DIA	Data-independent acquisition
DMEM	Dulbecco's Modified Eagle Medium
DMSO	Dimethyl sulfoxide
EC50	Half-maximal effective concentration

ECM	Extracellular matrix
EDTA	Ethylenediaminetetraacetic acid
eNOS	Endothelial nitric oxide synthase
ERK2	Extracellular signal-regulated kinase 2
FBS	Fetal bovine serum
FDP	Farnesyl diphosphate
FDR	False discovery rate
FH	Familial hypercholesterolemia
GLUT	Glucose transporters
GM1	monosialotetrahexosylganglioside1
GO	Gene ontology
GPx	Glutathione peroxidase
GSK3β	Glycogen synthase kinase 3 beta
H_2O_2	Hydrogen peroxide
HCl	Hydrochloric acid
HEK293	Human embryonic kidney cell line
HMG-CoA	3-hydroxy-3-methylglutaryl-CoA
HRP	Horseradish peroxidase
ICAM-1	Intercellular adhesion molecule 1
IgG	Immunoglobulin G
JNK	c-Jun N-terminal kinase
LDL	Low-density lipoprotein
LDL-C	Low-density lipoprotein cholesterol
LDLR	Low-density lipoprotein receptor
LDLRAP1	LDL receptor adaptor protein 1
LSD	Fisher's least significant difference
MAPK	Mitogen-activated protein kinase
MARK	Microtubule-affinity regulating kinase
mtDNA-CN	Mitochondrial DNA copy number
mtDNA	Mitochondrial deoxyribonucleic acid
MTT	3-(4, 5-Dimethylthiazol-2-yl)-2, 5-Diphenyltetrazolium Bromide
NFTs	Neurofibrillary tau tangles
NF-κB	Nuclear factor κB
NAD^+	Nicotinamide adenine dinucleotide
NADH	Reduced NAD^+ (plus hydrogen)
$NADP^+$	Phosphorylated NAD^+
NADPH	Nicotinamide adenine dinucleotide phosphate

NMDAR	N-methyl-D-aspartate receptor
NO	Nitric oxide
NOX	NADPH oxidase
Nrf2	Nuclear factor erythroid 2-related factor 2
NTCs	No-template controls
$ONOO^-$	Peroxynitrite anion
OS	Oxidative stress
oxLDL	Oxidised low-density lipoprotein
PBS	Phosphate-buffered saline
PBST	Phosphate-buffered saline tween
PCA	Protocatechuic acid
PCSK9	Pro-protein convertase subtilisin-kexin type 9
PHF	Paired helical fragments
PPI	Protein-protein interaction
p-tau	Phosphorylated tau
PVDF	Polyvinylidene fluoride
qPCR	Quantitative polymerase chain reaction
RAGE	Receptors for advanced glycation end products
RIPA	Radioimmunoprecipitation assay
ROS	Reactive oxygen species
sAPP-α	soluble APP-fragment
SDS	Sodium dodecyl sulphate
SDS-PAGE	Sodium dodecyl sulphate polyacrylamide gel electrophoresis
Sirt1	Silent information regulator factor 2-related enzyme 1
SREBP	Sterol regulatory element-binding protein
SSI	Squalene synthase inhibitor
STRING	Search Tool for Retrieval of Interacting Genes/Proteins
SWATH-MS	Sequential window acquisition of all theoretical fragment ion spectra mass spectrometry
TCA	Tricarboxylic acid cycle
TLR	Toll-like receptor
TNF- α	Tumour necrosis factor-α
WHO	World Health Organisation

List of Figures

Figure 1: The processing of amyloid precursor protein (APP) 20

Figure 2: The primary proteins that are mutated in familial hypercholesterolemia 25

Figure 3: The influence of cholesterol levels on APP processing 28

Figure 4: The involvement of reactive oxygen species (ROS) in amyloid-β (Aβ) and neurofibrillary tangle formation 31

Figure 5: Cholesterol biosynthesis pathway occurring in the central nervous system 36

Figure 6: SWATH-MS analysis of FH patient plasma samples identified 28 differentially expressed proteins (10 upregulated and 18 downregulated) 59

Figure 7: The top four gene ontology (GO) molecular functions that are enriched by the dysregulated proteins identified in the FH vs control dataset 64

Figure 8: Protein-protein interaction (PPI) network of the dysregulated proteins (FH vs control) with a fold-change ≥ 1.5, analysed via STRING database 65

Figure 9: Pathway enrichment (KEGG) of the Differentially Expressed Proteins (DEPs) identified in FH vs Control Groups using ShinyGO v0.8 70

Figure 10: Treatment with SSI does not significantly decrease cell viability in HEK293 cells at 25 nM and 50 nM 74

Figure 11: Treatment with SSI does not significantly decrease cell viability in SH-SY5Y cells at lower concentrations 77

Figure 12: Treatment with SSI causes a significant increase in LDLR protein expression in HEK293 cells 79

Figure 13: Treatment with SSI causes a significant increase in LDLR protein expression in SH-SY5Y cells 81

Figure 14: The effects of the hypercholesterolemic-Alzheimer's Disease treatment conditions on mitochondrial activity in (A) HEK293 and (B) SH-SY5Y 83

Figure 15: The effects of the hypercholesterolemic-Alzheimer's Disease treatment conditions on cellular metabolic activity in (A) HEK293 and (B) SH-SY5Y 87

Figure 16: SSI treatment decreases ROS production in the hypercholesterolemic-AD cell model 90

Figure 17: Treatment with SSI increases mtDNA-CN in the hypercholesterolemic-AD cell model (HEK293)..... 94

Figure 18: The top enriched pathways based on the differentially expressed proteins (DEPs) identified in FH vs Control groups, obtained from Reactome

..... 97

Figure 19: An overview of the main families of actin-binding proteins..... 104

Figure S1: Agarose gel electrophoresis of extracted DNA from HEK293 cells after 48-hour treatment 183

Figure S2: Amplification plot and Melt Curve analysis of the mtDNA and nuclear DNA sequences during qPCR 184

Figure S3: Representative non-truncated western blot images showing the detection of LDLR (left) and β-actin (right). 185

List of Tables

Table 1: Outline of the sources and dilutions for the primary and secondary antibodies used in the western blot analysis 52

Table 2: qPCR Master Mix 56

Table 3: Primer pairs and sequences used in the qPCR reaction for mtDNA-CN quantification (Refinetti et al., 2017) 57

Table 4: List of the dysregulated proteins (FH) ≥ 1.5-fold change and their gene ontology (GO) molecular functions as identified by STRING and UniProt databases 60

Table 5: List of the 15 dysregulated proteins (≥ 1.5-fold change) that overlapped in the FH vs control and FH vs FH+statin datasets 63

Table 6: Top 10 Enriched Gene Ontology (GO) Biological Processes in Differentially Expressed Proteins Identified in FH vs Control Groups (STRING) 67

Table 7: Top 10 Enriched Pathways based on Differentially Expressed Proteins Identified in FH vs Control Groups, obtained from Reactome 68

Table S1: 10× TBE Buffer Recipe (pH 8.3) 186

Table S2: 2× Radioimmunoprecipitation assay (RIPA) Lysis Buffer 186

Table S3: 10× Electrophoresis Running Buffer (pH 8.3) 187

Table S4: 10× Transfer Buffer 187

Table S5: SDS-PAGE Gel Recipe 187

1. Introduction

1.1 – Alzheimer's Disease

1.1.1 – Overview: Prevalence, symptoms, diagnosis & treatment

Considered as the leading cause of dementia, Alzheimer's disease (AD) is a progressive neurodegenerative disorder that is known to impair memory and cognitive function in elderly populations. According to the World Health Organization (WHO) (2023), the number of dementia cases increases by 10 million people each year, with already over 55 million dementia cases recorded in 2023 (World Health Organisation, 2023). In 2017, the World Alzheimer's Report estimated that 187 000 people in South Africa were living with AD-caused dementia and that by 2030 this number could rise to 250 000 people (De Jager et al., 2017). Similarly, the Global Burden of Disease forecasts that dementia prevalence in South Africa will increase by 181% between 2019 (241 937) and 2050 (680 045) (Nichols et al., 2022). This rise is believed to be due to the increase in population growth and demographic aging (i.e. An increase in the older proportion of the population) which is characteristic of middle- and low-income countries, such as South Africa. Considered to be an inevitable consequence of aging, a patient's "AD-status" is often dependent on their age. Individuals that are younger than 60 years old are often diagnosed with early-onset AD, and those that age above 60 years are diagnosed with late-onset AD (Chauhan & Chauhan, 2006). In addition to aging, family genetic history is the second strongest risk factor for AD onset (Tanzi, 2012). However, only approximately 10% of AD cases are found to be genetically linked by autosomal dominant transmission, termed familial AD, and hence, 90% of AD cases are sporadic, meaning that disease onset occurs due to a combination of genetic polymorphisms and environmental factors, such as lifestyle (Li, Lin & Huang, 2018). This predominance of sporadic AD cases highlights the importance of identifying and mitigating non-genetic risk factors to potentially reduce the onset of this devastating disease.

The term "progressive" is used to describe AD as disease symptoms gradually become worse over time such that this progression is termed the "Alzheimer's disease continuum". The continuum can be divided into three consecutive phases, starting with preclinical AD, mild cognitive impairment due to AD, and lastly, dementia due to AD (Gaugler et al., 2021). Although these phases of the continuum have been identified in this order, the duration of each phase varies for

each patient. This is due to factors such as the individual's age, genetics, lifestyle and many others. In particular, the duration of the preclinical phase of AD, where the patient exhibits no symptoms of AD but there are measurable biomarkers that could indicate the earliest signs of the disease, can range from five years to decades (Long et al., 2022). In fact, many studies have indicated that AD begins 20 years before noticeable symptoms arise such as memory deficits and language problems (Haque & Levey, 2019). As time progresses more clinical symptoms arise such as disturbances in visuospatial orientation and executive functioning (confusion, poor judgement and decision-making), which marks the beginning of the mild cognitive impairment phase of the AD continuum. Additionally, patients also experience noncognitive changes such as psychosis, mood disturbances, agitation, personality changes and sleep abnormalities (Gaugler et al., 2021). These symptoms are all signs of neuronal damage and death (neurodegeneration) in the brain, and currently, it is only at the onset of these symptoms that AD is diagnosed.

Due to the complexity and large number of symptoms of AD, there is no single diagnostic tool/test that can definitively determine if a patient has AD. The current diagnostic evaluation of patients includes an analysis of the patient's family history in terms of medical, neurological, and psychiatric histories followed by a physical and neurological examination that can include magnetic resonance imaging and/or computed tomography scans to assess the type and extent of damage in the brain (Bomasang-Layno & Bronsther, 2021). Additional clinical tests for neurodegeneration often look for the biological hallmarks of AD (discussed in 1.1.2 and 1.1.3). Psychiatric evaluations are often also performed which assess memory impairment, behavioural changes and other thinking skills (Albert et al., 2011). Studies have found that this diagnosis approach may require several appointments that may span several weeks or even months for a definite diagnosis of AD (Beach et al., 2012; Bomasang-Layno & Bronsther, 2021). Although neuropathological evaluation produces a 90% accuracy rate for the detection of AD, the issue remains that the presence of clinical symptoms suggests that the disease has already caused extensive damage to the brain of the patient. Additionally, this also implies that there is a substantial window of time in which the progression of the disease can be intervened.

Furthermore, diagnosis of AD at this stage of the disease leads to a limited treatment strategy since the neurodegeneration present cannot be reversed. The current aim of treatments targeted towards AD is to minimize the symptoms and behavioural disturbances to improve quality of life as

opposed to trying to stop the disease progression or remove the symptoms. This is often done via psychosocial treatments, such as environmental manipulation and family support structures, and pharmacotherapy which includes cognitive enhancers, mood stabilisers, antidepressants and antipsychotics (Gaugler et al., 2021). These multiple treatment and diagnostic approaches reflect an incomplete understanding of the pathophysiology of AD and that this knowledge gap is the biggest barrier to the improved diagnosis and treatment of the disease. Considering the global prevalence of AD, the severe degree of symptoms and the lack of an effective cure or treatment to slow down or stop disease progression, there is an urgent need to identify novel biomarkers involved in its aetiology or progression for an improved understanding of the disease. In turn, this could improve lives worldwide by allowing early diagnosis and improved treatment.

1.1.2 – Histopathological Hallmarks of AD: Neurofibrillary Tau Tangle Formation & Cytoskeletal Dysregulation

The current knowledge on AD shows that there are two primary histopathological features found in the AD brain that are believed to be the primary drivers in the pathology of AD by causing neurodegeneration. These features are called the hallmarks of AD and include the formation of protein aggregates of amyloid beta and neurofibrillary tangles (NFTs), and are often used for the diagnosis of AD (Bomasang-Layno & Bronsther, 2021).

The formation of NFTs occurs by the hyperphosphorylation of a microtubule-associated protein called tau. Tau protein consists of two functional domains, the microtubule binding domain at the C-terminus and the projection domain at the N-terminus (Šimić et al., 2016). In addition to stimulating tubulin assembly into microtubules, the C-terminus also functions in stabilizing the microtubules to allow neurite extensions for effective neuronal communication (Gong & Iqbal, 2008). Like any protein, tau is also modified post-translationally via several mechanisms, such as polyamination, nitration, ubiquitination, glycosylation, truncation, aggregation, and the most common modification, phosphorylation (Metaxas & Kempf, 2016). The microtubule-binding ability of tau is primarily regulated by phosphorylation at serine/threonine residues (Gong & Iqbal, 2008). Although the dynamic phosphorylation of tau occurs in both physiological and pathological conditions, the degree and locations of the phosphorylation differ. In particular, studies have found that the phosphorylation level of tau in the AD brain is three to four-fold higher than that of the normal brain (Köpke et al., 1993). Hyperphosphorylation of tau causes them to aggregate and

tangle around one another, due to conformational changes to tau and its dissociation from microtubules that causes them to depolymerise (Metaxas & Kempf, 2016). The dissociated tau then forms paired helical fragments (PHF) that polymerise into insoluble tangles that eventually form NFTs within the neuronal cytoplasm. The intracellular presence of NFTs can block the transport of nutrients and essential molecules needed for neuronal survival, such as brain-derived neurotrophic factors (Gaugler et al., 2021). Furthermore, due to the high localisation of tau at neuronal axons, the NFTs also impair axonal transport and cause synaptic dysfunction (Duan et al., 2012). Although multiple studies indicate a strong correlation between the number of NFTs in the brain and the severity of dementia (Arriagada et al., 1992; Brion et al., 2001), some studies have argued that the formation of NFTs is a defence mechanism used by the neurons to reduce the cytotoxic hyperphosphorylated tau (p-tau). This is due to the finding that the polymerisation of p-tau into NFTs actually eliminates its toxic activity of sequestering other microtubule-associated proteins (Gong & Iqbal, 2008). This finding indicates that the treatment strategy for NFTs should focus on the prevention or reversal of tau hyperphosphorylation prior to NFT formation.

When looking at the causes of tau hyperphosphorylation in AD, multiple studies have suggested that the dysregulation of the dynamic action of tau kinases (perform phosphorylation) and phosphatases (perform dephosphorylation) is responsible for the aberrant phosphorylation of tau (Brion et al., 2001; Gong & Iqbal, 2008). The major tau kinases that have higher activity levels in the AD brain include microtubule-affinity-regulating kinase (MARK), cyclin dependent kinase 5 (CDK5), cAMP-dependent protein kinase, extracellular signal-regulated kinase 2 (ERK2), glycogen synthase kinase 3 beta (GSK3β) and stress-activated protein kinases (Duan et al., 2012). On the other end, the primary tau phosphatases involved include protein phosphatase 1 and 2, which have been found to have a decreased activity of 20 – 30% in the AD brain (Gong et al., 1995). This large number of signalling enzymes involved illustrates possible cross-linking of many cellular pathways that could be involved in tauopathy. Moreover, the projection domain (N-terminus) of tau itself has been found to be involved in cell signalling such that it directly interacts with the Src-family kinases, growth factor receptor-bound protein 2, phosphatidylinositol and phosphatidylinositol biphosphate, among others, which are signalling molecules implicated in proliferation, growth, apoptosis and cytoskeletal rearrangement (Mueller et al., 2021).

In fact, it is important to note that cytoskeletal dysregulation is a significant feature of AD, affecting multiple components of the cytoskeleton, including microtubules, actin filaments and their associated regulatory proteins (Sen et al., 2022). The microtubule network is primarily impaired by disruptions in microtubule-associated proteins, such as tau (Bamburg & Bloom, 2009) and the formation of NFTs, as already discussed. For actin cytoskeleton abnormalities, studies have shown excessive actin polymerisation and aggregation in neurons, which contributes to synaptic dysfunction by affecting both the presynaptic release of neurotransmitters and the postsynaptic density of neuron dendrites, which can compromise synaptic integrity and strength (Penzes & VanLeeuwen, 2011; Pelucchi, Stringhi & Marcello, 2020). Additionally, key cytoskeletal regulatory proteins, such as Rho GTPases and cofilin, are dysregulated in AD, leading to impaired cytoskeletal remodelling (Sen et al., 2022). Rho GTPases are crucial regulators of the actin cytoskeleton and have been found to display aberrant activity in AD brains (Aguilar, Zhu & Lu, 2017). This aberrant activity of Rho GTPases has been associated with axonal degeneration and synaptic dysfunction due to the excessive actin polymerisation caused by their dysregulation (Schmidt et al., 2022). Similarly, cofilin, an actin-binding protein that regulates actin dynamics in dendritic spines, is also dysregulated in AD brains, whereby its phosphorylation is increased. This increased phosphorylation leads to the formation of cofilin-actin rods which contribute to neurodegeneration in AD by reducing dendritic spines and synaptic function, blocking the trafficking of mitochondria and promoting tauopathy by destabilising tau-induced microtubule assembly (Wurz et al., 2022).

In addition to these two key cytoskeletal regulatory proteins, there are multiple other proteins that form part of this regulatory system that are also dysregulated in AD pathogenesis (Bamburg & Bloom, 2009). The widespread dysregulation of cytoskeletal components in AD suggests a fundamental disruption in cytoskeletal dynamics that ultimately contributes to the widespread loss of neuronal integrity and synaptic function, leading to neurodegeneration. Moreover, the collapse of microtubule networks due to tau hyperphosphorylation, coupled with excessive actin polymerisation and impaired cytoskeletal dynamics, is also implicated in influencing signalling pathways as these cytoskeletal structures are important mediators for receptors and protein trafficking within the cell (Cooper, 2000). These pleiotropic functions of tau and the dynamic regulation of the cytoskeleton illustrate the possibility of more than one cellular pathway/mechanism in which upstream cellular changes or pathologies may occur that can lead to

the tauopathy implicated in AD pathogenesis. Thus, an in-depth analysis of these cellular pathways, the cross-linking thereof and the proteins within them in the AD context is necessary to improve the current understanding of this major hallmark.

1.1.3 – Histopathological Hallmarks of AD: Amyloid Beta Plaque Formation

The second histopathological hallmark of AD that is considered to be the main driver of AD pathogenesis is the presence of senile plaques. These plaques consist of deposits of insoluble protein aggregates of amyloid β-peptides (Aβ). These deposits can be found both inside and outside neurons but are predominantly located extracellularly where they disrupt interneuron communication at their cellular synapses (Fontana et al., 2020). The formation of Aβ occurs through the processing of amyloid precursor protein (APP) which is present as a transmembrane protein and is ubiquitously expressed in mammalian cells. The processing of APP can be divided into a non-amyloidogenic pathway and an amyloidogenic pathway by which Aβ is formed (Christensen et al., 2004; Li, Liu, et al., 2019; Gaugler et al., 2021), as illustrated in figure 1. The former pathway occurs when APP is cleaved by α-secretase enzymes in the middle of the "Aβ" region of APP which releases a soluble APP-fragment (sAPP-α) into the extracellular space. The remaining APP C-terminal fragment (APP-CTF83/αCTF) still spanning the cell membrane is then cleaved by γ-secretase to form a P3 fragment (released extracellularly) and an APP intracellular domain (AICD) (released intracellularly). This pathway has been implicated in physiological roles such as neuronal differentiation, neurite outgrowth and synapse formation (Kamenetz et al., 2003), where sAPP-α has been shown to be neuroprotective with contributions to neurogenesis (Zhou et al., 2011). In contrast, the amyloidogenic pathway occurs through the cleavage of APP by β-secretase at a point where the Aβ region of APP remains intact. This first cleavage releases the soluble fragment sAPP-β, where the remaining APP-CTF99 (βCTF) is further cleaved by γ-secretase to produce AICD and Aβ peptides (fig. 1) (Pająk, Kania & Orzechowski, 2016).

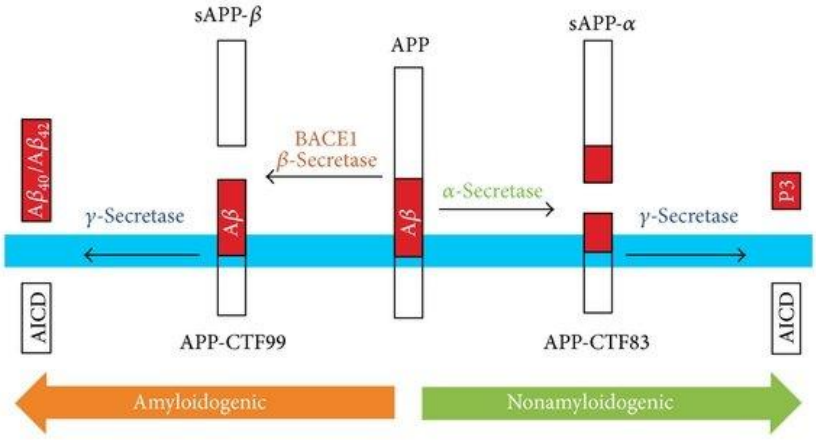


Figure 1: The processing of amyloid precursor protein (APP).

APP processing occurs at the cell membrane (shown in blue) via two pathways. The non-amyloidogenic pathway involves APP cleavage at the amyloid-β (Aβ) region (shown in red) by α-secretase to release soluble sAPP-α. The amyloidogenic pathways involves APP cleavage by β-secretase at a site that does not interrupt the Aβ region and releases sAPP-β. In both pathways, APP is further processed by γ-secretase to form AICD, however the non-amyloidogenic pathway releases P3 and the amyloidogenic pathway releases insoluble Aβ peptides that later form aggregates and senile plaques. Adopted from Pajak et. al. (2016).

The Aβ products of the amyloidogenic pathway can exist in multiple isoforms depending on the number of residues that make up the peptide (Gu & Guo, 2013). The two most common isoforms are Aβ40 (has 40 residues) and Aβ42 (has 42 residues) where high concentrations of Aβ40 have been observed in cerebral spinal fluids of AD patients and Aβ42 has been implicated as the major, and sometimes only, component of amyloid plaques in AD brains (Gu & Guo, 2013; Fontana et al., 2020). The cause of the activation of the amyloidogenic pathway in the AD brain, and thus the formation of Aβ42, is still unknown. While studies have shown that Aβ itself can further promote this amyloidogenic pathway in a self-amplifying cycle (O'Brien & Wong, 2011; Antonino et al., 2022), the initial trigger of this pathway before Aβ accumulation remains unclear. Since Aβ42 plays a vital role in AD pathogenesis, this cause requires further investigation.

The accumulation of NFTs and Aβ42 is believed to regulate one another where increasing Aβ production has been found to lead to increased NFT accumulation, causing further cellular damage

which can trigger more Aβ production, thus leading to a cycle of continuous neurodegeneration which could be the premise of the progressive nature of AD (Li, Marshall, et al., 2019). Several studies have implicated Aβ in the formation of NFTs as evidence has shown that Aβ is able to activate the calcium/calmodulin-dependent protein kinase kinase β (CaMKKβ) pathway which leads to the activation of the AMP-activated protein kinase (AMPK) family of kinases, which includes brain-specific kinases (BRSK1/2) and MARKS (Thornton et al., 2011). These enzymes are all involved in the phosphorylation of tau protein at specific epitopes, most commonly at the serine 262 and 396 residues of tau, which have been shown to cause the somatodendritic accumulation of tau proteins into NFTs. In particular, Aβ also causes the aberrant activation and increased expression of GSK3β which is the primary kinase that causes tau hyperphosphorylation as it can phosphorylate 3 epitopes alone (Reddy, 2013). These findings suggest that tau hyperphosphorylation can occur downstream of Aβ pathogenesis.

Furthermore, Aβ has also been seen to activate microglial cells, which are responsible for immune modulation in the brain (Gaugler et al., 2021). Stimulation of microglial cells through receptor interactions by extracellular Aβ causes chronic activation of the innate immune system where drastic increases in inflammatory molecules, such as cytokines and chemokines, impair microglial clearance of the accumulating Aβ and neuronal cell debris, which leads to microglia-mediated neuronal death by phagocytosis or cytotoxicity (Sun, Chen & Wang, 2015). Supporting the NFT-causing role of Aβ, studies have shown that certain cytokines produced through this Aβ-induced activation of the innate immune system, such as interleukin-1β, cause increased tau pathology by stimulating the kinase signalling pathways implicated in tau hyperphosphorylation (Heneka, Golenbock & Latz, 2015). Additionally, Aβ aggregation and accumulation leads to mass mitochondrial dysfunction and the onset of oxidative stress. Hence, the formation of Aβ is believed to account for the majority of neuronal loss seen in AD, compared to NFTs which account for approximately 8.1% of neuronal loss (Kril et al., 2002). Although newly approved drugs for treating or decreasing Aβ and NFTs have been developed, clinical trials have shown that although these therapies show promising results in the short term, there is still a need to investigate their long-term impacts (Huang et al., 2023). These findings highlight the need to explore preventative strategies that target early pathological changes in Aβ and tau, potentially offering more effective long-term protection against AD progression.

Although the causes of these pathological hallmarks, and hence, of AD have been attributed to non-modifiable risk factors such as genetics, age and family history, there are several modifiable risk factors that have shown significant associations with the onset and/or progression of AD. These include smoking, social and cognitive engagement, physical activity, diet and cardiovascular disease (Gaugler et al., 2021). In fact, in 2020 it was suggested that by addressing these modifiable risk factors, people might be able to prevent or delay up to 40% of dementia cases (Livingston et al., 2020). Notably, recent studies have shown that metabolic disorders, such as hypercholesterolemia (high cholesterol), can be a key factor in the onset of the pathological symptoms of AD. These contributions have been attributed to the increase in cellular cholesterol levels which cause a constant state of inflammation present in hypercholesterolemic patients which worsens with age (the primary risk factor for AD) and can lead to tissue damage in the central nervous system (Refolo et al., 2000). Furthermore, being the cholesterol-richest organ in the body, the brain is susceptible to changes in cholesterol levels needed to maintain homeostasis, where cholesterol concentrations have been implicated in driving Aβ production (Ehehalt et al., 2003). Additionally, common cellular markers between these diseases such as mitochondrial dysfunction and oxidative stress further illustrate a possible link between them. The exact cellular mechanisms and pathways constituting this link remain unclear and require further investigation in search of a deeper understanding of AD pathogenesis, and the identification of potential therapeutic targets.

1.2 – Familial Hypercholesterolemia

To assess the role of hypercholesterolemia in AD pathology, it is important to examine hypercholesterolemia more closely. When an individual is found to have high levels of cholesterol in their blood plasma, they are diagnosed as hypercholesterolemic. Individuals with hypercholesterolemia have an increased risk of cardiovascular disease as this excess cholesterol can deposit in the coronary arteries as seen in atherosclerosis (Youngblom, Pariani & Knowles, 1993). This occurs as a result of elevated levels of low-density lipoprotein (LDL), which is one of five major groups of lipoprotein composed of proteins (apolipoproteins), cholesterol, triglycerides and phospholipids that function in cholesterol and triglyceride transportation in the blood circulation (Khan, 2006). Hypercholesterolemia can be inherited from genetic mutations or acquired as “secondary” hypercholesterolemia due to diet, lifestyle or medical conditions, such as

diabetes mellitus, that influence cholesterol levels (Martinez-Hervas & Ascaso, 2019). The primary form of hypercholesterolemia arises from genetic predisposition and is referred to as familial hypercholesterolemia (FH) (Martinez-Hervas & Ascaso, 2019). Heterozygous FH occurs in the presence of an autosomal dominant mutation in genes that are inherited from one parent and is estimated to affect 1 in 200 to 250 people worldwide as the most common inherited condition that leads to cardiovascular disease (Zambón et al., 2010). Unfortunately, South Africa has one of the highest incidences of FH in the world where approximately 1 in 100 people are estimated to have FH (Marais, Firth & Blom, 2004). Hypercholesterolemia is diagnosed in adults when cholesterol levels are higher than 7.8 mmol/L and LDL levels are greater than 4.9 mmol/L where genetic testing is performed to confirm if it is FH (Martinez-Hervas & Ascaso, 2019). The histopathological symptoms of FH include the deposition of xanthomas around the tendons of joints, such as the knee and hands, as well as around the eyelids (Youngblom, Pariani & Knowles, 1993). However, the most common consequence of FH is coronary heart disease (CAD) which often leads to myocardial infarction, and in rare cases, stroke. In fact, untreated men with FH are at a 50% elevated risk for a fatal coronary event by the age of 50 years and women are at a 30% elevated risk by the age of 60 years (Martinez-Hervas & Ascaso, 2019).

Under physiological conditions, the LDL receptor (LDLR) is vital in maintaining cholesterol homeostasis through a tightly controlled intracellular regulation system. Once bound by LDL, the ligand-receptor complex undergoes clathrin-mediated endocytosis, followed by the dissociation of LDL from the receptor due to the acidic endosomal environment. The endosome is then fused with a lysosome for proteolysis of the LDL-cholesterol. A conformational change in LDLR protects it from degradation and instead, the receptor is either directed back to the cell membrane or to the Golgi apparatus for endosomal sorting, which ultimately leads to the recycling of LDLR to the cell membrane (Islam, Hlushchenko & Pfisterer, 2022). The primary genetic mutations implicated in FH are involved in the ligand interactions, internalisation and recycling of LDLR and hence, disrupt this regulation system.

The first and most common mutation implicated in FH, causing 60 – 80% of FH cases (Youngblom, Pariani & Knowles, 1993), is in the *LDLR* gene itself. This mutation often causes a structural, and hence functional, change that disables the receptor's ability to bind to its LDL ligand (Kerr et al., 2017). Additionally, mutations in the *LDLR* gene may suppress its synthesis,

translocation to the cell membrane and turnover (Mollazadeh et al., 2018). The second most common gene mutation causing FH is in the apolipoprotein B (*ApoB*) gene and accounts for 1-5% of FH cases (Youngblom, Pariani & Knowles, 1993). This gene codes for an important structural component of LDLs and when mutated leads to limited binding of LDL-cholesterol (LDL-C, when LDL is carrying cholesterol from the plasma) to LDLR (Mollazadeh et al., 2018). Finally, the third most common gene mutated in FH, that accounts for 0 – 3% of FH cases, is the pro-protein convertase subtilisin-kexin type 9 (*PCSK9*) gene. A mutation in this gene causes its increased expression and promotes LDLR internalisation and degradation (Guo, Feng & Zhou, 2020). In rare cases, the LDL receptor adaptor protein 1 (*LDLRAP1*) gene (encodes the protein required for LDLR internalisation) is also found to be mutated in FH patients (Martinez-Hervas & Ascaso, 2019). By interrupting the normal cycle of LDLR and the internalization of LDL and hence, its removal and degradation, these mutations lead to an accumulation of LDL in the blood plasma (fig. 2). In fact, people with heterozygous FH have a 50% deficiency of LDLR, which produces a two-fold increase in the number of LDL particles in blood from birth (Goldstein & Brown, 2009).

Considering that FH patients are at a severe risk of cardiovascular diseases which are the leading causes of death globally, representing 32% of all global deaths according to the WHO (2021), this condition should not be neglected and poses a serious health issue in the global population. Furthermore, high cholesterol levels, such as those seen in FH, have recently been found to be associated with other disease phenotypes such as type 2 diabetes, vascular hypertension and cognitive impairments (Cimminiello, Zambon & Polo Friz, 2016).

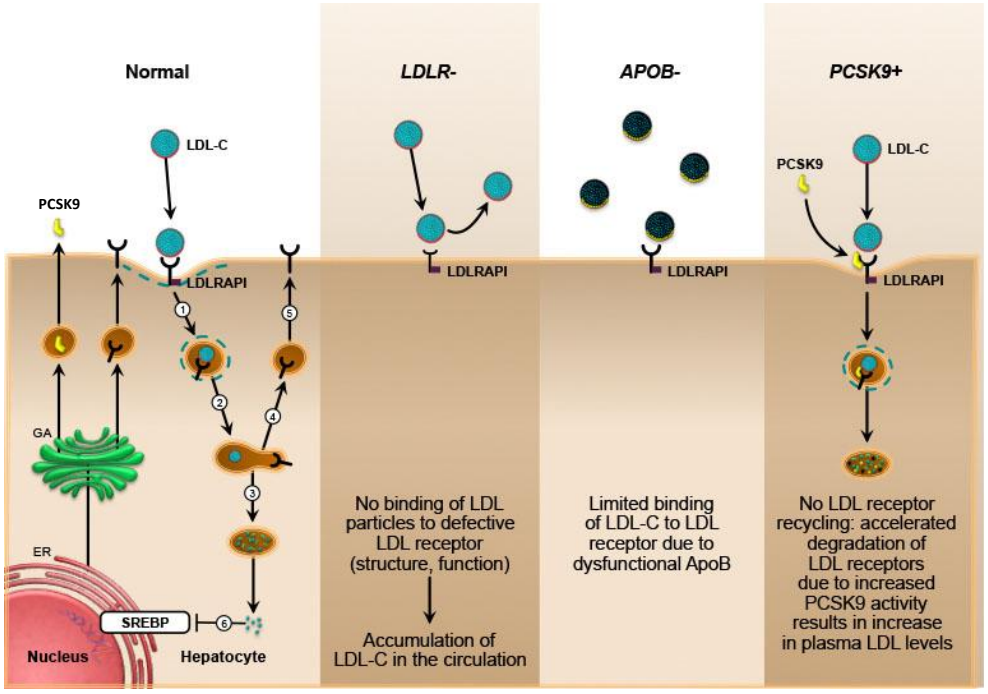


Figure 2: The primary proteins that are mutated in familial hypercholesterolemia.
The mutations in *LDLR*, *APOB* and *PCSK9+* genes lead to defects in physiological LDLR functioning and recycling, ultimately contributing to an accumulation of LDL (low-density lipoprotein) and LDL-C (cholesterol) in the circulation. Blue circles represent normal circulating LDL-C. Black circles indicate dysregulated or uncleared LDL-C due to *APOB* mutation, which impairs LDL receptor binding. Adapted from Martinez-Hervas & Ascaso (2019).

1.3 – Associations between AD and FH

1.3.1 – Altered cholesterol homeostasis in the AD brain

Cholesterol homeostasis is the dynamic balance of cholesterol biosynthesis, uptake, efflux, transport, metabolism and storage. Altered cholesterol homeostasis has been implicated in not only cardiovascular diseases but also in neurological disorders (Zhang & Liu, 2015). Since 22-30% of total body cholesterol is found in the brain, it can be considered as the cholesterol-richest organ (Jin et al., 2019). In neurons, cholesterol is crucial in neuron plasticity, function, axonal development and maintenance (Reitz, 2012). However, due to the blood-brain barrier (BBB), there is little to no direct transport of cholesterol between the peripheral circulation and the brain. Hence, cholesterol biosynthesis *in situ* is very active to meet the high demands of the brain. Although

neurons can synthesize cholesterol, the majority of cholesterol biosynthesis occurs in astrocytes, and this cholesterol is then transported to the neurons via apolipoprotein E (ApoE) containing lipoproteins (Varma et al., 2021). The neurons then import this cholesterol via receptor-mediated endocytosis where one of these receptors that mediate its uptake is LDLR (de Chaves et al., 2008). Recent evidence suggests that FH might weaken BBB function and cause a disruption in the balance of cholesterol transport between the brain and the periphery (Engel et al., 2019), with additional detrimental effects being caused by LDLR deficiency or malfunction that decreases cholesterol-bound ApoE endocytosis. This could lead to increased cholesterol infiltration and accumulation in the extracellular spaces of neurons which have been implicated in promoting the cleavage of APP via β-secretase (amyloidogenic processing) and Aβ aggregation (discussed in sections 1.3.2 and 1.3.3, respectively).

Excess cholesterol in the brain is primarily converted to 24 (S) hydroxycholesterol (24-HC) by the neuron-specific enzyme CYP46A1. The 24-HC product is a more polar metabolite that can cross the BBB, which is the primary route for the elimination of cholesterol from the brain (Zhang & Liu, 2015). Studies have shown that this conversion of excess cholesterol into 24-HC is reduced in AD brains which is associated with worsened neuritic plaque and NFT pathology (van der Kant et al., 2019). The alternative pathway for excess cholesterol is enzymatic conversion to cholesterol esters (CE) (storage form of cholesterol) by acyl-CoA cholesterol acyltransferase (ACAT) in the endoplasmic reticulum. Although CE levels make up only 1% of brain cholesterol in physiological conditions, studies have shown that CE levels are increased by 1.8 fold in the brains of late-onset AD patients (Chan et al., 2012). Furthermore, multiple studies have found that CEs could contribute to the production of Aβ both *in vivo* and *in vitro* as studies showed that CE reduction reduced Aβ levels and secretion in induced pluripotent stem cell-derived neurons (Puglielli et al., 2001; Hutter-Paier et al., 2004; Huttunen et al., 2009; Di Paolo & Kim, 2011).

Additionally, CE-storing lipid droplets have been demonstrated to regulate proteasome activity by acting as signalling organelles (Arrese et al., 2014). This has implications in p-tau proteostasis as van der Kant and colleagues (2019) found that the reduction of CE enhanced proteasome levels. As a result, proteasomal degradation of p-tau was increased by higher proteasome activity within the cell. These findings indicate that cholesterol metabolites and CEs could act upstream of AD pathogenesis, making them possible therapeutic targets for AD treatment. Further evidence

supporting the abovementioned aberrations in brain cholesterol homeostasis is that multiple genetic risk factors associated with AD include genes that encode components of this system, namely ApoE ε4, the apolipoprotein clusterin, CYP46A1, several members of the LDLR family, ACAT and many more (Huttunen & Kovacs, 2008; Di Paolo & Kim, 2011; Chang et al., 2021). Considering the strong genetic link between AD and cholesterol metabolism, AD can be regarded as a unique lipid disorder.

1.3.2 – Influence of high cholesterol on APP processing

The high cholesterol environment in the brain has been reported in many studies to directly influence the processing of APP, which occurs at the cell membrane (Frears et al., 1999; Riddell et al., 2001; Ehehalt et al., 2003; Wang et al., 2021). Cholesterol is a major component of cell membranes, contributing to the formation of distinct membrane domains that vary by the different density and composition of lipids at localised regions. One such domain is called a lipid raft, which is enriched in cholesterol and is implicated in signal transduction, protein trafficking and proteolytic processing (Riddell et al., 2001) by compartmentalisation of the cell membrane for these various functions. These lipid rafts are also known as monosialotetrahexosylganglioside1 (GM1) clusters due to the predominant presence of GM1 lipids (Wang et al., 2021).

A recent study demonstrated that the β- and γ-secretases implicated in the amyloidogenic processing of APP are found in these GM1 clusters, whereas α-secretase (responsible for the non-amyloidogenic processing of APP) is found in the border region of these lipid rafts, termed ‘disordered’ membrane regions (Wang et al., 2021). These secretases were observed to be fairly static compared to the more motile APP peptide that would move between the two regions. This movement of APP is dependent on its cholesterol environment, where high cholesterol conditions promote the movement of APP to the GM1 clusters where it would thus be cleaved by β-secretase to form the insoluble, pathogenic Aβ peptide. In contrast, low cholesterol conditions drove APP to the disordered region where α-secretase cleavage results in a soluble, nonamyloidogenic product (Zambón et al., 2010; Zhou et al., 2011) (fig. 3). This phenomenon illustrates the potential impact that high cholesterol levels, such as those occurring in FH individuals, could have on the production of Aβ and hence, in the pathogenesis of AD.

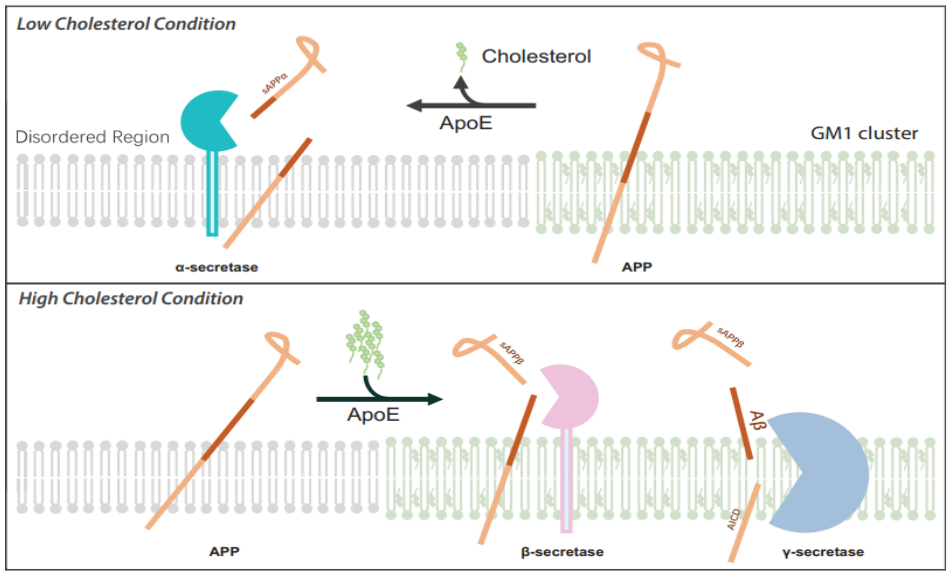


Figure 3*:* The influence of cholesterol levels on APP processing.
High cholesterol levels lead to amyloidogenic processing via β-secretase cleavage of APP in the GM1 cluster (also known as a lipid raft). Low cholesterol levels lead to non-amyloidogenic processing via α-secretase cleavage of APP in the disordered membrane region. Adopted from Wang et al. (2021).

1.3.3 – The role of LDLR in neurogenesis and Aβ clearance

The LDLR deficiency in FH is also speculated to influence the fibrillation and clearance of Aβ from the brain. As mentioned, LDLR is a major receptor of ApoE and is needed for neurons to endocytose extracellular cholesterol that can only be brought to them by ApoE. This function is of high importance in neurons as research shows that besides the need for cholesterol in new membrane production and maintenance, cholesterol uptake is vital for cell energetic states and acts as signalling molecules in neural precursor cells for their proliferation and differentiation (Engel et al., 2019). Thus, loss of LDLR as seen in FH could lead to decreased cholesterol uptake by neurons and consequently, slow down or impair neurogenesis and differentiation into specialised neuronal populations which illustrates a link between FH and neurocognition. Moreover, a study found that overexpression of LDLR enhanced brain-to-blood Aβ transport (Mollazadeh et al., 2018), which highlighted that AD treatment could be enhanced by targeting LDLR. In addition to cholesterol transportation, ApoE also interacts with Aβ through its carboxyterminal domain, which can induce Aβ fibrillation and aggregation, even from soluble forms of Aβ (Reitz, 2012). A study

by Kim et. al. (2009) found that only a 2-fold overexpression of LDLR was sufficient to decrease ApoE levels and Aβ accumulation in the brain by more than 50%. Additionally, Aβ clearance was increased and its aggregation was drastically reduced by LDLR overexpression (Kim et al., 2009). Thus, if ApoE-cholesterol complexes cannot be removed from the extracellular space by LDLR-mediated endocytosis then higher levels of ApoE become available to induce Aβ fibrillation. These findings suggest a vital role of LDLR and high cholesterol in not only cardiovascular disease risk but also in neurological diseases, especially AD.

1.3.4 – Mitochondrial Dysfunction and Oxidative Stress

Additional factors that have been suggested to play a role in the link between AD and FH include mitochondrial dysfunction and oxidative stress (OS). Mitochondrial dysfunction occurs when the mitochondria, the key organelle present in all cells and responsible for energy production in the form of adenosine triphosphate (ATP), experiences cellular damage which can result in loss of cellular viability and function (de Oliveira et al., 2011). Since electron leakage occurs during the electron transport chain, damage to mitochondria exacerbates this leakage which becomes the primary cause of oxidative stress (Chauhan & Chauhan, 2006). In general terms, OS occurs by the production of free radicals, known as reactive oxygen species (ROS). These include oxygen- and nitrogen-based molecules that have unpaired electrons. This results in these radicals being highly unstable and reactive as they search and 'grab' electrons from other molecules, such as proteins, nucleic acids and lipids, turning those molecules into unstable free radicals themselves (Chauhan & Chauhan, 2006). In normally functioning mitochondria this is avoided by the presence of an antioxidant system, comprising mostly of nitric oxide (NO) produced by endothelial nitric oxide synthase (eNOS), which is able to neutralize ROS before significant cell damage can occur. It has been found that the elevated levels of LDL occurring in FH patients leads to the increased generation of superoxide radicals (common ROS) which is known to reduce the activity of eNOS which reduces NO levels, and hence results in an imbalance between the free radicals and antioxidant levels which results in OS (Ganjali et al., 2021). Furthermore, high LDL levels present an attractive substrate to be oxidized by ROS due to its lipid and proteomic composition, which leads to increased lipid peroxidation products (Mollazadeh et al., 2018). These products are highly reactive and when found in high concentrations, as would occur in FH patients, cause protein and DNA damage, alterations in cell signalling and general cytotoxicity (de Oliveira et al., 2011).

Mitochondrial dysfunction, OS and lipid peroxidation are all contributing factors to the onset of AD (Wang et al., 2014). In fact, the brain is highly susceptible to OS due to its high energy demand, high oxygen consumption, high level of iron (a potent ROS catalyst) and is rare in antioxidants (Salim, 2017). Most of all, as mentioned, the brain is rich in polyunsaturated fatty acids that are easily peroxidizable (Chauhan & Chauhan, 2006). Studies have found that the occurrence of OS and associated events actually precedes the formation of the pathology (i.e. Aβ and NFT formation) (Chauhan & Chauhan, 2006; Wang et al., 2014). This supports the important role of OS in AD, and since FH-induced OS and mitochondrial dysfunction occur early on in FH patients (a genetic condition occurs from birth), there could be a contribution of FH to the onset of AD. In addition to general OS, damaged mitochondria are also prominent features of AD (Wang et al., 2014). A study by Yu et al. (2006) found that neuronal cells exposed to high glucose and cholesterol levels produced elevated ROS and exhibited mitochondrial fragmentation. Similarly, Zheng et al. (2020) found that oxidised LDL (oxLDL) caused irregular mitochondrial fusion and fission events, through observations of structurally damaged mitochondria, which led to ROS overproduction (Zheng & Lu, 2020). These findings further suggest a possible link between the FH phenotype (elevated LDL, OS and hence, oxLDL) and AD.

The role of OS and mitochondrial dysfunction in AD presents itself as a complex cycle. Since mitochondria themselves are also vulnerable to OS, it has been proposed that interactions between mitochondrial dysfunction and OS in and around the brain contribute to the initiation and/or amplification of ROS (Salim, 2017). Cell malfunction and degeneration are caused by this prevalent feature which leads to the pathogenesis of AD (Wang et al., 2014). Mitochondrial DNA (mtDNA) is especially vulnerable to ROS attack, and a study found that damage of mtDNA by OS is increased in AD brains by three-fold (Wang et al., 2014). This induces many adverse effects such as inhibition of mitochondrial RNA transcripts and protein synthesis, reduced ATP production (Mollazadeh et al., 2018) and excess ROS production which ultimately leads to cell death. In neurons, OS impairs axonal transport and disrupts intracellular calcium homeostasis, affecting neurotransmitter release and neuronal excitability, which can impair synaptic plasticity and affect learning and memory (Massaad & Klann, 2011). Additionally, excess ROS has been linked to the formation of Aβ and NFTs by stimulation of the respective enzymes involved in their processing (such as protein kinases for NFTs) or the substrates (APP for Aβ formation) (Chauhan & Chauhan, 2006; Wang & Zou, 2018). Both soluble and insoluble Aβ products have been shown

to cause loss of mitochondrial membrane potential and induce the oxidation of vital macromolecules such as DNA and proteins and induce lipid peroxidation (Sun, Chen & Wang, 2015), all of which lead to neurodegeneration characteristic of AD. In general, ROS are involved in Aβ and NFT formation, however, ROS production also increases with Aβ and NFT pathology (Chauhan & Chauhan, 2006). As a result, ROS is generated in an endless cycle (fig. 4). Given the known link between oxidative stress and hypercholesterolemia, patients with FH could represent the start of this cycle (i.e., the initial increase in ROS), potentially acting as an early driver of AD-related oxidative damage.

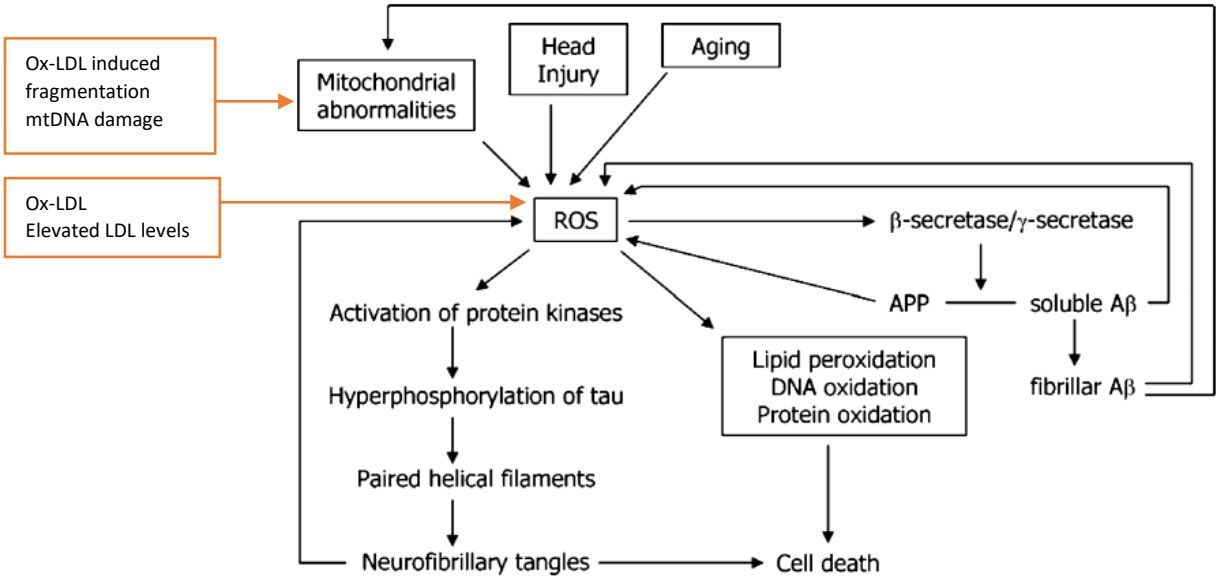


Figure 4: The involvement of reactive oxygen species (ROS) in amyloid-β (Aβ) and neurofibrillary tangle formation.

Excess ROS production can promote Aβ and neurofibrillary tangle formation, which in turn results in increased ROS levels. Orange boxes illustrate the possible involvement of oxidized LDL (oxLDL) and elevated LDL levels (characteristic of FH cases) in ROS-mediated pathogenesis in AD. Adapted from Chauhan & Chauhan (2006).

1.3.5 – Inflammation

Persistent oxidative stress not only has direct implications on cellular function and survival but also plays a role in driving chronic inflammation (Biswas, 2016). As part of its role as a risk factor for cardiovascular diseases such as atherosclerosis, hypercholesterolemia induces systemic inflammation, which significantly contributes to its pathophysiology. As mentioned, excess LDL is prone to oxidation to form oxLDL, which is known to trigger an immune response. This occurs primarily through the activation of macrophages which recognise oxLDL through macrophage pattern-recognition receptors (Sanjurjo et al., 2023). This process promotes pro-inflammatory secretion of cytokines and chemokines, such as interleukin-23, interleukin-6 and tumour necrosis factor-α (TNF- α), which are key molecules in regulating both systemic inflammation and the immune response (Kochumon et al., 2022). Additionally, these secretions enhance toll-like receptor (TLR) signalling and inflammasome activation, resulting in increased immune cell proliferation and production of inflammatory mediators which can exacerbate chronic metabolic diseases such as atherosclerosis (Tall & Yvan-Charvet, 2015a). Hence, studies have shown that elevated LDL cholesterol, and especially its oxidised form, can perpetuate the inflammatory cycle, which can lead to endothelial dysfunction (Tall & Yvan-Charvet, 2015a; Bogachkov et al., 2020). Endothelial cells form the inner lining of blood vessels and are critical to maintaining vascular homeostasis by regulating blood flow, vascular permeability and playing roles in the immune response (Endemann & Schiffrin, 2004). Loss of these physiological functions, often due to excess oxidative stress and inflammation, is referred to as endothelial dysfunction, which is implicated in many diseases, including neurodegeneration (Fang et al., 2023).

This is due to the vital role of endothelial cells in forming and maintaining the BBB, whereby they possess unique features such as tight junctions and low transcytosis rates, which are important to restrict the exchange of molecules and harmful substances between the blood and the brain (Fang et al., 2023). Therefore, endothelial dysfunction causes increased permeability of the BBB due to the loss of tight junction integrity, which allows paracellular leakage that enables toxins, cells, ions and pro-inflammatory cytokines to infiltrate the brain (Hughes et al., 2016). Additionally, elevated secretions of interleukins and TNF-α during endothelial dysfunction increase their expression of intercellular adhesion molecule (ICAM)-1 by activating nuclear factor (NF)-κB which promotes and facilitates the transmigration of peripheral immune cells (e.g. leukocytes) from the

bloodstream into the central nervous system (CNS) (Fang et al., 2023). This increased permeability and infiltration across the BBB is known to trigger neuroinflammation, a major contributor to neuronal cell loss and degeneration, implicated in AD. Many studies have shown that AD patients exhibit weakened BBBs and elevated neuroinflammation which has been found to correlate with increased Aβ accumulation and tau hyperphosphorylation in the brain (Rutkowsky et al., 2018; Rauchmann et al., 2023).

The disruption of the BBB and subsequent neuroinflammation can also activate microglia, the brain's resident immune cells. While acute microglial activation is necessary to maintain homeostasis by surveilling the brain parenchyma, phagocytosing debris and acting as the brain's first line of defence against pathogens, chronic microglial activation can inhibit adult neurogenesis and exacerbate the release of ROS and pro-inflammatory cytokines leading to further neuronal damage and loss (Heneka et al., 2015; Rather et al., 2021). Interestingly, microglia are also activated by Aβ deposition, resulting in the migration of these cells to plaque sites and the subsequent phagocytosis of Aβ fibrils, thus, contributing to Aβ clearance in the brain. However, studies have shown that the sustained activation of microglia also decreases its Aβ binding and phagocytosing efficiency, where the Aβ degrading enzyme activity present in microglia decreases, resulting in a reduced ability for microglia to break down Aβ plaques (Michelucci et al., 2009; Krabbe et al., 2013). Similarly to the oxidative stress cycle previously discussed, there exists a feed-forward loop of increasing neuroinflammation that can further promote Aβ plaque and neurofibrillary tau formation, which in turn is a potent activator of surrounding glial cells, prompting them to adopt a pro-inflammatory phenotype that further exacerbates the current inflammation in the brain (Heneka et al., 2015). Hence, it is clear that triggering neuroinflammation in the CNS could be a pivotal stage in the pathogenesis of AD. Overall, these studies show that the chronic inflammation stemming from the hypercholesterolemic condition may not be confined to the vasculature but may also initiate inflammatory cascades in neighbouring tissues such as the brain. This highlights a possible interplay between hypercholesterolemia-induced systemic inflammation and AD-related neuroinflammation.

1.4 – Induced LDLR upregulation through drug treatment

1.4.1 – Conventional Statin Treatment

Considering the high lipid content in the brain, there have been several studies that investigated the effect of lipid-lowering treatments on AD, including agents used to treat hypercholesterolemic states, such as statins (Li, Lin & Huang, 2018; Ward, Watts & Eckel, 2019). Almost all the cholesterol present in the brain is synthesised *de novo* through a metabolic pathway that begins with the conversion of acetyl-CoA to 3-hydroxy-3-methylglutaryl-CoA (HMG-CoA) in the mevalonate pathway. This product is then further processed to become farnesyl diphosphate (FDP) which can then enter either the non-sterol pathway or the sterol pathway by which cholesterol will be formed (fig. 5) (Zhang & Liu, 2015). The enzymes used in this cholesterol biosynthesis pathway are often targets of drugs aimed to reduce high cholesterol levels (Li, Lin & Huang, 2018). The most commonly used treatment to reduce high plasma cholesterol is the prescription of drugs called statins. The cholesterol-lowering ability of statins is attributed to inhibiting the enzyme called HMG-CoA reductase that functions in catalysing the final and rate-limiting step in the mevalonate pathway (i.e. the conversion of HMG-CoA to mevalonate). This is done by competitively blocking the active site of this enzyme and thus preventing substrate access (Kojro et al., 2010). In addition to blocking cholesterol synthesis itself, statins are also able to upregulate LDLR expression. This occurs since increased LDL cholesterol in cells inhibits the processing of sterol regulatory element-binding protein (SREBP). Processing of SREP is needed to fulfil its function as a transcription factor for the expression of multiple genes, including the gene for LDLR (Goldstein & Brown, 2009). Hence, by limiting cholesterol synthesis statins also indirectly increase LDLR levels.

Statins have been used widely to treat cardiovascular diseases and hypercholesterolemic states such as FH. A major limitation of statins is that it blocks cholesterol synthesis at the step prior to the formation of FDP and its downstream intermediates that are not involved in the sterol pathway for cholesterol synthesis. Studies have highlighted that this could have detrimental effects as most of these intermediates such as ubiquinone, heme A, isoprenoids and farnesylated proteins are important metabolic molecules involved in cell signalling, cell growth and inflammatory responses (Ugawa et al., 2000; Ward, Watts & Eckel, 2019). Moreover, the use of statins has its limitations in some patient populations, especially for those with FH. Patients with FH require additional

upregulation of LDLR above the normal levels of non-FH patients, however, compliance and potency issues for statin dosages mean that FH patients are unable to meet their targeted lipid levels even at the maximal dosage of statins (Kerr et al., 2017). Additionally, one study has also associated statin use with the acceleration of diabetes onset in individuals already predisposed to developing diabetes (Cimminiello, Zambon & Polo Friz, 2016). This is explained by the possible role of statins in impairing pancreatic beta-cell function and decreasing peripheral insulin sensitivity (Goldstein & Mascitelli, 2013). These limitations of statins illustrate that they are not the best solution to treating high cholesterol levels in patients of various disease states, and therefore, highlight the need for alternatives.

1.4.2 – Squalene Synthase Inhibitors: Novel compound SSI

A novel target for upregulating LDLR levels has been found in the cholesterol biosynthesis pathway. As previously mentioned, a step in this pathway involves the processing of FDP in either a non-sterol or sterol pathway. The enzyme, squalene synthase, is what determines which pathway will be taken by catalysing the dimerisation of two FDP molecules to form squalene (Ugawa et al., 2000), the key precursor to cholesterol (fig. 5). Inhibition of squalene synthase has been targeted as an alternative treatment strategy to the use of statins due to the fact that inhibiting this step of the cholesterol synthesis pathway does not lower the levels of the non-sterol intermediates required for cell growth and viability (Brusselmans et al., 2007). Similar to statins, by decreasing cholesterol levels, SREBP is allowed to promote LDLR expression which can further decrease LDL levels.

A recent study by Kerr et. al. (2017) discovered a set of novel compounds that were found to act as squalene synthase inhibitors (SSI). Among these novel SSI compounds, one demonstrated the highest potency and metabolic stability, where *in vivo* testing further revealed its ability to inhibit the conversion of FDP to squalene in a dose-dependent manner, with a half-maximal effective concentration (EC_{50}) of 26 nM (Kerr et al., 2017). This implies that small doses of the compound is able to be effective which illustrates the most pharmacological potential as patients would not require large doses for treatment (Kojro et al., 2010). Additional testing found that the compound SSI also drives LDLR upregulation and successfully inhibited squalene synthase activity in mice. Furthermore, a synergistic effect of using statins (simvastatin) and compound SSI was found to cause a 10-16-fold increase in LDLR upregulation compared to either drug used in isolation (Kerr

et al., 2017). As lipid goals become stricter, especially in the case of FH patients, the addition of a squalene synthase inhibitor such as compound SSI could ameliorate the issues of statin-intolerance and dosage setbacks experienced by non-negligible patient populations by requiring a smaller statin dose, and hence fewer side-effects from statin treatment. Moreover, with the increasing evidence linking FH to AD (as discussed), the application of FH-targeted treatments in the assessment of AD could help to uncover the molecular pathways linking these diseases.

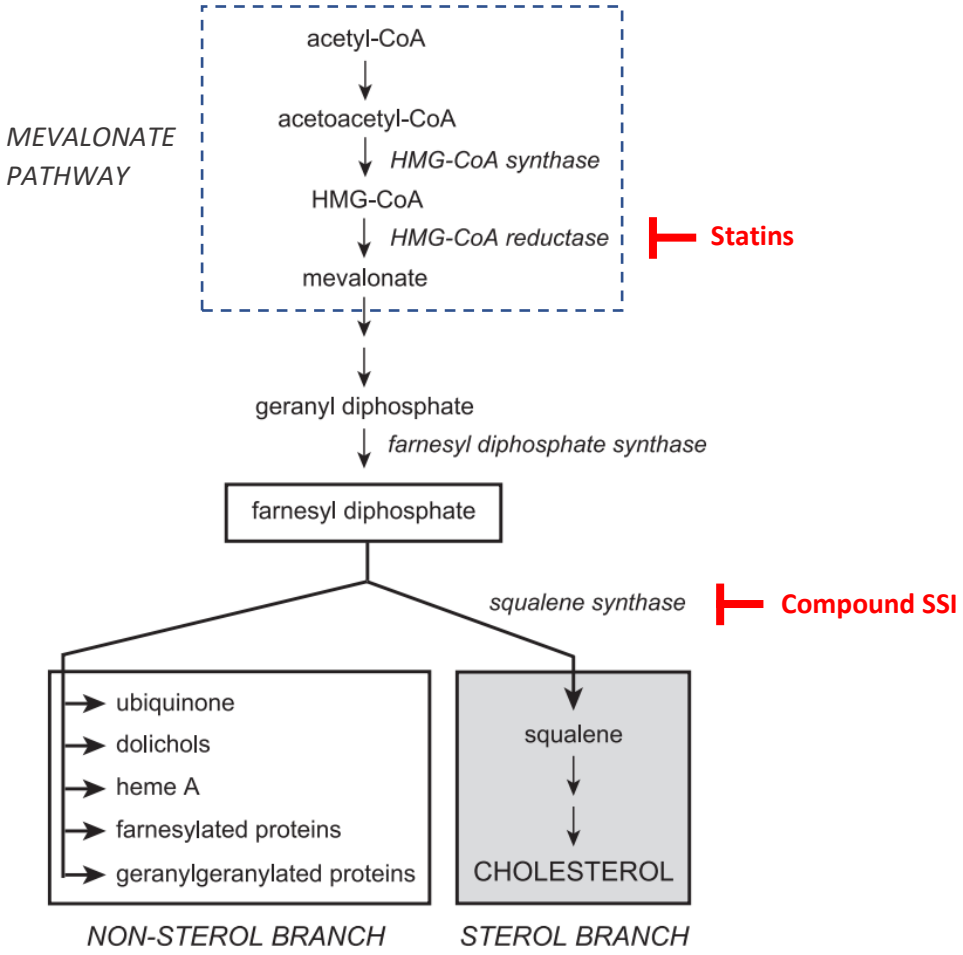


Figure 5: Cholesterol biosynthesis pathway occurring in the central nervous system. Statin therapy inhibits the HMG-CoA reductase enzyme implicated in the rate-limiting step of the mevalonate pathway. Squalene synthase inhibitors, such as compound SSI, inhibits the sterol branch in cholesterol synthesis and still enables the non-sterol branch to occur. Adapted from Brusselmans et. al., (2007).

1.5 – Rationale of the study

As life expectancy increases, the prevalence of AD is projected to increase fourfold by 2050 to 106.8 million with 1 in 86 individuals living with AD (Wang et al., 2014). Additionally, its costs are also predicted to double every 20 years (Reitz, 2012), this includes both direct medical care and informal costs. In 2019, an average of 5 hours per day was spent by informal caregivers (i.e. family members and friends) to provide care for those living with AD-induced dementia (World Health Organisation, 2023). In addition to the financial stress, caregivers experience overwhelming physical and emotional pressures that may further burden familial relationships and require further health, social and financial assistance (World Health Organisation, 2023). Considering the global impact of AD in all ethnic and socioeconomic classes, it is important to have a wider perspective on the factors and contributors affecting its pathogenesis for the improved treatment of the disease. Despite decades of research, the molecular mechanisms underlying AD pathogenesis remain incompletely understood, underscoring the need for innovative approaches. Recent evidence illustrates an association between the genotypic and phenotypic changes that occur in FH and AD, either by possible causative mechanisms, such as LDLR deficiency, or by common disease defects such as increased mitochondrial dysfunction and inflammation. Exploring this intersection provides an opportunity to uncover upstream mechanisms driving AD pathology, which may inform the development of targeted therapeutic strategies and alleviate the broader economic and social burden of this disease.

1.6 – Scope of the study

In this study, the associations between hypercholesterolemia and AD were investigated in an attempt to better understand the possible molecular links between both disease states. This was done by integrating proteomic analysis with targeted *in vitro* experiments. First, a proteomic analysis was conducted on plasma samples of FH patients to explore the molecular pathways that are dysregulated in the FH condition and gain insight into whether these dysregulations could potentially impact AD onset. This analysis highlighted a dysregulation in oxidative stress and ROS response processes which have been strongly implicated in AD development, as discussed. To further explore these findings at a cellular level, an *in vitro* hypercholesterolemic-AD cell model was created by treating human embryonic kidney (HEK) 293 and the SH-SY5Y human

neuroblastoma cell lines with Aβ protein, LDL and hydrogen peroxide to mimic early oxidative stress conditions. The novel compound SSI was used to induce LDLR upregulation in this model. The safety and efficacy of SSI were assessed using the MTT cell viability assay, western blot analysis of LDLR expression and cytotoxicity analysis by using light microscopy to evaluate cell morphology. To assess mitochondrial function in the cell models and after SSI treatment, mitochondrial metabolic activity was assessed using the MTT and Alamar Blue® assays in conjunction with assessing mtDNA copy number using quantitative PCR. Moreover, ROS production in the SSI-treated cell models was also assessed using fluorometric analysis.

2. Aims and Objectives

2.1 - Main aim

To assess the impact of hypercholesterolemia on Alzheimer's disease pathogenesis by examining proteomic alterations in familial hypercholesterolemic patient plasma and assessing associated oxidative stress, mitochondrial dysfunction and LDL receptor-related signalling pathways in a hypercholesterolemic-AD cell model.

2.2 – Objectives

1. Investigate the differential protein expression in plasma samples of FH patients compared to healthy controls using sequential window acquisition of all theoretical fragment ion spectra mass spectrometry (SWATH-MS) proteomics.
2. Create a hypercholesterolemic-AD cell model by treating HEK293 and SH-SY5Y cells with human amyloid-beta protein (Aβ42) and low-density lipoprotein (LDL).
3. Create an oxidative stress cell model by treating HEK293 and SH-SY5Y cells with hydrogen peroxide (H_2O_2) to mimic early-stage oxidative stress conditions in AD and hypercholesterolemia.
4. Induce LDLR upregulation in HEK293 and SH-SY5Y cells using novel compound SSI treatment.
5. Validate SSI-induced LDLR upregulation in the HEK293 and SH-SY5Y cells using western blot analysis.
6. Assess the mitochondrial activity of the hypercholesterolemic-AD cell model after SSI treatment using the 3-(4, 5-Dimethylthiazol-2-yl)-2, 5-Diphenyltetrazolium Bromide (MTT) assay.
7. Assess the cellular metabolic activity of the hypercholesterolemic-AD cell model after SSI treatment using the Alamar Blue® assay.
8. Assess the effect of SSI treatment on the production of reactive oxygen species (ROS) in the hypercholesterolemic-AD cell model using a fluorescence-based ROS assay.
9. Assess the effect of SSI treatment on mitochondrial DNA copy number (mtDNA-CN) in the hypercholesterolemic-AD cell model using quantitative PCR.

3. Methodology

3.1 - Proteomic Analysis: SWATH-MS

Proteomics is the large-scale study of the proteome within an organism. This includes the analysis of all isoforms of all proteins, the post-translational modifications of proteins and protein-protein interactions (Alaaeddine et al., 2017). Additionally, since the proteome is dynamic in nature and changes throughout development or in response to adverse occurrences (e.g. disease), proteomics has been a valuable and insightful tool in understanding the complexity of a disease state by gathering insights into cellular pathways and hence, the various mechanisms of a disease. One of the well-established methods for proteomic analysis is mass spectrometry, a technique whereby proteins and peptides are first ionised and assessed based on their characteristic mass-to-charge (m/z) ratios. The m/z values can then be matched to databases by computer algorithms to identify the proteins (Pan et al., 2009). This study utilised Sequential Windows Acquisition of All Theoretical Spectra-Mass Spectrometry (SWATH-MS), which is used to identify and quantify thousands of proteins in a single sample. SWATH-MS is advantageous as it maximises the acquisition of all protein data that a sample may contain by using an integrated data acquisition approach. Furthermore, this technique provides very accurate and reproducible quantification of proteins, which is necessary when assessing a disease state (Frederick & Ciborowski, 2016).

In this study, proteomic analysis was conducted on patient plasma samples (ethics clearance number: M210289, Appendix) obtained in collaboration with Prof. Derick Raal (Head of the Division of Endocrinology at the School of Clinical Medicine at the University of the Witwatersrand). The patient samples included 10 healthy individuals (negative FH status, negative statin status), 12 FH patients (positive FH status, negative statin status) and 12 FH patients on statin medication (positive FH status, positive statin status). Since FH is congenital, each of these groups included individuals with ages ranging from 7 to 50 years old, representing a broad range of disease progression and biological variability. Proteomic analysis (sample and data processing) of the patient plasma samples was performed at The Council for Scientific and Industrial Research (CSIR) centre. The SWATH-MS measurements were based on data-independent acquisition (DIA), such that the protein samples did not require any labelling before digestion and there was no selection of specific precursor ions that can limit the protein range that is measured in the

sample, as seen in data-dependent acquisition (DDA). Instead, DIA allows all ions within specified m/z regions to be analysed. This allows for the unbiased and wide proteomic coverage of the sample. After sample analysis, protein identification was performed using a DDA-derived protein spectral library such as ProteinPilot which runs the DIA-derived data through multiple databases (e.g. Swiss-Prot Uniprot). Due to the sample size, the identified proteins were considered as differentially expressed if the proteins had a fold change of ≥ 1.5, p-value ≤ 0.05 and q-value ≤ 0.05 (Karp & Lilley, 2007). These thresholds were placed to balance the need for statistical significance with the limitations of small sample size, ensuring that identified proteins had robust and reliable differences in expression.

To assess the biological implications of any differential protein expression observed via SWATH-MS, functional analysis was performed using the Search Tool for Retrieval of Interacting Genes/Proteins (STRING) database v12 (https://string-db.org/). STRING is a biological database of known and predicted protein-protein interactions. The database determines these interactions using information from multiple sources such as scientific text mining, computational prediction tools, experimental data and co-expression analyses (Szklarczyk et al., 2019). Each protein interaction examined is given a confidence score ranging from 0 to 1, calculated based on the integrated data from these various sources. This score is a measure of the likelihood that a predicted protein-protein interaction (PPI) is biologically meaningful, where higher confidence scores indicate stronger evidence supporting a specific interaction (Szklarczyk et al., 2019). For this analysis, a minimum confidence score of 0.400 (medium confidence) was chosen as a threshold to include interactions that have a reasonable level of support, ensuring that enough PPIs were captured to identify meaningful biological networks while excluding interactions with weaker or less reliable evidence. The STRING database was also used to determine the top gene ontology (GO) molecular functions and biological pathways enriched by the protein dataset. For this analysis, a minimum strength score of 1.00 was applied to filter both GO terms. The strength scores describe how large the enrichment effect is and represents the ratio between the number of proteins in the network that are annotated with a term to the number of proteins that STRING expects to be annotated with this term in a random network of the same size (Log10(observed/expected)). This threshold was chosen to focus on GO terms that are enriched at least 10 times more than would be expected by chance.

In addition to STRING, the Reactome Pathway Browser (https://reactome.org/) was also used to perform functional analysis of the differentially expressed proteins and identify the top 10 enriched molecular pathways. Reactome is a highly curated and peer-reviewed pathway annotation database that can be used to uncover, interpret and visualise cellular pathways from high-throughput data (Yu & He, 2016). This pathway analysis tool is known to be an accurate and reliable bioinformatics tool that integrates and cross-references both curated and external data. Reactome's robust cross-referencing and integration of curated data ensure the accuracy and relevance of its pathway analysis, uncovering key molecular mechanisms and interactions within complex datasets. Lastly, an interactive web-based tool called ShinyGO v0.8 (http://bioinformatics.sdstate.edu/go80/, South Dakota State University) was used to create a comprehensive visual representation of the top 20 enriched pathways, including molecular structures, cellular activities and disease states, providing a comprehensive overview of the broader implications of the dysregulated proteins found in the dataset. Therefore, using both protein expression proteomics and functional analysis, this study investigated insights into the primary cellular mechanisms involved in the pathogenesis of FH in addition to the effects of statin therapy on these mechanisms.

3.2 - Cell Culture

This study used the HEK293 (Fox Chase Cancer Centre, Pennsylvania) and SH-SY5Y (CELLONEX, Johannesburg) cell lines for the experimental procedures. The SH-SY5Y cell line is derived from the parent SK-N-SH neuroblastoma cell line (subcloned three times) and is commonly used for *in vitro* neurological studies, particularly relating to Alzheimer's disease (Patte-Mensah et al., 2012; Koriyama et al., 2015). This cell line is human-derived and able to express most AD-related proteins, including Aβ42 and tau, as well as the FH-related LDLR protein (Brodeur et al., 2012). Similarly, the HEK293 (human embryonic kidney) cells express neuronal markers, LDLR and can internalize amyloid-beta protein, as seen in previous studies (Domingues et al., 2007; Porrello et al., 2007). Hence, these cell lines were suitable for creating an AD-FH cell model to investigate the link between these diseases.

The HEK293 cells were cultured in T25 culture flasks using high glucose Dulbecco's Modified Eagle Medium (DMEM) (Hyclone, GE Life Sciences, Massachusetts, USA). For the SH-SY5Y cells, the high glucose Dulbecco's Modified Eagle Medium**:** Nutrient Mixture F-12 (DMEM/F12,

1:1) (Gibco, Fisher Scientific, Brussels, Belgium) was used for all cell culture-related methods in T25 culture flasks. All culture media was supplemented with 10% (v/v) fetal bovine serum (FBS) (Biowest, Nuaillé, France) to provide all the necessary growth factors and nutrients to support optimal cell growth. To prevent bacterial contamination, 1% (v/v) penicillin/streptomycin (Thermo Fisher Scientific, Massachusetts, USA) was also added to the media. The cells were then incubated at 37°C in a humidified incubator with 5% CO_2 to mimic *in vivo* conditions (Liste-Calleja et al., 2015).

3.2.1 - Harvesting and Passage

The Zeiss Primovert light microscope (Zeiss, Oberkochen, Germany) was used to monitor cell growth until the cells reached 70- 80% confluency. At this stage, the cells underwent passaging to allow continued cell growth and prevent contact inhibition (Masters & Stacey, 2007). The old culture media was carefully discarded and the cells were washed twice with 2 ml of phosphate-buffered saline (PBS). The cells were then harvested by the addition of trypsin-Ethylenediaminetetraacetic acid (EDTA) (Biowest, Nuaillé, France), where trypsin caused cell detachment by proteolytic cleavage of cell-flask adhesions. EDTA was present as a chelating agent to remove magnesium and calcium ions used by cell-adhesion receptors, such as cadherins, to remove the cell-cell adhesions (Segeritz & Vallier, 2017). Once cell detachment was confirmed (after 5-10 minute incubation at 37°C), the trypsin was neutralised by adding an equal volume of fresh media to the flask, to prevent loss of cell viability. The cells were then collected and pelleted via centrifugation at 1500 × g for 3 minutes. After the supernatant was discarded, fresh culture media was added to resuspend the cell pellet. The cells were then divided into new culture flasks where additional media was added per flask (5 ml for T25 flasks). Since cells should not be cultured exhaustively, to prevent the accumulation of mutations and altered phenotypes, and in case of unforeseen circumstances, such as equipment failure and contamination, cell stocks were also made by preparing a solution of 10% dimethyl sulfoxide (DMSO) (Thermo Fisher Scientific, USA) and 90% culture media which was used to resuspend the cell pellets, before being placed in cryovials. The cell stocks were then stored at -80°C until needed.

3.2.2 - Cell Quantification and Seeding

Cell quantification and cell viability were assessed via the trypan blue exclusion assay prior to treatment to ensure that a standard number of cells were used per treated cell group for each experiment/assay. Trypan blue was used to differentially stain live and dead cells due to dead cells having compromised cell membranes, allowing the solution to stain the cytoplasm (appear blue), whereas live cells with intact membranes are not stained (appear white) (Strober, 2001). Prior to treatment, the cells were harvested from the culture flasks using the same protocol outlined (section 3.2.1) until the cells were collected as a pellet. To the pellet, 2 ml of fresh culture media was added, and the cells were gently resuspended by pipetting up and down. A 20 µl aliquot of the cell suspension was transferred to a sterile 1.5 ml microcentrifuge tube and mixed with 20 µl of trypan blue dye (1:1). Thereafter, 20 µl of the mixed solution was inserted into a cell counting slide (Bio-Rad, California, USA). The counting slide was inserted into the TC- 20 Automated Cell Counter (Bio-Rad, California, USA) which reported the total cell count, live cell count and percentage cell viability. The live cell count was then used to calculate what volume of the 2 ml cell suspension to use per well for even seeding density for subsequent assays to be performed and to ensure the cells were at least 90% viable before seeding. Seeding densities included: 1×10^4 cells/well for 96-well plates (used for cell viability and ROS production analysis), 0.3×10^6 cells/well for 6-well plates (used for mtDNA-CN qPCR), and 2.2×10^6 cells/well for 100mm dishes (used for western blot analysis).

3.3 – Treatment

The HEK293 and SH-SY5Y cells were treated after being harvested and seeded as previously outlined (3.2.1 and 3.2.2). The seeded plates were left untreated and incubated for 24 hours to allow the cells to attach to the plate surface. The seeding density and cell viability were monitored across all wells using an inverted light microscope prior to treatment to ensure uniformity across the wells/dishes. All treatments were conducted using three biological repeats, each containing two or three technical repeats per treatment group.

3.3.1 - Compound SSI

To assess the effect of LDLR upregulation on the FH-AD cell model, the HEK293 and SH-SY5Y cells were treated with the novel compound named SSI, which is a squalene synthase inhibitor that reduces *de novo* cholesterol biosynthesis in cells and has been found to cause an upregulation of LDLR expression (Kerr et al., 2017). A 1 μM stock solution of the compound was made using culture media and a final concentration of 0.0023% DMSO, which was needed to solubilize the compound. To find the optimum concentration of the compound to maximize LDLR upregulation while minimizing cytotoxicity, the cells were first treated with four concentrations of SSI (25 nM, 50 nM, 100 nM and 150 nM) based around its EC_{50} of 26 nM (Kerr et al., 2017). The effect of these concentrations of SSI was assessed using the 3-(4, 5-Dimethylthiazol-2-yl)-2, 5-Diphenyltetrazolium Bromide (MTT) (3.5.1) cell viability assay and western blot analysis (3.6) after 24 hours and 48 hours of incubation under standard conditions. After optimisation, the 50 nM and/or 100 nM SSI concentrations were used for subsequent assays (MTT assay, Alamar Blue® assay, ROS assay and mtDNA-CN qPCR).

3.3.2 - Amyloid-beta Protein (Aβ42)

To create an AD-cell model, the human 42 amino acid isoform of amyloid beta (Aβ42) was used to treat the HEK293 and SH-SY5Y cells. This isoform is the most common isoform found in AD and hence, was ideal for inducing an AD state in the cell models (Li et al., 2019). In order to investigate the early stages of AD pathogenesis, the cells were treated with a non-lethal concentration of 1 μM Aβ42 (Terzioglu-Usak et al., 2017; Bernabeu-Zornoza et al., 2019).

The lyophilised Aβ42 peptide (Sigma-Aldrich, USA) was reconstituted in a 50 mM Tris-HCl buffer at pH 9 to a stock concentration of 1mg/ml. As per the manufacturer's instructions, this Aβ42 solution was then incubated at 37°C for 48 hours to induce oligomerisation of the peptides. Thereafter, the solution was diluted in 1× PBS to a new stock concentration of 5 μM, which was stored at -20°C until needed for treatment. This new stock was then diluted using cell culture media to a final concentration of 1 μM to be used for cell treatment. The cells were then incubated at 37°C for 24 and/or 48 hours prior to analysis in further assays.

3.3.3 – Low-density lipoprotein (LDL) cholesterol

To create a hypercholesterolemic cell model, the cells were treated with 150 μg/ml of low-density lipoprotein (LDL) (Sigma-Aldrich Merck, Darmstadt, Germany). This concentration falls in the mid-high range concentration used to mimic the hyperlipidemic state *in vitro* (Baumer et al., 2017). The LDL was reconstituted in PBS to a stock concentration of 5 mg/ml, which was stored at -20°C until needed for treatment. To treat the cells, the LDL was diluted using cell culture media to a final concentration of 150 μg/ml. After LDL treatment the cells were incubated at 37°C for 24 and/or 48 hours prior to analysis in further assays.

3.3.4 – Hydrogen Peroxide (H_2O_2)

Studies have illustrated that both hypercholesterolemia and AD exhibit high levels of oxidative stress as a key event that leads to cell damage and deterioration (Chauhan & Chauhan, 2006; de Oliveira et al., 2011), providing a possible mechanism linking the two diseases. Hence, to further mimic the pathological phenotype of these two diseases, the HEK293 and SH-SY5Y cells were treated with hydrogen peroxide (H_2O_2). Due to its high rate of decomposition, fresh stocks of 10 mM H_2O_2 were prepared using cell culture media just prior to treatment. The cells were treated with two concentrations of 300 and 500 μM, known to generate intracellular reactive oxygen species production, without causing excessive cytotoxicity (Gülden et al., 2010). Treatment with H_2O_2 was followed by 24 and/or 48-hour incubation at 37°C prior to analysis in further assays.

3.4 - Cell Morphology

After cell seeding, the HEK293 and SH-SY5Y cells were examined 24 and 48 hours after treatment using an inverted light microscope (Zeiss, Oberkochen, Germany) at 40× magnification. Digital images of the cells were taken using this microscope and analysed visually for any morphological signs of cellular stress or death, such as cell shrinkage, cell rounding, membrane blebbing or detachment (Saraste & Pulkki, 2000).

3.5 – Metabolic Activity Assays

To assess the effect of the treatments (3.3) on the metabolic activity of the HEK293 and SH-SY5Y cells, the MTT and Alamar Blue® cell viability assays were performed. These assays were first performed during the optimisation of the SSI concentrations. Thereafter, the two assays were used to assess the effects of the SSI compound on the FH-AD cell models. For the metabolic activity assays performed, protocatechuic acid (PCA) (8 mM) was used as the cell death/positive control in the SSI optimisation MTT assays, while triton-X (2%) was used as the cell death/positive controls in the remaining MTT and Alamar Blue® assays, as both solutions are known apoptotic inducers (Saraste & Pulkki, 2000). The untreated cells served as the negative control. The results were then calculated such that the treated cells were expressed as a percentage of the untreated cells (set to 100%) within each biological repeat.

3.5.1 - 3-(4, 5-Dimethylthiazol-2-yl)-2, 5-Diphenyltetrazolium Bromide (MTT) assay

The MTT assay is a common colourimetric assay used to determine cell viability by specifically measuring the metabolic activity of functional mitochondria within the cells. In viable cells, the mitochondrial succinate dehydrogenase enzymes use nicotinamide adenine dinucleotide (NAD^+)/reduced NAD^+ (NADH) to reduce the MTT tetrazolium salt into an insoluble purple formazan crystal product (Burton, 2005). Once dissolved, the formazan product can be measured by spectrophotometry. Thus, the quantity of formazan product produced is proportional to the number of functioning mitochondria.

Briefly, the HEK293 and SH-SY5Y cells were seeded into 96-well plates and treated. Once the treatment period was complete (24 or 48 hours), 100 µl of an MTT solution comprising 90% cell culture media and 10% of 5 mg/ml MTT was added to each well. The plate was then incubated in the dark for 2 hours at 37°C to allow the MTT to formazan conversion. After incubation, 100 µl of MTT neutralisation solution (10% sodium dodecyl sulphate and 10 mM HCl) was added to the MTT-containing media to solubilise the formazan crystals without disturbing them. The cells were then left to incubate at 37°C overnight for complete formazan solubilisation before the absorbance of each sample was measured at 570 nm using the VICTOR® Nivo™ Multimode Plate Reader (Avantor®, PerkinElmer, USA).

3.5.2 - Alamar Blue® Cell Viability Assay

Cellular metabolic activity of the treated cells was also assessed using the Alamar Blue® assay. The principle of the assay is the conversion of a blue non-fluorescent dye called resazurin, to a red, fluorescent compound called resorufin. The resazurin dye is able to permeate the cell membrane where it can be reduced by NADH dehydrogenase and nicotinamide adenine dinucleotide phosphate ($NADP^+$)/reduced $NADP^+$ (NADPH) dehydrogenase in the presence of NADH and NADPH both in mitochondria and the cytoplasm. Hence, the assay reflects overall cellular metabolic activity (Rampersad, 2012). Resorufin is a highly fluorescent compound compared to the non-fluorescent resazurin, and thus, metabolically active cells are indicated by an increase in fluorescence and a change in colour from blue to red in the culture medium (Rampersad, 2012). Although absorbance changes can also be used to measure resorufin, this approach is often less sensitive than using fluorescence measurements, which was the choice of measurement for this study.

Briefly, the HEK293 and SH-SY5Y cells were seeded into 96-well plates and treated as previously described. The treatment-containing media was removed from the cells followed by a subsequent wash with 1× PBS. Thereafter, resazurin dye solution was added to the wells at a volume that is 10% of the total volume of culture media per well (for 96-well plates: 10 µl dye and 90 µl media). The plates were then incubated at standard conditions for 2-4 hours. Thereafter, fluorescence was measured at 590 nm emission/ 560 nm excitation wavelengths using the VICTOR® Nivo™ Multimode Plate Reader (Avantor®, PerkinElmer, USA). Background fluorescence was accounted for by including blank wells containing the assay working solution without cells, and all raw fluorescence values were corrected by subtracting the corresponding blank readings.

3.6 - Western Blot Analysis

To assess the efficacy of SSI-induced LDLR upregulation in the HEK293 and SH-SY5Y cells, western blot analysis was performed. This method is highly specific as the proteins are first separated by molecular size followed by the use of target-specific antibodies, which allow specific proteins of interest to be analysed qualitatively and quantitatively. Additionally, western blot analysis is highly sensitive, as it is capable of detecting protein levels as low as 0.1 ng (Yang & Mahmood, 2012). Although this method produces semi-quantitative results, whereby the protein

levels are relative to an untreated control, this was sufficient for its purpose in assessing LDLR upregulation, as the primary goal was to confirm changes in expression rather than obtain absolute quantification.

3.6.1 - Protein Extraction

After treatment the HEK293 and SH-SY5Y cells were harvested by first removing and discarding the old culture media containing the treatments. Thereafter, the cells were washed with 2 ml of 1× PBS. The cells were then detached from the plate using 2 ml of trypsin/EDTA for 5 minutes at 37°C. To inactivate the trypsin/EDTA, 2 ml of fresh media was added to each plate. The cell suspension was then transferred to individual 15 ml falcon tubes and centrifuged at 4000 × g for 10 minutes. After removing the supernatant, 400 - 600 µl of 2× radioimmunoprecipitation assay (RIPA) buffer (Appendix, table S2) was added to the cell pellet (depending on the size of the pellet). RIPA buffer was used to lyse the cells due to the presence of both non-ionic detergents (e.g., Triton X-100) and anionic detergents, most commonly sodium dodecyl sulphate (SDS) which causes protein denaturation, decreases protein-protein interactions and ensures efficient protein solubilization (Niu et al., 2018). This solution was then transferred to 2 ml centrifuge tubes, where the cells were then sonicated on ice 3 times at 35 Hz for 10 seconds per burst, to ensure efficient cell lysis. Once complete, the solutions were vortexed before being incubated at 4°C for 15 minutes. To separate the protein and cell debris, the lysate was centrifuged at 5000 × g for 10 minutes. Thereafter, the protein-containing supernatant was transferred to fresh 2 ml centrifuge tubes. The BCA assay was then performed to quantify the protein concentration of the lysates.

3.6.2 - Protein Quantification: Bicinchoninic acid (BCA) assay

Before performing western blot analysis, the total protein concentration of each lysate was determined to ensure equal loading of protein for the western blot. The BCA assay consists of two reagents, namely, copper (II) sulphate and bicinchoninic acid (BCA). The principle of this assay is that the peptide bonds present in proteins reduce the Cu^{2+} ions found in the copper (II) sulphate reagent to Cu^{1+}. Thereafter, two molecules of BCA chelate with one Cu^{1+} ion to form a purple-coloured complex that absorbs light at a wavelength of 526 nm (Johnson, 2021). Thus, the concentration of protein will be directly proportional to the number of Cu^{2+} ions that are reduced and hence to the absorbance measured at 526 nm. This colourimetric-based assay was performed

as opposed to other popular assays, such as the Bradford assay, as it is more sensitive, being able to detect protein concentrations as low as 5 µg/ml, and contains less protein/protein variability compared to the Bradford assay, which relies on protein-dye binding (Shen, 2019).

To quantify the proteins using the absorbance spectra, a standard curve was first created using a set of bovine serum albumin (BSA) protein standards of known concentration (0, 0.2, 0.4, 0.6, 0.8, 1 mg/ml). These standards were loaded at 25 µl/well into a 96-well plate and samples of unknown concentration were added into separate wells at 5 µl/well and made up to 25 µl using distilled water. All samples were loaded in triplicate. The BCA working solution was then made up at a 1:50 ratio of copper (II) sulphate to bicinchoninic acid. This solution was added to the plate at 200 µl/well. The plate was then incubated at 37°C for ±45 minutes. Once a sufficient colour change was observed, the absorbance was measured at 526 nm using the VICTOR® Nivo™ Multimode Plate Reader (Avantor®, PerkinElmer, USA). The absorbance spectra for the BSA standards were used to create a standard curve where a linear regression model was calculated to obtain an equation for the curve (ensuring that the R^2 value is not less than 0.98, to ensure a strong correlation between absorbance and protein concentration for accurate protein quantification). The protein concentration of each sample was calculated using this equation. The samples were then made up for western blot analysis by diluting the lysate samples to a minimal final concentration of 1 mg/ml (including loading dye).

3.6.3 - SDS-PAGE and Western Blotting

Once the protein lysates were quantified, sodium dodecyl sulphate polyacrylamide gel electrophoresis (SDS-PAGE) was used to separate the different proteins in the lysate according to molecular weight. As mentioned, each lysate sample was first standardised to 1 mg/ml using distilled water and 3× loading dye (187.5 mM Tris-HCl pH 7, 6% SDS (w/v), 30% glycerol, 0.03% bromophenol blue (w/v)) which contains dithiothreitol, a reducing agent that breaks disulfide bonds in proteins. The presence of SDS and a reducing agent ensures that all the proteins are fully linearised and possess the same net negative charge. This ensures that the proteins can be resolved based solely on their molecular weights as they move across the gel in the presence of an electric field which causes them to migrate towards the positive electrode (Manns, 2011). The hydrocarbon tail in SDS binds the protein to initiate denaturation while imparting a negative charge along the protein length, and the reducing agent functions in breaking any disulfide bonds to ensure full

linearisation of the proteins (Rath et al., 2009). A discontinuous gel system was cast using 5% stacking and 10% resolving polyacrylamide gels (Appendix, table S5) to concentrate the proteins into sharp bands at the interface before their separation through the resolving gel matrix during electrophoresis. The prepared samples were heated for 5 minutes at 95°C to ensure protein denaturation before 30 µg of protein was loaded into separate wells of the gel system alongside 2 µl of PageRuler Prestained Protein Ladder (Thermo Fisher Scientific, USA). The protein samples were resolved for 60-90 minutes at 100 V using the Mini-PROTEAN Tetra Vertical Electrophoresis Cell Chamber System (Bio-Rad, California, USA) and 1× Electrophoresis Running Buffer (Appendix, table S3).

Next, 6 filter papers and 2 sponges were pre-soaked in 1× Transfer Buffer and polyvinylidene fluoride (PVDF) membrane was cut to size and activated in methanol for 5 minutes. After the proteins were separated and the dye front was 0.5 cm from the bottom, the proteins were transferred to the PVDF membrane using the Eco-MINI Biometra wet transfer tank system (Analytik Jena Company, Jena, Germany). The setup involved laying one sponge, three filter papers, the PVDF membrane, the gel, three filter papers and the last sponge (in this order) into a cassette. This transfer was performed in 1× Transfer buffer (Appendix, table S4) for 1 hour and 45 minutes at 100 V – 40 mA. Once transfer was complete, the membranes were cut according to the protein ladder to separate β-actin loading control (42 kDa) and the target protein, LDLR (100- 130 kDa), so that each could be incubated with their respective primary antibody separately. Each membrane was then incubated in 5% blocking buffer made with non-fat milk powder in 1× PBS and 0.1% Tween 20 (PBST) for 1 hour. This step was performed to prevent the primary antibody from binding non-specifically to the exposed areas of the membrane by blocking these sites. After blocking, the membranes were incubated with primary antibody (table 1) diluted in 3% BSA in 1× PBST overnight on a shaker at 4°C. Each membrane was then washed 4 times with 1× PBST for 5 minutes per wash with gentle shaking to remove any unbound antibody.

The membranes for the LDLR protein were then incubated with a secondary antibody (outlined in table 1) made up in 3% BSA and 1× PBST, shaking at room temperature in the dark for 1 hour. The secondary antibody is conjugated with horseradish peroxidase (HRP), a reporter enzyme, required to catalyse the chemical reaction with its substrate to generate a chemiluminescent signal that is detectable and can be used to quantify the amount of protein present. After incubation, the

membranes were washed 4 times with 1× PBST (5 minutes per wash). After the last wash, 2 ml of SuperSignal™ West Pico PLUS Chemiluminescent Substrate (Thermo Fisher Scientific, USA) was added to the membranes for up to 5 minutes to react with the HRP-conjugated LDLR secondary antibody and the already HRP-conjugated primary antibody for β-actin. The chemiluminescent signal was visualised using the ChemiDoc™ Imaging System (Bio-Rad, California, USA). In order to quantify the signals detected for each protein, densitometric analysis was performed on the bands using Image Lab 5.1 software (Bio-Rad, California, USA) where the target protein signals (LDLR) were normalised against the β-actin loading control band intensities.

Table 1: Outline of the sources and dilutions for the primary and secondary antibodies used in the western blot analysis

Target Protein	Antibody	Product Name	Dilution	Manufacturer
LDLR	Primary	Anti-LDLR monoclonal antibody, produced in goat	1:1000	Invitrogen, Thermo Fisher Scientific
	Secondary	Donkey anti-goat IgG-HRP conjugated	3:20 000	Santa Cruz Biotechnology
β-actin	Primary	Monoclonal anti-β-actin peroxidase, produced in mouse	1:10 000	Sigma Aldrich, Merck

3.7 - Total Reactive Oxygen Species (ROS) Assay

A major hallmark of both hypercholesterolemia and AD is the disruption in cellular redox balance leading to excess ROS formation and the oxidation of important biomolecules such as DNA, lipids and protein (Chauhan & Chauhan, 2006). Hence, this study used the Total Reactive Oxygen Species (ROS) Assay Kit 520 nm (Invitrogen, Thermo Fisher, USA) to assess the effects of SSI treatment on ROS production in the hypercholesterolemic-AD cell models. The HEK293 and SH-SY5Y cells were harvested and seeded into 96-well plates, left to attach overnight, and then treated as previously described. Since hydrogen peroxide already formed part of the treatment groups, it also acted as the positive control.

First, the 500× stock solution was made by adding 40 µl of DMSO into the provided ROS stain vial. Thereafter, a 1× ROS stain was made by adding 2 µl of the 500× ROS stain for every 1 ml of media. After a PBS wash of the seeded cells, 100 µl of the 1× ROS stain solution was added to

each well. The plates were then incubated for 60 min at 37°C and 5% CO_2. The stain functions as a sensor for free radicals by reacting with the ROS produced by the cells, resulting in the generation of fluorescence. After incubation, and without removing the 1× ROS stain solution, the cells were treated with the various treatment groups previously described. After 24 hours, the ROS levels were measured using the VICTOR® Nivo™ Multimode Plate Reader (Avantor®, PerkinElmer, USA) to detect the fluorescence emission (excitation/emission wavelength of 495/520 nm), which is directly proportional to the ROS present in the solution. Background fluorescence was accounted for by including blank wells containing the assay working solution without cells, and all raw fluorescence values were corrected by subtracting the corresponding blank readings.

3.8 - Mitochondrial DNA Copy Number (mtDNA-CN) Analysis

Serving as an indicator of mitochondrial abundance and health, this study measured the mitochondrial DNA copy number (mtDNA-CN) of the treated cells. This provides insights into how the treatments affect mitochondrial dynamics, particularly in conditions associated with oxidative stress and metabolic dysregulation. Due to treatment supply delays, the mtDNA-CN analysis was conducted in HEK293 cells only, due to their robust growth and metabolic activity compared to the SH-SY5Y cell line. The HEK293 cells were harvested and seeded into 6-well plates before being treated with 50 nM SSI, 150 µg/ml LDL, 500 µM H_2O_2, 1 µM Aβ42 and co-treatments of SSI with the LDL, H_2O_2 and Aβ42 groups. The treated cells were then incubated at 37°C for 48 hours.

3.8.1 – DNA Extraction

After 48-hour treatment, the HEK293 cells were harvested by trypsinisation, where two wells from the 6-well plates were combined to form one technical replicate. This cell suspension was centrifuged at 6000 × g for 1 minute to collect the cell pellet prior to DNA extraction using the Quick-DNA™ Miniprep Plus DNA Extraction Kit (Zymo Research Corporation, California, USA). Working in sterile conditions and on ice, the supernatant of the centrifuged cells was discarded before the cell pellets were resuspended in 1× PBS (100 µl per 1 × 10^6 cells). To the same tube, 100 µl of BioFluid & Cell Buffer was added. This buffer contains detergents and salts to facilitate the disruption of the cell membrane and maintain a stable pH and ionic strength suitable for cell disruption but still stabilizing the DNA to maintain its integrity. Subsequently, 10 µl of

Proteinase K was added to the same tube in order to digest and denature cellular proteins, including nucleases that could degrade the DNA, to enhance the purity of the extracted DNA by preventing protein contamination. The sample was then vortexed briefly for 10-15 seconds before being incubated at 55°C for 10 minutes. After incubation, 220 µl of Genomic Binding Buffer was added to the sample, which was then vortexed for 10-15 seconds. The entire sample was then transferred into a Zymo-Spin™ IIC-XLR Column in a Collection Tube, which was centrifuged at 12 000 × g for 1 minute. The Genomic Binding Buffer contains chaotropic salts, which disrupt the hydrogen bonding in proteins and other cellular components, and facilitate the binding of DNA to the silica matrix in the spin column by promoting hydrophobic interactions between the DNA and silica under high-salt conditions. This ensures that the DNA selectively adheres to the column while the other cellular components and debris remain in the solution and are deposited in the flow through. After centrifugation, the Collection Tube containing the flow-through was discarded and the spin column was placed into a new Collection Tube. To the column, 400 µl of DNA Pre-Wash Buffer was added to the spin column, which was then centrifuged at 12 000 × g for 1 minute. This buffer contains low concentrations of chaotropic salts to remove residual salts, proteins and other cellular components that are still present on the DNA and silica gel. After centrifugation, the Collection Tube was emptied before 700 µl of g-DNA Wash Buffer was added to the spin column, which was centrifuged again at 12 000 × g for 1 minute. This wash step was repeated (including the centrifugation) with 200 µl of g-DNA Wash Buffer. This buffer contains a high alcohol (ethanol/isopropanol) concentration to wash away any residual impurities while preserving the bound DNA. After the final wash step, the flow through and Collection Tube was discarded before the spin column was transferred to a new sterile microcentrifuge tube where 50 µl of pre-warmed (to 60°C) DNA Elution Buffer (10 mM Tris-HCl, pH 8.5, 0.1 mM EDTA) was added to the spin column, being careful not to touch the silica matrix nor the sides of the column to prevent contamination of the elute. This buffer facilitates the release of DNA from the silica matrix by disrupting the ionic interactions that hold the DNA to the silica surface. The spin column was incubated for 5 minutes at room temperature before being centrifuged at maximum speed for 1 minute to elute the DNA. To improve the DNA yield, the elute was loaded a second time into the same spin column, where it was incubated for 3 minutes at room temperature before being centrifuged again at maximum speed for 1 minute. The extracted DNA was then quantified using the NanoDrop® ND-1000 (Thermo Scientific, USA) which was also used to assess the DNA purity

by ensuring that the DNA extracts had A260/A280 (to assess protein contamination) and A260/A230 (to detect buffer/salt contamination) ratios of close to 1.8 and 2.0-2.2, respectively. Each sample was then made up to 50 ng/µl and/or 10 ng/µl (in cases where DNA yield was below 50 ng/µl).

3.8.2 – Agarose Gel Electrophoresis

To assess the DNA integrity after DNA extraction, the samples were resolved on a 1% agarose gel (0.5 g Electran agarose, 50 ml 1× TBE buffer and 3 µl EZ-Vision blue light DNA dye), which was run in 1× TBE buffer (Appendix, table S1). The DNA samples were prepared by adding 1 µl of 6× Orange DNA Loading Dye (Fermentas, Thermo Fisher Scientific) to 5 µl of DNA sample. Before running the gel, 3 µl of O'GeneRuler 1 kb DNA Ladder (Fermentas, Thermo Fisher Scientific) molecular weight marker was loaded into the first well of the gel. Thereafter, 5 µl of each of the prepared samples were loaded into the subsequent wells. The gel was then resolved at room temperature at 80 V for 1 hour. The resolved gel (Appendix, fig. S1) was viewed under UV light using the ChemiDoc™ Imaging System (Bio-Rad, California, USA).

3.8.3 – Quantitative Polymerase Chain Reaction (qPCR)

Following DNA extraction, real-time/quantitative polymerase chain reaction (qPCR) was performed to quantify mtDNA-CN in the cells after 48-hour treatment. This was done using primers targeting a mtDNA segment (chrM:10087-10192) and primers targeting a nuclear DNA segment (chr11:2170993-2171170). The nuclear DNA segment was targeted for amplification to act as the reference gene required to be normalised against for the relative quantification of the mtDNA using the Delta Ct (threshold cycle) method. This is required to reduce experimental bias by removing non-biological variation as much as possible and, thus, improve data validity.

The qPCR reaction mix consisted of (table 2) 10 µl of Luna® Universal qPCR Master Mix (SYBR) (New England Biolabs, Massachusetts, USA), 0.5 µM of each primer (table 3), 1 µl (50 ng/ml sample) or 5 µl (10 ng/ml sample) of DNA sample and 9 µl (if using the 50 ng/ml sample) or 5 µl (if using the 10 ng/ml sample) of PCR grade dH_2O for a final reaction volume of 22 µl containing 50 ng of DNA sample. This mix was made in duplicate per sample, one using the primers for the mtDNA and one using primers for the nuclear DNA (table 3).

Table 2: qPCR Master Mix

Reagent	Volume per well (µl)
Luna® Universal qPCR Master Mix (SYBR) (New England Biolabs, Massachusetts, USA)	10
Forward Primer (10 µM)	1
Reverse Primer (10 µM)	1
DNA sample (10 ng/ml / 50 ng/ml) /control (PCR grade dH_2O)	1 (50 ng/ml) / 5 (10 ng/ml) to load 50 ng DNA
PCR grade dH_2O	9 / 5 (depending on sample loaded)
TOTAL	22

The samples were plated into separate wells of a MicroAmp™ Optical 96-Well Reaction Plate (Thermo Fisher Scientific, USA). Additionally, no template controls (NTCs) were plated using the same reaction mix recipe (and for each primer set), but instead of DNA sample, PCR grade dH_2O was added to ensure that there was no nucleic acid contamination in the reaction mix, and to identify any presence of primer dimers (Appendix, fig. S2). Once all samples and NTCs were plated, the plate was briefly centrifuged to ensure all contents were collected at the bottom of each well. Thereafter, the plate was sealed using an optically clear plate sealer and placed in the QuantStudio™ 5 Real-Time PCR System (Thermo Fisher Scientific, USA). The qPCR reaction was performed using the following parameters: initial denaturation step at 95°C for 3 minutes, followed by 45 cycles of denaturation at 95°C for 10 seconds and annealing and extension at 60°C for 30 seconds. After the qPCR was complete, the Ct values for each sample was obtained using the QuantStudio™ Design & Anlaysis Software 2.8.0 (Thermo Fisher Scientific, USA). The qPCR Ct values were then analysed using the comparative Ct (ΔΔCt) method to calculate relative mtDNA expression levels normalised to the nuclear DNA. The $2^{-\Delta\Delta Ct}$ formula was then used to determine the fold-change in mtDNA-CN between the untreated and treated samples.

Table 3: Primer pairs and sequences used in the qPCR reaction for mtDNA-CN quantification (Refinetti et al., 2017)

Primer	Sequence (5' to 3')
Mitochondrial forward	ACA CCC TCC TAG CCT TAC TAC
Mitochondrial reverse	GAT ATA GGG TCG AAG CCG C
Nuclear forward	AGG GTA TCT GGG CTC TGG
Nuclear reverse	GGC TGA AAA GCT CCC GAT TAT

3.9 - Statistical analysis

Statistical analysis was performed using Microsoft Excel 365 (Miccrosoft Corporation, Redmond, WA, USA) and IMB SPSS Statistics (IMB Corporation, Armonk, NY, USA). Three biological replicates were used for each experimental assay. General data processing, including fold-change and percentage change determinations, was conducted in Excel. Additionally, the SSI optimization data (western blot analysis and initial MTT analysis) was statistically analysed by performing a paired, two-tailed student's t-test (confidence interval of 95%) between the treated samples and the untreated controls in Excel. The remaining assay data was assessed using SPSS, where normality of the data was assessed using the Shapiro-Wilk test, while homogeneity of variances was evaluated using the Levene's test. For data that passed both tests, one-way analysis of variance (ANOVA) was performed to determine if there was a significant difference between two or more treatment groups (95% confidence interval). This was followed by Fisher's Least Significant Difference (LSD) post hoc test for multiple comparisons between all treatment groups. For data that failed the Levene's test, Welch's ANOVA was used, which adjusts for unequal variances, followed by the Games-Howell post hoc test to account for unequal sample sizes and variances. All statistical tests were performed at a significance level of 0.05, with increasing significance attained at $p<0.01$ and $p< 0.001$.

4. Results

4.1 – Proteomic Analysis

This study aimed to assess the impact of hypercholesterolemia on AD pathogenesis by examining proteomic alterations in FH patient plasma and assessing associated oxidative stress, mitochondrial dysfunction and LDL receptor-related signalling pathways in a hypercholesterolemic-AD cell model. To address this, a two-part approach was used, where an untargeted proteomic analysis was conducted, followed by a more targeted *in vitro* investigation of specific signalling pathways and hallmarks highlighted in the proteomic analysis. Thus, to uncover specific proteins and biological processes that may link FH to the pathogenesis of AD, SWATH-MS analysis was conducted on plasma samples from 12 FH patients who were not on statin treatment. The analysis involved identifying proteins with significant alterations in expression compared to healthy control patients, followed by functional annotation and pathway analysis enrichment using multiple bioinformatic databases such as STRING database, Reactome and ShinyGO.

There were 30 differentially expressed proteins (DEPs) identified from the SWATH-MS analysis of which 10 proteins were upregulated and 20 were downregulated. The fold-change within this dataset ranged from -3.105316 to 3.536205. Since there were 10 control samples and 12 FH samples, a subset of significant proteins was identified that exhibited a fold change of 1.5 and above (Karp & Lilley, 2007). Therefore, further enrichment analysis was only performed on proteins with a fold-change of 1.5 and above, and those with statistically significant differential expression (p-value <0.05, q-value<0.05). This filter criteria resulted in 28 DEPs, 10 upregulated and 18 downregulated (fig. 6) to be further analysed and reported on.

Additionally, to assess the effects of statin treatment within the FH context, DEPs were also identified in the FH vs FH+statin dataset obtained from the plasma samples of 12 FH patients who were on statin treatment and the same 12 FH patients that were not on statin treatment. From this dataset, 44 proteins were found to be differentially expressed, however, rather than analysing all 44 DEPs, only the 15 DEPs that overlapped between the FH vs control and FH vs FH + statin datasets were focused on in this study. This approach was taken so as not to evaluate the effects of statins independently but to determine how statin treatment influences proteins already altered in FH patients. Using this approach, this study assessed whether statins reversed, exacerbated or had

no effect on the proteomic changes induced by FH, thereby providing insight into their role within the FH condition rather than as a standalone treatment.

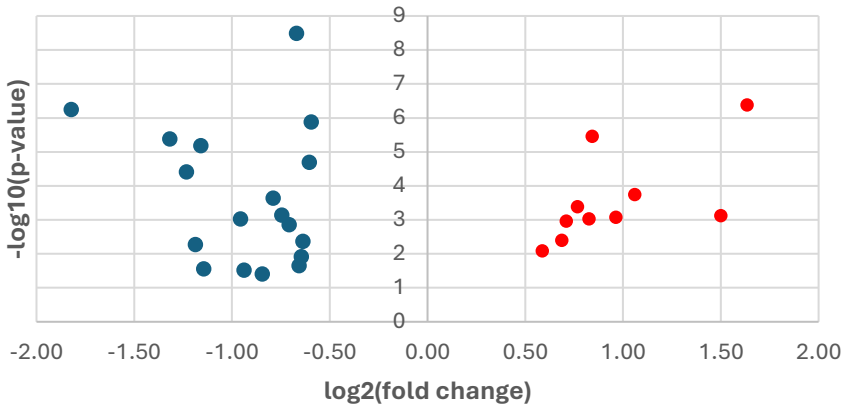


Figure 6: SWATH-MS analysis of FH patient plasma samples identified 28 differentially expressed proteins (10 upregulated and 18 downregulated).

Scatter plot showing the relationship between the magnitude of protein expression changes and their statistical significance in the comparison of FH patients (no statins) to control groups. The x-axis represents the log2(fold change) of protein expression, where positive values indicate upregulation (10 proteins, red) and negative values indicate downregulation (18 proteins, blue). The y-axis represents the -log10(p-value), where higher values indicate greater statistical significance.

After identifying each DEP in the FH group, functional annotation was performed by cross-referencing publicly available databases, such as UniProt, STRING and Reactome pathway browser (table 4). The 15 overlapping proteins found in the FH vs control and FH vs FH+statin datasets are found in table 5, which indicates that 13 of the 15 overlapping proteins exhibited a reversible effect due to statin treatment. These 13 proteins were: S100A9, SAA2, PFN1, ALDOB, PF4V1, GSTP1, THBS1, ACTB, SAA1, CA1, TPM4, IGHV3-43D and MBL2. If the protein was downregulated in the FH vs control group, that meant there was less protein in the FH patients compared to healthy controls. Similarly, if the same protein is downregulated in the FH vs FH+statin group, then that protein is less abundant in the FH patients compared to the FH+statin patients, indicating that the statin treatment increased that protein abundance, which would negate its downregulation in relation to the control group. Similar logic is also applied to the case of

upregulation. There were two proteins in the overlapping DEP group where the statin treatment further increased (SOD3) and further decreased (IGHG4) the protein expression.

Table 4: List of the dysregulated proteins (FH) ≥ 1.5-fold change and their gene ontology (GO) molecular functions as identified by STRING and UniProt databases.

	Fold Change	Genes	Protein Descriptions	GO Molecular Function
Downregulated	-3.53620489	SAA2	Serum amyloid A-2 protein	chemoattractant activity
	-2.493498244	ALDOB	Fructose-bisphosphate aldolase B	fructose-bisphosphate aldolase activity, protein binding, cytoskeletal protein binding, identical protein binding, ATPase binding, fructose-1-phosphate aldolase activity, fructose binding
	-2.351295613	S100A9	Protein S100-A9	signal transducer activity, calcium ion binding, protein binding, microtubule binding, zinc ion binding, antioxidant activity, Toll-like receptor 4 binding, arachidonic acid binding, RAGE receptor binding
	-2.277076838	GSTP1	Glutathione S-transferase P	glutathione transferase activity, glutathione peroxidase activity, protein binding, drug binding, JUN kinase binding, kinase regulator activity, S-nitrosoglutathione binding, dinitrosyl-iron complex binding, glutathione binding, nitric oxide binding
	-2.234274839	PFN1	Profilin-1	adenyl-nucleotide exchange factor activity, RNA binding, actin binding, actin monomer binding, protein binding, phosphatidylinositol-4,5-bisphosphate binding, Rho GTPase binding, cadherin binding, proline-rich region binding
	-2.210927631	PF4V1	Platelet factor 4 variant	chemokine activity, heparin binding, CXCR chemokine receptor binding
	-1.939849177	TPM4	Tropomyosin alpha-4 chain	calcium ion binding, protein binding, structural constituent of muscle, identical protein binding, protein homodimerization activity, protein heterodimerization activity, actin filament binding

	-1.916130452	TUBA3C; TUBA3D; TUBA1B; TUBA4A; TUBA3E; TUBA1A; TUBA1C; TUBA8	Tubulin alpha-3C chain; Tubulin alpha-3D chain; Tubulin alpha-1B chain; Tubulin alpha-4A chain; Tubulin alpha-3E chain; Tubulin alpha-1A chain; Tubulin alpha-1C chain; Tubulin alpha-8 chain	double-stranded RNA binding, GTPase activity, structural molecule activity, structural constituent of cytoskeleton, protein binding, GTP binding, ubiquitin protein ligase binding; GTPase activity, structural constituent of cytoskeleton, protein binding, GTP binding, protein kinase binding; molecular_function, GTPase activity, structural constituent of cytoskeleton, protein binding, GTP binding; GTPase activity, structural molecule activity, structural constituent of cytoskeleton, protein binding, GTP binding, protein domain specific binding; GTPase activity, structural molecule activity, structural constituent of cytoskeleton, protein binding, GTP binding; GTPase activity, structural constituent of cytoskeleton, GTP binding
	-1.795925272	IGHG4	Immunoglobulin heavy constant gamma 4	antigen binding, serine-type endopeptidase activity, immunoglobulin receptor binding
	-1.72890127	ACTB	Actin, cytoplasmic 1	structural constituent of cytoskeleton, protein binding, ATP binding, kinesin binding, protein kinase binding, Tat protein binding, identical protein binding, nitric-oxide synthase binding, structural constituent of postsynaptic actin cytoskeleton, RNA polymerase II core promoter proximal region sequence-specific DNA binding, RNA polymerase II distal enhancer sequence-specific DNA binding, nucleosomal DNA binding
	-1.676850863	SAA1	Serum amyloid A-1 protein	G-protein coupled receptor binding, heparin binding, chemoattractant activity
	-1.633061483	THBS1	Thrombospondin-1	phosphatidylserine binding, fibronectin binding, integrin binding, calcium ion binding, protein binding, heparin binding, fibroblast growth factor binding, low-density lipoprotein particle binding, identical protein binding, laminin binding, proteoglycan binding, transforming growth factor beta binding, fibrinogen binding, collagen V binding
	-1.591467149	APCS	Serum amyloid P-component	complement component C1q binding, calcium ion binding, carbohydrate binding, identical protein binding, virion binding, unfolded protein binding, low-density lipoprotein particle binding

	-1.576627354	MPO	Myeloperoxidase	chromatin binding, peroxidase activity, heparin binding, heme binding, metal ion binding
	-1.563697537	TLN1	Talin-1	phosphatidylserine binding, integrin binding, structural constituent of cytoskeleton, protein binding, vinculin binding, LIM domain binding, phosphatidylinositol binding, cadherin binding, actin filament binding
	-1.555351369	ABCF3	ATP-binding cassette sub-family F member 3	protein binding, ATP binding, ATPase activity, cadherin binding
	-1.520958984	CA1	Carbonic anhydrase 1	arylesterase activity, carbonate dehydratase activity, protein binding, zinc ion binding, hydro-lyase activity
	-1.510460373	HP	Haptoglobin	protein binding, antioxidant activity, hemoglobin binding
Upregulated	1.502829479	IGHV3-64	Immunoglobulin heavy variable 3-64	antigen binding, immunoglobulin receptor binding
	1.611042736	IGLV2-14	Immunoglobulin lambda variable 2-14	antigen binding, serine-type endopeptidase activity
	1.635978848	IGLC7	Immunoglobulin lambda constant 7	antigen binding, serine-type endopeptidase activity, immunoglobulin receptor binding
	1.701895482	IGHV3-43D	Immunoglobulin heavy variable 3-43D	antigen binding
	1.773574226	KRT2	Keratin, type II cytoskeletal 2 epidermal	structural constituent of cytoskeleton, protein binding, cytoskeletal protein binding, structural constituent of epidermis
	1.793894416	MBL2	Mannose-binding protein C	serine-type endopeptidase activity, receptor binding, calcium ion binding, protein binding, mannose binding, calcium-dependent protein binding, carbohydrate binding
	1.951138301	SOD3	Extracellular superoxide dismutase [Cu-Zn]	superoxide dismutase activity, copper ion binding, protein binding, heparin binding, zinc ion binding
	2.085005403	IGLV7-43	Immunoglobulin lambda variable 7-43	antigen binding, serine-type endopeptidase activity

	2.83143215	IGHD	Immunoglobulin heavy constant delta	antigen binding, immunoglobulin receptor binding
	3.105316379	IGLV5-37	Immunoglobulin lambda variable 5-37	antigen binding

* *Oxidative Stress and Antioxidant Defence, Cytoskeletal Dynamics and Regulation, Inflammation and Immune Regulation, Metabolism and Energy Regulation*

Table 5: List of the 15 dysregulated proteins (≥ 1.5-fold change) that overlapped in the FH vs control and FH vs FH+statin datasets.

Fold Change (FH/FH+statin)	Genes	Protein Descriptions	Up- or Down-regulation *	
			FH/FH+statin	FH/control
-4.496457659	S100A9	Protein S100-A9	DOWN	DOWN
-3.520924234	SAA2	Serum amyloid A-2 protein	DOWN	DOWN
-3.189259522	PFN1	Profilin-1	DOWN	DOWN
-2.9584362	ALDOB	Fructose-bisphosphate aldolase B	DOWN	DOWN
-2.435968774	PF4V1	Platelet factor 4 variant	DOWN	DOWN
-2.41024569	GSTP1	Glutathione S-transferase P	DOWN	DOWN
-2.366184111	SOD3	Extracellular superoxide dismutase [Cu-Zn]	DOWN	UP
-2.352732958	THBS1	Thrombospondin-1	DOWN	DOWN
-2.068869782	ACTB	Actin, cytoplasmic 1	DOWN	DOWN
-1.832854319	SAA1	Serum amyloid A-1 protein	DOWN	DOWN
-1.803231923	CA1	Carbonic anhydrase 1	DOWN	DOWN
-1.543909135	TPM4	Tropomyosin alpha-4 chain	DOWN	DOWN
1.559524835	IGHG4	Immunoglobulin heavy constant gamma 4	UP	DOWN
1.565648456	IGHV3-43D	Immunoglobulin heavy variable 3-43D	UP	UP
1.568784796	MBL2	Mannose-binding protein C	UP	UP

** Matching regulatory changes (UP or DOWN) indicate a reversible effect of statin treatment.*

Considering that proteins are multifunctional depending on factors such as cellular location and microenvironment, all the gene ontology (GO) molecular functions were determined and summarised in table 6. GO molecular functions describe the specific functions that the protein can perform at a molecular level independent of context (i.e. when and where in the cell). To assess the GO molecular functions, the data was further filtered to only include proteins with a minimum

strength score of 1.00. The strength score is the Log10(observed / expected), which describes how large the enrichment effect is. It's the ratio between i) the number of proteins in a network that are annotated with a term and ii) the number of proteins that are expected to be annotated with this term in a random network of the same size. Thereafter, the STRING database identified four GO molecular functions that were enriched by the DEPs, namely (in order of decreasing strength): antioxidant activity (MPO, HP, S100A9, SOD3, GSTP1), structural constituent of the cytoskeleton (KRT2, TLN1, TUBA8, ACTB), heparin-binding (MPO, PF4V1, THBS1, SOD3, SAA1) and sulfur compound binding (MPO, PF4V1, THBS1, SOD3, GSTP1, SAA1) (fig. 7). Additionally, STRING was unable to identify 6 proteins (IGLV5-37, IGLV7-43, IGLC7, IGLV2-14, IGLHV3-64 and IGHG4) from the input of 28 proteins. These proteins were variable isoforms of immunoglobin, with a primary molecular function of antigen binding in the immune response.

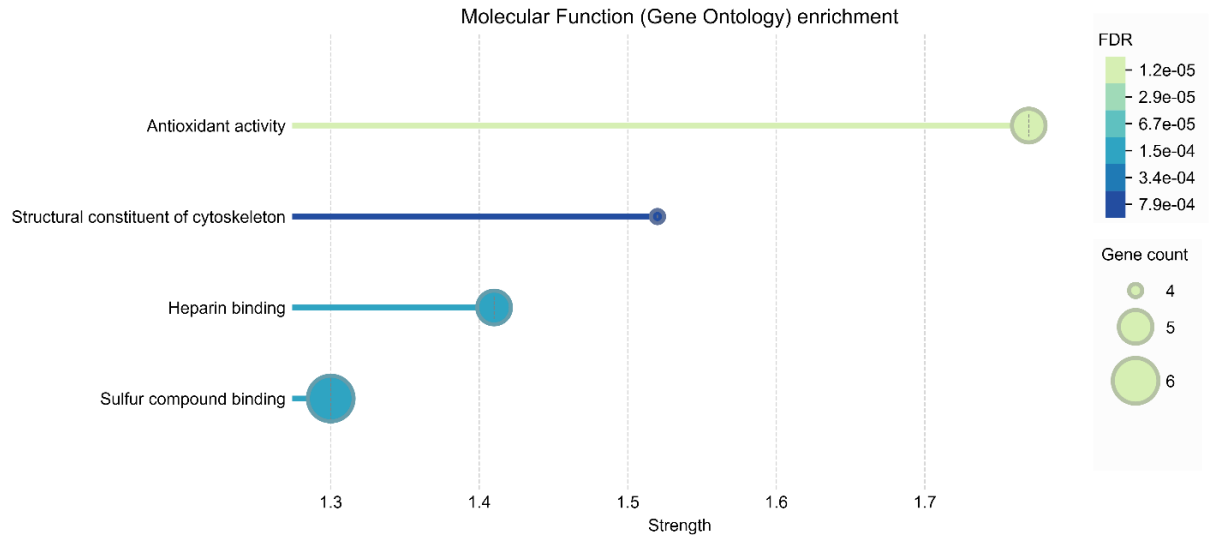
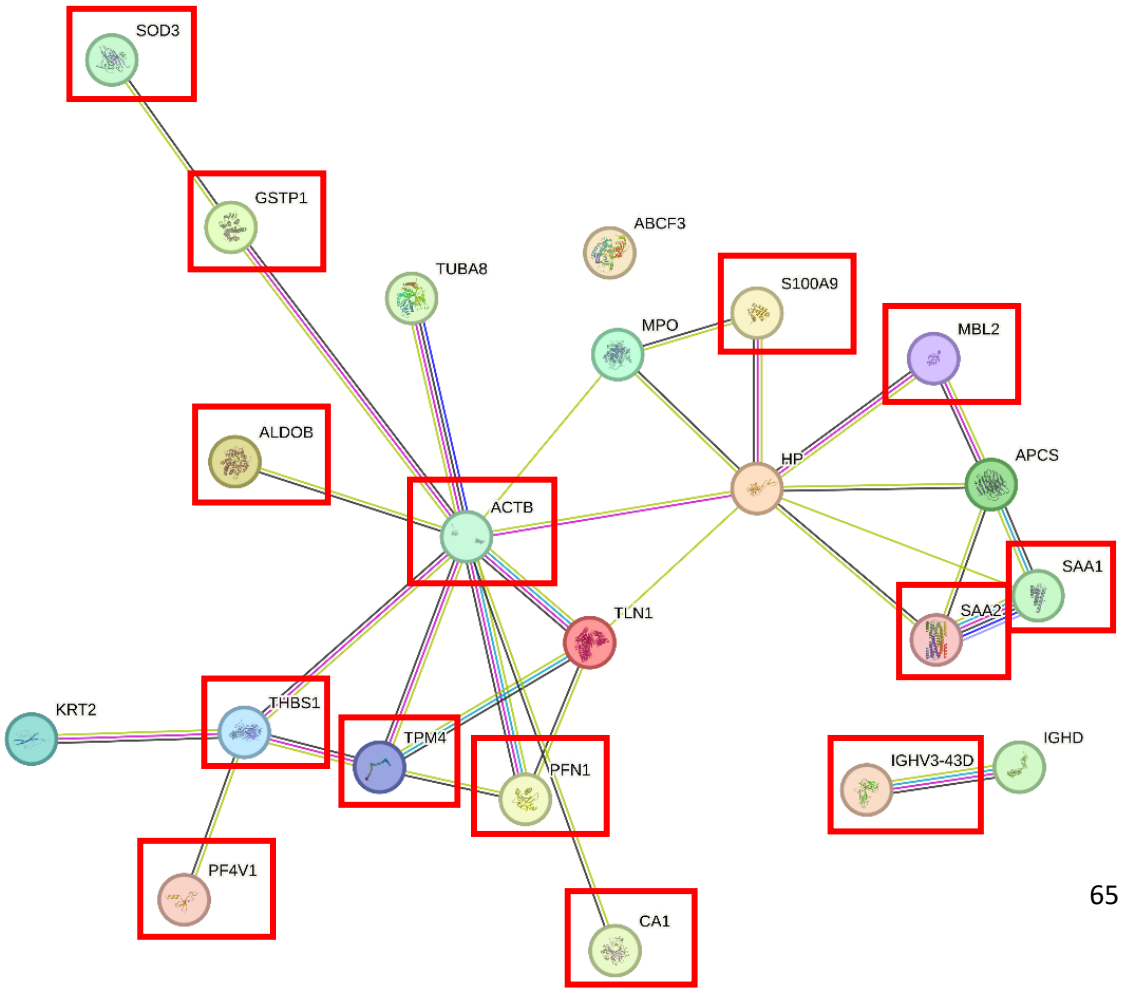


Figure 7: The top four gene ontology (GO) molecular functions that are enriched by the dysregulated proteins identified in the FH vs control dataset.

FDR: false discovery rate; represents the expected proportion of false positives among the significant DEPs, smaller FDRs indicate greater confidence that the DEPs are not false positives. Strength: log10(observed/expected); describes how large the enrichment effect is.

These proteins were then used to construct a protein-protein interaction (PPI) network using the STRING database to explore the interactions between the DEPs (fig. 8). Each node in the network represents a protein, while the edges indicate predicted functional associations based on experimental data, co-expression, and curated biological pathways. The network highlights clusters of interacting proteins, suggesting potential involvement in shared biological processes or pathways relevant to familial hypercholesterolemia. This dataset had a PPI enrichment p-value of 6.04e-10, which indicates that the proteins interact with each other more frequently than would be expected for a random set of proteins of similar size and connectivity drawn from the genome. Such enrichment suggests that these proteins are partially biologically interconnected as a group. Of the 22 proteins identified by STRING, only one protein (ABCF3) appeared as an unconnected node with no evidence (to date) of any interactions with the rest of the protein network. Similarly, a protein pair (IGHV3-43D and IGHD) was also disconnected from the larger protein network but still exhibited an interaction between them. The proteins possessing the highest number of interactions were ACTB (10 interactions) and HP (8 interactions), which also appeared central in the observed PPI network image (fig. 8).



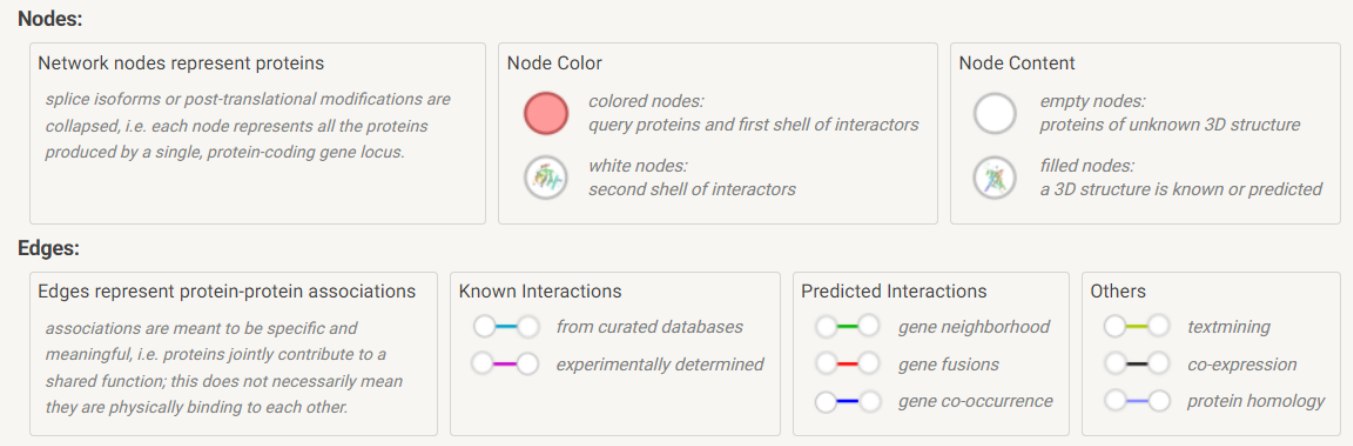


Figure 8: Protein-protein interaction (PPI) network of the dysregulated proteins (FH vs control) with a fold-change ≥ 1.5, analysed via STRING database.

The different coloured circles represent the query proteins, referred to as "nodes". The lines between the nodes, called "edges", indicate the protein-protein interactions, with each colour representing different types of evidence for each interaction. Red square boxes are placed on the proteins that were also differentially expressed in the FH vs FH+statin dataset. Minimum interaction score: medium confidence (0.400).

To attain a broader overview of the significance of these molecular functions and how the proteins interact within the PPI, a list of the top 10 enriched GO biological processes (table 6) identified from the interactions and enrichment of the DEPs was obtained from STRING. These GO terms represent broad, multistep processes that involve multiple proteins working together to accomplish a specific biological objective. Table 6 indicates which of the DEPs are involved in these top processes and highlights dysregulation in the immune, inflammatory and oxidative stress response processes in the FH patients.

Table 6: Top 10 Enriched Gene Ontology (GO) Biological Processes in Differentially Expressed Proteins Identified in FH vs Control Groups (STRING).

FDR: false discovery rate; represents the expected proportion of false positives among the significant DEPs, smaller FDRs indicate greater confidence that the DEPs are not false positives. *Strength*: log10(observed/expected); describes how large the enrichment effect is.

Term ID	Term description	Strength	False discovery rate	Matching proteins in the network (labels)
GO:0006953	Acute-phase response	2.03	2.47E-05	APCS, HP, MBL2, SAA1, SAA2
GO:0006958	Complement activation, classical pathway	1.83	0.0108	MBL2, IGHD, IGHV3-43D
GO:0006911	Phagocytosis, engulfment	1.72	0.0196	THBS1, IGHD, IGHV3-43D
GO:0030168	Platelet activation	1.57	0.0038	PF4V1, TLN1, SAA1, ACTB
GO:0030593	Neutrophil chemotaxis	1.53	0.0482	PF4V1, S100A9, SAA1
GO:0000302	Response to reactive oxygen species	1.33	0.0242	MPO, HP, SOD3, GSTP1
GO:0042742	Defence response to bacterium	1.24	0.00094	MPO, HP, S100A9, MBL2, IGHD, IGHV3-43D
GO:0006959	Humoral immune response	1.22	0.0083	PF4V1, S100A9, MBL2, IGHD, IGHV3-43D
GO:0006954	Inflammatory response	1.12	0.00019	PF4V1, APCS, THBS1, HP, S100A9, MBL2, SAA1, SAA2
GO:0006979	Response to oxidative stress	1.09	0.0253	MPO, HP, MBL2, SOD3, GSTP1

To gain a deeper understanding of the specific biochemical pathways involved, the DEPs were further analysed using Reactome, a curated database of biological pathways offering detailed insights into the molecular reactions and interactions in which these proteins participate. Reactome

identified 31 out of the 35 identifiers in the sample, where 309 pathways were hit by at least one of them. Four identifiers were not found nor mapped to any entity in Reactome, namely: ABCF3, IGHV3-43D, IGHV3-64 and SAA2. The top 10 enriched pathways identified by Reactome consisted of the most enriched pathway being "RHO GTPases activate IQGAPs", followed by pathways that overlapped regarding gap junction and tubulin assembly and function (table 7). Lastly, the tenth most enriched pathway was the "Activation of AMPK downstream of NMDARs". These results illustrate both the enrichment of biologically significant cell signalling pathways and specific molecular pathways involving the cytoskeleton, which correlates with the GO molecular function "structural constituent of cytoskeleton" identified in STRING.

Table 7: Top 10 Enriched Pathways based on Differentially Expressed Proteins Identified in FH vs Control Groups, obtained from Reactome.

FDR: false discovery rate; represents the expected proportion of false positives among the significant DEPs, smaller FDRs indicate greater confidence that the DEPs are not false positives

Pathway name	Entities			Reactions	Matching proteins in the network (labels)
	Found	p-value	FDR	Found	
RHO GTPases activate IQGAPs	9/36	1.55e-15	3.10e-13	2/5	ACTB, TUBA1A, TUBA1B, TUBA1C, TUBA3C, TUBA3D, TUBA3E, TUBA4A, TUBA8
Cooperation of Prefoldin and TriC/CCT in actin and tubulin folding	9 / 37	1.89e-15	3.10e-13	6 / 6	ACTB, TUBA1A, TUBA1B, TUBA1C, TUBA3C, TUBA3D, TUBA3E, TUBA4A, TUBA8
Microtubule-dependent trafficking of connexons from Golgi to the plasma membrane	8 / 22	3.22e-15	3.51e-13	1 / 2	TUBA1A, TUBA1B, TUBA1C, TUBA3C, TUBA3D, TUBA3E, TUBA4A, TUBA8
Transport of connexons to the plasma membrane	8 / 23	4.55e-15	3.73e-13	1 / 3	TUBA1A, TUBA1B, TUBA1C, TUBA3C, TUBA3D, TUBA3E, TUBA4A, TUBA8
Post-chaperonin tubulin folding pathway	8 / 25	8.77e-15	5.70e-13	6 / 9	TUBA1A, TUBA1B, TUBA1C, TUBA3C, TUBA3D, TUBA3E, TUBA4A, TUBA8
Formation of tubulin folding intermediates by CCT/TriC	8 / 30	3.73e-14	1.83e-12	2 / 2	TUBA1A, TUBA1B, TUBA1C, TUBA3C, TUBA3D, TUBA3E, TUBA4A, TUBA8

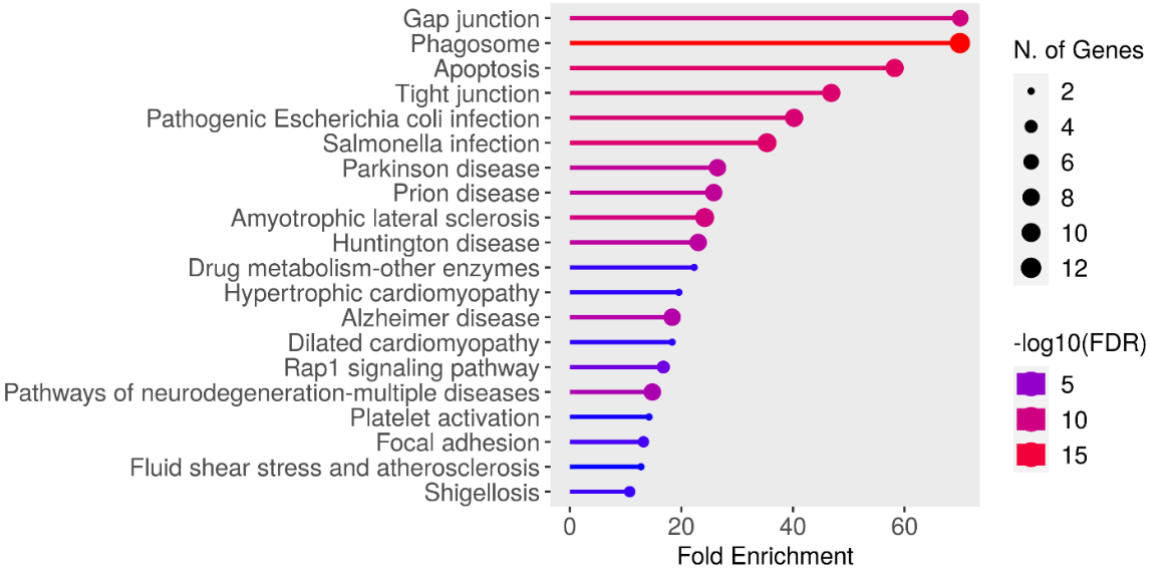
Gap junction trafficking	9 / 52	3.97e-14	1.83e-12	7 / 20	ACTB, TUBA1A, TUBA1B, TUBA1C, TUBA3C, TUBA3D, TUBA3E, TUBA4A, TUBA8
Recycling pathway of L1	9 / 55	6.54e-14	2.68e-12	5 / 14	ACTB, TUBA1A, TUBA1B, TUBA1C, TUBA3C, TUBA3D, TUBA3E, TUBA4A, TUBA8
Gap junction trafficking and Regulation	9 / 57	8.98e-14	3.22e-12	7 / 24	ACTB, TUBA1A, TUBA1B, TUBA1C, TUBA3C, TUBA3D, TUBA3E, TUBA4A, TUBA8
Activation of AMPK downstream of NMDARs	8 / 34	1.01e-13	3.22e-12	1 / 3	TUBA1A, TUBA1B, TUBA1C, TUBA3C, TUBA3D, TUBA3E, TUBA4A, TUBA8

A web-based graphical tool called ShinyGO v0.8 was utilised to further explore and represent the pathways enriched by the DEPs, identifying the top 20 pathways with significant fold enrichment (fig. 9A). Although ShinyGO utilises multiple databases including Reactome and STRING, which were used separately in this proteomic analysis, the enriched pathways seen in figure 9A were obtained from the KEGG (Kyoto Encyclopedia of Genes and Genomes) database which provided broader pathway terms compared to the more detailed molecular pathways provided in Reactome. This broader scope of pathways allows for a more comprehensive view that connects molecular pathways directly to disease states, offering insights into how these pathways may contribute to specific health conditions. Considering this, there were multiple disease states identified ranging from bacterial infections ("Pathogenic Escherichia coli infection", "Salmonella infection", "Shigellosis"), cardiovascular pathologies ("Hypertrophic cardiomyopathy", "Dilated cardiomyopathy", "Fluid shear stress and atherosclerosis") and, interestingly, many neurodegenerative diseases ("Parkinson disease", "Prion disease", "Huntington disease", "Alzheimer disease", "Pathways of neurodegeneration-multiple diseases"). This strong enrichment of neurodegenerative disease pathways, particularly AD, is noteworthy given that the samples were derived from FH patients. The identification of AD-related pathways suggests a potential mechanistic link between FH and neurodegeneration. Of importance to this study, Alzheimer's disease had a fold enrichment score of 18.33413462, where 8 genes (TUBA1B, TUBA3E, TUBA3D, TUBA8, TUBA4A, TUBA3C, TUBA1A, TUBA1C) were matched to this pathway. The fold enrichment score measures the magnitude of enrichment, whereby the higher the score, the stronger the enrichment.

In addition to the disease states, the top four enriched pathways included “Gap junction”, “Phagosome”, “Apoptosis” and “Tight junction” which correlate to the GO molecular functions and Reactome molecular pathways identified previously. These pathways were also determined by the same protein set (TUBA1B, TUBA3E, TUBA3D, TUBA8, TUBA4A, TUBA3C, TUBA1A, TUBA1C) with the most enriched pathway being “Gap junction” which had a fold enrichment score of 70.00305944. The high enrichment of these pathways suggests potential disruptions in cellular communication and cell survival mechanisms in FH patients, with the high enrichment of the “Gap junction” pathway, in particular, indicating a strong overrepresentation of this pathway in the DEPs, suggesting its potential significance in FH-related molecular changes.

To better evaluate the connections (if any) between these identified pathways, ShinyGO generated a hierarchical clustering tree (fig. 9B). This clustering tree illustrates how pathways with many shared genes are grouped, offering insights into the interconnected nature of these biological processes. There were two distinct cluster groups illustrated. The largest cluster has the “Gap junction” pathway in the centre notably surrounded by the pathways related to neurodegenerative diseases. The second cluster included disease states related to cardiac health, and the bacterial infection pathways were present in both clusters.

(A)



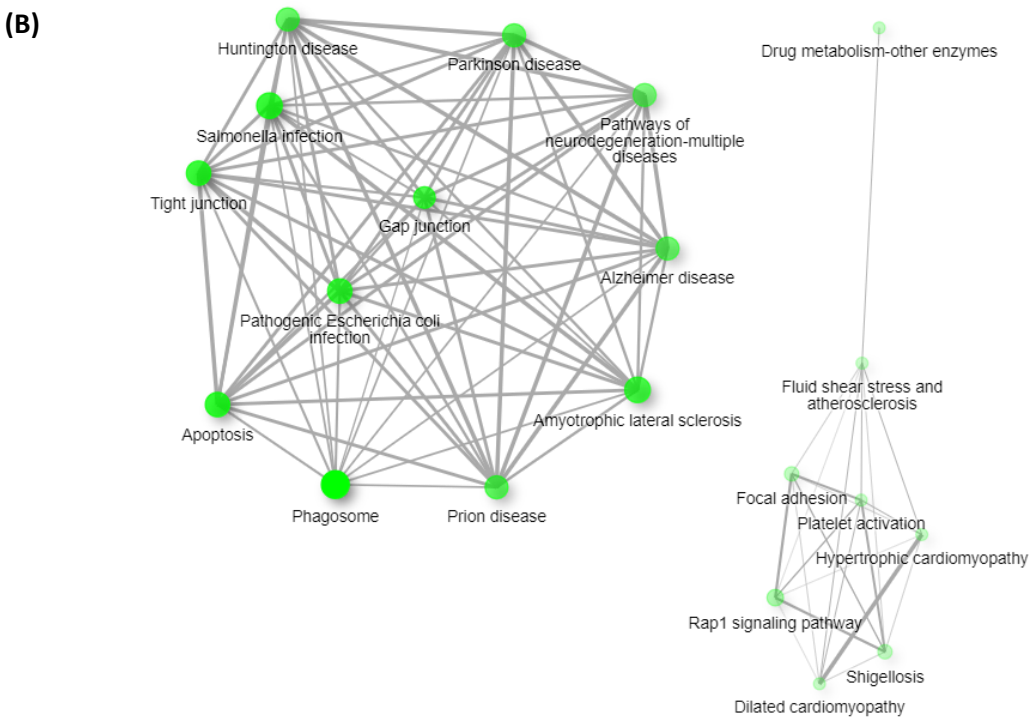


Figure 9: Pathway enrichment (KEGG) of the Differentially Expressed Proteins (DEPs) identified in FH vs Control Groups using ShinyGO v0.8.

(A) Graphical representation of the most enriched pathways, where the y-axis lists the enriched pathways in order of decreasing fold enrichment (shown on the x-axis). The -log10(false discovery rate) represents statistical significance, where higher values denote stronger enrichment. "N. of Genes": the number of DEPs that overlap with the total number of genes assigned to each pathway in the KEGG database. **(B)** A hierarchical clustering tree summarises the correlation amongst enriched pathways. Pathways with many shared genes are clustered together. Larger dots indicate more significant p-values.

The proteomic analysis of FH patients' plasma revealed significant alterations in protein expression, with pathway enrichment highlighting multiple disease-related processes, including neurodegenerative diseases such as AD. Furthermore, the comparison between FH and FH+statin patients provided insights into how statin therapy modulates these changes, potentially mitigating some of the dysregulated pathways. Notably, the proteomic data highlighted disruptions in

pathways involved in oxidative stress and ROS-related processes. Given that mitochondrial dysfunction is a key driver of oxidative stress in neurodegenerative diseases, these findings provided a strong basis for further investigation at the cellular level using the hypercholesterolemic-AD cell model. Overall, the proteomic findings reinforce the growing recognition of hypercholesterolemia as a risk factor for AD and suggest that lipid-lowering therapies such as statins and SSI may have broader neuroprotective effects.

4.2 – *In vitro* Results

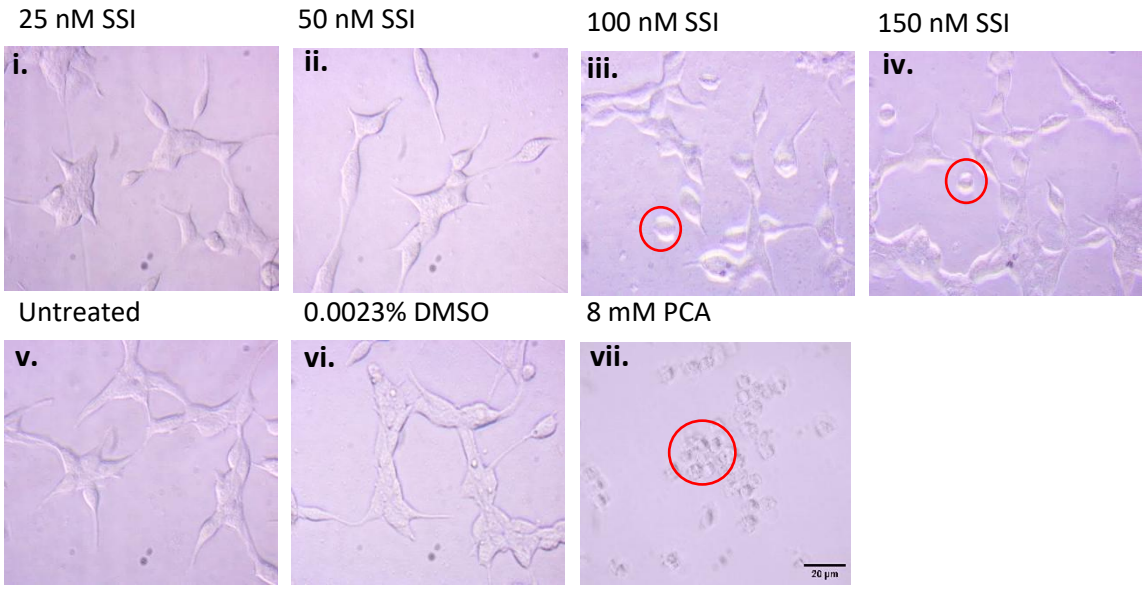
Mitochondrial dysfunction is a pivotal factor connecting hypercholesterolemia and AD, with both conditions characterised by increased oxidative stress and disrupted mitochondrial activity. The elevation in oxidative stress and mitochondrial dysfunction present in hypercholesterolemic patients can activate a cascade whereby ROS production promotes Aβ production and tau hyperphosphorylation, leading to further amplification of oxidative stress, ultimately leading to neurodegeneration (de Oliveira et al., 2011; Cheignon et al., 2018). Hence, this study assessed mitochondrial health under hypercholesterolemic-AD conditions and SSI treatment. This was done using the MTT assay to evaluate mitochondrial activity, the Alamar Blue® assay to measure overall metabolic activity and quantitative PCR to measure mitochondrial DNA copy number.

4.2.1 – Dose- and time-dependent effect of SSI on cell viability in HEK293 and SH-SY5Y cells

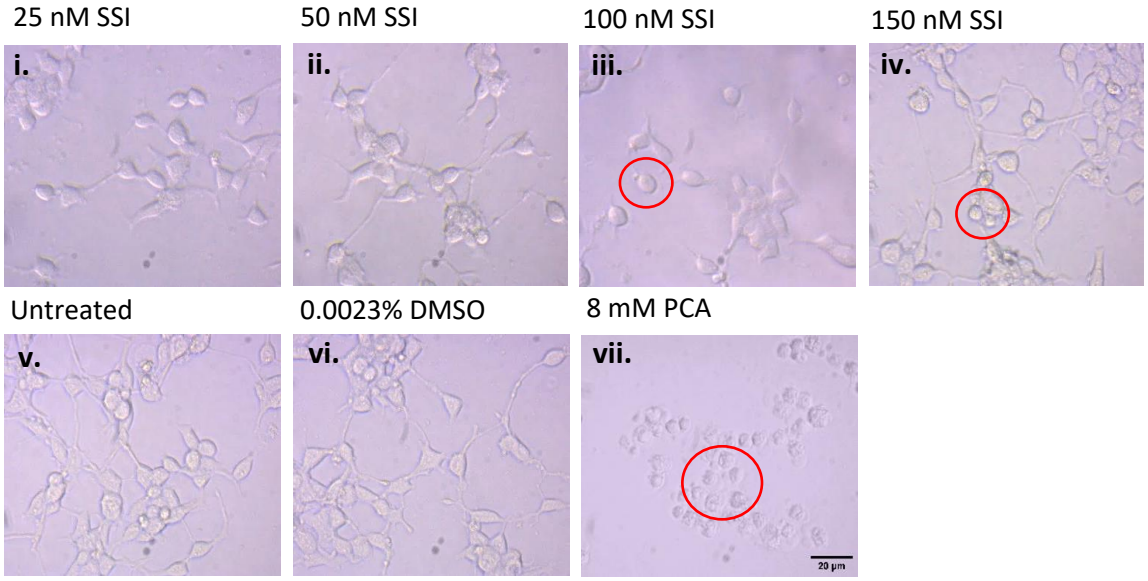
This study aimed to assess the effects of familial hypercholesterolemia on Alzheimer's disease hallmarks and signalling pathways by low-density lipoprotein receptor (LDLR) upregulation in FH-AD cell models. To do this, a squalene synthase inhibitor (SSI), was used to treat HEK293 and SH-SY5Y cells. Before evaluating the impact of SSI on the hypercholesterolemic-AD cell model, the compound's safety and efficacy were confirmed.

The toxicity of SSI was assessed by performing a concentration study (25 nM, 50 nM, 100 nM and 150 nM) and a time study of 24 and 48 hours on both cell lines. Cell morphology analysis in the HEK293 cells for both the 24- and 48-hour treatments showed no signs of cell death in the vehicle control and all the SSI-treated cells compared to the untreated cells, which exhibited polygonal, epithelial-like morphology characteristic of HEK293 cells (fig. 10A and B). The vehicle control cells closely resembled the untreated cells, confirming that the DMSO solvent had no observable effects on cell morphology. However, cells treated with 100 nM and 150 nM SSI exhibited signs of cellular stress, such as cell rounding (red circles). In contrast, the cell death control, treated with 8 mM protocatechuic acid (PCA), a known apoptotic inducer, exhibited significant cell shrinkage and rounding, indicating cell detachment and death (fig. 10Avii and Bvii).

(A) 24 hours



(B) 48 hours



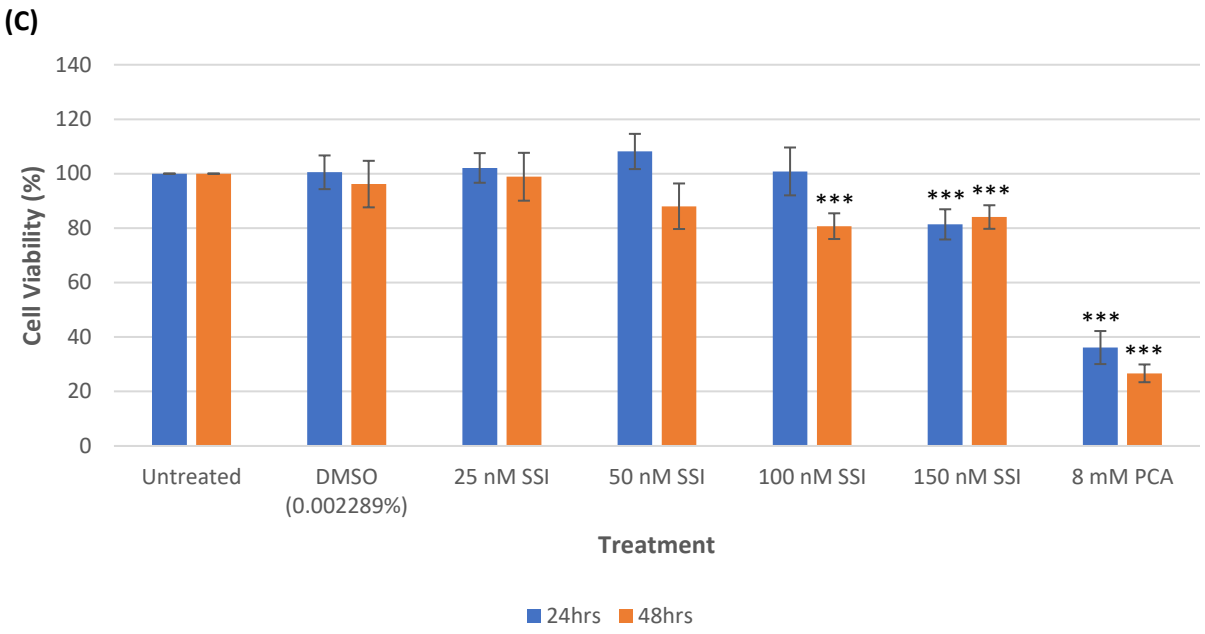


Figure 10: Treatment with SSI does not significantly decrease cell viability in HEK293 cells at 25 nM and 50 nM.

Cell morphology images of HEK293 cells after **(A)** 24-hour and **(B)** 48-hour treatment with the following compounds: **(i)** 25 nM SSI, **(ii)** 50 nM SSI, **(iii)** 100 nM SSI, **(iv)** 150 nM SSI, **(v)** untreated, **(vi)** 0.0023% DMSO vehicle control and **(vii)** 8 mM protocatechuic acid (PCA) cell death control. Red circles indicate signs of cell rounding and cellular stress. Images were taken using an inverted light microscope (Zeiss, Oberkochen, Germany) at 40x magnification. **(C)** Percentage cell viability of HEK293 cells after 24-hour and 48-hour SSI treatment assessed using the MTT assay. Treated cells are expressed as a percentage of the untreated cells (set to 100%). Error bars represent standard deviation *(Student's t-test: *p≤ 0.05, **p≤ 0.01 ***p ≤ 0.001, n = 3 biological repeats, 3 technical repeats each).*

The observations seen in the cell morphology analysis were further investigated by conducting the MTT assay (fig. 10C) on the same set of cells (24- and 48-hour SSI treatment). After 24 hours, the DMSO vehicle control, and 25, 50 and 100 nM SSI-treated cells caused insignificant decreases of 0.51% ± 6.19%, 2.10% ± 5.44%, 8.15% ± 6.47% and 0.82% ± 8.79% (respectively) in cell viability compared to the untreated cells (set to 100%). Only at 150 nM SSI was there a significant decrease of 18.62% ± 5.55% observed in the HEK293 cells, confirming a mild cytotoxic effect. The PCA-treated cells showed a 63.86% ± 6.06% decrease in viability, verifying the assay's responsiveness

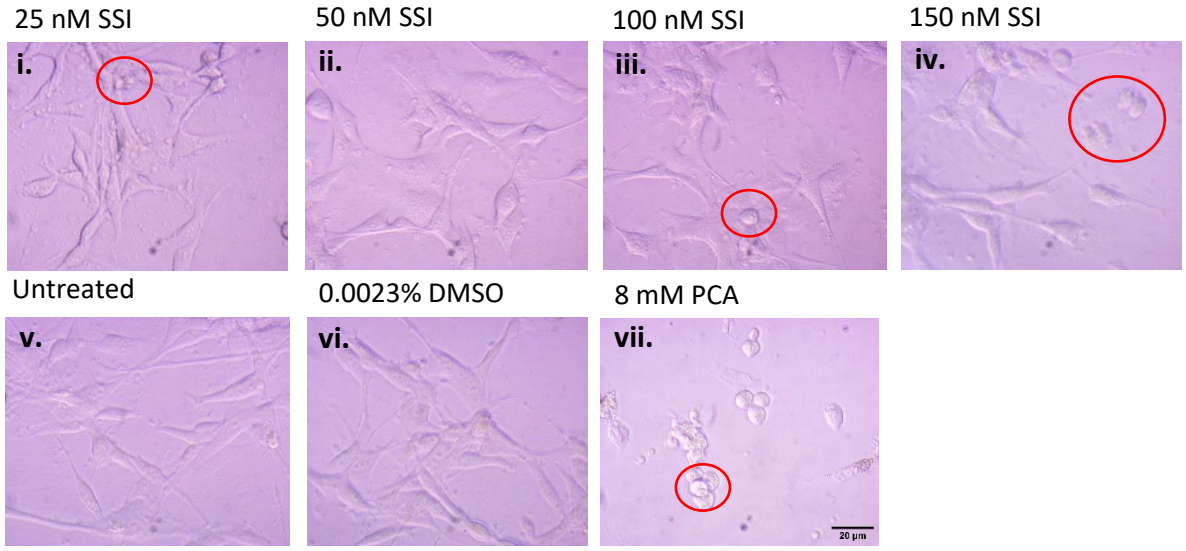
to a known cytotoxic agent. In contrast, 48-hour treatment with SSI caused larger decreases in cell viability across each concentration: DMSO (3.83% ± 8.55%), 25 nM (1.14% ± 8.79%), 50 nM (11.96% ± 8.37%), 100 nM (19.28% ± 4.72%), 150 nM (15.93% ± 4.33%) and 8 mM PCA (73.33% ± 3.26%). According to statistical analysis via the student's t-test, the 19.28% and 15.93% decreases in cell viability seen in the 100 nM and 150 nM SSI-treated cells (respectively) were significant ($p \leq 0.01$). These observations indicate that SSI treatment is non-toxic after 24 hours but might cause cytotoxic effects after 48 hours at higher concentrations greater than or equal to 100 nM in HEK293 cells.

In addition to HEK293 cells, the SSI concentration and time studies were also conducted on the SH-SY5Y (neuronal) cell line. As seen in the HEK293 cells, cell morphology analysis of the SH-SY5Y cells after 24 and 48-hour SSI treatment showed no visible signs of significant cell death where most of the cells exhibit the slightly neuronal elongated morphology with projections, as seen in the untreated cells, in contrast to the cell death control group that exhibited significant cell shrinkage and loss of those progressions (fig. 11A and B). However, there were still some signs of cellular stress as slight shrinkage and cell rounding were also observed in the 100 nM and 150 nM SSI-treated cells at both time points (red circles).

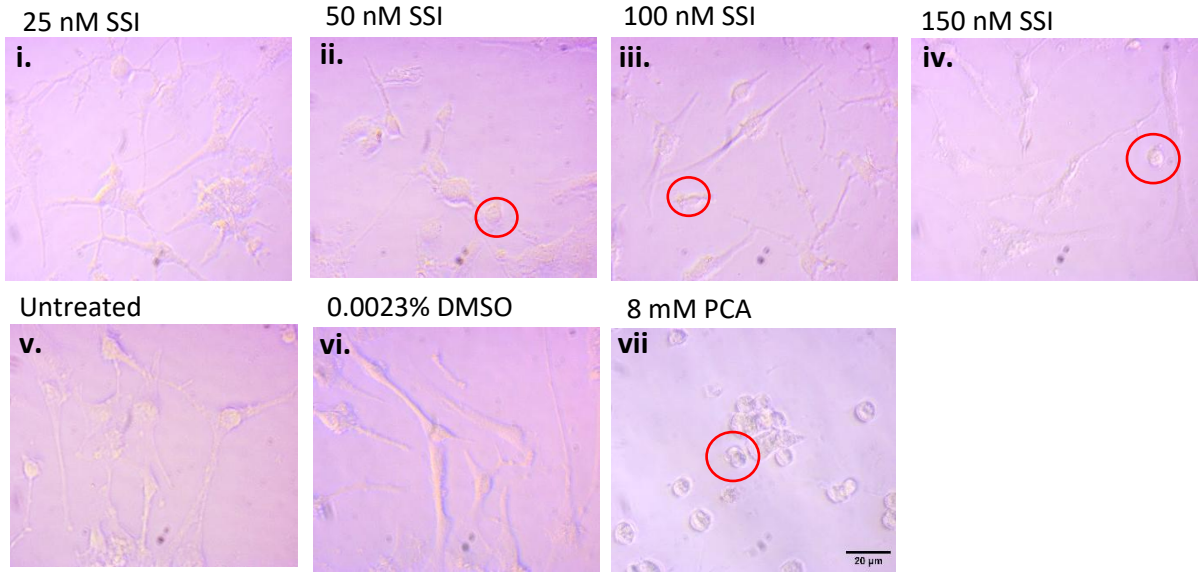
The MTT assay results indicated that the SSI treatment did cause a slightly higher cytotoxic effect on the SH-SY5Y cells as compared to the HEK293 cells, even at 24 hours, as there were slight decreases in cell viability for the 25 nM (5.78% ± 4.13%), 50 nM (4.66% ± 5.73%), 100 nM (7.24% ± 9.56%) and 150 nM (10.16% ± 4.78%) SSI treated cells (fig. 11C). Statistical analysis indicated that only the 10.16% decrease in cell viability from the 150 nM SSI treatment was significant alongside the 54.03% ± 8.50% decrease seen in the 8mM PCA cell death control. Similarly, the 48-hour treatment also showed a significant decrease in cell viability for the 150 nM SSI-treated cells (11.78% ± 3.68%), while the lower SSI concentrations did not cause significant decreases in cell viability (3.95% ± 6.60%, 5.97% ± 5.28% and 7.23% ± 5.63%, for the 25, 50 and 100 nM SSI-treated cells, respectively). Moreover, the DMSO control also had a significant decrease in cell viability (6.31% ± 1.20%) after 48-hour treatment, which could be the reason why the highest SSI concentration exhibited a significant decrease in cell viability. These results could suggest that at higher concentrations close to 150 nM and at prolonged periods of more than 24 hours, SSI could be slightly cytotoxic. In contrast, lower concentrations of SSI (25-50 nM) had

very minimal cytotoxic effects as seen in the cell morphology and MTT analysis, indicating their potential suitability for investigating SSI's ability to modulate high LDL and AD markers without compromising cell viability.

(A) 24 hours



(B) 48 hours



(C)

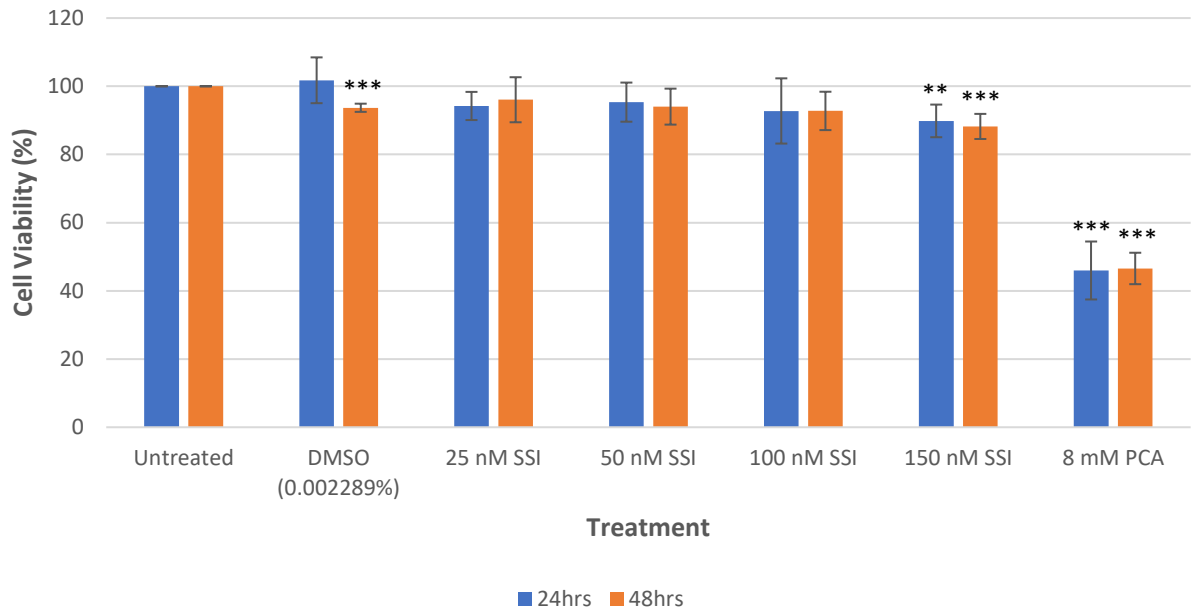


Figure 11: Treatment with SSI does not significantly decrease cell viability in SH-SY5Y cells at lower concentrations.

Cell morphology images of SH-SY5Y cells after **(A)** 24-hour and **(B)** 48-hour treatment with the following compounds: **(i)** 25 nM SSI, **(ii)** 50 nM SSI, **(iii)** 100 nM SSI, **(iv)** 150 nM SSI, **(v)** untreated, **(vi)** 0.0023% DMSO vehicle control and **(vii)** 8 mM protocatechuic acid (PCA) cell death control. Red circles indicate signs of cell rounding and cellular stress. Images were taken using an inverted light microscope at 40x magnification. **(C)** Percentage cell viability of SH-SY5Y cells after 24-hour and 48-hour SSI treatment assessed using the MTT assay. Treated cells are expressed as a percentage of the untreated cells (set to 100%). Error bars represent standard deviation *(Student's t-test: *p≤ 0.05, **p≤ 0.01 ***p ≤ 0.001; n = 3 biological repeats, 3 technical repeats each).*

4.2.2 - Treatment with SSI causes a significant increase in LDLR protein levels in HEK293 and SH-SY5Y cells

After assessing the cytotoxic effects of SSI on the HEK293 and SH-SY5Y cells, western blot analysis was performed to validate the LDLR upregulating effects of SSI on these cell lines. This was done using the same concentration and time study design (25 nM, 50 nM, 100 nM and 150

nM SSI for 24 and 48 hours). Western blot analysis showed an observable increase in protein band intensity as the SSI concentration increased (fig. 12).

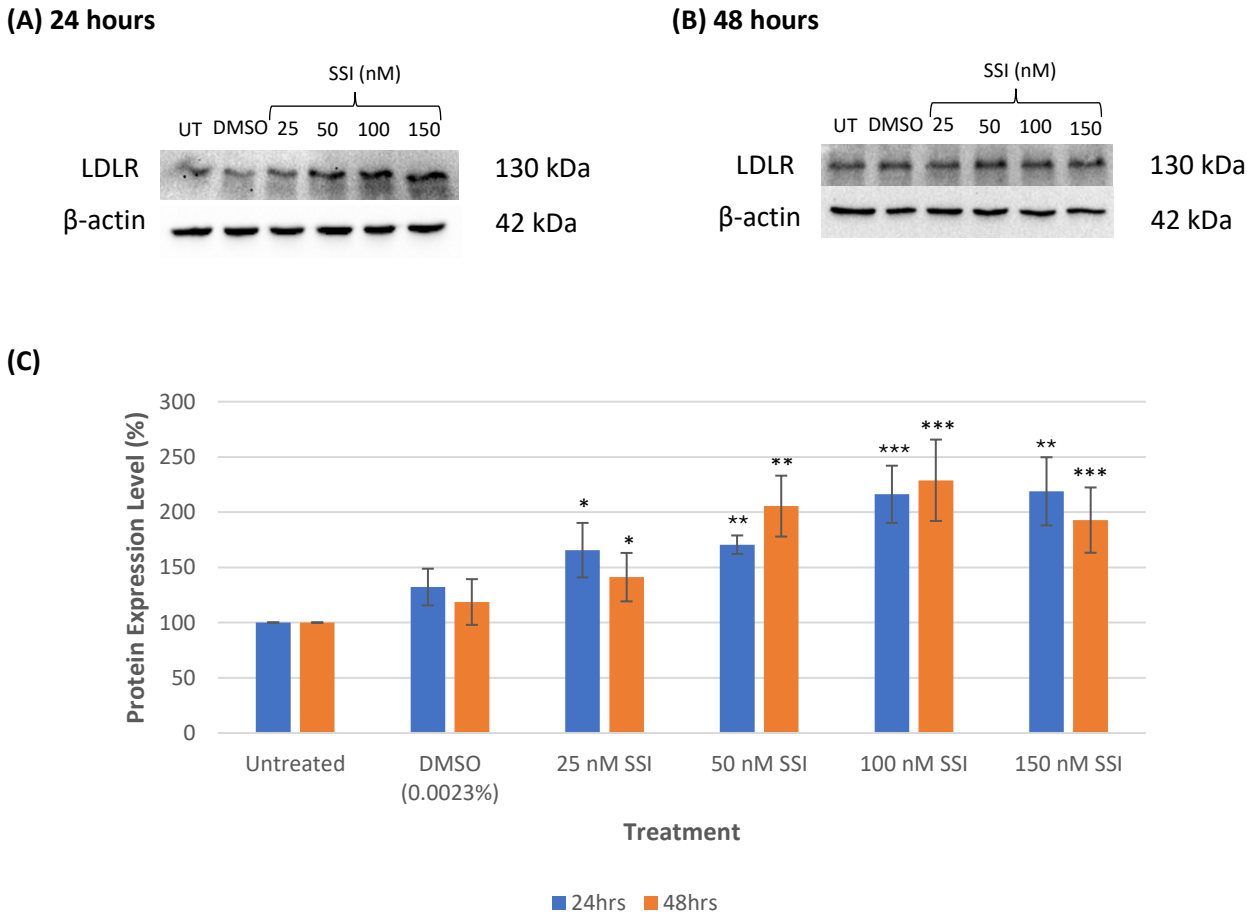


Figure 12: Treatment with SSI causes a significant increase in LDLR protein expression in HEK293 cells.

Western blot images of the target protein, low-density lipoprotein receptor (LDLR), and the loading control protein, β-actin, present in the HEK293 cell lysates after **(A)** 24-hour and **(B)** 48-hour treatment. **(C)** Densitometric analysis indicated a significant increase in LDLR expression levels with increased SSI concentration. LDLR signals (1:1000 antibody dilution, Thermo Fisher Scientific) were normalised against the β-actin (1: 10 000 antibody dilution, Sigma Aldrich, Merck) loading control. Treated cells are expressed as a percentage of the untreated cells (set to 100%). Error bars represent the standard deviation *(Student's t-test: *p≤ 0.05, **p≤ 0.01 ***p ≤ 0.001; n = 3 biological repeats, 3 technical repeats each).*

Densitometric analysis was performed to confirm the observed increase in band intensity. This was done by normalising the LDLR band intensities against the β-Actin loading control bands. Figure 12C indicates that there was a proportional relationship between SSI concentration and LDLR protein expression levels, as the protein levels increased (compared to the untreated control set to 100%) by 65.60% ± 24.65%, 70.52% ± 8.38%, 116.16% ± 25.90% and 118.87% ± 30.85% for 25 nM, 50 nM, 100 nM and 150 nM SSI, respectively (24-hour treatment). This was also observed for the 48-hour treatment where LDLR levels increased by 41.14% ± 21.92% (25 nM), 105.46% ± 27.58% (50 nM), 128.86% ± 36.85% (100 nM) and 92.80% ± 29.57% (150 nM). Statistical analysis via the student's t-test indicated that the SSI induced increases in LDLR expression across the concentration range of 25 nM – 100 nM were all significant, in contrast to the DMSO vehicle control which exhibited non-significant increases of 32.22% ± 16.58% and 18.64% ± 20.71% after 24 and 48 hours, respectively.

Similar results were also obtained for the SH-SY5Y cells, whereby there was also an increase in LDLR protein levels with increased SSI concentration for both 24- and 48-hour treatment (fig. 13). After 24 hours, each rise in LDLR expression after SSI treatment (33.81% ± 6.54%, 30.34% ± 14.85%, 58.34% ± 14.82% and 64.69% ± 6.82% for 25 nM, 50 nM, 100 nM and 150 nM SSI, respectively) was statistically significant. After 48-hour treatment, all SSI concentrations, except for 25 nM SSI, induced a significant increase in LDLR levels compared to the untreated control. The LDLR levels increased by 3.14% ± 6.72% (25 nM), 32.69% ± 5.75% (50 nM), 55.72% ± 14.90% (100 nM) and 60.50% ± 16.60% (150 nM) after 48-hours which were very close to those seen after the 24-hour treatment. As seen in the HEK293 cells, the DMSO vehicle control did not cause any significant increase in LDLR expression (9.04% ± 5.60% and 4.82% ± 11.15%, after 24 and 48 hours, respectively), indicating that the LDLR upregulation is due to SSI and not the solvent.

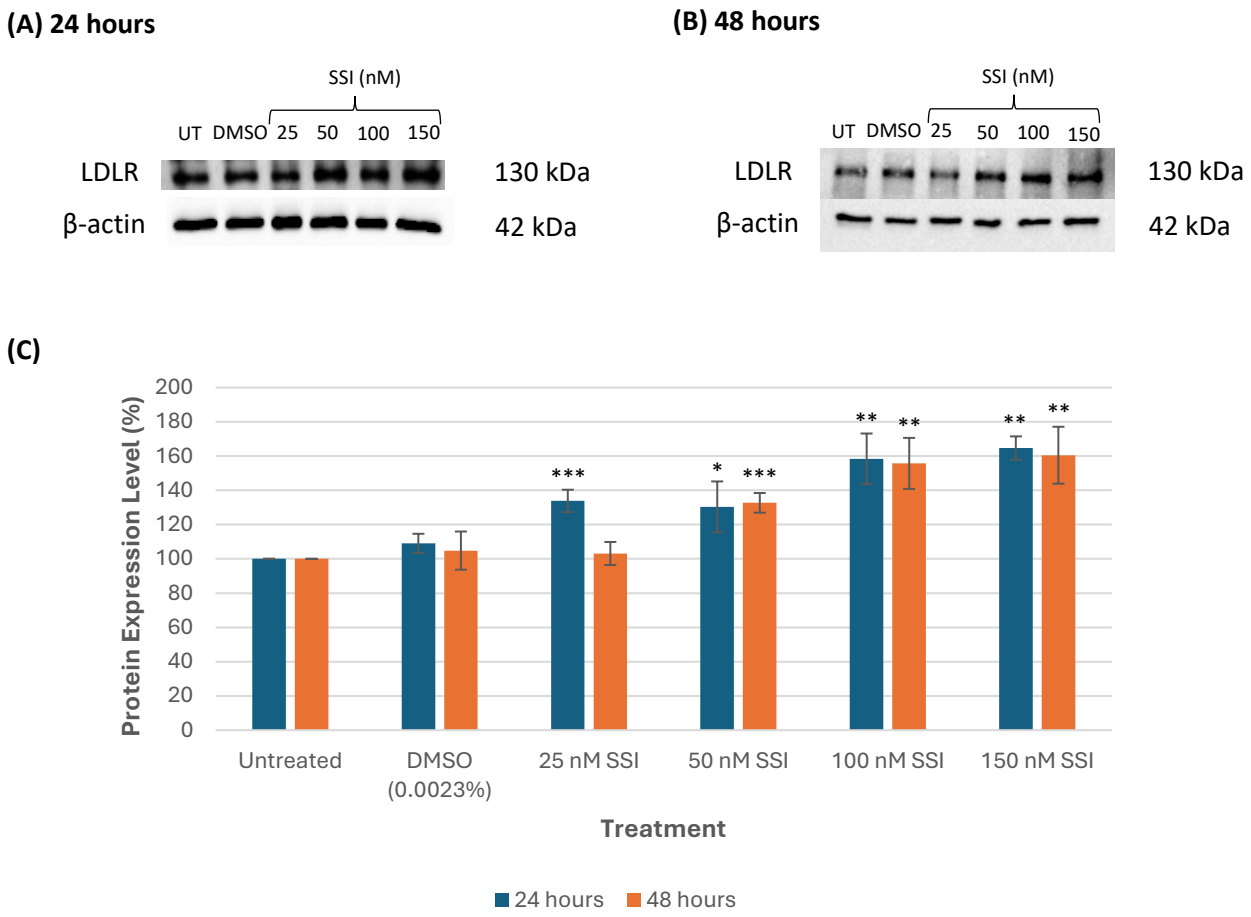


Figure 13: Treatment with SSI causes a significant increase in LDLR protein expression in SH-SY5Y cells.

Western blot images of the target protein, low-density lipoprotein receptor (LDLR), and the loading control protein, β-actin, present in the cell lysate of SH-SY5Y cells after **(A)** 24-hour and **(B)** 48-hour treatment. **(C)** Densitometric analysis indicated a significant increase in LDLR expression levels with increased SSI concentration. LDLR signals (1:1000 antibody dilution, Thermo Fisher Scientific) were normalised against the β-actin (1: 10 000 antibody dilution, Sigma Aldrich, Merck) loading control. Treated cells are expressed as a percentage of the untreated cells (set to 100%). Error bars represent the standard deviation *(Student's t-test: *p≤ 0.05, **p≤ 0.01, ***p ≤ 0.001; n = 3 biological repeats, 3 technical repeats each).*

When comparing the level of LDLR upregulation between the cell lines, it was observed that LDLR expression was higher in the HEK293 cells where levels were recorded above 200% (maximum level being 228.85% for 100 nM SSI, after 48-hour treatment), whereas the SH-SY5Y

cells had a maximum protein expression level of 164.69% (150 nM SSI; after 24-hour treatment). Even so, the western blot analysis indicates that SSI does cause a concentration-dependent upregulation of LDLR *in vitro*. To investigate the effects of SSI on mitochondrial metabolic activity and overall ROS production when treating the hypercholesterolemic-AD cell model, the 50 nM and 100 nM SSI concentrations were selected based on the cytotoxicity results showing no significant effect on cell viability at 24 hours. Additionally, the western blot analysis revealed significant upregulation of LDLR at these two concentrations across both cell lines.

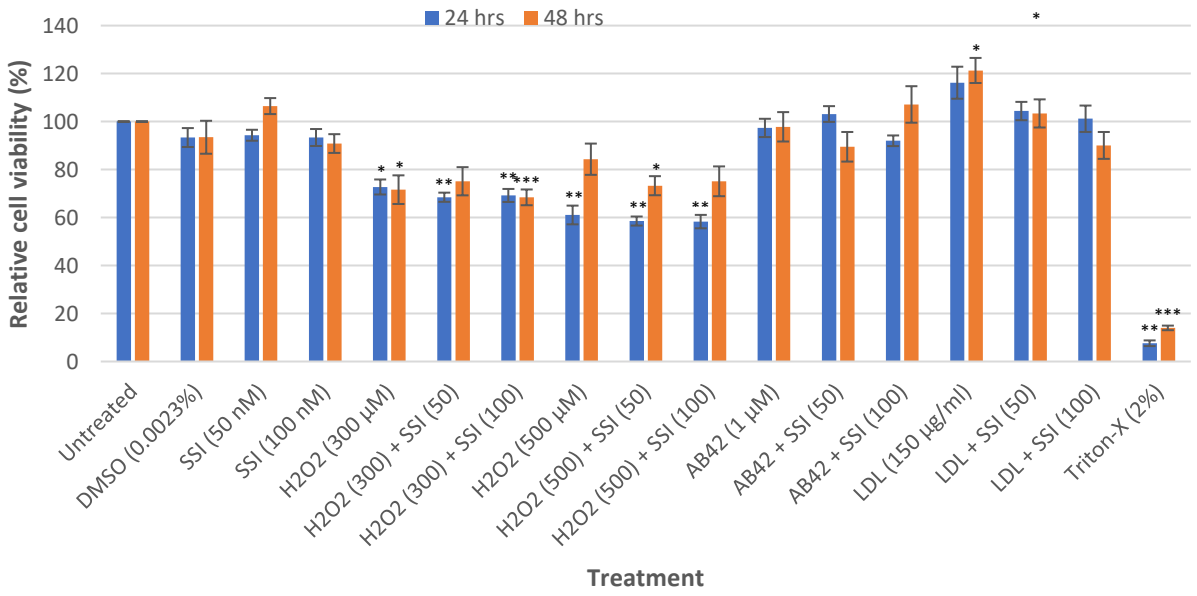
4.2.3 - SSI treatment and the hypercholesterolemic-AD conditions decrease mitochondrial activity but do not significantly affect overall cell metabolic activity

To assess mitochondrial activity, the MTT assay was performed on the HEK293 and SH-SY5Y cells 24- and 48-hours post-treatment with 50 nM and 100 nM SSI, 300 μM and 500 μM H_2O_2, 1 μM Aβ, 150 μg/ml LDL and co-treatments thereof (fig. 14). This assay was used as it directly measures the activity of mitochondrial dehydrogenases present in the electron transport chain in oxidative phosphorylation (Burton, 2005). As seen in the SSI optimisation results, the 50 nM and 100 nM SSI treatments did not significantly affect the mitochondrial activity of the HEK293 cells (compared to the untreated cells) at both 24 hours (decreases of 5.71% ± 2.29% and 6.65% ± 3.53%, respectively) and 48 hours (increase of 6.45% ± 3.34% and decrease of 9.17% ± 3.91%, respectively). This was also seen in the DMSO control, which caused non-significant decreases of 6.67% ± 3.95% and 6.55% ± 6.87% at 24- and 48-hours, respectively. Similarly, treatment with 1 μM Aβ42 also caused non-significant effects on mitochondrial activity in the HEK293 cells, where decreases of 2.66% ± 3.81% and 2.20% ± 6.13% in mitochondrial activity were seen after 24 and 48 hours, respectively. When 50 nM SSI was added to the Aβ42 group, the mitochondrial activity increased slightly by 5.80% ± 3.28% after 24 hours but decreased by 8.32% ± 6.17% after 48 hours. For the 100 nM SSI, its addition to the Aβ42 group caused a decrease of 5.35% ± 2.22% after 24 hours and an increase of 9.33% ± 7.61% after 48 hours. All of these changes were non-significant, suggesting that SSI and Aβ42 treatments, both in isolation and in combination, did not substantially affect mitochondrial activity in HEK293 cells at the tested concentrations and time points.

Conversely, the H_2O_2 treatments did cause significant decreases in mitochondrial activity in the HEK293 cells. After 24 hours, the 300 μM and 500 μM H_2O_2 treatments caused significant

decreases of 27.27% ± 3.13% and 38.93% ± 3.90% (respectively) in mitochondrial activity compared to the untreated cells. However, these reductions in mitochondrial activity were still not as large as the 92.40% ± 1.19% and 86% ± 0.96% reductions seen in the 2% Triton-X cell death control group after 24 and 48 hours, respectively. When SSI was added to the H_2O_2 groups, the mitochondrial activity decreased slightly by 4.27% ± 1.91% (50 nM SSI) and 3.53% ± 2.71% (100 nM SSI) for the 300 µM H_2O_2 groups, and by 2.53% ± 1.89% (50 nM SSI) and 2.76% ± 2.80% (100 nM SSI) for the 500 µM H_2O_2 group, all of which were non-significant. Similarly, after 48 hours, the 300 µM and 500 µM H_2O_2 treatments caused decreases of 28.38% ± 5.97% and 15.69% ± 6.52%, respectively, of which only the former was significant. When SSI was added, the mitochondrial activity increased slightly by 3.51% ± 5.88% (50 nM SSI) and decreased by 3.20% ± 3.29% (100 nM SSI) for the 300 µM H_2O_2 groups, and decreased by 11.04% ± 3.97% (50 nM SSI) and 9.21% ± 6.21% (100 nM SSI) for the 500 µM H_2O_2 group, all of which were also non-significant. These results suggest that H_2O_2 treatment significantly reduces mitochondrial activity in HEK293 cells, particularly after 24 hours. However, the addition of SSI to H_2O_2-treated cells does not appear to have a significant impact on mitochondrial activity, as the observed changes were minimal and statistically non-significant. This indicates that SSI may not play a substantial role in modulating the effects of H_2O_2 on mitochondrial function in these cells under the tested conditions.

(A) HEK293



(B) SH-SY5Y

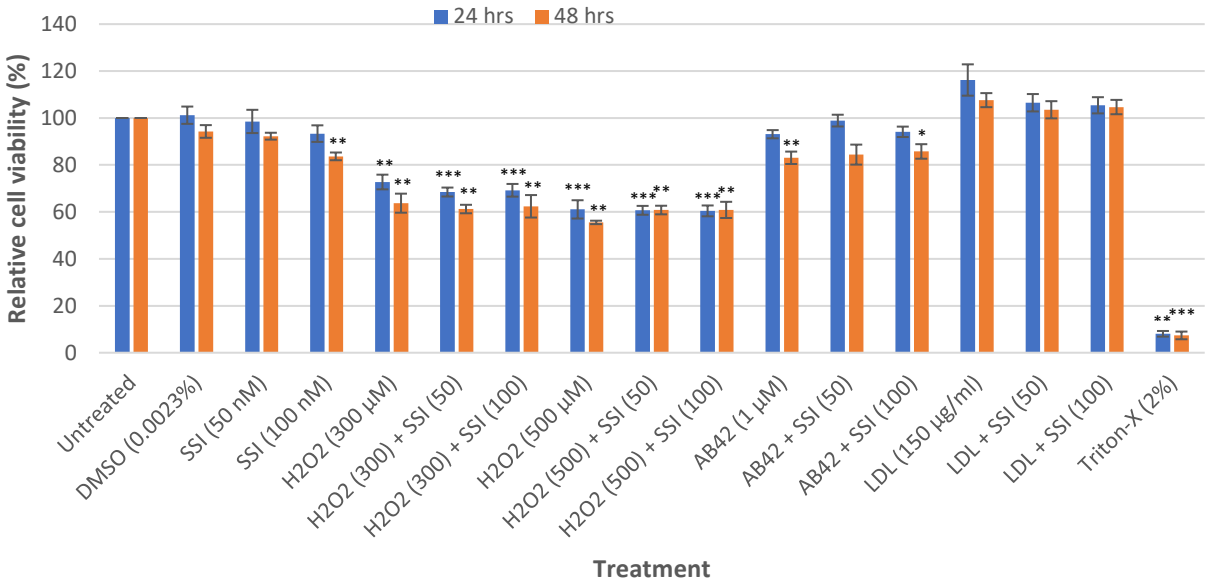


Figure 14: The effects of the hypercholesterolemic-Alzheimer's Disease treatment conditions on mitochondrial activity in (A) HEK293 and (B) SH-SY5Y.

The relative mitochondrial activity of the hypercholesterolemic-AD cell models was investigated using the MTT assay after 24- and 48-hour treatment with squalene synthase inhibitor (50 nM and 100 nM SSI), hydrogen peroxide (300 µM and 500 µM H_2O_2), amyloid beta 42 (1 µM Aβ42), low-density lipoprotein (150 µg/ml LDL), DMSO vehicle control and 2% Triton-X as the cell death control. Co-treatment with SSI showed no significant effect on the hypercholesterolemic-AD cell models. Treated cells are expressed as a percentage of the untreated cells (set to 100%). Error bars represent standard deviation (*Welch's ANOVA followed by Games-Howell post hoc test: *p≤ 0.05, **p≤ 0.01 ***p ≤ 0.001, n = 3 biological repeats, 3 technical replicates each).*

In contrast to the other treatment conditions, the LDL treatment group caused an increase in mitochondrial activity at both 24- (16.19% ± 13.35%) and 48- (21.29% ± 10..44%) hours (of which the latter was statistically significant) in the HEK293 cells. The addition of SSI to the LDL group decreased the mitochondrial activity by 11.81% ± 7.64% (50 nM SSI) and 15.02% ± 10.99% (100 nM SSI) after 24 hours, and by 17.91% ± 11.72% (50 nM SSI) after 48 hours, bringing the mitochondrial activity levels closer to the untreated control (100%), although these changes were non-significant. Interestingly, after 48 hours the addition of 100 nM SSI to the LDL group caused

a significant decrease of 31.24% ± 11.20% to 90.05% relative mitochondrial activity, suggesting that higher concentrations of SSI may have a more pronounced effect on mitigating LDL-induced increases in mitochondrial activity over longer exposure periods.

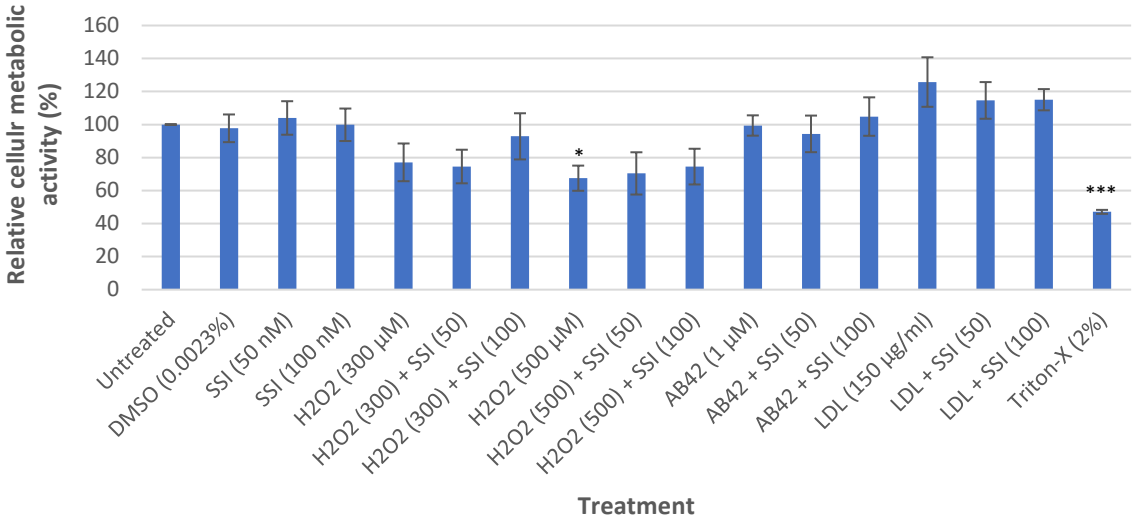
As seen in the SSI optimisation results in the SH-SY5Y cells, treatment with 50 and 100 nM SSI did not cause any significant reduction in mitochondrial metabolic activity after 24 hours (with decreases of 1.47% ± 9.91% and 6.65% ± 7.06%, respectively). Only at 48 hours did the 100 nM SSI treatment cause a significant 16.35% ± 3.30% reduction in mitochondrial activity, whereas the 7.75% ± 2.93% reduction from the 50 nM SSI was still non-significant. The DMSO vehicle control caused a 1.19% ± 7.37% increase in mitochondrial activity after 24 hours, and a 5.73% ± 5.39% decrease after 48 hours, both of which were non-significant. In contrast to the HEK293 cells, the 1 μM Aβ treatment caused a significant 16.95% ± 5.29% reduction in mitochondrial activity in the SH-SY5Y cells after 48 hours, although the 6.90% ± 3.50% reduction seen after 24 hours was non-significant. However, as observed in the HEK293 cells, the addition of SSI to the Aβ-treated SH-SY5Y cells caused non-significant changes in mitochondrial activity, where the activity increased by 5.80% ± 5.02% (50 nM SSI) and 1.02% ± 4.44% (100 nM SSI) after 24-hour treatment, and by 1.35% ± 8.53% (50 nM SSI) and 2.70% ± 6.19% (100 nM SSI) after 48-hour treatment. Additionally, unlike in the HEK293 cells, treatment with 150 μg/ml LDL did not significantly affect the mitochondrial activity in the SH-SY5Y cells (16.19% ± 13.35% and 7.61% ± 5.98% increases after 24- and 48-hour treatment, respectively). The addition of SSI to the LDL treatment did not cause any significant changes in mitochondrial activity, where the activity decreased by 9.69% ± 7.41% (50 nM SSI) and 10.77% ± 6.90% (100 nM SSI) at 24 hours, and by 4.10% ± 7.33% (50 nM SSI) and 2.95% ± 6.11% (100 nM SSI) at 48 hours. Although non-significant, these changes still exhibit a trend of returning the mitochondrial activity in the LDL-treated cells closer to the untreated control levels (100%).

Comparable to the HEK293 cells, treatment with 300 μM and 500 μM H_2O_2 caused significant reductions in mitochondrial activity after both 24-hour treatment (27.27% ± 4.57% and 38.93% ± 7.80%, respectively) and 48-hour treatment (36.29% ± 8.12% and 44.48% ± 1.47%, respectively). However, this reduction was not as large as the 91.94% ± 2.39% (24 hours) and 92.63% ± 3.28% (48 hours) decreases in the 2% Triton-X cell death control group. When SSI was added to the 300 μM treated cells, the mitochondrial activity decreased by 4.29% ± 3.81% (50 nM SSI) and 3.53%

± 5.42% (100 nM SSI) after 24 hours, and by 2.50% ± 3.62% (50 nM SSI) and 1.33% ± 9.58% (100 nM SSI) after 48 hours. Similarly, for the 500 μM H_2O_2-treated cells, the mitochondrial activity decreased by 0.40% ± 3.78% (50 nM SSI) and 0.64% ± 4.62% (100 nM SSI) after 24 hours and increased by 5.27% ± 3.68% (50 nM SSI) and 5.34% ± 6.90% (100 nM SSI) after 48 hours. These changes in mitochondrial activity after SSI treatment were all non-significant, suggesting that SSI may not be able to mitigate the negative effects of H_2O_2 on mitochondrial activity in SH-SY5Y cells, as also seen in the HEK293 cells. However, in both cell lines, these results also demonstrate that SSI treatment did not exacerbate the reduction in mitochondrial activity caused by H_2O_2, indicating that SSI is not detrimental to cellular health at these concentrations (except 100 nM at 48 hours in SH-SY5Y cells), as also observed in the optimisation results.

Following the MTT assay, which specifically assessed mitochondrial metabolic activity, the Alamar Blue® assay was performed to evaluate overall cellular metabolic activity as it can also reflect contributions from non-mitochondrial enzymes. This assay was conducted to determine whether the effects observed in the MTT assay were specific to mitochondrial metabolic activity or if they extended to overall cell viability and metabolism. Figure 15 shows the results from the Alamar Blue® assay whereby the HEK293 and SH-SY5Y cells were treated with the same treatment groups from the MTT assay (fig. 14) for 24 hours. Compared to the untreated cells (set to 100%), the DMSO vehicle control, triton-X cell death control, 50 nM SSI and 100 nM SSI treatment groups had relative cellular metabolic activities of 97.73% ± 8.39%, 47.11% ± 1.20%, 103.98% ± 10.15% and 99.86% ± 9.84% (respectively) in the HEK293 cells, and 87.06% ± 3.63%, 18.66% ± 0.59%, 92.05% ± 7.48% and 92.80% ± 4.23% (respectively) in the SH-SY5Y cells. The changes in relative cellular metabolic activity in these groups were all non-significant.

(A) HEK293



(B) SH-SY5Y

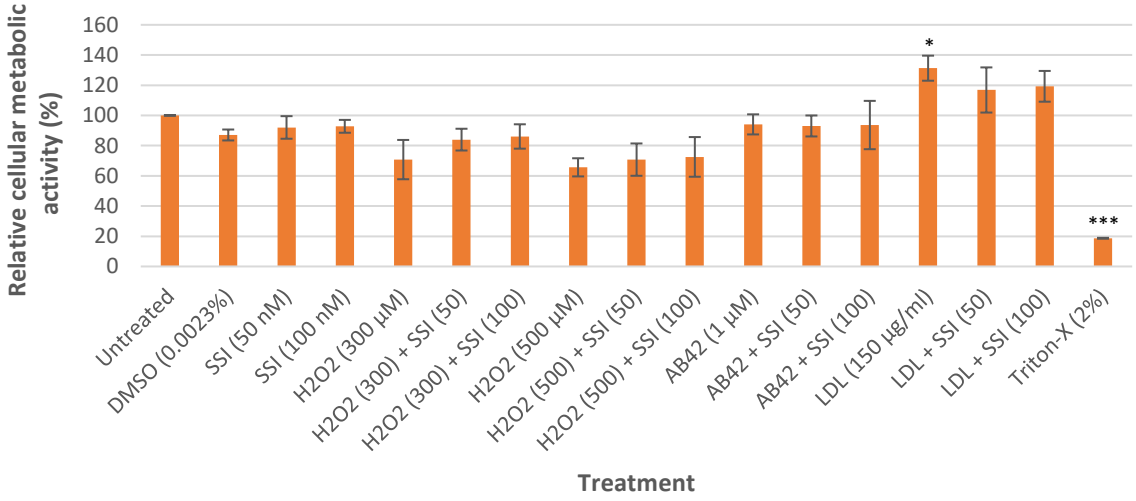


Figure 15: The effects of the hypercholesterolemic-Alzheimer's Disease treatment conditions on cellular metabolic activity in (A) HEK293 and (B) SH-SY5Y.

The relative cellular metabolic activity of the hypercholesterolemic-AD cell models was measured using the Alamar Blue® assay after 24-hour treatment with squalene synthase inhibitor (50 nM and 100 nM SSI), hydrogen peroxide (300 µM and 500 µM H_2O_2), amyloid beta 42 (1 µM Aβ42), low-density lipoprotein (150 µg/ml LDL), DMSO vehicle control and 2% Triton-X as the cell death control. Co-treatment with SSI showed no significant effect on the cellular metabolic activity in the hypercholesterolemic-AD cell models. Treated cells are expressed as a percentage of the untreated cells (set to 100%). Error bars represent standard deviation (*Welch's ANOVA followed by Games-Howell post hoc test: *p≤ 0.05, **p≤ 0.01 ***p ≤ 0.001, n = 3 biological repeats, 3 technical replicates each).*

Similarly, treatment with 1 μM Aβ also caused non-significant changes in cellular metabolic activity in both cell lines, where the levels decreased to 99.43% ± 6.16% in the HEK293 cells and 94.08% ± 6.66% in the SH-SY5Y cells. When the Aβ-treated cells were then treated with SSI, the cells did not exhibit any significant changes nor any observable trend in cellular metabolic activity. In the HEK293 cells, the cellular metabolic activity decreased to 94.35% ± 11.09% after 50 nM SSI treatment and increased to 104.83% ± 11.65% after 100 nM SSI treatment. In the SH-SY5Y cells, the cellular metabolic activity decreased slightly to 93.04% ± 6.95% after 50 nM SSI treatment and to 93.65% ± 16% after 100 nM SSI treatment. As expected, treatment with 150 μg/ml LDL caused the cellular metabolic activity to increase to 125.74% ± 15.00% in the HEK293 cells and to 131.29% ± 8.30% in the SH-SY5Y cells, where only the latter was significant. When SSI was added to the LDL groups, the cellular metabolic activity decreased to 114.62% ± 11.11% (50 nM SSI) and 115.04% ± 6.43% (100 nM SSI) in the HEK293 cells, and to 116.86% ± 14.95% (50 nM SSI) and 119.29% ± 10.19% (100 nM SSI) in the SH-SY5Y cells. Although these changes were non-significant, the decrease in cellular metabolic activity after SSI addition to the LDL group suggests that SSI may help regulate metabolic imbalances caused by high LDL treatment, potentially stabilising cellular metabolism under these conditions.

Like the MTT assay results, the 300 μM H_2O_2 treatment groups exhibited decreased levels of 77.12% ± 11.43% and 70.76% ± 13.01% for the HEK293 and SH-SY5Y cells (respectively), however, these reductions were non-significant. Interestingly, when SSI was added to the 300 μM H_2O_2 treatment group, there was a general trend whereby the SSI increased the relative cellular metabolic activities of the cells treated with 300 μM H_2O_2. This was more consistent in the SH-SY5Y cells where the SSI treatment increased the cellular metabolic activity of the 300 μM H_2O_2 treated cells to 84% ± 7.21% (50 nM SSI) and 86.07% ± 8.08% (100 nM SSI), compared to the HEK293 cells which exhibited a decreased level of 74.59% ± 10.17% after 50 nM SSI treatment, but then a large increase to 92.86% ± 13.98% after 100 nM SSI treatment. Similarly, the 500 μM H_2O_2 treatment also caused decreased levels of 67.51% ± 7.63% and 65.64% ± 6.01% for the HEK293 and SH-SY5Y cells, respectively, with the former being significant. Once again, the addition of SSI to this group caused increases in cellular metabolic activity in both cell lines. For the HEK293 cells, the new levels were 70.41% ± 12.80% (50 nM SSI) and 74.53% ± 10.81% (100 nM SSI), and for the SH-SY5Y cells the levels increased to 70.75% ± 10.7% (50 nM SSI) and 72.55% ± 13.14% (100 nM SSI).

Despite this trend seen for both concentrations of H_2O_2, the increases in cellular metabolic activity seen after SSI treatment were all non-significant, however, so were the decreases seen by the H_2O_2 treatments alone (except for the 500 μM H_2O_2 treatment in the HEK293 cells). This suggests that while these observed increases in cellular metabolic activity following SSI treatment were not statistically significant, the consistent upward trend across both H_2O_2 concentrations indicates that SSI may be able to mitigate oxidative stress-induced metabolic impairments and further supports the notion that SSI does not exacerbate cellular damage. Although SSI treatment did not significantly protect mitochondrial activity, as measured by the MTT assay, the Alamar Blue® results suggest that SSI may help preserve overall cellular metabolic activity, particularly under oxidative stress conditions. To further explore the potential antioxidant properties of SSI and its role in mitigating oxidative stress, a ROS production assay was conducted to assess how SSI influences ROS levels under the same treatment conditions.

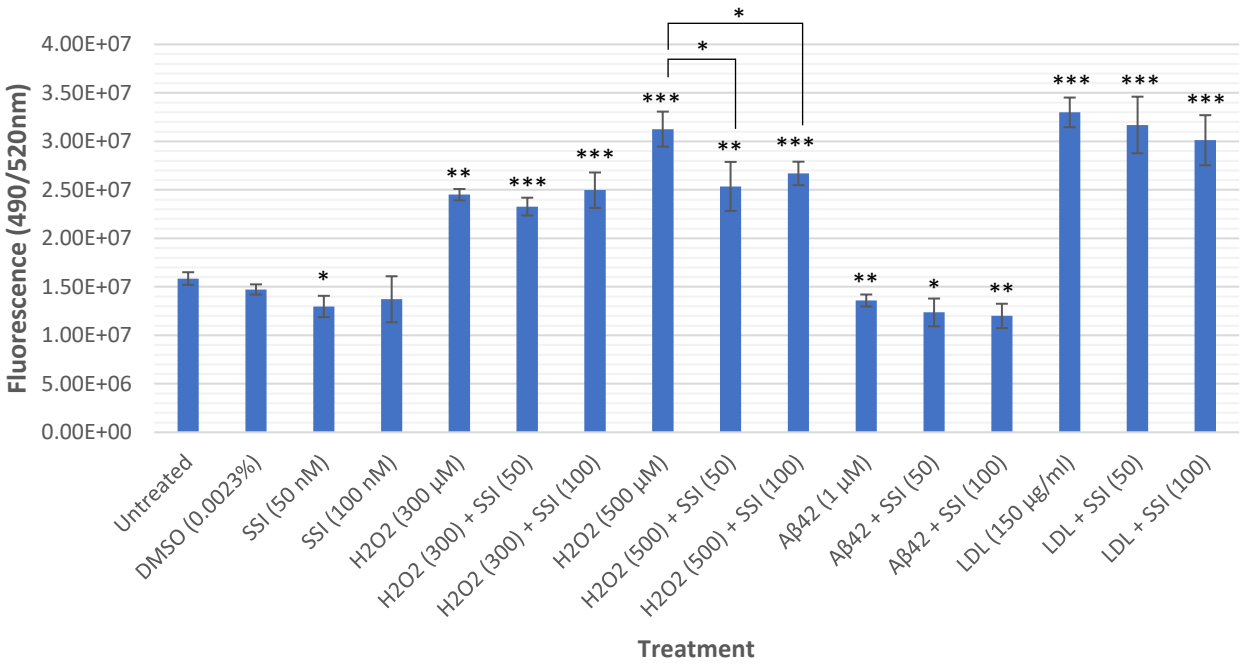
4.2.4 - Treatment with SSI shows a promising trend of decreasing total ROS production in the hypercholesterolemic-AD cell model

This study measured total ROS production in HEK293 and SH-SY5Y cell models to assess oxidative stress under hypercholesterolemic-AD conditions. As mentioned, ROS plays a critical role in both hypercholesterolemia and AD, as excessive ROS production contributes to oxidative stress that damages cellular components, promotes inflammation, and accelerates neurodegenerative and vascular pathologies linked to these conditions (Wang et al., 2014; Mollazadeh et al., 2018). Using the Total ROS Assay Kit 520 nm (Invitrogen, Thermo Fisher, USA), total ROS levels were quantified to evaluate the impact of these stressors on oxidative balance, a critical factor in AD pathogenesis.

The fluorescence signals of the treated HEK293 cells (fig. 16A) showed a significant decrease in ROS detection in the 50 nM (18.14% ± 4.12%) but not the 100 nM (13.45% ± 7.4%) SSI-treated cells and the DMSO control group (7.07% ± 0.47%). As expected, both the 300 μM and 500 μM H_2O_2-treated cells showed significant increases in ROS production of 54.60% ± 2.54% and 97.27% ± 3.48%, respectively, confirming the ROS-inducing effects of hydrogen peroxide. When SSI was added to the 300 μM H_2O_2 group, the co-treatment with both SSI concentrations did not cause any significant change in ROS production. However, when SSI was added to the 500 μM H_2O_2 group, the ROS levels decreased significantly by 37.30% ± 10.10% (50 nM SSI) and 28.84%

± 4.70% (100 nM SSI) compared to 500 µM H_2O_2 treatment alone. Similarly, LDL treatment also caused a significant spike (an increase of 108.14% ± 5.25%) in ROS levels, reflecting its pro-oxidant effect at elevated levels. When SSI was added to the LDL group, this ROS spike decreased by 8.19% ± 8.80% (50 nM SSI) and 18.10% ± 8.97% (100 nM SSI). While these reductions were non-significant, they suggest that SSI may modulate LDL-induced oxidative stress, possibly through LDLR upregulation.

(A) HEK293



(B) SH-SY5Y

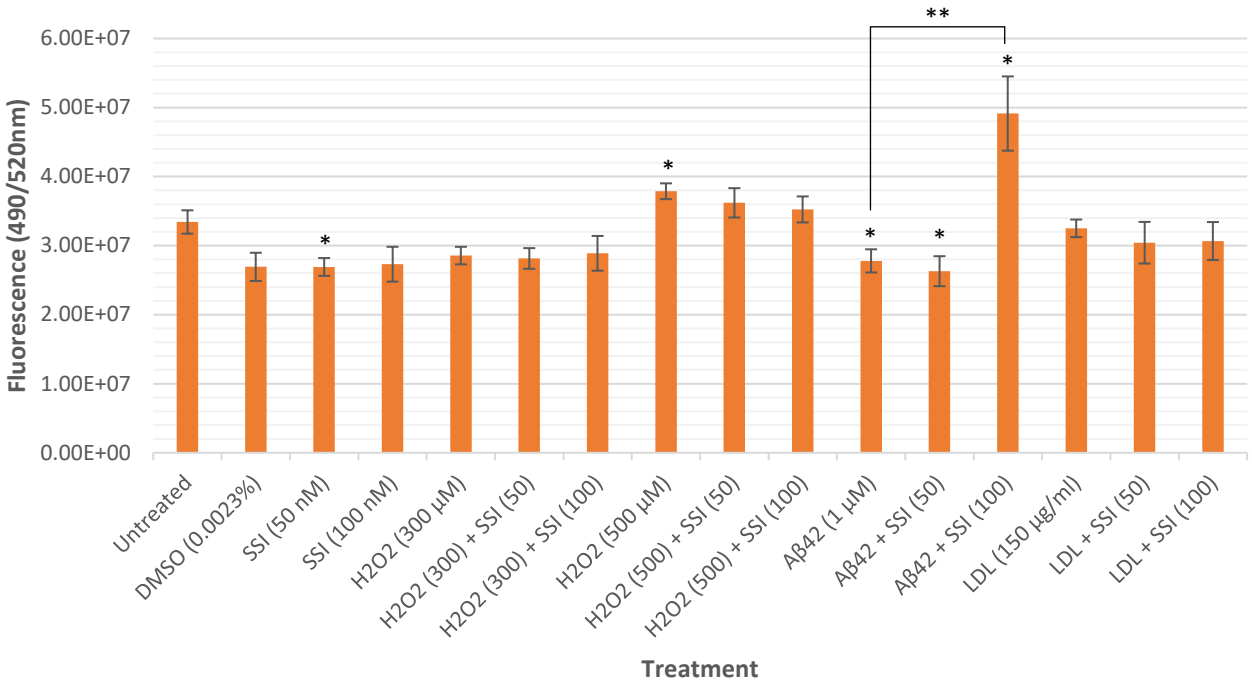


Figure 16: SSI treatment decreases ROS production in the hypercholesterolemic-AD cell model.

A fluorescent based Total ROS assay measured total ROS production of **(A)** HEK293 and **(B)** SH-SY5Y cells after 24-hour treatment with hydrogen peroxide (300 µM and 500 µM H_2O_2), low-density lipoprotein (150 µg/ml LDL), amyloid beta (1 µM Aβ42), squalene synthase inhibitor (50 nM and 100 nM SSI) and co-treatments thereof. Statistical analysis showed significant decreases in total ROS production for selective SSI treated groups. Error bars represent standard deviation (*Welch's ANOVA followed by Games-Howell post hoc test: *p≤ 0.05, **p≤ 0.01 ***p ≤ 0.001, n = 3 biological repeats, 3 technical replicates each).*

Although SSI treatment caused significant decreases in ROS levels in the 500 µM H_2O_2 treated group, the overall ROS levels were still significantly higher than the untreated cells, indicating that SSI cannot fully restore ROS levels to baseline. In contrast to the H_2O_2 and LDL treatment groups, the Aβ42 treatment caused a significant decrease in ROS levels by 14.27% ± 0.63%, which could indicate a possible compensatory cellular response to Aβ42. When SSI was co-administered with Aβ42, ROS levels decreased further by 7.72% ± 3.58% (50 nM) and 10.03% ± 3.32% (100 nM),

though these reductions were not statistically significant. Overall, in the HEK293 cells, the addition of SSI to the H_2O_2, LDL and Aβ42 treatment groups showed a consistent trend of lowering total ROS production after 24-hour treatment.

Similar to the HEK293 cells, only the 50 nM SSI treatment caused a significant decrease of 19.48% ± 4.12% in ROS production in the SH-SY5Y cells, whereas the 100 nM SSI (18.3% ± 10.60% decrease) and DMSO vehicle control (19.45% ± 6.03% decrease) groups did not cause any significant changes (fig. 16B). Interestingly, the 300 μM H_2O_2 treatment did not cause an expected spike in ROS production, but rather a decrease of 14.56% ± 6.12% in ROS levels, although this was not significant. When SSI was added to this group, the ROS levels exhibited minute changes of no more than 1.3%, which were not significant. In contrast, the 500 μM H_2O_2 treatment caused a significant increase of 13.32% ± 7.03% in ROS levels compared to the untreated control. As observed in the HEK293 cells, the SSI treatment caused a decrease in ROS levels in the 500 μM H_2O_2 group, where the 50 nM and 100 nM SSI caused decreases of 5.03% ± 9.96% and 7.89% ± 8.12%, respectively, albeit non-significant. Similar to the 300 μM H_2O_2 groups, the LDL treatment did not cause any significant change in ROS levels compared to the untreated control, where the ROS levels decreased slightly by 2.76% ± 6.41%, which may reflect variability in the LDL-mediated oxidative response in SH-SY5Y cells. When SSI was added to the LDL group, the levels dropped by 6.23% ± 11.85% (50 nM SSI) and 5.48% ± 9.59% (100 nM SSI). A notable result also seen in the SH-SY5Y cells was the significant decrease in ROS levels after Aβ42 treatment (16.86% ± 5.75%). The addition of 50 nM SSI to Aβ42 caused a slight decrease of 4.46% ± 6.03% in ROS levels, however, the addition of 100 nM SSI caused an unexpected spike in ROS levels, which were significantly increased by 63.83% ± 19.92% compared to the Aβ42 treatment group.

Overall, these results showed a promising trend whereby the addition of SSI, particularly at 50 nM, reduced ROS levels across all treatment groups. A decrease in ROS generally suggests improved cellular redox balance, which can protect cells from the oxidation-induced damage of cellular components implicated in elevated ROS conditions. These findings highlight SSI's potential as a modulator of oxidative stress in various contexts, though its effectiveness appears to vary depending on the ROS inducer and its concentration. To build upon these findings, mitochondrial DNA copy number was assessed to evaluate whether the observed reduction in ROS corresponds with changes in mitochondrial integrity and biogenesis.

4.2.5 - Treatment with SSI increases mtDNA-CN in the hypercholesterolemic-AD cell model

In line with evaluating mitochondrial dysfunction, this study also assessed mitochondrial DNA copy number (mtDNA-CN) using quantitative PCR (qPCR). Assessing mtDNA-CN is widely used as a test for mitochondrial dysfunction as changes in mtDNA-CN can reflect the organelle's response to cellular stress by indicating mitochondrial biogenesis or damage. To complement the findings from the MTT and Alamar Blue® assays, the mtDNA-CN was assessed at 48 hours to investigate the long-term effects of the treatments on mitochondrial health. Additionally, only the 500 μM H_2O_2 treatment was used as the ROS production assay revealed that it caused higher ROS production compared to 300 μM H_2O_2, making it more relevant for evaluating mitochondrial responses. This concentration also caused significant decreases in mitochondrial and cellular metabolic activity, as seen in the MTT and Alamar Blue® assays. Moreover, the choice of only using 50 nM SSI reflects its ability to mitigate oxidative damage without compromising cell viability, which was a concern as the optimisation results showed a significant reduction in cell viability in the SH-SY5Y cells after 48-hour treatment with 100 nM SSI.

Figure 17 shows that treatment with 50 nM SSI did not significantly change the mtDNA-CN levels (1.08-fold change/increase of 7.47% ± 0.11%) of the HEK293 cells, whereas the DMSO vehicle control did exhibit a 21% ± 0.06% decrease in mtDNA-CN compared to the untreated cells, however, this was also found to be non-significant. These results imply that SSI treatment in isolation does not significantly affect mtDNA-CN. In comparison, treatment with H_2O_2 and LDL caused significant increases of 68.53% ± 0.18% and 49.56% ± 0.13% (respectively) in mtDNA-CN compared to the untreated cells. Interestingly, when SSI was added to these two groups, the mtDNA-CN levels increased further by 19.73% ± 0.20% and 26.24% ± 0.10% for the H_2O_2 and LDL-treated groups (respectively), although these increases were non-significant. In contrast to these two groups, treatment with Aβ42 caused a 0.69-fold change in mtDNA-CN compared to the untreated cells. This significant reduction (30.95% ± 0.06%) in mtDNA-CN levels suggests a potential impairment in mitochondrial biogenesis or increased mitochondrial degradation, consistent with mitochondrial dysfunction associated with Aβ42 toxicity. As seen in the other treatment groups, the addition of SSI to the Aβ42 treatment resulted in a significant 57.19% ±

0.14% increase in mtDNA-CN, suggesting that SSI may mitigate Aβ42-induced mitochondrial damage by promoting mitochondrial biogenesis or stabilisation.

These results provide key insights into the mitochondrial dynamics under different treatment conditions relating to the hypercholesterolemic-AD cell model, highlighting potential mechanisms of mitochondrial dysfunction.

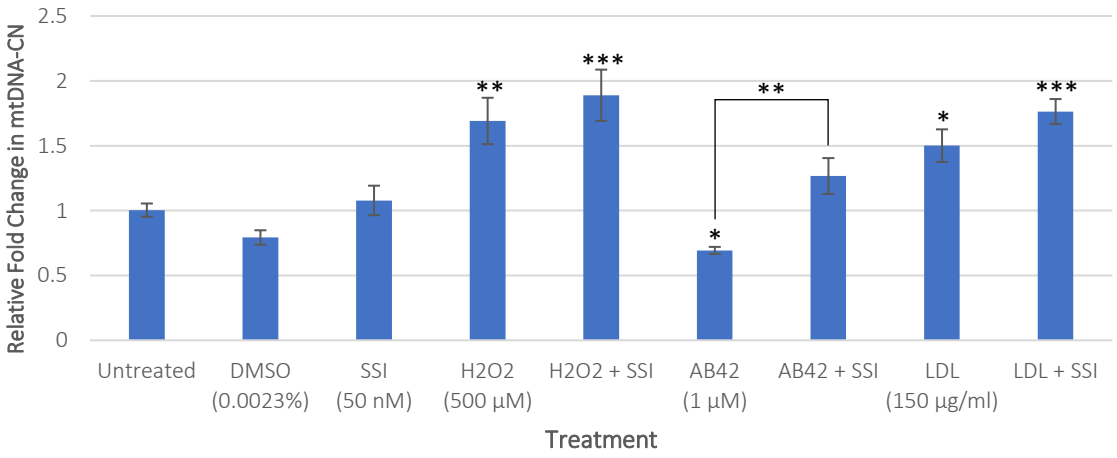


Figure 17: Treatment with SSI increases mtDNA-CN in the hypercholesterolemic-AD cell model (HEK293).

Bar graph of the fold change in mitochondrial DNA copy number (mtDNA-CN) of HEK293 cells after 48-hour treatment with squalene synthase inhibitor (SSI), hydrogen peroxide (H_2O_2), amyloid beta (AB42) and low-density lipoprotein (LDL). The ch11: 2170993 – 2171170 nuclear DNA region was used as the reference gene. Fold-change is compared to the untreated control group (1). Error bars represent standard deviation *(One-way ANOVA followed by LSD post hoc test: *p ≤ 0.05, **p ≤ 0.01, ***p ≤ 0.001; n = 3 biological replicates, 3 technical replicates each).*

5. Discussion

Alzheimer's disease is a neurodegenerative disorder characterised by hallmark features such as amyloid-beta (Aβ) plaques, neurofibrillary tangles (NFTs), and extensive neuronal loss. While the precise mechanisms driving AD remain elusive, emerging evidence points to metabolic disorders, such as hypercholesterolemia, as significant risk factors that can exacerbate the disease's progression. Hypercholesterolemia has been linked to increased Aβ aggregation, oxidative stress, and neuroinflammation, all of which are implicated in AD pathology (Refolo et al., 2000; Gamba et al., 2015). Current therapeutic strategies for hypercholesterolemia, including statins and LDLR upregulation, aim to restore cholesterol homeostasis by reducing circulating LDL levels, thereby potentially mitigating these AD-related mechanisms. This study conducted proteomic analysis on FH patient plasma samples to identify novel biomarkers that could be potential therapeutic targets that may further inform therapeutic strategies against AD. Based on these findings, the effects of a squalene synthase inhibitor (SSI) on mitochondrial dysfunction and metabolic activity in hypercholesterolemic-AD cell models were also evaluated, to identify therapeutic strategies that may reduce hypercholesterolemia-associated contributions to AD pathogenesis.

5.1 – Proteomics Discussion

Proteomics is the large-scale study of proteins, focusing on their expression, structure, functions, and interactions within a biological system. Proteins are central to virtually all biological processes, making proteomics a powerful tool for understanding cellular functions and disease mechanisms. This study aimed to use proteomic analysis to investigate the molecular changes associated with FH and explore potential links to AD. Using SWATH-MS, 28 differentially expressed proteins (DEPs) with significant alterations in expression between FH patients (not on statin medication) and healthy controls were identified. Additionally, data was also collected from FH patients who were on statin medication. This study only focused on the 15 proteins that were differentially expressed in both the FH vs control and FH vs FH+statin dataset, to assess the statin effects on the FH condition specifically. These proteins were further analysed through functional annotation and pathway enrichment, revealing their involvement in a range of biological processes, molecular functions, and pathways. Notably, enriched pathways spanned cytoskeletal regulation

and dynamics, oxidative stress and antioxidant defence, inflammation and immune regulation and metabolism and energy regulation.

5.1.1 - Dysregulated proteins in cytoskeletal dynamics and regulation

The cytoskeleton is a dynamic network of protein filaments, namely microfilaments (actin), microtubules (tubulin) and intermediate filaments, all of which serve multiple essential functions within cells. These include providing structural support, maintaining cell shape, division and movement, and facilitating the movement of materials within the cell (Hohmann & Dehghani, 2019). The cytoskeleton is integral to cellular communication and mechanotransduction, allowing cells to detect and respond to both external and internal stimuli. Moreover, it is essential for maintaining tissue integrity and aids in vital processes such as cell migration and adhesion, which are vital for development and its dysregulation is implicated in many diseases (Fletcher & Mullins, 2010). Several of the downregulated proteins identified in the FH plasma samples are proteins integral to cytoskeletal regulation. These proteins are tropomyosin (TPM4), actin (ACTB), profilin-1 (PFN1), thrombospondin-1 (THBS1), talin-1 (TLN1) and alpha-tubulin isoforms (TUBA3C, TUBA3D, TUBA1B, TUBA4A, TUBA3E, TUBA1A, TUBA1C, TUBA8). Only one upregulated protein, keratin type 2 (KRT2) is also involved in the cytoskeleton. This was also evidenced in the Reactome pathway enrichment analysis where 7 out of the top 10 pathways were directly related to microtubule dynamics and gap junction regulation (table 7), whilst the remaining 3 were still linked to microtubules. These pathways have been briefly illustrated in figure 18 and will be discussed in further detail. While research into the possible effects of FH on the cytoskeleton has not been performed explicitly, some studies have shown that a hyperlipidaemic state, which is akin to hypercholesterolemia, has altered cytoskeletal regulation and dynamics, by remodelling membrane-cytoskeletal structures (Rajkumar et al., 2010), and altering actin-dependent signalling pathways (Suica et al., 2015).

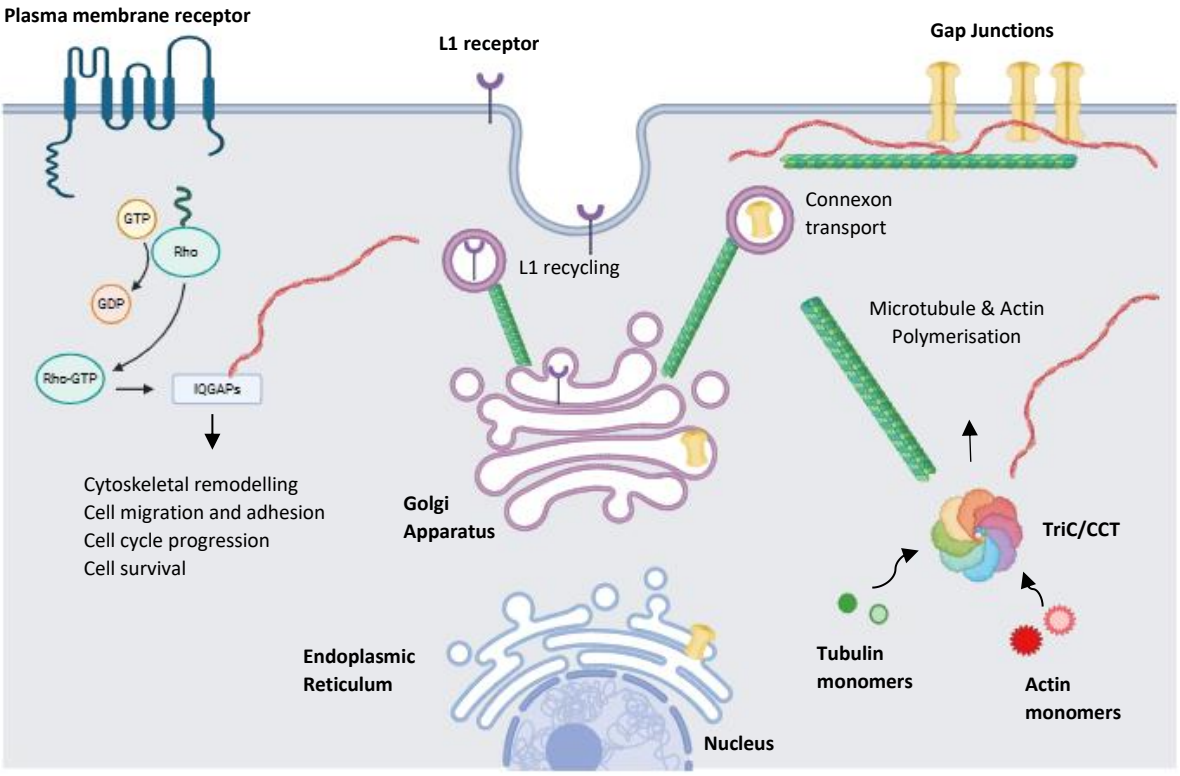


Figure 18: The top enriched pathways based on the differentially expressed proteins (DEPs) identified in FH vs Control groups, obtained from Reactome.

The enriched pathways obtained from Reactome were all matched to the tubulin and/or actin DEPs, emphasising the involvement of these cytoskeletal structures in various cellular processes. The pathways highlighted the role of these proteins in connexon transport from the Golgi apparatus to the plasma membrane, gap junction trafficking and regulation, the recycling pathway of L1, involvement in RHO GTPase activation of IQGAPs as well as the TriC/CCT mediated folding of tubulin and actin monomers to facilitate microtubule and actin polymerization. Diagram was created using Biorender.com.

5.1.1.2 - Intermediate Filaments: Structural Stability and Cellular Integrity

As mentioned, there was only one cytoskeletal-related protein that was upregulated in the FH patient samples, where keratin type 2 (KRT2) had a 1.77-fold increase in protein levels compared to healthy controls. Keratins form the largest subset of intermediate filaments, which is a permanent structure within the cytoskeleton, important for cell structure anchorage to other cells and the extracellular matrix (Herrmann et al., 2007). Additionally, keratins are also implicated in

signalling pathways, inflammation and disease states. While there are currently no studies investigating KRT2 and cholesterol disorders such as FH, recent studies have looked at the role of keratins in AD. Through genome-wide genotyping, it was observed that certain keratin types were positively associated with AD phenotypes, specifically keratin 9 (KRT9, a type I keratin), which was detected in the cerebrospinal fluid of AD patients, but not in healthy brains. Concentrations of KRT9 were also found to correlate with AD-related proteins (i.e. Amyloid beta, tau, apolipoprotein E etc.) making it a new biomarker with high diagnostic accuracy for AD (Wong et al., 2023). This study also looked into single nucleotide polymorphisms (SNPs) in keratins and found that SNPs in KRT2 were associated with higher cerebrospinal fluid-Aβ42 concentrations in AD patients. Thus, it could be speculated that elevated levels of KRT2, as seen in the FH patients, could be related to an increase in Aβ in AD.

5.1.1.3 - Microtubules: Intracellular Transport and Dynamics

The FH patients had a 1.92-fold decrease in protein expression of multiple isoforms of alpha tubulins, a vital monomer of microtubules, which are hollow cylinders formed by a 1:1 ratio of alpha- and beta-tubulin subunits. Humans express 9 alpha-tubulin isoforms that exhibit tissue specificity and interestingly, the brain expresses the 1A-, 1B-, 1C-, 4A-, and 8-alpha tubulin isoforms (Fukushima et al., 2009) all of which were dysregulated in the FH patient samples. In neurons, microtubules are the main protein filaments of the cytoskeleton (Burbaeva, Androsova & Savushkina, 2020), and constitute approximately 10% of the total protein in the brain (Cleveland et al., 1980). As mentioned, microtubules have many functions in cells, but in adult neurons, they are vital in facilitating the efficient trafficking of proteins, organelles, mRNAs and other molecules across the axons, making them important components in cellular communication (Aiken et al., 2017). Additionally, microtubule function is essential for neuronal migration, a process necessary for forming the cortical layers and various other brain structures (Buck & Zheng, 2002). These studies emphasise the importance of microtubules in the brain where evidence has shown that cytoskeletal defects and altered microtubule-mediated processes have been linked to neurodevelopmental disorders (Kumar et al., 2010) and play important roles in neurodegeneration. For instance, the pathogenesis of NFTs, a major histopathological hallmark of AD, is associated with the fact that tau is a microtubule-associated protein, whereby its hyperphosphorylation in AD hinders tubulin and microtubule assembly, leading to microtubule disintegration and

destabilisation (Brion et al., 2001). For this reason, microtubule stabilisers have been investigated in the search for a therapeutic strategy against AD and have shown largely positive results, improving the pathogenesis of the disease (Ballatore et al., 2012; Guo et al., 2020; Yao et al., 2024). A very recent study found that a microtubule stabiliser significantly reduced Aβ plaques and tau pathology in mouse models of AD, where it was also able to reduce axonal dystrophy and gliosis (a fibrous proliferation of glial cells in response to brain injury) (Yao et al., 2024).

Considering the abundant research and evidence regarding the role of microtubule stability and dynamics in AD, it can be speculated that dysregulation of microtubules could be a possible pathway contributing to the pathogenesis of AD. The Reactome pathway enrichment analysis did identify 3 pathways directly linked to the correct folding of the tubulin monomers. These pathways included, "Cooperation of Prefoldin and TriC (tailless complex polypeptide 1-ring complex)/CCT (chaperonin containing tailless complex polypeptide 1) in actin and tubulin folding", "Formation of tubulin folding intermediates by CCT/TriC" and "Post-chaperonin tubulin folding pathway". As part of the pathway analysis done by Reactome, the number of reactions involved within a specific pathway that the proteins are involved in is noted (table 7) and these three pathways exhibited found reactions of 6/6, 2/2 and 6/9 (respectively), suggesting that there could be a dysregulation in these processes in the FH patients. These pathways mention the role of prefoldin and TriC/CCT, both of which are chaperonin proteins (Jin et al., 2019; Grantham, 2020). In fact, TriC/CCT is considered an essential eukaryotic chaperonin complex that functions in the assisted folding of 10% of cytosolic proteins (Jin et al., 2019), including those vital to the cytoskeleton (actin and tubulin), which in turn allows them to properly assemble into microfilaments and microtubules, respectively (Grantham, 2020). This is an important process in cells whereby a defect/dysregulation of this complex or process has been implicated in many diseases, including neurodegeneration and AD (Pavel et al., 2016). The enrichment of these pathways and the significant downregulation of the alpha-tubulin proteins could indicate a major disruption in tubulin, and hence, microtubule assembly and function in FH patients. Interestingly, a study found a 65% reduction in total alpha-tubulin levels in the brains of AD patients compared to age-matched control brains (Zhang et al., 2015). This similarity in alpha-tubulin downregulation between FH and AD suggests a potential overlap in cytoskeletal dysregulation between them.

5.1.1.4 - Microfilaments and Actin-Binding Proteins: Cytoskeletal Remodelling and Cell-Cell Interactions

In addition to tubulin, the actin (ACTB) protein exhibited a 1.73-fold decrease in protein expression in the FH patients compared to healthy controls. Actin is a globular protein that is present in both the cytoplasm and nuclei of cells, where it forms part of the cytoskeleton and can regulate gene transcription by binding to transcription factors and forming a component of chromatin remodelling complexes (Miralles & Visa, 2006). Actin can exist as a monomer, called G-actin, which can then polymerise into filaments called F-actin, leading to dynamic polymerisation and depolymerisation that constitutes the basis of the protein's involvement in the cytoskeleton and its functions in cell shape, polarity and motility (Dominguez & Holmes, 2011). Despite its role in gene transcription regulation, the pathways highlighted by the proteomic analysis focused on its role in the cytoskeleton. As mentioned in the results, the ACTB protein had the most protein-protein interactions (10) as identified by STRING, with the PPI network illustrating a central role of actin in connecting many of the DEPs (fig. 8). Four of the proteins that interacted with ACTB have important functions in influencing actin polymerisation and some of its functions in the cytoskeleton. These proteins are: PFN1, TPM4, THBS1 and TLN1, and all four proteins were downregulated in the FH patient samples.

Profilin-1 (PFN1) is an actin monomer-binding protein that regulates actin polymerisation by binding to G-actin and catalysing its formation to F-actin through mediator proteins called formins (Alkam et al., 2016) (fig. 19). This action of PFN1 is concentration-dependent, where high concentrations inhibit actin polymerisation and low concentrations enhance it (Schutt, Karlén & Karlsson, 2022). This implies that the levels of PFN1 are carefully regulated to maintain actin polymerisation dynamics, whereby the depolymerisation of actin filaments is just as important as its polymerisation, where a balanced dynamic is essential for cellular functions. The significant decrease in PFN1 in the FH patient samples compared to the healthy control patients could signify a dysregulation in this protein expression and hence by association, in actin polymerisation dynamics. Interestingly, in a recent genome-wide association study of AD, an analysis of the top functional networks exhibited in the AD brain found that one of these networks in the amygdala was "cytoskeletal and organelle organisation" which included PFN1 (Brabec et al., 2021). Additionally, PFN1 was the highest-ranking functional gene in the hippocampus. These results

supported previous studies indicating how alterations to the function of PFN1 could lead to alterations in synaptic maintenance, which in turn could contribute to neurodegeneration (Schweinhuber et al., 2015). In addition to its vital role in regulating actin dynamics, a possible new function of PFN1 was investigated very recently where authors found that PFN1 knockout in CAD (Cath.a-differentiated) neuronal cells led to a disruption in mitochondrial dynamics (Read et al., 2024). These authors reported the depolarisation of the mitochondria, a change in mitochondrial morphology to large and elongated as well as an increase in superoxide production. These changes were said to be independent of actin polymerisation in the cytosol, further emphasising the importance of PFN1's independent functionality in cells and providing a novel role of PFN1 in maintaining mitochondrial integrity. These studies highlight PFN1 as an unrecognised protein that may have essential functions in cells, where its dysregulation could contribute to disease. The finding that it is downregulated in the FH patient samples could highlight it as a potential new biomarker.

Tropomysosin alpha-4 (TPM4) is a protein that forms part of a family of actin-binding proteins with functions related to actin regulation in the cytoskeleton. TPMs form coiled-coil dimers creating a polymer along the length of actin filaments (Pelucchi, Stringhi & Marcello, 2020). There are four mammalian *TPM* genes, namely *TPM1, TPM2, TPM3* and *TPM4,* which can each form multiple protein isoforms through alternative exon splicing (Gunning, O'neill & Hardeman, 2008). Neurons mainly express isoforms deriving from TMP1, TPM3 and TPM4 (Brettle, Patel & Fath, 2016), where the latter two have been found to localise in the postsynaptic region of mouse hippocampal neurons (Guven, Gunning & Fath, 2011). This is in part due to the functions of TPMs in protecting actin filaments from severing proteins and pointed-end depolymerisation by binding along the length of the filaments and competing with actin depolymerising factor (ADF)/cofilin for actin binding (Ono & Ono, 2002) (fig. 19). This suggests that a decreased level of TPMs, as seen in the FH patient samples, could lead to increased binding of ADF/cofilin to actin filaments, leading to its depolymerisation. Additionally, TPMs interact with many different actin-binding proteins, forming protein complexes with actin that contribute to maintaining normal cell function (Brettle, Patel & Fath, 2016). This is supported by the STRING analysis where the PPI figure illustrates that TPM4 interacts with THBS1, PFN1 and TLN1, which are the other actin-associated proteins in the DEPs. Considering that the actin cytoskeleton is the predominant cytoskeletal structure in postsynaptic neurons in the brain, its constant remodelling and crucial regulation of its

dynamics is vital for the correct functioning of excitatory synapses in the brain which is important during memory and learning (Guven, Gunning & Fath, 2011), both of which are disrupted in AD. While there are very limited papers investigating TPM4 specifically being involved in FH or AD, its functional role in actin polymerisation regulation indicates that it could be implicated in diseases that show detrimental effects when the regulation of the actin cytoskeleton is disrupted.

In addition to proteins that regulate the actin cytoskeleton directly, there were two downregulated proteins that have roles in connecting the actin cytoskeleton to the plasma membrane, Thrombospondin-1 (THBS1) and talin-1 (TLN1). These two proteins had a 1.63- and 1.56-fold decrease (respectively) in protein levels in the FH patient samples. THBS1 is a glycoprotein that mediates cell-to-cell and cell-to-matrix interactions where it has been implicated in many functions including cell migration, apoptosis, immune response and angiogenesis (Taraboletti, Roberts & Liotta, 1987; Good et al., 1990; Guo et al., 1997). Studies have found that THBS1 has a role in the pathogenesis of metabolic diseases, such as obesity, diabetes and cardiovascular disease (Gutierrez & Gutierrez, 2021). The role of THBS1 in cell metabolism could be why there was a dysregulation observed in the FH patient samples. In the brain, thrombospondins are secreted by astrocytes and perform their known function in modulating synaptogenesis and neurogenesis (Son et al., 2015) due to their ability to mediate cell-to-cell interactions. A study by Risher and colleagues found that loss of the THBS1 receptor led to significant deficits in synapse number and structure in the mouse brain (Risher et al., 2018). Interestingly, another study found that THBS1 expression was decreased in AD brains and that Aβ-mediated reduction of synaptic proteins and related signalling pathways was mitigated by the intrasubicular injection of THBS1 into AD mouse brains (Son et al., 2015). Moreover, THBS1 was also found to inhibit Aβ-induced mitochondrial fission in Aβ-treated mouse hippocampal neuroblastoma cells, where the protein appeared to improve mitochondrial dynamics and functions after Aβ treatment (Kang et al., 2018). This suggests that the downregulation of THBS1 could be a factor in AD pathogenesis.

Compared to THBS1, TLN1 has a more focused function as a cytoplasmic adapter protein capable of directly connecting the actin cytoskeleton to integrins. In addition to its three known actin-binding sites, TLN1 also has binding sites for many proteins, mostly those that also bind actin (Franco-Cea et al., 2010), as seen in the PPI network (fig. 8). This property allows TLN1 to act as an essential linker protein forming cytoplasmic adhesion complexes that link the transmembrane

adhesion receptor and integrin proteins to the cytoskeleton (Camp et al., 2024) (fig. 19). Additionally, by linking integrins to actin, TLN1 also mediates the conversion of mechanical signals into biochemical signals, which may influence disease progression (Wang et al., 2024). This idea has been investigated in AD, where a study found that TLN1 can bind to amyloid precursor protein (APP) due to APP possessing the same cytoplasmic motif as integrins, creating an APP/TLN1 complex at the cell membrane (Ellis et al., 2024). The authors found that APP forms an extracellular meshwork that can exert mechanical signals to cells. Hence, the APP/TLN1 complex can mechanically couple the cytoskeletons of pre- and post-synaptic neurons. Additionally, the authors proposed that APP processing (which can lead to amyloidogenic products as discussed in the introduction) may also be influenced by a mechanical signalling pathway, whereby under tension, the cleavage sites in APP may have varying accessibility to the respective secretases responsible for its processing. This was further supported by the same authors who found that TLN1 silencing in HEK293-APP 695WT cells caused an accumulation of APP processing products from alpha-, beta- and gamma-secretases, and hence includes Aβ production. Considering that TLN1 was significantly reduced in the FH patient samples, in addition to influencing APP processing through elevated LDL levels influencing lipid raft formation (as discussed in the introduction), the dysregulation of TLN1 in FH patients could also be implicated in APP processing, especially in the brain environment, as seen in this very recent and interesting study (Ellis et al., 2024). These papers indicate that more researchers are investigating the roles of these perhaps often-overlooked cytoskeletal proteins in neurodegenerative disorders and other disease states.

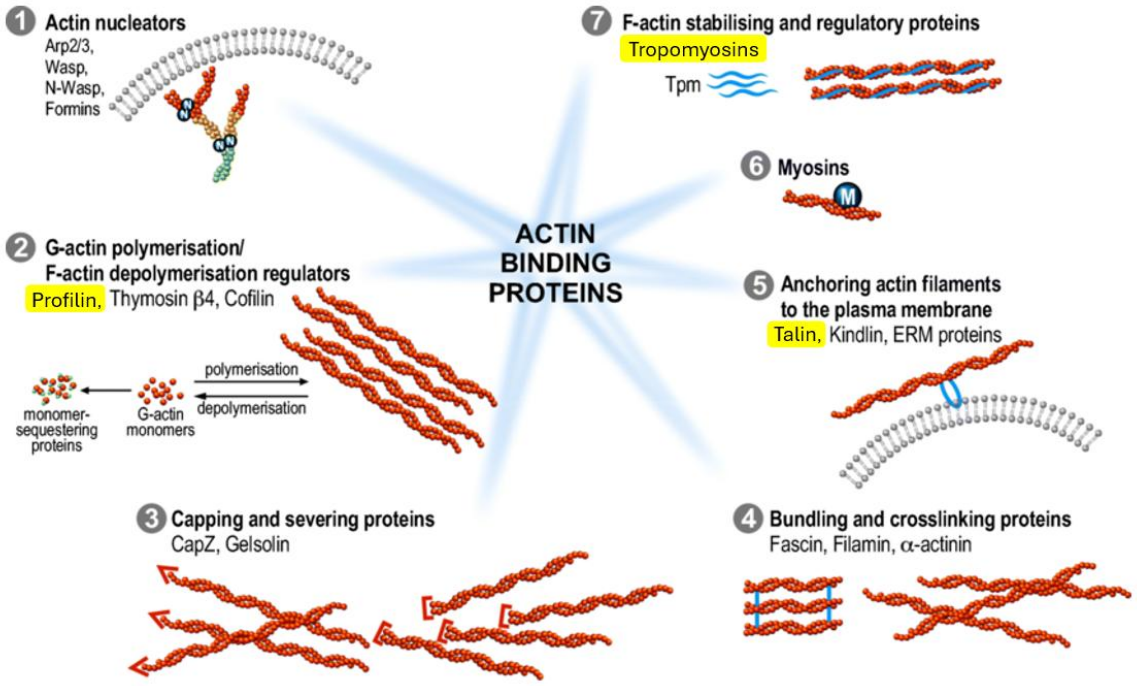


Figure 19: An overview of the main families of actin-binding proteins.

Actin-binding proteins can be divided into seven groups according to their functions on actin polymers and/or monomers. Highlighted in yellow are the actin-binding proteins that were found dysregulated in the FH patient dataset, namely, Profilin (2 – G-actin polymerisation/F-actin depolymerisation regulators), Talin (5 – Anchoring actin filaments to the plasma membrane) and Tropomyosin (7 – F-actin stabilising and regulatory proteins). Thrombospondin (not illustrated) was also dysregulated, with functions including the modulation of actin dynamics and influencing cell-cell and cell-matrix interactions. This diagram highlights a broad disruption of actin cytoskeletal dynamics in the FH patient dataset. Adapted from Ruggiero & Lalli (2021).

5.1.1.5 - Pathway Enrichment Analysis of Cytoskeletal Dysregulation

The importance of the cytoskeleton in disease is further highlighted in the proteomic results by all of the top 10 enriched pathways from Reactome being matched to the alpha-tubulin and actin proteins downregulated in the FH patients. As discussed, some of these pathways were directly related to tubulin/microtubule folding regulation. The remaining pathways link these proteins to

secondary functions beyond the cytoskeleton, such as modulating cell signalling pathways and gap junctions. The top enriched pathway was “RHO GTPases activate IQGAPs”. This pathway was matched due to the activity of RHO GTPases by the cell membrane, where these cytoskeletal proteins reside. Constituting a family of scaffolding proteins, IQGAPs are actin-binding proteins that integrate multiple signalling pathways and coordinate a wide range of cellular activities such as cell migration and polarity (Watanabe, Wang & Kaibuchi, 2015). Additionally, through its interactions with extracellular signal-regulated kinase 2 (Erk2) and B-Raf protein, IQGAPs function as a scaffold for the mitogen-activated protein kinase (MAPK) pathway, an essential pathway in cell proliferation, differentiation and death (Roy, Li & Sacks, 2005; Ren, Li & Sacks, 2007). However, the more prominent role of IQGAPs is in forming cell-cell adhesions by binding to E-cadherins and β-catenins (Brandt & Grosse, 2007). Although Reactome does not specify the exact implications of the dysregulation of actin and alpha-tubulin proteins on this pathway, it is clear that a disruption of the regulation of this multifaceted protein could be very detrimental to cells. The expression and activity of IQGAPs in the brain have also been linked to proper neuronal proliferation and migration, where its facilitation in actin cytoskeletal dynamics is required for correct neurite growth essential for synapse formation, plasticity and overall neuronal communication (Hedman, Smith & Sacks, 2015). Furthermore, the ability of IQGAPs to integrate multiple signalling pathways suggests that they play a critical role in neuronal development and potentially, in neurodegenerative processes.

Adding to the common theme of cell-cell adhesions, four of the top ten enriched Reactome pathways are related to gap junction formation, trafficking and regulation (table 7). Gap junctions consist of connexins, which form hexamer channels called connexons at the cell membrane, allowing the passage and exchange of small ions and molecules between the cytoplasm of neighbouring cells (Goodenough & Paul, 2009). The Reactome pathways highlight a dysregulation in the microtubule-dependent trafficking of connexons from the Golgi apparatus, where they are assembled, to the plasma membrane. Considering the significant downregulation of the alpha-tubulin proteins in the FH patients, this would imply that there could be a resulting disruption in this trafficking system, as highlighted by the 4 pathways in Reactome. This speculation is evidenced by a study that has shown that the use of a microtubule-disrupting agent abolished the motility of connexin-transporting vesicles, thus proving the reliance on microtubules for their delivery to the cell membrane (Fort et al., 2011). Additionally, the KEGG pathway enrichment

analysis from ShinyGO v0.8 (fig. 9A) identified “Gap junction” as the highest enriched pathway. Moreover, its location at the centre of the hierarchical clustering tree correlating the enriched pathways implies that this disruption in gap junction trafficking could have detrimental implications on many diseases, especially neurodegenerative diseases (e.g. AD, Parkinson's disease and Huntington's disease) as seen in figure 9B. Since gap junctions allow the direct exchange of ions and molecules between cells, they are known as electrical synapses in the brain, important for the rapid communication and synchronisation of electrical discharges in pre- and post-synaptic neurons (Purves et al., 2001). It is well-evidenced that gap junction dysregulation contributes to neurodegeneration (Nakase & Naus, 2004; Huang et al., 2021), particularly in AD, where it has been found that reduced connectivity of astrocyte-oligodendrocyte gap junctions, may contribute to AD progression by impairing oligodendrocyte homeostasis and myelination (Angeli et al., 2020). Hence, a disruption in gap junction trafficking and regulation could be another plausible link between FH and AD, and further research should be done on this topic in FH.

Another cell-adhesion-related pathway enriched in the FH patients was the “Recycling pathway of L1”. Interestingly, L1 is a cell adhesion glycoprotein that belongs to the immunoglobulin supergene family that is predominantly expressed in the brain, compared to the rest of the body, where it plays many important roles in neuronal migration and differentiation, axonal outgrowth and guidance, myelination and synaptic plasticity (Cotman et al., 1998; Sytnyk, Leshchyns’ka & Schachner, 2017). These functions require coordination between L1 and the actin cytoskeleton. The physiological recycling of L1 is a dynamic process involving exo- and endo-cytosis and allows for the rapid renewal of L1 adhesions necessary for its many functions (Dequidt et al., 2007). This Reactome pathway shows that the downregulation of the actin and alpha-tubulin proteins disrupts the recycling of L1 at the cell membrane, specifically affecting the movement of the clathrin-coated endocytic vesicles and endosomes. Although there are limited studies that address the direct implications of disrupting this recycling pathway, there are studies that show its involvement in disease. In AD, it was found that the recycling pathway of L1 interacts with autophagy mechanisms and the ubiquitin-proteasome system (a complex process that regulates protein homeostasis and trafficking in cells), where through this interaction, L1 may facilitate the transport of Aβ to autophagosomes for degradation (Loers, Bork & Schachner, 2024). Considering its predominant role in the brain, it is interesting that this pathway was enriched in the FH patient samples, posing

an opportunity for further investigation into the role of altered cholesterol metabolism in this pathway and the implications thereof.

Lastly, the tenth pathway enriched in this proteomic dataset was the "Activation of AMPK downstream of NMDARs". N-methyl-D-aspartate receptors (NMDARs) are ligand-gated cation channels that are activated by an excitatory neurotransmission in the central nervous system (Hansen et al., 2017). These receptors are critically involved in modulating synaptic plasticity, learning and memory. The activation of NMDARs initiates an influx of calcium and sodium ions into the neuron, which initiates a series of signalling cascades, including the activation of adenosine monophosphate-activated protein kinase (AMPK) (Stahmann et al., 2006). This Reactome pathway was matched to the dysregulated alpha-tubulin proteins, as they are involved not only in the stabilisation of NMDARs at the cell membrane, but also in mediating the signalling cascade whereby AMPK is phosphorylated by calcium/calmodulin-dependent protein kinase kinase (CaMKK) with ATP used as a phosphate source (Woods et al., 2005). Many studies have shown that AMPK signalling is important in maintaining energy balance as it is activated by a rise in the AMP:ATP ratio in cells (Woods et al., 2005; Salminen & Kaarniranta, 2012). The associations of these enzymes and ATP are all mediated by microtubules, and hence a dysregulation of the alpha-tubulin proteins (which were matched to this pathway in Reactome) could disrupt this signalling cascade and could also contribute to the FH phenotype, which exhibits altered energy metabolism. In the context of AD, the role of AMPK activity remains unclear. While some studies have found that AMPK activation can cause a decrease in mTOR signalling, which in turn facilitates autophagy and lysosomal Aβ degradation (Cai et al., 2012), others have found a relationship whereby AMPK activity is increased due to Aβ-NMDAR-dependent mechanisms (Thornton et al., 2011). This latter study found that Aβ42 could interact with NMDARs, leading to activation of CaMKK and AMPK, which correlated with an increase in tau phosphorylation (Thornton et al., 2011). These studies illustrate a context-dependent relationship between NMDAR activation, AMPK signalling and AD pathology. It is possible that AMPK activity could initially be a protective mechanism to counteract metabolic disturbances in AD, however, excessive activation could contribute to tau phosphorylation and Aβ production (Salminen et al., 2011). Overall, further research is needed to elucidate this relationship, as well as the role of altered cholesterol metabolism, as seen in FH, and a disruption in microtubule regulation.

Since the cytoskeleton can connect multiple cellular compartments, mediate cell-cell and cell-matrix communication and influence cell signalling pathways, it is imperative to develop an in-depth understanding of the factors and surrounding proteins involved in cytoskeletal dynamics and homeostasis as evidence already illustrates that even when a single component of this intricate system becomes dysregulated, it can create a cascade of reactions that can result in disease. Currently, there is limited research investigating these specific proteins in hypercholesterolemic disease states. The results of this proteomics study have shown that there could be a significant dysregulation of the cytoskeleton in FH, involving the fundamental cytoskeletal proteins, keratin-2, actin and alpha-tubulin, as well as multiple regulatory proteins with which they interact. As discussed, many of these proteins have also been implicated in the pathogenesis of AD. This overlap suggests a potential link between FH and AD, offering new avenues for exploring shared molecular mechanisms underlying these conditions. By shedding light on these under-investigated proteins, this study contributes to a deeper understanding of their relevance and highlights the need for further research into their dual roles in lipid metabolism disorders and neurodegeneration.

5.1.2 - Dysregulated proteins in oxidative stress and antioxidant defence

As discussed in the introduction, oxidative stress is a key factor that occurs in both FH and AD, presenting as a possible link between the two diseases. Unsurprisingly, the proteomics data revealed the dysregulation of a few proteins involved in the oxidative stress response and antioxidant system. The proteins that are directly involved in these systems include glutathione S-transferase P (GSTP1) and haptoglobin (HP) which were downregulated, and extracellular superoxide dismutase (SOD3) which was upregulated. Other DEPs also have roles in oxidative stress, but these will be discussed in the inflammation and immune regulation section, where their primary roles are involved.

Glutathione S-transferase P (GSTP1) is an enzyme that plays an important role in the cellular antioxidant system where it functions in catalysing the conjugation reaction of glutathione to electrophiles in cells (Keen & Jakoby, 1978). Having such an integral role in oxidative stress regulation, GSTP1 is widely expressed, with especially high expression in the brain (Berhane et al., 1994). In addition to its direct role in removing ROS, it is also involved in multiple signalling pathways where a knockdown of GSTP1 has been shown to elevate oxidative stress and result in

altered phosphorylation activity of c-Jun N-terminal kinase (JNK), extracellular signal-regulated kinase (ERK), mitogen-activated protein (MAP) kinases and NF-κB signalling, all leading to the increased expression of apoptosis-promoting genes (Singh et al., 2020). The FH patient samples had a 2.28-fold decrease in GSTP1 levels compared to healthy controls. Considering the important functional roles of GSTP1, this could result in elevated oxidative stress as well as dysregulation in important cell signalling pathways in FH patients. The top two pathways that have been extensively investigated include GSTP1's inhibitory effects on JNK activity (Liu et al., 2021). The JNK family of protein kinases play central roles in stress signalling pathways involved in cell death, gene expression, neuronal plasticity, regeneration and regulation of cellular senescence (Yarza et al., 2016). These pathways are often activated after exposure to stress factors, such as oxidative stress, cytokines and even Aβ peptides, and its activation has been studied as a key factor responsible for the regulation of apoptosis signals, and hence its overactivation has been implicated in many diseases, including AD (Yan et al., 2024). Thus, being a principal regulator of JNK activity, a downregulation of GSTP1 could not only increase oxidative stress but also enhance JNK activity contributing to increased apoptosis and cellular damage.

This could also explain the KEGG pathway enrichment of "Apoptosis" from ShinyGO v8.0 (fig. 9A). Moreover, GSTP1 also has inhibitory effects on cyclin-dependent kinase-5 (Cdk5) activity, an enzyme that plays a key role in many cellular activities such as membrane dynamics and functions, cell-cell adhesions, wound healing, tissue regeneration and cell survival and apoptosis, among others (Shupp, Casimiro & Pestell, 2017). In the brain, it regulates synaptic plasticity and neuronal survival, playing a key role in memory and learning (Sun et al., 2011). Despite its many important functions, it is well known that Cdk5 is hyperactivated in many disease states such as cancer and neurodegenerative diseases, including AD (Shupp, Casimiro & Pestell, 2017). Recent studies observed that a decrease in GSTP1 levels correlated with an increase in Cdk5 activity in both cancer and neuronal lines and in AD brains (Sun et al., 2011; Shah & Lahiri, 2014), suggesting that even in different tissue types, GSTP1 still acts as a regulator of Cdk5 activity. Hence, the downregulation of GSTP1 is being considered as a possible biomarker for the diagnosis of oxidative stress and disease phenotypes. Even in AD, studies have shown that GSTP1 activity and levels are reduced in all brain areas of AD patients, where researchers speculate that its downregulation could promote oxidative stress, contributing to AD pathogenesis (Lovell, Xie &

Markesbery, 1998; Wang, 2015). Overall, the reduced levels of GSTP1 in the FH patients could highlight a possible pathway behind the role of oxidative stress in linking FH and AD.

Another antioxidant protein that was downregulated in the FH patient samples was haptoglobin (HP). Produced by the liver to get rid of free hemoglobin in the blood, HP is predominantly found in the vascular system where it also has roles in antioxidant and anti-inflammatory activities (Bertaggia et al., 2014). Although the change in HP levels was slight (1.51-fold decrease) compared to healthy controls, this protein presented as a connection point between many of the other proteins, as it had the second-highest number of interactions (8 interactions) in the PPI network from STRING (fig. 8). Considering its primary location in the blood, it makes sense that the proteins that it interacts with are mainly involved in the inflammatory response (e.g. S100A9, SAA2, SAA1 and MPO). There are limited studies that look into the association of HP and serum LDL levels, however, studies have shown that HP could act as an antioxidant in the prevention of LDL oxidation (Bernard et al., 2003), a phenomenon critical to the pathogenesis of many metabolic diseases including atherosclerosis and FH (Manzoor et al., 2022). The mechanism behind the antioxidant effect of HP involves its function in removing hemoglobin from the bloodstream, as free hemoglobin is known to have pro-oxidant properties where it undergoes auto-oxidation and produces hydrogen peroxide and superoxide. This can then lead to the oxidation of other small molecules present in the bloodstream and promote oxidative stress (Miller, Altamentova & Shaklai, 1997; Rifkind, Mohanty & Nagababu, 2015). Thus, a downregulation of HP could promote hemoglobin-mediated oxidative stress mechanisms. These proteomic results highlight a possible mechanism that contributes to the oxidative stress state in FH patients, particularly concerning LDL oxidation. In terms of how HP downregulation could relate to AD, studies have shown that AD patients exhibit increased levels of HP both in blood plasma and various brain regions (Song et al., 2015; Philbert et al., 2021). This elevation is associated with a microvasculopathy that involves erythrocyte leakage and is speculated to be a compensatory response to oxidative stress and inflammation in the brain. Thus, the detection of elevated HP in AD patients could be dependent on the stage and progression of the disease at the time of sampling. Nonetheless, the role of HP in oxidative stress regulation is worth investigating further.

In contrast to HP, the antioxidant protein superoxide dismutase 3 (SOD3) was upregulated (1.95-fold increase in protein levels compared to controls) in the FH patient samples. SOD3 is an

extracellular enzyme known for its principal function in maintaining redox balance by detoxifying reactive nitrogen species and ROS by catalysing the conversion of superoxide anion free radicals into oxygen and hydrogen peroxide (Chidambaram et al., 2024). This antioxidant enzyme is expressed in many cells, but particularly by fibroblasts in vascular tissues, hence it is predominantly found on cell surfaces and in the extracellular matrix (ECM), where it displays a high affinity to ECM proteins such as collagen and heparin sulfate proteoglycans (Nguyen et al., 2004). Thus, it has also been observed that SOD3 inhibits the oxidative damage of these ECM proteins (Kliment et al., 2008; Yao et al., 2010), further highlighting its critical role in antioxidation in the body. Another important antioxidant function of SOD3 is to regulate nitric oxide (NO, vasodilator) bioavailability (Pineda et al., 2001). This implicates SOD3 in playing a crucial role in vascular function, where dysregulation of NO contributes to disease states such as atherosclerosis (Fukai et al., 1998; Fukai, 2002). Free NO participates in a spontaneous reaction with superoxide to form the highly reactive peroxynitrite anion ($ONOO^-$). Studies have shown that SOD3 prevents the pro-oxidant reactions of $ONOO^-$, such as lipid peroxidation and protein nitration of surrounding molecules, which leads to many disease states (Zachariae, Hu & Petersen, 2020).

Overall, SOD3 is a key modulator of oxidative stress, and its upregulation in the FH patients suggests an elevated oxidative stress environment in the FH patients, where its upregulation could be a compensatory mechanism against excess ROS and other reactive species in these patients. This is plausible considering the STRING analysis indicating that the highest shared GO molecular function amongst the DEPs is “antioxidant activity” (fig. 7), as well as the PPI network (fig. 8) showing an interaction between GSTP1 and SOD3, the two primary proteins directly involved in antioxidant activity. Furthermore, studies have shown that SOD3 overexpression in cells exposed to oxidative agents leads to a decrease in ROS levels and improved cell viability (Yang et al., 2016, 2017). These studies also found that SOD3 influences the expression of apoptosis-related genes, reducing markers such as cytochrome c and caspases, which are critical in the apoptotic process, further illustrating the importance of this protein in maintaining cell health. Albeit at lower levels compared to other SOD proteins, SOD3 is also expressed in the brain, in both intra- and extra-cellular spaces and particularly in regions such as the hippocampus (Zou et al., 2009), the region responsible for memory and learning, and the region most affected in AD. This suggests that its presence could be important in reducing oxidative stress in the brain. However, while primarily an antioxidant, SOD3 has also been investigated as having potential prooxidant properties due to its

role in hydrogen peroxide generation (Zachariae, Hu & Petersen, 2020). This duality suggests that the context of SOD3 elevation is crucial in determining its overall impact on cellular health and disease states.

The upregulation of SOD3 alongside the downregulation of HP and GSTP1, suggests a complex and potential compensatory response to oxidative stress in FH patients. While SOD3 elevation could indicate an adaptive mechanism to mitigate excessive ROS in the hypercholesterolemic environment, the concurrent downregulation of HP and GSTP1, which are critical for detoxifying ROS and reducing oxidative damage, might reflect an overall impaired antioxidant capacity in these patients. All three proteins also matched the enriched STRING GO biological processes, "Response to reactive oxygen species" and "Response to oxidative stress," further highlighting the central role of oxidative stress in this condition. This context implies that while SOD3 elevation may initially act as a protective mechanism, its prooxidant potential through hydrogen peroxide generation could exacerbate oxidative damage if not adequately neutralised by downstream antioxidant systems. This imbalance in oxidative stress regulation may contribute to cellular dysfunction and increased vulnerability to oxidative damage in FH patients, linking it to the pathogenesis of diseases like AD, where oxidative stress is a well-documented hallmark (as discussed in the introduction).

5.1.3 - Dysregulated proteins in inflammation and immune regulation

Inflammation and immune regulation play an important role in the pathology of FH, where cholesterol accumulation in macrophages and immune cells promotes inflammatory responses (Tall & Yvan-Charvet, 2015b). Contrary to this, the proteomic analysis of the FH vs control dataset found most of the inflammation- and immune-associated proteins to be downregulated in the FH patients. One possible explanation is that some FH patients may be on anti-inflammatory medications, which could influence protein expression levels of these inflammatory markers. Additionally, pathway enrichment analysis using ShinyGO.v0.8 (fig. 9A) highlighted multiple bacterial-related diseases (e.g. *Escherichia coli* infection, *Salmonella* infection, Shigellosis), suggesting that some patients may have had underlying infections at the time of sampling, further complicating the inflammatory and immune profile. Nonetheless, the identified proteins were still differentially expressed and may have potential roles in FH pathology.

Playing dual roles in oxidative stress and immune regulation, myeloperoxidase (MPO) had a 1.58-fold decrease in expression in the FH patients compared to the controls. This protein belongs to the peroxidase subfamily of enzymes and forms part of the host defence system of polymorphonuclear leukocytes, lymphocytes, monocytes and macrophages, where they exhibit antimicrobial activity (Van Der Veen, De Winther & Heeringa, 2009). This is achieved primarily by its production of different reactive oxygen and nitrogen species, where it uses H_2O_2 to oxidise several halides and pseudohalides, and chemically modify important molecules (e.g. Lipoprotein membranes) of pathogens, essentially killing them (Arnhold, 2020). Hence, MPO function plays important roles in both oxidative stress and immune response, which was also highlighted in table 6, where the STRING database matched it to the GO biological processes: "Response to reactive oxygen species", "Defence response to bacterium" and "Response to oxidative stress". Interestingly, MPO is the most abundant pro-inflammatory biomarker in neutrophilic granulocytes, where its enhanced level of activity is often used as the best diagnostic tool for inflammation and oxidative stress in many common diseases, including cardiovascular disease, rheumatoid arthritis and neurodegenerative disorders such as AD (Khan, Alsahli & Rahmani, 2018). This is also the case for hypercholesterolemia, where studies find significant increases in MPO expression and activity in response to high cholesterol (Puntoni et al., 2011). For instance, a study found a 7.2-fold increase in neutrophil MPO expression in a rabbit model of hypercholesterolemia (Liu et al., 2008).

This elevated expression of MPO is speculated to correlate with cholesterol levels as a study found that cholesterol reduction in FH patients led to reductions in MPO expression levels (Puntoni et al., 2011). Considering that elevated MPO expression and activity are also reported in the plasma and brains of AD patients (Green et al., 2004; Tzikas et al., 2014), along with the increased prevalence of its oxidation products, there could be a correlation between the elevated MPO levels in hypercholesterolemic individuals (in response to high cholesterol) initiating the increased MPO levels in AD. Interestingly, a study investigated the effects of MPO deficiency in a mouse model of AD and found that hematological MPO deficiency led to lower inflammatory responses and increased protection against cognitive decline (Volkman et al., 2019), highlighting the potential role of MPO in exacerbating neuroinflammation and cognitive impairment in AD. As mentioned, the downregulation of MPO could be due to secondary effects of other (non-statin) medications

such as anti-inflammatories, where even supplements such as melatonin have also been found to lower MPO levels (Van Der Zwan, Scheffer & Teerlink, 2010).

Another set of proteins that were downregulated in the FH patients was serum amyloid A 1 and 2 (SAA1 and SAA2) with fold decreases of 1.68 and 3.54 (respectively) in the FH patients compared to the controls. These proteins form part of the acute phase response to inflammation, infection or injury, produced primarily by the liver from which it is released to the blood circulation (Kurvits et al., 2019). SAAs have cytokine-like properties that stimulate the production and release of cytokines, chemokines and induce monocyte and neutrophil migration (Jumeau et al., 2019). This aligns with the matched GO biological pathways (STRING), "Acute-phase response", "Platelet activation", "Neutrophil chemotaxis" and "Inflammatory response" (table 6). In addition to its major roles in immune response, SAAs have also been found to modulate cholesterol homeostasis by interacting with lipoproteins, potentially influencing cholesterol transport and metabolism due to its primary biosynthesis occurring at the liver (Frame & Gursky, 2017). Interestingly, a study found that free SAA delays lipoprotein oxidation, exhibiting a mild anti-oxidant effect (Jayaraman, Haupt & Gursky, 2016). Not only is this beneficial against HDL and LDL oxidation, but also for decreasing the pathogenic oxidation of phospholipids and cholesterol in damaged cell membranes. This would suggest that the downregulation seen in the FH patients could contribute to increased vulnerability of the excess LDL to be oxidised, leading to increased oxidative stress and inflammatory response.

In the context of AD, SAA concentration has been found to be much higher in the CSF of AD subjects compared to controls (Chen & Xia, 2020), where studies have also shown that SAA is predominantly localised to Aβ neuritic plaques, axonal membranes and myelin sheaths (Chung et al., 2000). Additionally, a recent study found that SAA inhibits astrocyte proliferation and migration, potentially inhibiting the migration of astrocytes to Aβ plaques (Lin et al., 2020). This study attributed this to the activation of the p38 MAPK signalling pathway and SAA inhibitory effects on actin and microtubule reorganisation in astrocyte protrusions. This interplay between SAA, a major acute phase protein, and the cytoskeletal network in astrocytes is interesting and supports the STRING PPI network (fig. 8) which illustrates an interaction between SAA1 and SAA2 to ACTB, through HP, which is also involved in mitigating lipid oxidation, a seemingly shared function of HP and SAAs. These results could indicate a potential role for SAA in

cytoskeletal remodelling within astrocytes, particularly in the context of neuroinflammation. The implications of this cytoskeletal remodelling in astrocytes involve the potential to impair Aβ clearance, which is predominantly regulated via astrocytes (Fong et al., 2018). This would suggest that elevated SAA levels, which have been found to inhibit astrocyte proliferation and migration, could contribute to Aβ plaque formation, making SAA depletion a therapeutic strategy. However, SAA deficiency, which has been shown to elevate the activation of astrocytes in the brain of AD mice (Lin et al., 2020), could also be detrimental as evidence shows that overactivation of astrocytes enhances neuroinflammation and can contribute to Aβ plaque formation (as discussed in the introduction) (Perez-Nievas & Serrano-Pozo, 2018). Overall, these findings highlight the complex and potentially dual role of SAAs in inflammation and AD pathology and underscores the need for further investigation into whether the dysregulation of SAA1 and SAA2 expression in FH patients could be implicated in AD pathogenesis.

Also contrary to current literature, S100A9 was downregulated in the FH patients with a 2.35-fold decrease in these patients compared to controls. S100A9 is a calcium- and zinc-binding protein, highly pro-inflammatory and classified as a damage-associated molecular pattern (DAMP) molecule with prominent roles in the regulation of inflammatory processes and immune response (Chen et al., 2015). It can stimulate neutrophil migration and adhesion, enhance their bactericidal activity by promoting phagocytosis through the activation of PI3K/AKT and ERK1/2 pathways, and trigger neutrophil degranulation via a MAPK-dependent mechanism (Wang, Song, et al., 2018). These functions align with the GO biological processes, “Neutrophil chemotaxis”, Defence response to bacterium”, “Humoral immune response” and ”Inflammatory response”, with which S100A9 was matched to. In hypercholesterolemic conditions, which is the highest risk factor for atherosclerosis, the deficiency of S100A9 has been seen to reduce atherosclerotic lesions (Averill et al., 2011). Evidence has shown that S100A9 interacts with receptors for advanced glycation end products (RAGE receptors), which trigger pro-inflammatory pathways that exacerbate endothelial dysfunction and promote atherosclerosis (Ehlermann et al., 2006). As discussed in the introduction (section 1.3.5), endothelial dysfunction can contribute to AD by impairing cerebral blood flow, disrupting the BBB and promoting neuroinflammation.

In AD, S100A9 has been shown to be at similar levels to Aβ in the CSF (Wang, Iashchishyn, et al., 2018), speculated to be due to its own amyloidogenicity, where it can self-assemble into amyloids

which may lead to an acquired amyloid cytotoxicity (Iashchishyn et al., 2017). Thus, it is speculated that the rising S100A9 levels during inflammation may lead to its amyloid formation that can trigger and aggravate Aβ amyloid fibrilisation, further enhancing amyloid cytotoxicity in AD (Zhao et al., 2013; Wang, Klechikov, et al., 2014). Thus, it is clear that the elevated levels of S100A9, both in response to and as a trigger of inflammation, can contribute to the pathogenesis of both hypercholesterolemic conditions and AD. However, in this study, the proteomic results found S100A9 to be downregulated and not upregulated, which would imply that there was limited inflammation in the FH patients, which contrasts with current literature stating otherwise. Given S100A9's involvement in both hypercholesterolemia and AD, further investigation is needed to determine whether its downregulation in these FH patients reflects a protective response, a disease-specific adaptation, or an effect of external factors such as medication use.

Similarly, the elevation of another acute-phase protein, serum amyloid P component (APCS) has also been found to potentially contribute to AD pathology, where it promoted the deposition of amyloid, prevented its proteolysis and stabilised amyloid plaques *in vitro* (Hamazaki, 1995; Tennent, Lovat & Pepys, 1995). This protein was found downregulated in the FH patients (1.59-fold decrease). Having matched to the GO biological processes, "Acute-phase response" and "Inflammatory response", APCS is a key mediator of the innate immune response, binding to pattern-recognition sequences on microbes and recognising cell damage (Du Clos & Mold, 2011), which activates the complement activation cascade, and hence inflammation (Sjöberg et al., 2006). Thus, it has been recently proposed that APCS and its protein family (pentraxins) may be a possible mediator between chronic inflammation and AD, as studies have shown that APCS deposition on NFTs occurs prior to complement activation which could initiate local inflammation (Veerhuis, 2011). This implies that elevated APCS levels would be detrimental in the context of AD.

In contrast, studies have shown APCS to have an anti-atherosclerotic role by binding to lipoproteins and facilitating cholesterol efflux from macrophages, which is critical in preventing macrophage to foam cell formation (Xi et al., 2018). Hence, a downregulation in APCS, as seen in the proteomic analysis of the FH patients, could be detrimental in the context of hypercholesterolemia, as reduced APCS levels may impair its protective role in foam cell prevention. If this downregulation observed in this study is not due to possible external intervention, then the possible increase in foam cell formation would result in the subsequent

increase in endothelial dysfunction, oxidative stress and inflammation (Gui, Zheng & Cao, 2022), which have all been shown to contribute to AD pathogenesis (Estudillo et al., 2023; Tucker et al., 2023). Hence, while there may not seem to be a direct link between the downregulated APCS in FH and AD initially, there may be further long-term consequences which may be worth investigating.

Similarly, while platelet factor 4 variant (PF4V1) elevation correlates with heightened inflammatory markers in hypercholesterolemic patients (Ferroni, Basili & Davi, 2003; Bhatnagar et al., 2012), PF4V1 elevation is being investigated as a therapeutic strategy against AD where it has been found to enhance synaptic plasticity, restore cognitive deficits and reduce inflammation (Schroer et al., 2023; Sun et al., 2025). PF4V1 is a chemokine released upon platelet activation (a GO biological process to which it was matched, alongside "Neutrophil chemotaxis" and "Inflammatory response"; table 6) that primarily functions as an inhibitor of angiogenesis (Lakka Klement, Shai & Varon, 2013). This protein had a 2.21-fold decreased expression in the FH patients compared to the controls, which contrasts existing literature which found increased PF4V1 levels, as well as decreased angiogenesis in FH patients, although the latter has also been reported to be due to LDL-mediated inhibition of endothelial proliferation (Bogachkov et al., 2020). Given its proposed protective role in AD, the decreased PF4V1 levels could indicate a reduced capacity to counteract neurodegenerative mechanisms, particularly in the context of impaired angiogenesis and endothelial dysfunction.

The last immune-associated protein that was downregulated (1.80-fold) in the FH patients was immunoglobulin heavy constant gamma 4 (IGHG4) which forms part of the immunoglobulin G (IgG) subclass of antibodies and is involved in antigen binding, antibacterial humoral response and complement activation ("IGHG4 immunoglobulin heavy constant gamma 4 (G4m marker) [Homo sapiens (human)] - Gene - NCBI", n.d.). Interestingly, this protein was not identified in the STRING database, and there is little to no literature that has investigated its specific role in any AD or hypercholesterolemic context. However, given the increasing recognition of immune dysfunction in both FH and AD, the downregulation of IGHG4 could highlight alterations in humoral immune responses. This could impair immune surveillance and contribute to altered inflammatory balance, both of which are prominent in the progression of FH and AD. However, contrary to IGHG4, there were seven immunoglobulin proteins (table 4) that were upregulated in

the FH patients. Although there were seven of these immunoglobulins that were differentially expressed, only IGHD and IGHV3-43D were identified by the STRING database, where they were completely disconnected from the other proteins in the PPI network (fig. 8) and matched to the following GO biological processes (table 6): “Complement activation, classical pathway”, “Phagocytosis engulfment”, “Defence response to bacterium”, and “Humoral immune response”. This could be due to the other variables reflecting antigen-specific responses to possible bacterial infections, which were detected in the pathway enrichment analysis using ShinyGO v0.8 (fig. 9).

While the upregulation of the immunoglobulins in the FH patients could be related to possible infections in the patients, this observation is supported by literature which states that hypercholesterolemia is linked to increased levels of immunoglobulin production against oxidised lipoproteins (Zhou et al., 1998; Khoo et al., 2015). In the context of AD, recent studies have found that higher IgG levels are associated with worse cognitive test outcomes and increased Aβ deposition (Park et al., 2022), however, higher IgM levels were associated with a decreased risk of dementia (Khan et al., 2021), highlighting a complex interplay between the adaptive immune system and AD. Hence, despite the possibility that the oxLDL-induced elevation of immunoglobulins in FH patients could initiate an increased adaptive immune response, leading to increased inflammation and immunoglobulin production extending to the brain, more research is needed to address the implications of the dysregulation of specific immunoglobulins in this context.

In addition to the immunoglobulins, mannose-binding protein C (MBL2) was also upregulated (1.79-fold increase) in the FH patients. MBL2 is a lectin protein that forms part of the innate immune system and interacts with carbohydrates on microbes, activating the complement system (Reveille & Bruce, 2004), as supported by MBL2 matching 6 out of the top 10 GO biological processes, mainly centred on immune and inflammatory processes (table 6). Studies have also shown that MBL2 may promote non-inflammatory sequestration of dying host cells by interacting with exposed structures of late apoptotic and necrotic cells and facilitating their uptake by macrophages (Nauta et al., 2003). The role of MBLs in hypercholesterolemia remains unclear, as some studies found higher serum MBL levels in coronary artery disease patients, suggesting a potential link to cardiovascular risk factors (Meneghetti Da Rosa et al., 2024), while a Mendelian randomisation study reported that higher serum mannose levels do not significantly affect lipid

profiles, suggesting no direct causal relationship between mannose and hypercholesterolemia (Mazidi et al., 2021). Similarly, while higher MBL levels have been found to colocalise with Aβ, to which it can bind, possibly facilitating the activation of local neuroinflammation and immune response (Larvie et al., 2012), studies have also observed lower MBL levels in the CSF of AD patients (Fakruddin et al., 2013). These discrepancies in studies for both hypercholesterolemia and AD indicate that more research is needed before inferences about the contribution of dysregulated MBL2 can be made.

Overall, the proteomic analysis of FH patients leaned towards the downregulation of proteins associated with the innate immune system, including acute-phase response proteins, and the upregulation of multiple immunoglobulins, indicating a possible increased involvement of the adaptive immune response. This shift in immune profile suggests a possible chronic, antibody-driven inflammatory state in FH patients, potentially driven by persistent lipid dysregulation and prolonged immune activation. However, it must be noted that there could have been external interference (such as infections, medications etc.) that could have heavily affected the immune profile of these patients. Furthermore, factors such as cohort age, population dynamics and lifestyle, may have influenced the immune-related protein expression in these FH patients. Since the FH cohort had a wide age range (7 to 50 years old), differences in immune system maturity and responsiveness may have contributed to variations in protein expression, where younger individuals typically have more robust immune responses compared to older individuals who typically experience immunosenescence and chronic-low-grade inflammation (Wu & Meydani, 2008). Additionally, genetic and environmental differences between populations may result in distinct immune regulation patterns that do not fully align with previous studies. Lifestyle factors such as diet, physical activity and smoking can also modulate systemic inflammation (Monye & Adelowo, 2020), potentially affecting the observed protein expression profiles. Nonetheless, these results highlight the complexity of inflammatory responses in hypercholesterolemia and AD, suggesting that while chronic inflammation is widely recognised as a driver of disease pathology, specific inflammatory mediators may be differentially regulated under certain conditions. In the end, these results emphasise the need for further research into the interplay between acute-phase proteins, lipid metabolism, and neuroinflammation, particularly in relation to FH and its implications for AD risk.

5.1.4 - Dysregulated proteins in metabolism and energy regulation

There were three DEPs within the FH vs control dataset that were categorised to have primary functions relating to metabolism and/or energy regulation. These proteins were, carbonic anhydrase 1 (CA1), ATP-binding cassette sub-family F member 3 (ABCF3) and aldolase B (ALDOB), which were all downregulated in the FH patients. While there are no studies that look at the direct relationship between CA1 and hypercholesterolemia, its function in the reversible conversion of carbon dioxide to carbonic acid might have indirect effects on cholesterol homeostasis. A dysregulation of CA1 expression can result in the imbalance of blood pH and ion homeostasis, which can disrupt many physiological processes such as electrolyte secretion, gluconeogenesis and lipogenesis, among others (Occhipinti & Boron, 2019). Interestingly, studies have shown that carbon dioxide levels can modulate cholesterol metabolism as carbon dioxide triggers SREBP2 activation through changes in endoplasmic reticulum membrane cholesterol levels (Bolshette et al., 2023). As mentioned in section 1.4.2 of the introduction, the SREBPs are transcription factors that activate the expression of key genes, such as HMG-CoA reductase (which statins inhibit) and other enzymes in the cholesterol biosynthesis pathway, as well as LDLR for increased extracellular cholesterol uptake (Madison, 2016). Hence, there could be an interplay between CA1 dysregulation and cholesterol and fatty acid synthesis and uptake.

In AD, studies have shown that CA levels are significantly increased in the plasma of AD patients (Jang et al., 2010) where they are said to disrupt the multicellular neurovascular unit of the CNS. This unit is involved in the regulation of cerebral blood flow, delivery of oxygen and nutrients, barrier functions and CNS homeostasis (Lemon et al., 2021). Hence, CA inhibitors have been widely investigated as a therapeutic strategy for AD, where studies have reported decreased hyperphosphorylated tau and neuronal cell loss in AD mice models treated with CA inhibitors, due to the improved regulation of lysosomal acidification, promoting lysosomal exocytosis (Lopez et al., 2024). Considering the important role of CA1 in many physiological processes which may influence both cholesterol and neurovascular regulation, its dysregulated expression in the FH patients may be worth investigating further.

Although ABCF3 is part of the ATP-binding cassette (ABC) transporter family, where ABCA1 (ATP-binding cassette transporter A1) is heavily involved in cholesterol homeostasis by controlling cholesterol export from cells (Ye, Lu & Wu, 2020), the role of ABCF3 specifically is

not heavily investigated in hypercholesterolemia. However, a recent study did show that ABCF3 possesses active ATPase activity (breakdown of ATP) and that cholesterol inhibited this activity, potentially dysregulating ATP hydrolysis and hence, energy homeostasis (Peterson et al., 2019). This suggests that elevated cholesterol levels in FH patients could impair ABCF3 function, potentially disrupting cellular energy balance and metabolic processes. Interestingly, ABCF3 was isolated in the STRING PPI network, where it did not have any known interaction with the other DEPs, possibly indicating that it may function independently of the major protein networks identified in this study or that there is a gap in current protein interaction databases regarding ABCF3's functional partners or contribution to metabolic processes. Currently, there is also limited research that investigated the role of ABCF3 in AD, but given the critical role of ATPase activity in various cellular functions, including protein synthesis and immune response, dysregulation of ABCF3 may contribute to broader metabolic dysfunctions that could play a role in AD.

Similarly to ABCF3, the current literature on the role of ALDOB in hypercholesterolemia and AD is limited. ALDOB is an enzyme that breaks down fructose in glycolysis, primarily expressed in the liver, kidney and small intestine (Ahmad & Sharma, 2024). While there are studies on aldolase A being present in brain lysates of AD patients (Mor, Izak & Cohen, 2005), little is known on the specific role of ALDOB, and what its downregulation observed in the FH patients could mean in the context of AD. However, given ALDOB's role in fructose metabolism and its primary expression in metabolic organs, its downregulation may be linked to impaired energy homeostasis or altered glucose-fructose balance. A dysfunction in glucose metabolism is increasingly being recognised as a contributing factor in both AD and hypercholesterolemia, where studies have shown that it can influence lipid synthesis in the liver (Herman & Samuel, 2016) and oxidative stress pathways where fructose accumulation (which could occur when ALDOB is downregulated) can induce oxidative stress and activate inflammatory pathways such as the NF-κB- signalling pathway, where it has particularly been linked to endothelial dysfunction (Baharuddin, 2024). Thus, ALDOB dysregulation in FH patients may indicate broader metabolic disturbances that could contribute to major cellular pathologies, such as oxidative stress, warranting further investigation into its potential mechanistic links. Overall, the downregulation of CA1, ABCF3 and ALDOB in FH patients highlights potential disruptions in metabolic and energy regulation pathways that may influence both FH and AD pathogenesis.

5.1.5 - Statin therapy mitigates hypercholesterolemic-induced changes in proteomic expression

Given that statins are commonly prescribed to FH patients, this study included a comparison of FH patients on statins to assess the potential effects of statin therapy on protein expression related to potential AD-associated pathways. For the cytoskeletal-associated proteins, the proteomic results from the FH vs FH+statin dataset showed that statin therapy increased the expression of ACTB, PFN1, THBS1 and TPM4 compared to the FH patients not on statin medication. Since these proteins were downregulated compared to the controls, this implies that the statin therapy partially restored their expression toward control levels. This aligns with existing literature which has found that statin treatment causes elevated actin polymerisation and increased F-actin content (Sarkar et al., 2022). Interestingly, this effect of statins was only found after chronic cholesterol depletion and not during acute cholesterol depletion, suggesting that these changes are time-dependent. Another study found that statins influenced actin cytoskeletal reorganisation through the inhibition of the ERK-1/2 and p38 pathways which regulate the activity of actin-regulatory proteins such as PFN1 (Han & Kim, 2018), further supporting the results seen in this proteomic analysis. The statin treatment appeared to selectively influence the actin cytoskeleton by increasing the expression of ACTB and proteins involved in its regulation while having no notable effect on the microtubule-associated proteins such as the alpha-tubulin isoforms (TUBA-). However, this could be due to the differential effects of different statins, where lovastatin and mevastatin, in particular, have been found to alter the microtubule system (Fan et al., 2001) whereas simvastatin was predominantly used in the studies that found the actin cytoskeleton to be affected (Sarkar & Chattopadhyay, 2023). Nonetheless, these results imply that statin therapy could mitigate the hypercholesterolemic-induced dysregulation of the actin cytoskeleton in FH patients, which could in turn extend to possible effects regarding the role of the cytoskeleton in neurodegeneration.

Analysis of the oxidative stress-associated proteins found that the FH+statin group exhibited an increase in GSTP1 and SOD3 levels compared to the FH patients not on statin medication. The GSTP1 protein was downregulated in the FH group compared to the control and, hence, implies that the statin therapy increased the protein expression closer to the control levels. Since GSTP1 is important to the antioxidant system, its upregulation in response to statin therapy suggests a potential protective effect against oxidative stress in FH patients. In contrast, SOD3 was found to be upregulated in the FH group compared to the controls but was downregulated compared to the

FH+statin group. This implies that the statin treatment increased SOD3 expression further in the FH patients. A recent systemic review looked at fourteen clinical trials using statin therapy and its effects on oxidative stress, and found that SOD levels were increased in six studies, remained the same in seven and were reduced in one (Daliri et al., 2023). These studies used different statins and measured SOD levels in different mediums (i.e. plasma, venous blood, serum etc.) making it difficult to directly compare them to one another and agree to a single stance on the effects of statins on SOD levels. However, the majority of the studies seem to report on the antioxidant effects of statins and their ability to upregulate SOD expression, where one study found that simvastatin treatment doubled SOD3 activity (Landmesser et al., 2005), specifically, which also highlights that not only is there an increase in expression, but also in functional activity. Overall, these findings suggest that statin therapy may exert beneficial effects on oxidative stress regulation in FH patients by enhancing the expression of key antioxidant proteins such as GSTP1 and SOD3. The observed upregulation of SOD3 in the FH+statin group supports the notion that statins can augment antioxidant defence mechanisms, which could have important implications for reducing oxidative damage associated with FH and its possible relation to AD. However, further research is needed to determine whether these effects translate into long-term clinical benefits for FH patients.

For the inflammation- and immune regulation-associated DEPs, the results found that for all but one of these DEPs, the FH+statin group exhibited a reversible effect of the statin treatment on the expression of these DEPs. The DEPs that were downregulated in both the FH vs control and FH vs FH+statin datasets were S1009A, SAA1, SAA2 and PF4V1, which implies that the statins caused an increase in expression of these proteins in the FH patients. As discussed, the elevation of these proteins is typically associated with an elevated inflammatory profile which may contribute to disease pathogenesis. On the other hand, IGHV3-43D and MBL2 were upregulated in both the FH vs control and FH vs FH+statin datasets, indicating that the statin treatment was decreasing the expression of these proteins in the FH patients. It was only IGHG4 that exhibited a further decrease in expression in the statin-treated FH patients. Interestingly, literature has shown that statins can reduce inflammation in some contexts while also provoking an immune response under specific conditions. Studies have shown that statins can inhibit the NF-κB pathway, which decreases pro-inflammatory cytokine production and enhances anti-inflammatory signalling (Koushki et al., 2021). Many studies also report that statins promote the polarisation of macrophages to the M2 phenotype, which corresponds to an anti-inflammatory response (Sadeghi

et al., 2024). However, in the case of existing infections, a study found that statins enhanced the immune response against *Mycobacterium tuberculosis* by promoting pro-inflammatory cytokine production (Guerra-De-Blas et al., 2019). This highlights the importance of context in determining the immunomodulatory effects of statins, as the effects may vary depending on the current immune environment. The observed results suggest that there is an inflammatory and/or immune-mediated response to statin therapy, however, one cannot conclude whether this is entirely pro- or anti-inflammatory, and what the possible implications of this could mean as a risk factor for AD.

The final DEPs that were also differentially expressed in the FH vs FH+statin dataset were CA1 and ALDOB, which were both downregulated in the FH vs control and FH vs FH+statin groups, indicating that the statin therapy increased the expression of these two proteins. There are limited studies that look at the direct link between statins and CA1 and ALDOB, suggesting that their increased expression could be an indirect effect of statin therapy on metabolic pathways. While there is limited evidence regarding the direct links between statin therapy and these proteins, since ALDOB is involved in fructose metabolism, its increase could reflect improved metabolic function or a compensatory response to altered energy demands in FH patients undergoing statin therapy. Similarly, given the potential influence of CA1 on cholesterol homeostasis through its role in pH balance regulation, its upregulation may also be in response to the broader metabolic adjustments related to the inhibition of cholesterol biosynthesis and the subsequent increase in SREBP2 caused by statin treatment. As mentioned, elevated levels of CA1 have been associated with the disruption in the multicellular neurovascular unit in the CNS of AD patients (Jang et al., 2010), hence, the increase in CA1 expression in the FH+statin group, along with the dysregulation of immune and inflammatory components, raises the question of whether prolonged statin use could potentially contribute to AD progression.

The relationship between statin therapy and AD remains complex, with studies reporting both protective, detrimental and neutral effects, depending on factors such as statin type, dosage and patient characteristics. In the studies that found neuroprotective effects of statins, this has mainly been attributed to the antioxidant and anti-inflammatory effects of statins, as was seemingly observed in this study by the increase in SOD3 expression (Rezakhani et al., 2023). A recent systematic review and meta-analysis illustrated that statins, mainly high-potency statins, had no harmful effects on the neurocognitive function in AD patients (Alsubaie et al., 2022), and similarly,

another study found that statins had neither positive nor negative associations with cognitive function or dementia risk (Murphy et al., 2023). In contrast, other studies have also reported statin-induced cognitive dysfunction and highlighted that there could be a differential effect of statins on cognitive impairment based on whether they are hydrophilic or lipophilic (Zhang, Wen & Zhang, 2018). Due to their increased penetrative capabilities, lipophilic statins have been found to cause greater negative impacts on cognition related to the induction of a pro-inflammatory microenvironment (Kiener et al., 2001), which contradicts the proposed anti-inflammatory effects used to support the neuroprotective effects of statins.

There is debate on whether these effects of statins are due to the prolonged cholesterol depletion or to statin pleiotropy (Butterfield, Barone & Mancuso, 2011), due to the inhibition of HMG-CoA reductase, which is early in the cholesterol biosynthesis pathway and hence, inhibits the production of many downstream molecules, such as isoprenoids and ubiquinone/coenzyme Q10 (CoQ10), which are vital for many cellular activities (Butterfield, Barone & Mancuso, 2011). In fact, the statin-induced reduction of CoQ10 has been reported to impair mitochondrial function and cause oxidative stress and neuronal injury, where Dumont et al. reported on the potential protective effects of CoQ10 in improving cognition and reducing Aβ pathology in a transgenic mice model of AD (Dumont et al., 2011). Hence, despite the increasing evidence linking hypercholesterolemia to AD pathogenesis, there is still a need to investigate the molecular mechanisms and pathways that are implicated in the progression of these diseases, to infer exactly where or how they are linked. Moreover, research is needed to find an effective treatment strategy that not only reduces excess cholesterol but also minimises the adverse effects associated with statin therapy. Squalene synthase inhibitors like SSI present a promising alternative, as they target cholesterol biosynthesis further downstream in the mevalonate pathway, potentially reducing the risk of off-target effects while still effectively lowering cholesterol levels.

5.2 – *In vitro* Investigation Discussion

To further explore the molecular disruptions identified in the proteomic analysis, particularly those related to oxidative stress, mitochondrial dysfunction and ROS production, this study employed an *in vitro* hypercholesterolemic-AD cell model. While proteomic analysis provides valuable insights into dysregulated pathways and protein interactions, investigating these findings at the cellular level allows for a deeper understanding of their functional consequences. This was done by replicating key aspects of the hypercholesterolemic and AD-associated cellular environment to determine whether the proteomics-identified disruptions translate into measurable cellular impairments. Through a series of functional assays, including metabolic activity, ROS detection and mitochondrial DNA copy number analysis, this study assessed the impact of hypercholesterolemic-AD conditions on these cellular markers. Furthermore, by evaluating the potential of squalene synthase inhibition in mitigating these effects, this research provides a mechanistic link between the proteomic findings and cellular responses, offering further insight into potential therapeutic strategies.

5.2.1 - Treatment with SSI is non-toxic and causes significant upregulation of LDLR in HEK293 and SH-SY5Y cells

As a possible statin alternative, this study utilised a squalene synthase inhibitor (SSI) known for its ability to suppress cholesterol biosynthesis and significantly upregulate LDLR expression. To investigate its potential in mitigating the hypercholesterolemic state and its influence on the AD model, HEK293 and SH-SY5Y cells were treated with four concentrations (25 nM, 50 nM, 100 nM and 150 nM) of SSI over 24- and 48-hour periods. These concentrations were selected based on the compound's EC_{50} value of 26 nM (Kerr et al., 2017). Morphological analysis showed that SSI treatment did not induce significant cell death or disrupt the characteristic morphology of either cell line at lower concentrations (25–100 nM SSI) over 24 and 48 hours. Signs of cellular stress, such as cell rounding and shrinkage, were noted only at higher concentrations (100 nM and 150 nM SSI). The MTT assay further supported these findings, showing minimal effects on cell viability at concentrations less than 100 nM after 24 hours. However, at 150 nM, a statistically significant decrease in viability (18.62%) was observed in HEK293 cells, and cytotoxicity became more pronounced after 48 hours. Similarly, SH-SY5Y cells exhibited slight reductions in viability

at 24 hours, with significant decreases (10.16% and 11.78%) occurring at 150 nM for 24- and 48-hour treatments, respectively. While this could be attributed to the DMSO solvent, which caused a significant, although slight (6.31%), decrease in cell viability after 48 hours, the larger reductions observed with SSI treatment suggest additional contributing factors that are caused by SSI itself. For instance, cholesterol depletion has been linked to mitochondrial dysfunction due to compromised membrane integrity and lipid raft stability (Goicoechea et al., 2023), which could contribute to decreased metabolic activity over time. Another potential mechanism could involve off-target effects of SSI, such as interference with intracellular signalling networks that regulate cell survival (Shapira et al., 2021). These results suggest that SSI is generally non-toxic at lower concentrations but may have mild cytotoxic effects at higher concentrations or extended exposure times. Furthermore, *in vivo* studies demonstrated that the compound was non-toxic even with repeated administration over several days (Kerr et al., 2017). While the exact plasma concentration in treated mice was not reported, the 40 mg/kg dose is likely to result in systemic concentrations higher than the cellular EC_{50} of 26 nM, suggesting that the compound remains well-tolerated even at doses exceeding the levels required for cellular activity. Nonetheless, these findings confirmed that the compound is suitable for evaluating LDLR upregulation *in vitro*.

The western blot analysis showed that SSI treatment caused statistically significant upregulation of LDLR in a dose-dependent manner in both cell lines. The highest LDLR expression, 228.85%, was reached in HEK293 cells after being treated with 100 nM SSI for 48 hours. Similarly, significant upregulation of LDLR levels was also observed in SH-SY5Y cells at slightly lower levels, with the highest being 164.69% at 150 nM after 24 hours. Since an increase in both SSI concentration and upregulation of LDLR protein levels are predicted to be linear, understanding the effects of various doses is much easier, thereby making it more useful. Statins have also exhibited a dose-dependent ability to upregulate LDLR (Yang et al., 2012). These findings suggest that the LDLR upregulation observed with both compounds is primarily driven by their cholesterol-lowering effects. By reducing intracellular cholesterol biosynthesis, drugs like statins and SSI indirectly trigger the increased transcription of SREBP2 which then further promotes the transcription of genes involved in increasing intracellular cholesterol, such as LDLR (Madison, 2016). Increased levels of LDLR promote the removal of LDL from the extracellular environment, potentially leading to additional advantages such as lowered risks of LDL-related disorders. The western blot analysis validates the effectiveness of SSI in boosting LDLR expression, a primary

aim of this research, given LDLR's crucial function in regulating cholesterol balance and its potential to alleviate conditions associated with hypercholesterolemia. In the context of AD, research has shown that overexpressing LDLR enhances the clearance of Aβ and reduces its aggregation in the brain through an ApoE-dependent pathway (Kim et al., 2009). Furthermore, a study found that LDLR-mediated clearance of ApoE-containing lipoproteins may indirectly influence tau pathology by altering lipid raft composition and reducing tau hyperphosphorylation (Shi et al., 2021). Beyond Aβ clearance and reducing tauopathy, LDLR upregulation may also help regulate brain lipid homeostasis, which is closely linked to neuronal integrity and neuroinflammation (Corraliza-Gomez, Sanchez & Ganfornina, 2019). This highlights the therapeutic potential of drugs capable of modulating LDLR expression for managing hypercholesterolemia and presenting a promising multi-faceted strategy for mitigating AD-related pathology.

5.2.2 - SSI treatment and the hypercholesterolemic-AD conditions decrease mitochondrial activity but do not significantly affect overall cellular metabolic activity

Mitochondrial dysfunction is a hallmark of both hypercholesterolemia and AD, contributing to increased oxidative stress and impaired bioenergetics that are known to drive amyloid beta production and tau hyperphosphorylation (de Oliveira et al., 2011; Cheignon et al., 2018). Hence, this study assessed mitochondrial function and dynamics to provide insights into the differential responses of mitochondrial and cellular metabolic activity under distinct treatment conditions.

Treatment with SSI alone caused no significant changes in mitochondrial metabolic activity at 24 hours in both cell lines. Still, it showed a moderate (albeit non-significant in the HEK293 cells) reduction at 48 hours, particularly at 100 nM in the SH-SY5Y cells (fig. 14). Although the majority of the results show no significant effect of SSI on mitochondrial and cellular metabolic activity, studies have shown that the inhibition of squalene synthase can actually improve mitochondrial function (Hiyoshi et al., 2003). This is due to the increase in intracellular farnesol, leading to reduced triglyceride biosynthesis. Since SSI inhibits the conversion of farnesyl pyrophosphate (FPP) to squalene, a study found that there is a subsequent increase in the FPP substrate levels (Wasko et al., 2010). These authors saw more than a 20-fold accumulation of FPP in HepG2 cells after 24-hour treatment with a potent squalene synthase inhibitor (9-biphenyl geranyl bisphosphonate). As seen in figure 5 (introduction), there are two pathways for FPP

metabolism, one via the conversion to squalene, and the other results in the formation of many derivatives. One such derivative is the formation of farnesol, which is produced by the hydrolysis of FPP by farnesyl phosphatases (Staines et al., 2004). Notably, triglyceride accumulation is a lesser-known marker of mitochondrial dysfunction, and its reduction by farnesol-mediated inhibition may contribute to improved mitochondrial health (Vankoningsloo et al., 2005).

While the reduction in mitochondrial metabolic activity seen at 100 nM SSI could initially be speculated to be due to the DMSO solvent used to dissolve the compound, the same DMSO percentage used as the vehicle control group did not cause a significant decrease in both mitochondrial and cellular metabolic activity. Another reason for the 16.35% reduction in mitochondrial activity from 48-hour treatment with 100 nM SSI in the SH-SY5Y cells could be due to the inhibition of squalene biosynthesis. Animal studies in ageing mice have found that squalene is important in maintaining key enzymes involved in the tricarboxylic acid (TCA) cycle and respiratory chain, such as NADH-, succinate- and isocitrate- dehydrogenases (Buddhan et al., 2007; Obulesu et al., 2014). This maintenance is important to preserve mitochondrial activity. Hence, an inhibition of squalene synthesis could disrupt this maintenance system, leading to a decrease in mitochondrial metabolic activity, as observed. While literature shows that squalene synthase inhibitors could cause both positive and negative effects on mitochondrial activity, this could largely depend on the cell type, inhibition mechanism, and dose conditions used in these studies (Hiyoshi et al., 2003; de Macedo-Silva et al., 2022). As seen in this study, the SH-SY5Y cells were more sensitive to the same SSI concentration at 48 hours compared to the HEK293 cells, which are known to be more robust compared to the neuronal cell line. This increased sensitivity in SH-SY5Y cells may be due to their neuronal lineage, as neurons are highly dependent on cholesterol for membrane integrity, synaptic function and signalling (Pfrieger & Ungerer, 2011). Since SSI inhibits intracellular cholesterol biosynthesis, neuronal cells may be more vulnerable due to their high reliance on endogenous cholesterol production, unlike HEK293 cells which can acquire cholesterol more readily from the environment (Zhang & Liu, 2015).

Similarly, treatment with 1 μM Aβ42 did not significantly affect mitochondrial metabolic activity in HEK293 cells at both 24 and 48 hours but did cause a significant decrease of 16.95% in the SH-SY5Y cells at 48 hours. This aligns with literature demonstrating that neuronal cells are more susceptible to Aβ42-induced mitochondrial toxicity than non-neuronal cells (Bloom, Ren & Glabe,

2005). Moreover, one study found that extracellular soluble Aβ at concentrations as low as 1 nM were taken up by SH-SY5Y cells but not by HEK293 cells, potentially through selective membrane receptors not abundantly expressed in the HEK293 cells compared to the SH-SY5Y cells (Hu et al., 2009). This study also treated the SH-SY5Y cells with 1 μM Aβ42 for several days and found that there was a time-dependent increase in Aβ42 accumulation intracellularly (Hu et al., 2009). This accumulation of Aβ has been shown in many studies to localise at mitochondrial membranes, interact with mitochondrial proteins, block the import of nuclear-encoded proteins to the mitochondria and disrupt the electron transport chain, all of which leads to mitochondrial dysfunction (Chen & Yan, 2007; Spuch, Ortolano & Navarro, 2012). This time-dependent Aβ accumulation could explain why the SH-SY5Y cells exhibited a significant decline in mitochondrial activity only at 48 hours, while the HEK293 cells were not significantly affected at both time points. If there is reduced Aβ uptake in HEK293 cells, then there would be reduced intracellular accumulation necessary to induce mitochondrial dysfunction, thereby preserving their mitochondrial activity despite exposure to Aβ42.

Another factor to consider is the concentration and structural state of Aβ42 used. Studies have shown that oligomerised Aβ is more toxic than the monomeric form (Kamalaldinezabadi et al., 2024; Rodriguez, Tatulian & Teter, 2024). Although the Aβ42 used in this study was pre-incubated according to the manufacturer's instructions to induce oligomerisation, the oligomerised state of the Aβ42 was not confirmed before treatment. Hence, there is a possibility that the cells were treated with a mixture of monomeric and oligomeric Aβ42, rather than predominantly oligomeric forms, which could account for the lack of significant toxicity observed. While oligomerised Aβ42 is generally considered more toxic than the monomeric form, there is a study that treated SH-SY5Y cells with monomeric Aβ42 and observed a reduction in cell viability, but this was at a higher concentration of 10 μM (Seino et al., 2018), which is ten times what was used in this study aiming to mimic the early stages of AD. Moreover, many studies also state that differentiated SH-SY5Y cells are much more susceptible to Aβ-induced toxicity compared to non-differentiated SH-SY5Y cells (Krishtal et al., 2015, 2017; Sarkar et al., 2025), as was used in this study. Despite these considerations, the results obtained provide insights into early-stage Aβ42 exposure.

When SSI was added to the Aβ42-treated cells, there were no significant changes in mitochondrial activity nor overall cellular metabolic activity in both cell lines. When the 100 nM SSI was added

to the SH-SY5Y cells at 48 hours, the mitochondrial activity was significantly reduced compared to the untreated cells, although this was not observed for the 50 nM SSI. Considering that treatment with only 100 nM SSI caused a significant decrease at the same time point, this concentration combined with the Aβ42 treatment could suggest a cumulative effect that may interfere with mitochondrial function. Although the addition of SSI did not improve the mitochondrial activity, it is important to note that it also did not further decrease the metabolic activity of the cells. It is also interesting to note that the Alamar Blue® assay showed no significant decrease in overall cellular metabolic activity for all Aβ42-treated cells, regardless of whether SSI was present. This suggests that the Aβ42-induced disruption in mitochondrial activity observed in the SH-SY5Y cells after 48 hours could be specific to the mitochondria, rather than affecting overall cellular metabolism. Overall, these results suggest that SSI does not exacerbate nor mitigate Aβ42-induced disruption in mitochondrial activity. However, literature still shows an important role for LDLR in Aβ clearance and neuronal development (Kim et al., 2009; de Oliveira et al., 2020), prompting future studies to explore whether SSI can exert long-term neuroprotective effects by modulating Aβ uptake and clearance pathways.

In contrast to the Aβ42 treatment, the 150 μg/ml LDL treatment caused an increase in mitochondrial and overall metabolic activity in both cell lines. Statistical analysis showed that only the 21.29% increase observed in the HEK293 cells after 48 hours was significant. These results were unexpected, as literature shows that excess LDL can cause a dysregulation in mitochondrial dynamics and disrupt membrane fluidity and function (Goicoechea et al., 2023). However, many of these studies reflect changes due to oxidised LDL and not native LDL, as was used in this study. Another factor to consider is the concentration of LDL used, where previous studies have used 250 μg/ml (Baumer et al., 2017) and 300 μg/ml (Farias et al., 2024) LDL as “high dose” levels and 50 μg/ml as “low dose”, with 150 μg/ml falling between these levels, suggesting that significant disruptions in mitochondrial activity may primarily occur at higher LDL concentrations. It is also worth considering that high levels of LDL could lead to increased metabolic activity as cells attempt to metabolise the excess LDL. However, this increase in metabolic activity may contribute to cellular stress and excess ROS production, which could be detrimental to cell health in the long term (Guo et al., 2024). Interestingly, the study by Farias et al. (2024) also performed an MTT assay in a mouse hippocampal neuronal cell line (HT-22) after treatment with both 50 and 300 μg/ml LDL for 24 hours and found no significant change in mitochondrial activity/cell viability

(Farias et al., 2024). Being a neuronal cell line, this result is comparable to the one seen in this study and could suggest that the lack of significant changes seen in the SH-SY5Y cells is not an isolated occurrence but could rather be a common trend in neuronal cells. While there was no major disruption in mitochondrial activity at the chosen concentration, it is important to note that this study aimed to investigate early events of the slow rise in LDL levels, rather than focusing on higher doses that may induce larger disruptions.

The Alamar Blue® results also indicate that the LDL treatment significantly increased metabolic activity in the SH-SY5Y cells, which could suggest an increase in compensatory metabolic pathways. One such pathway is beta-oxidation, the process where long-chain fatty acids are broken down in peroxisomes and mitochondria to generate acetyl coA and, ultimately, ATP (Rogers et al., 2014). Since LDL is a major carrier of cholesterol and lipids, cells exposed to elevated LDL levels may shift toward lipid metabolism as an alternative energy source (Liu & Czaja, 2013). However, excessive lipid metabolism can lead to increased ROS production, lipid peroxidation and metabolic stress (van Tits et al., 2003), which could have implications for neurodegenerative conditions where lipid dysregulation is a known factor (Zhang & Liu, 2015). This increase in metabolic activity was also seen in the HEK293 cells but was non-significant. When SSI was added to the LDL-treated cells there was a clear trend across both cell lines where SSI treatment reduced the elevated mitochondrial activity and overall metabolic activity. Despite this observable trend, the statistical analysis only found the 100 nM SSI treatment in the LDL-treated HEK293 cells to be significant after 48 hours. Nonetheless, this trend is expected due to the mechanism of action of SSI in upregulating LDLR, which enhances LDL uptake and clearance, thereby reducing extracellular LDL levels and potentially mitigating LDL-induced metabolic alterations.

Compared to the other treatment groups under investigation, the hydrogen peroxide (H_2O_2) treatment, mimicking oxidative stress in hypercholesterolemic-AD conditions, significantly reduced mitochondrial activity in both HEK293 and SH-SY5Y cells, particularly at higher concentrations (500 μM), as was expected. This aligns with current literature which has shown that exposure to H_2O_2, a potent reactive oxygen species, impairs mitochondrial function and integrity by damaging mitochondrial DNA and electron transport chain components, such as succinate dehydrogenase, ketoglutarate dehydrogenase and aconitase, all of which leads to bioenergetic failure (Nulton-Persson & Szweda, 2001). The addition of SSI to the H_2O_2-treated

cells resulted in minimal, non-significant alterations in mitochondrial activity, with no observable trend or dose-dependent response. This suggests that SSI does not effectively counteract H_2O_2-induced mitochondrial damage under the tested conditions. However, in the Alamar Blue® assay results (fig. 15), which can detect non-mitochondrial enzymatic activity such as those occurring in the cytoplasm (Rampersad, 2012), SSI co-treatment demonstrated a consistent trend of slightly increasing cellular metabolism, with increased concentration (albeit statistically non-significant). Additionally, this could also imply that the metabolic effects of SSI are subtle and may require longer treatment durations above the 24-hour treatment period used in this experiment.

Nonetheless, the trend may suggest a compensatory metabolic shift where non-mitochondrial pathways are upregulated to sustain energy requirements under oxidative stress conditions. One such pathway could be glycolysis, which is the breakdown of glucose to pyruvate (aerobic conditions) in the cytoplasm (Kierans & Taylor, 2024). When considering the hypothesis that SSI may be indirectly contributing to an increase in farnesol production, due to a lack of FPP conversion to squalene, literature has shown that farnesol can enhance the AMP-activated protein kinase (AMPK) signalling pathway (Cho et al., 2021). Activation of the AMPK signalling pathway stimulates the translocation of glucose transporters (GLUT) to the cell membrane to increase glucose uptake by the cell, as well as activating other key glycolytic enzymes like phosphofructokinase-1 by phosphorylating regulatory proteins, ultimately leading to increased glycolysis activity (Jeon, 2016). This could explain the observed trend where SSI treatment increased overall metabolic activity. On the same note, oxidative stress conditions have also been reported to induce an increase in AMPK signalling, and hence glycolysis, as an adaptive response to increase survival under these conditions (Wu & Wei, 2012; Zhu et al., 2022). This could also be why the reduction in metabolic activity detected by the Alamar Blue® assay for the H_2O_2-treated cells was not as significant compared to those seen in the MTT assay results, however, the Alamar Blue® results still measure mitochondrial activity, and hence we do see that there is still that decrease in overall metabolic activity, especially with the 500 μM H_2O_2 concentration, with a significant reduction of 32.49% found in the HEK293 cells.

Interestingly, AMPK signalling is intricately involved in the pathophysiology of AD, however, this involvement remains debated. While studies have stated that AMPK activity is decreased in AD brains, contributing to decreased mitochondrial biosynthesis and function in the brain (Zhao et al.,

2024), others have reported on the hyperactivity of AMPK in degenerating neurons contributing to loss of synaptic integrity (Domise et al., 2019). Similarly, some studies found that amyloid beta suppresses AMPK activity, potentially contributing to the metabolic dysregulation seen in AD (Lin et al., 2016), while other studies have also stated that amyloid beta activates AMPK, which, as a kinase, can also contribute to tau phosphorylation, and hence to NFT formation (Thornton et al., 2011; Domise et al., 2019). These contrasting views on the role of AMPK in AD pathogenesis have also led to contrasting views and ongoing research on the therapeutic potential of AMPK agonists. While AMPK activation can enhance autophagy and mitigate oxidative stress, its influence on amyloid beta accumulation and tau phosphorylation remains debated (Assefa et al., 2020; Yang et al., 2020). Although farnesol production has been proven to increase in response to squalene synthase inhibitors (Hiyoshi et al., 2003) more investigation would need to be done to confirm whether that leads to AMPK activation. From a speculative view, there is potential for SSI and squalene synthase inhibitors to be investigated as AMPK agonists in the wider ongoing research into this particular therapeutic strategy against AD.

Overall, these results provide insight into the metabolic effects of hypercholesterolemic-AD conditions and SSI treatment, highlighting cell-type specific effects and the need for further investigation into the molecular mechanisms underlying squalene synthase inhibition and LDLR upregulation in relation to AD pathogenesis.

5.2.3 - Treatment with SSI shows a promising trend of decreasing total ROS production in the hypercholesterolemic-AD cell model

Oxidative stress, driven by an imbalance between ROS production and antioxidant defences, plays a critical role in the pathophysiology of both hypercholesterolemia and AD. In FH patients, elevated levels of LDL contribute to oxidative stress through lipid peroxidation and the activation of pro-oxidant pathways, which exacerbate vascular inflammation and damage (Seo et al., 2019; Ganjali et al., 2021). Similarly, in AD, excessive ROS generation is a hallmark feature linked to Aβ42 aggregation, mitochondrial dysfunction, and neuronal damage, all of which accelerate neurodegenerative processes (Chauhan & Chauhan, 2006). Given the well-documented role of oxidative stress in both FH and AD, with the potential of FH-induced oxidative stress mechanisms contributing to those seen in neurodegeneration, exploring therapeutic strategies that mitigate ROS production is crucial. Furthermore, proteomic analysis of FH patient plasma samples in this study

further supported the established role of oxidative stress in FH by revealing significant enrichment of oxidative stress-related pathways and the dysregulation of key enzymes involved in ROS response. These findings prompted an *in vitro* investigation into ROS production in hypercholesterolemic-AD cell models to further explore the extent of oxidative stress under these disease conditions and assess the potential effects of SSI treatment in mitigating ROS levels.

The results indicate that SSI treatment alone had a notable effect on reducing basal ROS production in both HEK293 and SH-SY5Y cell models. In HEK293 cells, treatment with 50 nM SSI resulted in a significant decrease in ROS production by 17.76%, while 100 nM SSI caused a 13.32% reduction, although this was not statistically significant. Similarly, in SH-SY5Y cells, both 50 nM and 100 nM SSI treatments led to significant decreases in ROS production, with reductions of 19.48% and 18.30%, respectively. These findings suggest that SSI may influence the antioxidant system, potentially mitigating oxidative stress in both neuronal and non-neuronal cell types. There are limited studies addressing the exact effects or mechanisms of squalene synthase inhibition on oxidative stress, however, there are studies that suggest that there could be indirect influences. As previously mentioned, since SSI inhibits the conversion of FPP to squalene, there is a subsequent accumulation of FPP (Wasko et al., 2010). This accumulation of FPP could drive the cellular pathway leading to increased farnesol production as seen in *C.albicans* cells, which exhibited an 8-fold increase in farnesol production post-treatment with zaragozic acid B, a potent squalene synthase inhibitor (Hornby, Kebaara & Nickerson, 2003). Most studies have investigated plant-derived farnesol, which has been shown to significantly reduce oxidative stress markers in different cell/animal models, however, the chemical composition of farnesol appears to be identical regardless of its origin, whether from human or plant sources. Both produce the same sesquiterpenoid compound, which has the molecular formula C15H26O ("Farnesol (CHEBI:28600)", n.d.). This similarity suggests that the effects observed from plant-derived farnesol might also be present in human-derived farnesol. However, additional research would be necessary to confirm this hypothesis.

Studies have shown that farnesol exhibited protective effects against oxidative stress in rat models of cancer. In a study on hepatocellular carcinoma induced by diethyl nitrosamine, farnesol reduced markers of oxidative stress while boosting antioxidant levels in cells (Balaraman et al., 2021). Comparable results were observed in research on colon cancer induced by 1,2-dimethylhydrazine,

where farnesol mitigated oxidative damage. This was achieved through a reduction in lipid peroxidation and an increase in the activity of antioxidant enzymes, including superoxide dismutase (SOD), catalase, and glutathione peroxidase (Khan & Sultana, 2011). Interestingly, the proteomic analysis found an increased expression of SOD3 in the FH patients, with statin therapy further increasing its expression. This aligns with the findings from the cancer study that suggests that antioxidant enzymes, like SOD, are upregulated in response to oxidative damage and further highlights the potential for molecules involved in cholesterol synthesis (i.e. Statins and farnesol) to exert potential antioxidant modulation in managing oxidative stress.

In addition to cancer models, farnesol has also been shown to have neuroprotective effects. In an animal model of acrylamide-induced neurotoxicity in rats, administration of farnesol prior to exposure to acrylamide showed neuroprotective effects by reducing reactive gliosis, a glial response to injury, thus preserving brain integrity (Santhanasabapathy et al., 2015). Additionally, farnesol caused significant reductions in inflammatory cytokines including TNF-α and interleukin-6, which are commonly associated with neuroinflammation (Heneka, Golenbock & Latz, 2015). A possible mechanism behind these observations could be that farnesol activates the silent information regulator factor 2-related enzyme 1 (Sirt1)/ nuclear factor erythroid 2-related factor 2 (Nrf2) signalling pathway, as was found in a study whereby farnesol was administered to mice after chronic sleep deprivation-induced cognitive impairment (Li et al., 2023). The levels of Sirt1, Nrf2, heme oxygenase1, and glutathione peroxidase (GPx) 4 were all significantly increased in the hippocampi of these mice, which attenuated oxidative stress damage, pro-inflammatory cytokine activation, and microglial activation (Li et al., 2023). While there is no direct evidence linking the observed ROS reduction after SSI treatment to the upregulation of FPP, and subsequently farnesol, the existing literature outlined provides a speculative mechanism that may explain these findings.

In addition to reducing ROS production when treated in isolation, SSI also caused a reduction in ROS levels in the H_2O_2-treated cells. Both the HEK293 and SH-SY5Y cells exhibited significant increases in ROS production after 500 μM H_2O_2 treatment, but only the HEK293 cells had a significant increase after 300 μM H_2O_2 treatment, further highlighting a cell-type-specific response. This could be due to differences in mitochondrial metabolism between the two cell lines whereby HEK293 cells, having a shorter doubling time compared to the SH-SY5Y cells (Cervera et al., 2011; Feles et al., 2022), may have higher mitochondrial activity, leading to an earlier

increase in ROS levels when exposed to the lower H_2O_2 concentration. These results align with the established role of H_2O_2 as a key mediator of oxidative damage, particularly through its ability to penetrate cellular membranes and interact with transition metals, producing highly reactive hydroxyl radicals that can compromise mitochondrial function and activate pro-oxidant pathways such as NADPH oxidases (Sies, 2017). For the 300 μM H_2O_2 treatment group, co-treatment with SSI did not significantly change ROS production compared to treatment with H_2O_2 alone. In contrast, the addition of SSI to the 500 μM H_2O_2 treatment group led to significant reductions in ROS production in the HEK293 cells only. Despite no statistical significance, the SSI treatment in the SH-SY5Y cells still caused decreases in ROS production as the SSI concentration increased. This suggests that SSI may exert its antioxidant effects more effectively under conditions of high H_2O_2-induced ROS production (500 μM H_2O_2). It is possible that the cells may still maintain their endogenous antioxidant capacity at lower oxidative stress levels (300 μM H_2O_2), making the effects of SSI less pronounced (Poljsak, Šuput & Milisav, 2013). The mechanisms underlying the SSI-induced reduction in ROS production might involve the proposed influence of SSI on GPx activation (Li et al., 2023) (discussed earlier). Increasing GPx activity would increase the rate at which H_2O_2 is neutralised (converted into water), thereby reducing ROS accumulation and oxidative damage (Ren et al., 2002; Liddell et al., 2006).

In the LDL treatment groups, the results demonstrated a significant increase in ROS production, particularly in HEK293 cells, where ROS levels rose by 172.07% compared to untreated controls. This marked increase reflects the oxidative stress induced by LDL, despite its lack of effects on cell metabolism, likely through mechanisms such as the activation of NADPH oxidases (NOX) (O'Donnell et al., 2003; Piccoli et al., 2011). NADPH oxidases are proteins embedded in membranes, primarily responsible for facilitating electron transfer from the interior to the exterior of the plasma membrane, where molecular oxygen is the recipient. This process leads to the formation of the superoxide anion, which subsequently generates various reactive oxygen species, including hydrogen peroxide and hydroxyl radicals (Bedard & Krause, 2007; Gao, Zhou & Hong, 2012). LDL particles, especially when oxidised, are known to be potent inducers of oxidative stress, driving inflammatory responses and cellular damage in non-neuronal cells (Chien et al., 2003; Fearon, 2006). The co-treatment of LDL with SSI resulted in a partial reduction of ROS levels. In HEK293 cells, SSI at 50 nM and 100 nM decreased ROS by 10.71% and 23.65%, respectively, suggesting a promising role of SSI in reducing LDL-induced ROS production.

In addition to the proposed mechanism that SSI causes increased activation of antioxidant enzymes such as SOD and GPx, the LDLR upregulation coupled with the inhibition of squalene synthesis, could result in increased uptake of LDL leading to its catabolism, and hence limiting its interactions on the cell surface. Studies have found that LDL can interact with various cell membrane receptors such as G-protein coupled receptors, which activates a signalling cascade that includes Src tyrosine kinase, phospholipase C-gamma, phosphatidylinositol 3-kinase, p42/p44 MAPK kinase, p38 MAPK, protein kinase C, and cytosolic phospholipase A(2) (Pedreño et al., 2001; O'Donnell et al., 2003). This pathway ultimately leads to NOX activation and increased ROS, as was exhibited in endothelial cells (O'Donnell et al., 2003). Additionally, activation of lipoprotein-associated phospholipase A2 activity by high levels of LDL has been found to negatively impact nitric oxide (antioxidant) production in endothelial cells (Searle et al., 2011). In fact, a reduction in nitric oxide has been reported in hypercholesterolemic patients (Feron et al., 1999; Böger et al., 2004). Interestingly, a study found that treatment of endothelial cells with two squalene synthase inhibitors caused an increase in endothelial nitric oxide synthase expression (Tavridou et al., 2007). These studies suggest that SSI may mitigate LDL-induced ROS production not only by enhancing LDL uptake but also by restoring nitric oxide homeostasis.

In contrast, the SH-SY5Y cells did not show a significant increase in ROS levels upon LDL treatment, with only a slight decrease of 2.76% compared to untreated controls. Subsequent SSI co-treatment caused further reductions in ROS levels by 6.23% (50 nM) and 5.48% (100 nM), though these changes were not statistically significant. Despite these slight decreases in ROS after the addition of SSI, all three treatment groups showed no significant change in ROS levels compared to the untreated control, indicating no effect of the LDL treatments on ROS production. This is in contrast to another study whereby treatment with LDL, even at lower concentrations compared to what was used in the current study, significantly affected cell redox-regulating proteins (Dias et al., 2014). However, this study only performed the treatment with LDL at 2 and 16 hours. Since the current study assessed ROS production after 24-hour treatment, there could have been compensatory mechanisms activated by the SH-SY5Y cells to combat the acute increase in ROS production that could have possibly been detected at earlier time points, as seen in the study by Dias et. al. (2014). Additionally, the authors did not specify whether the SH-SY5Y cells were differentiated prior to treatments and assays. This may be important as it has been found that differentiation of SH-SY5Y cells may increase their vulnerability to oxidative stress (Forster et al.,

2016). These authors observed increased electrical plasma membrane activity and reduced expression of oxidative stress response genes post-differentiation of the SH-SY5Y cells. Thus, these studies emphasise the importance of considering various experimental factors, such as cell differentiation status and treatment durations which can significantly influence the observed outcomes and the overall interpretation of results. When considering the hypothesis that extracellular LDL could activate a signalling pathway leading to increased NOX activity, the current literature does not explicitly report such a relationship between LDL and NOX activity in neuronal cells. Rather, NOX activation in neuronal cells primarily occurs through a complex process involving protein-protein interactions, which originate from cytosolic subunits (Nayernia, Jaquet & Krause, 2014).

In the amyloid-beta (Aβ42) treatment groups, ROS levels were lower than those in untreated controls. Specifically, Aβ42 caused a 13.97% decrease in ROS production in HEK293 cells and a 16.86% decrease in SH-SY5Y cells. This finding contrasts with the typical association of Aβ42 with oxidative stress, especially in neuronal models (Kim et al., 2007; Schilling & Eder, 2011). However, these studies used remarkedly higher concentrations of Aβ42, in the 300 – 500 μM range, compared to the 1 μM used in this study. An additional study examined a smaller range of concentrations (0 μM, 2.5 μM, 5 μM, and 10 μM) of Aβ42 and determined that the 10 μM concentration was most effective in inducing significant mitochondrial damage (Han et al., 2017). In contrast, studies have also shown that Aβ42 may also possess antioxidant properties. This is due to its ability to chelate transition metal ions, which are potent catalysts of oxidation (Kontush, 2006). While it has been speculated that it is the monomeric form of Aβ that is antioxidant and the fibrillar/aggregated form that is pro-oxidant, a study still found that a range of 2 – 20 μM of aggregated Aβ42 inhibited the formation of hydroxyl radicals and H_2O_2 in cell-free systems (Sinha et al., 2013). Moreover, another study using 100 μM Aβ42 also found antioxidant effects of both monomeric and oligomeric forms of Aβ42 (Mitra, Prasad & Chakraborty, 2018). However, this study also concluded that these effects were different depending on how the Aβ42 was prepared, where they found that the oligomers prepared in PBS were more pro-oxidant compared to those prepared in a 10 mM HCl buffer solution or phenol-free cell culture medium (Mitra, Prasad & Chakraborty, 2018). These conflicting studies surrounding the role of Aβ42 in ROS production could be due to differences in methods regarding the choice of Aβ42 concentration and preparation. More studies need to be conducted to elucidate these discrepancies.

Studies have also proposed that Aβ species exhibit a dual role in oxidative stress depending on the disease stage, with monomers acting as antioxidants during early stages, while oligomers adopt a pro-oxidant function in later stages of the disease (Mitra, Prasad & Chakraborty, 2018). In the case of this study, the concentration of 1 μM, chosen to mimic early stages of AD and be non-lethal, showed antioxidant effects, which could be a realistic and or desirable result with regards to the context of this study. Moreover, emerging evidence suggests that aggregated Aβ may not directly drive ROS production but rather causes mitochondrial functional impairment in the form of membrane depolarisation independent of ROS (Sinha et al., 2013). However, ROS from pre-existing mitochondrial dysfunction has been implicated in initiating Aβ aggregation (Cheignon et al., 2018), creating a cycle where aggregated Aβ exacerbates mitochondrial damage, increasing ROS and oxidative stress. This cascade forms a positive feedback loop central to AD pathogenesis. Elevated LDL levels, known to induce significant ROS production, as seen in this study, could act as a trigger for Aβ aggregation, enhancing this cascade and accelerating neurodegenerative processes. The ability of SSI to reduce ROS across the conditions investigated suggests its potential to disrupt this harmful cycle. Despite the non-significance, the addition of SSI to the Aβ42 treatment still caused a decrease in ROS levels with increased SSI concentration. There was an unexpected spike in ROS levels observed when 100 nM SSI was added to the Aβ42-treated SH-SY5Y cells. As observed in the MTT results (fig. 11), this concentration of SSI has exhibited slightly cytotoxic effects on SH-SY5Y cells, indicating a possible cytotoxicity-induced ROS production due to the compounding effect of exposure to both compounds simultaneously.

Overall, the addition of SSI demonstrated a promising trend in reducing ROS production across various treatment conditions in both HEK293 and SH-SY5Y cell models. This effect was particularly evident in the H_2O_2 and LDL treatment groups, where SSI significantly mitigated the ROS production induced by these factors. The observed reduction in ROS levels suggests that SSI may have therapeutic potential in addressing the oxidative stress component common to both hypercholesterolemia and AD. As mentioned, SSI's mechanism of action may involve the activation of antioxidant pathways, potentially through increased farnesol production and activation of the Sirt1/Nrf2 signalling pathway. Many studies have indicated that overexpression of Sirt1 has been shown to have protective effects against AD (Donmez, 2012), as it modulates key pathological processes. Sirt1 has been shown to increase α-secretase activity, thereby promoting the non-amyloidogenic processing of APP, and reducing the production of amyloid-beta

(Li et al., 2018). Moreover, as a deacetylase enzyme, Sirt1 has been found to deacetylase tau protein as well as phosphorylating enzymes such as glycogen synthase kinase-3-beta (GSK-3β), leading to its inhibition. This was found to correlate with reduced hyperphosphorylation of tau and its subsequent aggregation into NFTs (Min et al., 2010, 2018). Moreover, the Nrf2 transcription factor signalling pathway, which activates antioxidant mechanisms in cells, is impaired in patients with AD (De Plano et al., 2023). Hence, the reactivation of this pathway is regarded as a potential strategy for managing the disease (Sidiropoulou, Metaxas & Kourti, 2023), and could be possible through SSI treatment. These findings provide valuable insights into the potential of SSI as a therapeutic strategy for addressing the interplay between hypercholesterolemia and Alzheimer's disease, particularly in relation to oxidative stress management.

5.2.4 - Treatment with SSI increases mitochondrial DNA copy number in the hypercholesterolemic-AD cell model (HEK293 cells)

Mitochondrial DNA copy number (mtDNA-CN) is a measure of the number of copies of mtDNA in a cell and can serve as an important indicator of mitochondrial functions as it can reflect changes in mitochondrial biogenesis and enzymatic activity (Castellani et al., 2020). Alterations in mtDNA-CN have been associated with various pathological conditions, such as cancer, cardiovascular and neurodegenerative diseases. While an increase in mtDNA-CN is often associated with mitochondrial biogenesis, either as a compensatory response to stress or improved cell viability, it can also indicate an accumulation of dysfunctional mitochondria if quality control mechanisms, such as mitophagy, are impaired (Castellani et al., 2020). Conversely, a decrease in mtDNA-CN may suggest mitochondrial damage or dysfunction but could also reflect an adaptive response to remove damaged mitochondria and maintain cellular homeostasis (Filograna et al., 2021). Hence, in addition to assessing oxidative stress and metabolic activity, investigating the effects of treatments on mtDNA-CN provides valuable insights into the potential long-term and overall effects of the treatments on mitochondrial health and function, as studies have shown that cell models of reduced mtDNA-CN exhibited reduced expression of vital complex proteins, lower enzymatic activity and even altered cellular morphology, which was rescued after restoring mtDNA-CN to wild-type levels (Jeng et al., 2008).

In the HEK293 cells, 48-hour treatment with 50 nM SSI did not significantly change the mtDNA-CN (1.08-fold change) compared to the DMSO control and untreated groups. However, the DMSO vehicle control group exhibited a 21% decrease compared to the untreated cells, which was found to be non-significant. This result suggests that SSI alone does not significantly induce nor impair mitochondrial biogenesis and function, as was also seen in the MTT results. This contrasts the effects seen by statins, which have been reported to significantly decrease mtDNA-CN levels, especially in statin-induced myopathy (Stringer et al., 2013). This reduction in mtDNA-CN due to statins is reported to be due to the depletion of ubiquinone/coenzyme Q10 (CoQ10) which is produced downstream of the mevalonate pathway that is inhibited by statins (Mollazadeh et al., 2021). In fact, studies have found that statins may reduce CoQ10 levels by 16-54% (Marcoff & Thompson, 2007). CoQ10 plays an important role in mitochondrial energy production as it accepts electrons in the electron transport chain, as well as exhibits anti-oxidant properties and a role in mitochondrial membrane protection (Quinzii & Hirano, 2010). Despite SSI and statins sharing the ability to inhibit cholesterol biosynthesis and upregulate LDLR, the observation that SSI does not significantly affect mtDNA-CN and metabolic activity may be due to the fact that it only inhibits the sterol pathway downstream of the mevalonate pathway (fig. 5), and hence, does not affect the non-sterol pathway which leads to the production of CoQ10 and other important molecules, suggesting that SSI may be a better statin alternative in this regard.

Unlike the SSI treatment group, treatment with the hypercholesterolemic-AD conditions all had significant effects on the mtDNA-CN in the HEK293 cells. Firstly, treatment with 500 μM H_2O_2 caused a significant 68.53% increase in mtDNA-CN levels compared to the untreated cells. This aligns with literature which has shown that oxidative stress and ROS can stimulate mtDNA replication (Liu et al., 2003), where a study found a significant increase in mtDNA-CN in peripheral blood mononuclear cells after 72-hour treatment with 200 μM H_2O_2 (Borghini et al., 2024), suggesting that mitochondria may increase biogenesis as a compensatory mechanism for oxidative stress. However, some studies have found that hydrogen peroxide treatment reduced mtDNA-CN levels, especially at higher concentrations of H_2O_2 in the mM range, as was seen in prostate cancer cells (Chan et al., 2011). Additionally, there was a study done on human osteosarcoma 143B cells which found that low doses of H_2O_2 in the 100 – 300 μM range increased mtDNA-CN levels after 48 hours, however, when the H_2O_2 concentration increased above 300 μM, the mtDNA-CN levels decreased (Lee et al., 2005). This suggests that the effect of H_2O_2 on

mtDNA-CN may be dose-dependent, where lower doses may initially stimulate mitochondrial biogenesis as a protective mechanism, while higher doses lead to mitochondrial damage and degradation of mtDNA. The increase in mtDNA-CN observed in this study after treatment with 500 μM H_2O_2 could indicate that the HEK293 cells are still in the compensatory phase at this concentration, further suggesting that the effects of H_2O_2 are also cell-type specific.

While this increase is suggestive of a compensatory mechanism, the MTT assay results still showed that the 500 μM H_2O_2 treatment caused a significant decrease in mitochondrial metabolic activity at both 24 and 48 hours, indicating that this increase in mtDNA-CN does not reflect improved mitochondrial function, but rather a cellular stress response or loss of mitochondrial quality control. This could be due to impaired mitophagy, a type of autophagy that specifically removes damaged mitochondria to maintain cellular homeostasis (Ding & Yin, 2012). This hypothesis is supported by a study that found that H_2O_2 treatment in pancreatic β-cells reduced the expression of mitophagy-related proteins, such as prohibitin 2 and parkin, which correlated to impaired mitophagy (Liu et al., 2024). When mitophagy is impaired, the number of damaged mitochondria can accumulate, leading to an increase in total mtDNA-CN without functional recovery (Ding & Yin, 2012). This may explain why the H_2O_2 treatment caused an increase in mtDNA-CN but decreased mitochondrial metabolic activity in the HEK293 cells.

When SSI was added to the H_2O_2-treatment group, the mtDNA-CN levels increased by 19.73%, although this was non-significant. Since this increase was not statistically significant and the mtDNA-CN levels did not change after treatment with only SSI, it is unclear whether this observation is indicative of a positive effect of SSI on mitochondrial biogenesis, or simply an increased compensatory response to the additional effect of cholesterol biosynthesis inhibition. Even though the MTT assay indicated a non-significant effect of SSI on modulating H_2O_2-induced reduction in mitochondrial metabolic activity, the ROS production assay did show that SSI significantly decreased ROS production when added to the 500 μM H_2O_2-treated HEK293 cells, suggesting that while SSI may not directly modulate mitochondrial function, the increase in mtDNA-CN could indicate a further compensatory response to improve cellular resilience to oxidative stress (Lee et al., 2000).

Similar to the H_2O_2 treatment group, treatment with 150 μg/ml LDL caused a significant 49.56% increase in mtDNA-CN levels compared to the untreated cells. This result contrasts literature that

found high LDL levels to be associated with decreased blood-derived mtDNA-CN and subsequently, increased cardiovascular disease outcomes in individuals (Liu et al., 2023). However, this discrepancy may be due to differences in experimental conditions, where the cited study was performed in a clinical setting, whereas the present study used a relatively short-term *in vitro* model with a moderate LDL concentration. Interestingly, a study found that LDL exposure in a mouse hippocampal neuronal cell line (HT-22) caused an increase in the expression of genes associated with mitochondrial fusion (Farias et al., 2024), and similarly, another study found that high oxLDL levels induced the upregulation of mitochondrial fission and fusion processes in HL-1 cardiomyocytes (Zheng et al., 2021). These studies suggest that high LDL can influence mitochondrial dynamics *in vitro*. This may explain the observed increase in mtDNA-CN after LDL treatment as mitochondrial fusion (when two mitochondria merge) is reported to be critical for mtDNA regulation (Silva Ramos et al., 2019). The MTT assay also exhibited an increase in mitochondrial metabolic activity in the LDL-treated HEK293 cells, which correlates with the observed increase in mtDNA-CN levels, which could suggest that the current LDL concentration and treatment duration may have stimulated mitochondrial adaptation rather than induced mitochondrial dysfunction. However, the ROS production assay did indicate a large increase in ROS production in the LDL-treated HEK293 cells after 24 hours. Similar to the H_2O_2 treatment group, this elevation in ROS could have also triggered the compensatory increase in mtDNA-CN. When SSI was added to the LDL group, the mtDNA-CN increased by 26.24%, though this was non-significant. Given that this increase is non-significant, it remains unclear whether this effect is a direct consequence of SSI treatment or simply a continuation of the mitochondrial response to LDL exposure, possibly due to the upregulation of LDLR.

In contrast to the other treatment conditions, the 1 μM Aβ42 treatment caused a significant 69.05% reduction in mtDNA-CN levels in the HEK293 cells. There are conflicting reports in current literature on the effects of Aβ42 on mtDNA-CN, where some studies have noted that mtDNA-CN is inversely correlated with insoluble Aβ40 and Aβ42 levels (Coskun et al., 2010; Parmar et al., 2017), while another found that sublethal concentrations of Aβ42 caused a slight increase in mtDNA-CN *in vitro* said to be a compensatory response to mtDNA damage, which was also increased after Aβ42 treatment (Diana et al., 2008). This discrepancy in findings may be attributed to differences in Aβ42 concentration, exposure duration and cell type used across studies. Interestingly, a study found that treatment with 1 μM Aβ in SH-SY5Y cells caused an increase in

mitophagy and mitochondrial fission-associated proteins (de la Cueva et al., 2022), suggesting that the observed decrease in mtDNA-CN may not solely reflect mitochondrial damage, but could also indicate an active quality control mechanism to remove dysfunctional mitochondria. Given that the MTT assay showed no significant effect of Aβ42 treatment on mitochondrial metabolic activity, the decline in mtDNA-CN may not immediately translate to impaired mitochondrial function, at least within the timeframe of this study.

The addition of SSI to the Aβ42-treated cells caused a significant 57.19% increase in mtDNA-CN compared to when the cells were treated with Aβ42 only. Furthermore, the new mtDNA-CN levels (Aβ42 + SSI) were not significantly different compared to the untreated cell group suggesting that not only did SSI increase the mtDNA-CN levels, but it restored them closer to normal levels. These results suggest that SSI may mitigate Aβ42-induced mitochondrial damage by promoting mitochondrial biogenesis. However, there are limited studies that can suggest the mechanism behind this observed result. One possible explanation could be the speculated ability of SSI to indirectly increase intracellular farnesol levels (as previously discussed) which has been shown to induce mitochondrial biogenesis by enhancing pathways such as the AMPK signalling pathway (Cho et al., 2021). However, the lack of a significant increase in mtDNA-CN with SSI treatment alone may suggest that its effects on mitochondrial biogenesis may be more pronounced under conditions of mitochondrial stress.

In general, these results suggest that mtDNA-CN is highly responsive to oxidative stress and hypercholesterolemic-AD treatment conditions. However, further analyses, such as assessing mitochondrial mass, membrane potential and ATP production would help clarify whether these changes in mtDNA-CN are associated with alterations in mitochondrial function. Overall, the current results indicate that SSI increases mtDNA-CN when combined with these conditions, especially when added to the Aβ42 treatment group, suggesting a role in mitochondrial biogenesis which could be investigated by examining key mitochondrial replication and fusion markers.

6. Conclusion

Alzheimer's disease (AD) is a complex neurodegenerative disorder characterised by mitochondrial dysfunction, oxidative stress and dysregulated lipid metabolism (Di Paolo & Kim, 2011; Wang et al., 2014). Given the increasing evidence linking hypercholesterolemia to AD pathology (Dias et al., 2015; Wu et al., 2022), this study aimed to assess the effects of hypercholesterolemia on AD hallmarks and signalling pathways by investigating the proteomic profile of FH patients and the impact of a novel squalene synthase inhibitor (SSI) on mitochondrial function in cell models of hypercholesterolemia and AD.

The proteomic analysis of FH patient plasma samples revealed key alterations in protein networks related to cytoskeletal dynamics and regulation, oxidative stress and antioxidant defence, inflammation and immune regulation and metabolism and energy regulation. This dysregulation of proteins spanning multiple networks highlights the widespread impact of hypercholesterolemia on essential cellular functions, many of which are also implicated in AD pathology. The altered expression of cytoskeletal regulatory proteins matched molecular pathways predominantly suggesting a dysregulation in gap junction regulation which may be linked to disruptions in neuronal integrity and synaptic activity, which are key pathologies in AD (Penzes & VanLeeuwen, 2011). Additionally, the observed changes in inflammatory and immune-related proteins further support the notion that systemic metabolic disturbances may contribute to neuroinflammatory disruptions that could potentially exacerbate AD progression (Thirumangalakudi et al., 2008). Statin therapy in FH patients appeared to partially restore the expression of cytoskeletal proteins and antioxidant proteins toward control levels, suggesting potential benefits in cytoskeletal regulation and oxidative stress defence. However, its effects on immune and inflammatory proteins were mixed, highlighting the complex immunomodulatory role of statins. While some findings align with the neuroprotective potential of statins, concerns remain regarding their impact on metabolic pathways and neuroinflammation.

Given that the proteomic analysis highlighted a dysregulation in oxidative stress response pathways in the FH patients, to further explore these findings, the *in vitro* investigation focused on assessing the molecular effects of a hypercholesterolemic-AD cell model on mitochondrial health markers, such as metabolic activity, ROS production and mtDNA-CN. Moreover, the effects of

cholesterol modulation were also evaluated through SSI treatment under these conditions. The *in vitro* results illustrated that SSI treatment had no major cytotoxic effects at lower concentrations but showed slight cytotoxicity at 100 nM in the SH-SY5Y cells after 48 hours. The hypercholesterolemic-AD conditions (LDL, Aβ42 and H_2O_2) had distinct effects on mitochondrial metabolic activity, where the chosen concentration of Aβ42 (representing early stages of AD) showed no significant impact on mitochondrial metabolic activity (as measured by the MTT assay). The LDL treatment, representing moderate hypercholesterolemic conditions, exhibited a trend of increasing mitochondrial metabolic activity, particularly in the HEK293 cells. In contrast, H_2O_2 treatment significantly reduced mitochondrial metabolic activity in both the HEK293 and SH-SY5Y cells, suggesting that oxidative stress may impact mitochondrial function more prominently than LDL or Aβ42 under these conditions. The addition of SSI to these treatment groups revealed no significant effect on improving the mitochondrial metabolic activity, except in the case of the LDL treatment whereby SSI treatment appeared to partially restore metabolic activity closer to untreated levels. Interestingly, the Alamar Blue® assay, which measures cellular metabolic activity via redox potential (from mitochondrial and non-mitochondrial activity), indicated that none of the treatments significantly affected overall metabolic function over the treatment period, which may suggest that while mitochondrial metabolic activity may be altered under the chosen conditions, overall cellular metabolism remains largely intact, at least within the tested timeframe.

The ROS production assay revealed more prominent results whereby H_2O_2 treatment caused a significant increase in ROS production, as expected, confirming its role as a strong oxidative stressor. In contrast, the 50 nM SSI and Aβ42 treatment groups significantly reduced ROS production in both cell lines. Moreover, SSI treatment in the 500 μM H_2O_2 treatment group caused a significant decrease in ROS production in the HEK293 cells, indicating a promising antioxidant role of SSI. The Aβ42 results suggested that the sublethal concentration of 1 μM Aβ42 may not be sufficient to enhance ROS production and oxidative stress, potentially suggesting that in the early stages of AD, the initiation of oxidative stress may occur due to other factors that precede Aβ42 toxicity. One such factor could be elevated LDL, which caused a significant increase in ROS production in the HEK293 cells, but not in the SH-SY5Y cells. However, the lack of effect in the SH-SY5Y cells may be influenced by their non-differentiated state, the treatment concentration

and differences in response and metabolic rates between the cell types, all of which could have impacted the observed results.

To further explore how these treatments impacted mitochondrial health, mtDNA-CN was assessed as a marker of mitochondrial biogenesis. The qPCR results indicated significant increases in mtDNA-CN after H_2O_2 and LDL treatment, possibly as a compensatory response to oxidative stress or an impairment in mitochondrial quality control mechanisms, such as mitophagy, which could drive the accumulation of dysfunctional mitochondria. In contrast, the Aβ42 treatment significantly reduced mtDNA-CN levels, suggesting a different mechanism of mitochondrial dysfunction that may not be related to inducing oxidative stress but could involve direct damage to mtDNA or enhanced mitophagy. Lastly, although SSI did not significantly affect mtDNA-CN on its own, its addition to the other treatment conditions caused an increase in mtDNA-CN, particularly in the Aβ42-treated cells, indicating a potential role of SSI in mitochondrial biogenesis. Overall, the *in vitro* results illustrate the distinct effects of the hypercholesterolemic-AD conditions on mitochondrial function, highlighting a more prominent role of ROS (H_2O_2) in early mitochondrial changes in the AD model, where elevated LDL levels may contribute to ROS production with SSI showing potential to mitigate these oxidative stress-induced effects.

Overall, the results of this study provided both *in vitro* and systemic insights into the complexity of cholesterol modulation and the potential molecular pathways that may link hypercholesterolemia and AD. Moreover, while statins are widely used to manage hypercholesterolemia and have shown potential neuroprotective effects, the findings suggest that squalene synthase inhibition may offer an alternative approach to modulating cholesterol metabolism where future studies could investigate the direct mechanisms by which SSI modulates the highlighted pathways as a potential therapeutic strategy for AD.

7. Future studies

For future studies, the proteomic study should increase the sample size to improve statistical power and representation. To mitigate the biological variance that could have been introduced due to the wide age range (7 to 50 years old) of the patients, the patients could be stratified into narrower age groups or adjusted for age-related effects during analysis. Moreover, future studies should

implement stricter participant inclusion criteria, to screen for potential confounding factors, such as the use of medications other than statins, which could influence the proteomic profile.

For the *in vitro* study, the AD cell model could be improved by differentiating the SH-SY5Y cell line to enhance the neuronal features and generate more physiologically relevant insights. Furthermore, the current treatment conditions could be further refined by optimising the concentrations to better represent certain stages of disease progression for both the hypercholesterolemic and AD contexts. Notably, for the Aβ42 treatment, future studies should verify the oligomerisation state of the protein (e.g. transmission electron microscopy) to ensure a consistent interpretation of the effects of Aβ42 treatment. Moreover, for the LDL treatment, it may be more relevant to include oxLDL to better mimic the pathological condition of hypercholesterolemia, as oxLDL is more biologically active in driving oxidative stress, inflammation and mitochondrial dysfunction (Chien et al., 2003). It would also be interesting to extend the treatment duration (above 48 hours) to further investigate the long-term effects of the treatments and confirm whether the observed effects in this study are compensatory or if they change over time.

Considering the results indicate a complex effect of the treatment conditions on mitochondrial function and mtDNA-CN, it would be highly insightful to include additional assays that further investigate the mechanisms of mitochondrial dysfunction. This includes assays that assess mitochondrial membrane potential, ATP production and the expression of mitochondrial biogenesis genes, such as those related to fission and fusion events (Brand & Nicholls, 2011). Additionally, future studies could investigate antioxidant enzyme levels (e.g. SOD) and mitochondrial superoxide levels (ROS produced by mitochondria) to determine whether the increased ROS production observed in the study reflects insufficient antioxidant defences and if it is primarily generated by mitochondria or other cellular sources.

To better assess the link between hypercholesterolemia and AD, assays assessing Aβ42 production and tau phosphorylation (e.g. ELISA or western blot analysis) would help determine whether cholesterol modulation influences these histopathological hallmarks of AD. Lastly, to assess the potential of SSI in modulating this link, proteomic analysis could be performed on an optimised cell model of hypercholesterolemia and AD. This would provide deeper insights into the molecular pathways influenced by SSI.

8. Study limitations

This study had several limitations that should be considered. Firstly, the SH-SY5Y cell line, while relevant for studying neurodegenerative processes, does not fully represent the complexity of mature neurons, particularly in functional responses, when undifferentiated. Additionally, while previously published protocols were followed to prepare the Aβ42 treatment, confirmation of its aggregation state would have provided greater clarity in interpreting the observed effects of its treatment. Similarly, the proteomic study used a small sample pool of 10 and 12 individuals which may limit the generalisability of the findings. Moreover, the wide age range of the patients (7 to 50 years old) could have introduced biological variance due to age-related differences in lipid metabolism and immune responses, potentially affecting the proteome profiles. The proteomic results could have also been influenced by the presence of other infections or medications that were not screened for, such as anti-inflammatories, which could have influenced the observed protein expression patterns. Furthermore, it is important to consider that changes in circulating protein levels may not directly reflect alterations within specific tissues, such as the brain.

9. References

Aguilar, B.J., Zhu, Y. & Lu, Q. 2017. Rho GTPases as therapeutic targets in Alzheimer's disease. *Alzheimer's Research & Therapy*. 9(1):97. DOI: 10.1186/s13195-017-0320-4.

Ahmad, U. & Sharma, J. 2024. Fructose-1-Phosphate Aldolase Deficiency. In *StatPearls*. Treasure Island (FL): StatPearls Publishing. Available: http://www.ncbi.nlm.nih.gov/books/NBK557761/ [2024, November 19].

Aiken, J., Buscaglia, G., Bates, E.A. & Moore, J.K. 2017. The α-Tubulin gene TUBA1A in Brain Development: A Key Ingredient in the Neuronal Isotype Blend. *Journal of Developmental Biology*. 5(3):8. DOI: 10.3390/jdb5030008.

Alaaeddine, R., Fayad, M., Nehme, E., Bahmad, H.F. & Kobeissy, F. 2017. The Emerging Role of Proteomics in Precision Medicine: Applications in Neurodegenerative Diseases and Neurotrauma. In *Personalised Medicine*. V. 1007. S. El-Khamisy, Ed. (Advances in Experimental Medicine and Biology). Cham: Springer International Publishing. 59–70. DOI: 10.1007/978-3-319-60733-7_4.

Albert, M.S., DeKosky, S.T., Dickson, D., Dubois, B., Feldman, H.H., Fox, N.C., Gamst, A., Holtzman, D.M., et al. 2011. The diagnosis of mild cognitive impairment due to Alzheimer's disease: Recommendations from the National Institute on Aging-Alzheimer's Association workgroups on diagnostic guidelines for Alzheimer's disease. *Alzheimer's & dementia : the journal of the Alzheimer's Association*. 7(3):270. DOI: 10.1016/j.jalz.2011.03.008.

Alkam, D., Feldman, E.Z., Singh, A. & Kiaei, M. 2016. Profilin1 biology and its mutation, actin(g) in disease. *Cellular and Molecular Life Sciences: CMLS*. 74(6):967–981. DOI: 10.1007/s00018-016-2372-1.

Alsubaie, N., Al-kuraishy, H.M., Al-Gareeb, A.I., Alharbi, B., De Waard, M., Sabatier, J.-M., Saad, H.M. & Batiha, G.E.-S. 2022. Statins Use in Alzheimer Disease: Bane or Boon from Frantic Search and Narrative Review. *Brain Sciences*. 12(10):1290. DOI: 10.3390/brainsci12101290.

Angeli, S., Kousiappa, I., Stavrou, M., Sargiannidou, I., Georgiou, E., Papacostas, S.S. & Kleopa, K.A. 2020. Altered Expression of Glial Gap Junction Proteins Cx43, Cx30, and Cx47 in the 5XFAD Model of Alzheimer's Disease. *Frontiers in Neuroscience*. 14:582934. DOI: 10.3389/fnins.2020.582934.

Antonino, M., Marmo, P., Freites, C.L., Quassollo, G.E., Sánchez, M.F., Lorenzo, A. & Bignante, E.A. 2022. Aβ Assemblies Promote Amyloidogenic Processing of APP and Intracellular Accumulation of Aβ42 Through Go/Gβγ Signaling. *Frontiers in Cell and Developmental Biology*. 10. DOI: 10.3389/fcell.2022.852738.

Arnhold, J. 2020. The Dual Role of Myeloperoxidase in Immune Response. *International Journal of Molecular Sciences*. 21(21):8057. DOI: 10.3390/ijms21218057.

Arrese, E.L., Saudale, F.Z. & Soulages, J.L. 2014. Lipid Droplets as Signaling Platforms Linking Metabolic and Cellular Functions. *Lipid insights*. 7:7–16. DOI: 10.4137/LPI.S11128.

Arriagada, P.V., Growdon, J.H., Hedley-Whyte, E.T. & Hyman, B.T. 1992. Neurofibrillary tangles but not senile plaques parallel duration and severity of Alzheimer's disease. *Neurology*. 42(3 Pt 1):631–639. DOI: 10.1212/wnl.42.3.631.

Assefa, B.T., Tafere, G.G., Wondafrash, D.Z. & Gidey, M.T. 2020. The Bewildering Effect of AMPK Activators in Alzheimer's Disease: Review of the Current Evidence. *BioMed Research International*. 2020(1):9895121. DOI: 10.1155/2020/9895121.

Averill, M.M., Barnhart, S., Becker, L., Li, X., Heinecke, J.W., LeBoeuf, R.C., Hamerman, J.A., Sorg, C., et al. 2011. S100A9 Differentially Modifies Phenotypic States of Neutrophils, Macrophages, and Dendritic Cells: Implications for Atherosclerosis and Adipose Tissue Inflammation. *Circulation*. 123(11):1216–1226. DOI: 10.1161/CIRCULATIONAHA.110.985523.

Baharuddin, B. 2024. The Impact of Fructose Consumption on Human Health: Effects on Obesity, Hyperglycemia, Diabetes, Uric Acid, and Oxidative Stress With a Focus on the Liver. *Cureus*. 16(9):e70095. DOI: 10.7759/cureus.70095.

Balaraman, G., Sundaram, J., Mari, A., Krishnan, P., Salam, S., Subramaniam, N., Sirajduddin, I. & Thiruvengadam, D. 2021. Farnesol alleviates diethyl nitrosamine induced inflammation and protects experimental rat hepatocellular carcinoma. *Environmental Toxicology*. 36(12):2467–2474. DOI: 10.1002/tox.23359.

Ballatore, C., Brunden, K.R., Huryn, D.M., Trojanowski, J.Q., Lee, V.M.-Y. & Smith, A.B. 2012. Microtubule Stabilizing Agents as Potential Treatment for Alzheimer's Disease and Related Neurodegenerative Tauopathies. *Journal of medicinal chemistry*. 55(21):8979–8996. DOI: 10.1021/jm301079z.

Bamburg, J.R. & Bloom, G.S. 2009. Cytoskeletal pathologies of Alzheimer disease. *Cell Motility*. 66(8):635–649. DOI: 10.1002/cm.20388.

Baumer, Y., McCurdy, S., Weatherby, T.M., Mehta, N.N., Halbherr, S., Halbherr, P., Yamazaki, N. & Boisvert, W.A. 2017. Hyperlipidemia-induced cholesterol crystal production by endothelial cells promotes atherogenesis. *Nature Communications*. 8(1):1129. DOI: 10.1038/s41467-017-01186-z.

Beach, T.G., Monsell, S.E., Phillips, L.E. & Kukull, W. 2012. Accuracy of the Clinical Diagnosis of Alzheimer Disease at National Institute on Aging Alzheimer Disease Centers, 2005–2010. *Journal of Neuropathology & Experimental Neurology*. 71(4):266–273. DOI: 10.1097/NEN.0b013e31824b211b.

Bedard, K. & Krause, K.-H. 2007. The NOX Family of ROS-Generating NADPH Oxidases: Physiology and Pathophysiology. *Physiological Reviews*. 87(1):245–313. DOI: 10.1152/physrev.00044.2005.

Berhane, K., Widersten, M., Engström, A., Kozarich, J.W. & Mannervik, B. 1994. Detoxication of base propenals and other alpha, beta-unsaturated aldehyde products of radical reactions and lipid peroxidation by human glutathione transferases. *Proceedings of the National Academy of Sciences*. 91(4):1480–1484. DOI: 10.1073/pnas.91.4.1480.

Bernabeu-Zornoza, A., Coronel, R., Palmer, C., Calero, M., Martínez-Serrano, A., Cano, E., Zambrano, A. & Liste, I. 2019. Aβ42 Peptide Promotes Proliferation and Gliogenesis in Human Neural Stem Cells. *Molecular Neurobiology*. 56(6):4023–4036. DOI: 10.1007/s12035-018-1355-7.

Bernard, D., Christophe, A., Delanghe, J., Langlois, M., De Buyzere, M. & Comhaire, F. 2003. The effect of supplementation with an antioxidant preparation on LDL-oxidation is determined by haptoglobin polymorphism. *Redox Report*. 8(1):41–46. DOI: 10.1179/135100003125001233.

Bertaggia, E., Scabia, G., Dalise, S., Verso, F.L., Santini, F., Vitti, P., Chisari, C., Sandri, M., et al. 2014. Haptoglobin Is Required to Prevent Oxidative Stress and Muscle Atrophy. *PLoS ONE*. 9(6):e100745. DOI: 10.1371/journal.pone.0100745.

Bhatnagar, P., Lu, X., Evans, M.K., LaVeist, T.A., Zonderman, A.B., Carter, D.L., Arking, D.E. & Fletcher, C.A. 2012. Genetic Variants in Platelet Factor 4 Modulate Inflammatory and Platelet Activation Biomarkers. *Circulation: Cardiovascular Genetics*. 5(4):412–421. DOI: 10.1161/CIRCGENETICS.111.961813.

Biswas, S.K. 2016. Does the Interdependence between Oxidative Stress and Inflammation Explain the Antioxidant Paradox? *Oxidative Medicine and Cellular Longevity*. 2016:5698931. DOI: 10.1155/2016/5698931.

Bloom, G.S., Ren, K. & Glabe, C.G. 2005. Cultured cell and transgenic mouse models for tau pathology linked to β-amyloid. *Biochimica et Biophysica Acta (BBA) - Molecular Basis of Disease*. 1739(2):116–124. DOI: 10.1016/j.bbadis.2004.08.008.

Bogachkov, Y.Y., Chen, L., Le Master, E., Fancher, I.S., Zhao, Y., Aguilar, V., Oh, M.-J., Wary, K.K., et al. 2020. LDL induces cholesterol loading and inhibits endothelial proliferation and angiogenesis in Matrigels: correlation with impaired angiogenesis during wound healing. *American Journal of Physiology - Cell Physiology*. 318(4):C762–C776. DOI: 10.1152/ajpcell.00495.2018.

Böger, R.H., Tsikas, D., Bode-Böger, S.M., Phivthong-ngam, L., Schwedhelm, E. & Frölich, J.C. 2004. Hypercholesterolemia impairs basal nitric oxide synthase turnover rate: a study investigating the conversion of l-[guanidino-15N2]-arginine to 15N-labeled nitrate by gas chromatography–mass spectrometry. *Nitric Oxide*. 11(1):1–8. DOI: 10.1016/j.niox.2004.07.008.

Bolshette, N., Ezagouri, S., Dandavate, V., Karavaeva, I., Golik, M., Wang, H., Espenshade, P.J., Osborne, T.F., et al. 2023. Carbon dioxide regulates cholesterol levels through SREBP2. *PLOS Biology*. 21(11):e3002367. DOI: 10.1371/journal.pbio.3002367.

Bomasang-Layno, E. & Bronsther, R. 2021. Diagnosis and Treatment of Alzheimer's Disease: An Update. *Delaware Journal of Public Health*. 7(4):74. DOI: 10.32481/djph.2021.09.009.

Borghini, A., Ndreu, R., Canale, P., Campolo, J., Marinaro, I., Mercuri, A., Turchi, S. & Andreassi, M.G. 2024. Telomere Length, Mitochondrial DNA, and Micronucleus Yield in Response to Oxidative Stress in Peripheral Blood Mononuclear Cells. *International Journal of Molecular Sciences*. 25(3):1428. DOI: 10.3390/ijms25031428.

Brabec, J.L., Lara, M.K., Tyler, A.L. & Mahoney, J.M. 2021. System-Level Analysis of Alzheimer's Disease Prioritizes Candidate Genes for Neurodegeneration. *Frontiers in Genetics*. 12. DOI: 10.3389/fgene.2021.625246.

Brand, M.D. & Nicholls, D.G. 2011. Assessing mitochondrial dysfunction in cells. *Biochemical Journal*. 435(Pt 2):297. DOI: 10.1042/BJ20110162.

Brandt, D.T. & Grosse, R. 2007. Get to grips: steering local actin dynamics with IQGAPs. *EMBO Reports*. 8(11):1019. DOI: 10.1038/sj.embor.7401089.

Brettle, M., Patel, S. & Fath, T. 2016. Tropomyosins in the healthy and diseased nervous system. *Brain Research Bulletin*. 126:311–323. DOI: 10.1016/j.brainresbull.2016.06.004.

Brion, J.P., Anderton, B.H., Authelet, M., Dayanandan, R., Leroy, K., Lovestone, S., Octave, J.N., Pradier, L., et al. 2001. Neurofibrillary tangles and tau phosphorylation. *Biochemical Society Symposium*. (67):81–88. DOI: 10.1042/bss0670081.

Brodeur, J., Thériault, C., Lessard-Beaudoin, M., Marcil, A., Dahan, S. & Lavoie, C. 2012. LDLR-related protein 10 (LRP10) regulates amyloid precursor protein (APP) trafficking and processing: evidence for a role in Alzheimer's disease. *Molecular Neurodegeneration*. 7:31. DOI: 10.1186/1750-1326-7-31.

Brusselmans, K., Timmermans, L., Sande, T.V. de, Veldhoven, P.P.V., Guan, G., Shechter, I., Claessens, F., Verhoeven, G., et al. 2007. Squalene Synthase, a Determinant of Raft-associated Cholesterol and Modulator of Cancer Cell Proliferation *. *Journal of Biological Chemistry*. 282(26):18777–18785. DOI: 10.1074/jbc.M611763200.

Buck, K.B. & Zheng, J.Q. 2002. Growth Cone Turning Induced by Direct Local Modification of Microtubule Dynamics. *The Journal of Neuroscience*. 22(21):9358–9367. DOI: 10.1523/JNEUROSCI.22-21-09358.2002.

Buddhan, S., Sivakumar, R., Dhandapani, N., Ganesan, B. & Anandan, R. 2007. Protective effect of dietary squalene supplementation on mitochondrial function in liver of aged rats. *Prostaglandins, leukotrienes, and essential fatty acids*. 76 6:349–55. DOI: 10.1016/J.PLEFA.2007.05.001.

Burbaeva, G.Sh., Androsova, L.V. & Savushkina, O.K. 2020. Binding of Colchicine to Tubulin in the Brain Structures in Normal Conditions and in Schizophrenia. *Neurochemical Journal*. 14(2):235–238. DOI: 10.1134/S1819712420010067.

Burton, J.D. 2005. The MTT Assay to Evaluate Chemosensitivity. In *Chemosensitivity: Volume 1 In Vitro Assays*. R.D. Blumenthal, Ed. (Methods in Molecular Medicine™). Totowa, NJ: Humana Press. 69–78. DOI: 10.1385/1-59259-869-2:069.

Butterfield, D.A., Barone, E. & Mancuso, C. 2011. Cholesterol-Independent Neuroprotective And Neurotoxic Activites Of Statins: Prespectives For Statin Use In Alzheimer Disease And Other Age-Related Neurodegenerative Disorders. *Pharmacological research : the official journal of the Italian Pharmacological Society*. 64(3):180–186. DOI: 10.1016/j.phrs.2011.04.007.

Cai, Z., Yan, L.-J., Li, K., Quazi, S.H. & Zhao, B. 2012. Roles of AMP-activated Protein Kinase in Alzheimer's Disease. *NeuroMolecular Medicine*. 14(1):1–14. DOI: 10.1007/s12017-012-8173-2.

Camp, D., Venkatesh, B., Solianova, V., Varela, L., Goult, B.T. & Tanentzapf, G. 2024. The actin binding sites of talin have both distinct and complementary roles in cell-ECM adhesion. *PLOS Genetics*. 20(4):e1011224. DOI: 10.1371/journal.pgen.1011224.

Castellani, C.A., Longchamps, R.J., Sun, J., Guallar, E. & Arking, D.E. 2020. Thinking outside the nucleus: Mitochondrial DNA copy number in health and disease. *Mitochondrion*. 53:214–223. DOI: 10.1016/j.mito.2020.06.004.

Cervera, L., Gutiérrez, S., Gòdia, F. & Segura, M.M. 2011. Optimization of HEK 293 cell growth by addition of non-animal derived components using design of experiments. *BMC Proceedings*. 5(Suppl 8):P126. DOI: 10.1186/1753-6561-5-S8-P126.

Chan, R.B., Oliveira, T.G., Cortes, E.P., Honig, L.S., Duff, K.E., Small, S.A., Wenk, M.R., Shui, G., et al. 2012. Comparative lipidomic analysis of mouse and human brain with Alzheimer disease. *The Journal of Biological Chemistry*. 287(4):2678–2688. DOI: 10.1074/jbc.M111.274142.

Chan, S.W., Nguyen, P.-N., Ayele, D., Chevalier, S., Aprikian, A. & Chen, J.Z. 2011. Mitochondrial DNA damage is sensitive to exogenous H2O2 but independent of cellular ROS production in prostate cancer cells. *Mutation Research/Fundamental and Molecular Mechanisms of Mutagenesis*. 716(1–2):40–50. DOI: 10.1016/j.mrfmmm.2011.07.019.

Chang, T.Y., Chang, C.C.Y., Harned, T.C., De La Torre, A.L., Lee, J., Huynh, T.N. & Gow, J.G. 2021. Blocking cholesterol storage to treat Alzheimer's disease. *Exploration of neuroprotective therapy*. 1(3):173–184. DOI: 10.37349/ent.2021.00014.

Chauhan, V. & Chauhan, A. 2006. Oxidative stress in Alzheimer's disease. *Pathophysiology*. 13(3):195–208. DOI: 10.1016/j.pathophys.2006.05.004.

de Chaves, E.P., Narayanaswami, V., Christoffersen, C. & Nielsen, L.B. 2008. Apolipoprotein E and cholesterol in aging and disease in the brain. *Future Lipidology*. 3(5):505–530. DOI: 10.2217/17460875.3.5.505.

Cheignon, C., Tomas, M., Bonnefont-Rousselot, D., Faller, P., Hureau, C. & Collin, F. 2018. Oxidative stress and the amyloid beta peptide in Alzheimer's disease. *Redox Biology*. 14:450–464. DOI: 10.1016/j.redox.2017.10.014.

Chen, J.X. & Yan, S.D. 2007. Amyloid-β-Induced Mitochondrial Dysfunction. *Journal of Alzheimer's disease : JAD*. 12(2):177–184.

Chen, M. & Xia, W. 2020. Proteomic Profiling of Plasma and Brain Tissue from Alzheimer's Disease Patients Reveals Candidate Network of Plasma Biomarkers. *Journal of Alzheimer's disease : JAD*. 76(1):349. DOI: 10.3233/JAD-200110.

Chen, B., Miller, A.L., Rebelatto, M., Brewah, Y., Rowe, D.C., Clarke, L., Czapiga, M., Rosenthal, K., et al. 2015. S100A9 Induced Inflammatory Responses Are Mediated by Distinct Damage Associated Molecular Patterns (DAMP) Receptors In Vitro and In Vivo. *PLoS ONE*. 10(2):e0115828. DOI: 10.1371/journal.pone.0115828.

Chidambaram, S.B., Anand, N., Varma, S.R., Ramamurthy, S., Vichitra, C., Sharma, A., Mahalakshmi, A.M. & Essa, M.M. 2024. Superoxide dismutase and neurological disorders. *IBRO Neuroscience Reports*. 16:373–394. DOI: 10.1016/j.ibneur.2023.11.007.

Chien, M.-W., Chien, C.-S., Hsiao, L.-D., Lin, C.-H. & Yang, C.-M. 2003. OxLDL induces mitogen-activated protein kinase activation mediated via PI3-kinase/Akt in vascular smooth muscle cells. *Journal of Lipid Research*. 44(9):1667–1675. DOI: 10.1194/jlr.M300006-JLR200.

Cho, S.Y., Lim, S., Ahn, K.S., Kwak, H.J., Park, J. & Um, J.-Y. 2021. Farnesol induces mitochondrial/peroxisomal biogenesis and thermogenesis by enhancing the AMPK signaling pathway *in vivo* and *in vitro*. *Pharmacological Research*. 163:105312. DOI: 10.1016/j.phrs.2020.105312.

Christensen, M.A., Zhou, W., Qing, H., Lehman, A., Philipsen, S. & Song, W. 2004. Transcriptional regulation of BACE1, the beta-amyloid precursor protein beta-secretase, by Sp1. *Molecular and Cellular Biology*. 24(2):865–874. DOI: 10.1128/MCB.24.2.865-874.2004.

Chung, T.F., Sipe, J.D., McKee, A., Fine, R.E., Schreiber, B.M., Liang, J.S. & Johnson, R.J. 2000. Serum amyloid A in Alzheimer's disease brain is predominantly localized to myelin sheaths and axonal membrane. *Amyloid: The International Journal of Experimental and Clinical Investigation: The Official Journal of the International Society of Amyloidosis*. 7(2):105–110. DOI: 10.3109/13506120009146246.

Cimminiello, C., Zambon, A. & Polo Friz, H. 2016. [Hypercholesterolemia and cardiovascular risk: advantages and limitations of current treatment options]. *Giornale Italiano Di Cardiologia (2006)*. 17(4 Suppl 1):6S – 13. DOI: 10.1714/2254.24276.

Cleveland, D.W., Lopata, M.A., MacDonald, R.J., Cowan, N.J., Rutter, W.J. & Kirschner, M.W. 1980. Number and evolutionary conservation of α- and β-tubulin and cytoplasmic β- and γ-actin genes using specific cloned cDNA probes. *Cell*. 20(1):95–105. DOI: 10.1016/0092-8674(80)90238-X.

Cooper, G.M. 2000. Signal Transduction and the Cytoskeleton. In *The Cell: A Molecular Approach. 2nd edition*. Sinauer Associates. Available: https://www.ncbi.nlm.nih.gov/books/NBK9964/ [2025, March 03].

Corraliza-Gomez, M., Sanchez, D. & Ganfornina, M.D. 2019. Lipid-Binding Proteins in Brain Health and Disease. *Frontiers in Neurology*. 10. Available: https://www.frontiersin.org/articles/10.3389/fneur.2019.01152 [2024, January 30].

Coskun, P.E., Wyrembak, J., Derbereva, O., Melkonian, G., Doran, E., Lott, I.T., Head, E., Cotman, C.W., et al. 2010. Systemic mitochondrial dysfunction and the etiology of Alzheimer's disease and down syndrome dementia. *Journal of Alzheimer's disease: JAD*. 20 Suppl 2(0 2):S293-310. DOI: 10.3233/JAD-2010-100351.

Cotman, C.W., Hailer, N.P., Pfister, K.K., Soltesz, I. & Schachner, M. 1998. Cell adhesion molecules in neural plasticity and pathology: similar mechanisms, distinct organizations? *Progress in Neurobiology*. 55(6):659–669. DOI: 10.1016/S0301-0082(98)00025-2.

de la Cueva, M., Antequera, D., Ordoñez-Gutierrez, L., Wandosell, F., Camins, A., Carro, E. & Bartolome, F. 2022. Amyloid-β impairs mitochondrial dynamics and autophagy in Alzheimer's disease experimental models. *Scientific Reports*. 12(1):10092. DOI: 10.1038/s41598-022-13683-3.

Daliri, M., Simental-Mendía, L.E., Jamialahmadi, T., Kesharwani, P., Reiner, Ž. & Sahebkar, A. 2023. Effect of Statins on Superoxide Dismutase Level: A Systematic Review. *Current Medicinal Chemistry*. (August, 31). DOI: 10.2174/0929867331666230831145809.

De Jager, C.A., Msemburi, W., Pepper, K. & Combrinck, M.I. 2017. Dementia Prevalence in a Rural Region of South Africa: A Cross-Sectional Community Study. *Journal of Alzheimer's Disease*. 60(3):1087–1096. DOI: 10.3233/JAD-170325.

De Plano, L.M., Calabrese, G., Rizzo, M.G., Oddo, S. & Caccamo, A. 2023. The Role of the Transcription Factor Nrf2 in Alzheimer's Disease: Therapeutic Opportunities. *Biomolecules*. 13(3):549. DOI: 10.3390/biom13030549.

Dequidt, C., Danglot, L., Alberts, P., Galli, T., Choquet, D. & Thoumine, O. 2007. Fast Turnover of L1 Adhesions in Neuronal Growth Cones Involving Both Surface Diffusion and Exo/Endocytosis of L1 Molecules. *Molecular Biology of the Cell*. 18(8):3131–3143. DOI: 10.1091/mbc.e06-12-1101.

Di Paolo, G. & Kim, T.-W. 2011. Linking Lipids to Alzheimer's Disease: Cholesterol and Beyond. *Nature Reviews. Neuroscience*. 12(5):284–296. DOI: 10.1038/nrn3012.

Diana, A., Simić, G., Sinforiani, E., Orrù, N., Pichiri, G. & Bono, G. 2008. Mitochondria morphology and DNA content upon sublethal exposure to beta-amyloid(1-42) peptide. *Collegium Antropologicum*. 32 Suppl 1:51–58.

Dias, H.K.I., Brown, C.L.R., Polidori, M.C., Lip, G.Y.H. & Griffiths, H.R. 2015. LDL-Lipids from patients with hypercholesterolaemia and Alzheimer's disease are inflammatory to microvascular endothelial cells: Mitigation by statin intervention. *Clinical science (London, England : 1979)*. 129(12):1195–1206. DOI: 10.1042/CS20150351.

Dias, I.H.K., Mistry, J., Fell, S., Reis, A., Spickett, C.M., Polidori, M.C., Lip, G.Y.H. & Griffiths, H.R. 2014. Oxidized LDL lipids increase β-amyloid production by SH-SY5Y cells through glutathione depletion and lipid raft formation. *Free Radical Biology and Medicine*. 75:48–59. DOI: 10.1016/j.freeradbiomed.2014.07.012.

Ding, W.-X. & Yin, X.-M. 2012. Mitophagy: mechanisms, pathophysiological roles, and analysis. *Biological chemistry*. 393(7):547–564. DOI: 10.1515/hsz-2012-0119.

Domingues, A., Almeida, S., da Cruz e Silva, E.F., Oliveira, C.R. & Rego, A.C. 2007. Toxicity of β-amyloid in HEK293 cells expressing NR1/NR2A or NR1/NR2B N-methyl-d-aspartate receptor subunits. *Neurochemistry International*. 50(6):872–880. DOI: 10.1016/j.neuint.2007.03.001.

Dominguez, R. & Holmes, K.C. 2011. Actin Structure and Function. *Annual review of biophysics*. 40:169–186. DOI: 10.1146/annurev-biophys-042910-155359.

Domise, M., Sauvé, F., Didier, S., Caillerez, R., Bégard, S., Carrier, S., Colin, M., Marinangeli, C., et al. 2019. Neuronal AMP-activated protein kinase hyper-activation induces synaptic loss by an autophagy-mediated process. *Cell Death & Disease*. 10(3):1–15. DOI: 10.1038/s41419-019-1464-x.

Donmez, G. 2012. The Effects of SIRT1 on Alzheimer's Disease Models. *International Journal of Alzheimer's Disease*. 2012:509529. DOI: 10.1155/2012/509529.

Du Clos, T.W. & Mold, C. 2011. Pentraxins (CRP, SAP) in the process of complement activation and clearance of apoptotic bodies through Fcγ receptors. *Current opinion in organ transplantation*. 16(1):15–20. DOI: 10.1097/MOT.0b013e32834253c7.

Duan, Y., Dong, S., Gu, F., Hu, Y. & Zhao, Z. 2012. Advances in the Pathogenesis of Alzheimer's Disease: Focusing on Tau-Mediated Neurodegeneration. *Translational Neurodegeneration*. 1(1):24. DOI: 10.1186/2047-9158-1-24.

Dumont, M., Kipiani, K., Yu, F., Wille, E., Katz, M., Calingasan, N.Y., Gouras, G.K., Lin, M.T., et al. 2011. Coenzyme Q10 Decreases Amyloid Pathology and Improves Behavior in a Transgenic Mouse Model of Alzheimer's Disease. *Journal of Alzheimer's Disease*. 27(1):211–223. DOI: 10.3233/JAD-2011-110209.

Ehehalt, R., Keller, P., Haass, C., Thiele, C. & Simons, K. 2003. Amyloidogenic processing of the Alzheimer β-amyloid precursor protein depends on lipid rafts. *The Journal of Cell Biology*. 160(1):113–123. DOI: 10.1083/jcb.200207113.

Ehlermann, P., Eggers, K., Bierhaus, A., Most, P., Weichenhan, D., Greten, J., Nawroth, P.P., Katus, H.A., et al. 2006. Increased proinflammatory endothelial response to S100A8/A9 after preactivation through advanced glycation end products. *Cardiovascular Diabetology*. 5(1):6. DOI: 10.1186/1475-2840-5-6.

Ellis, C., Ward, N.L., Rice, M., Ball, N.J., Walle, P., Najdek, C., Kilinc, D., Lambert, J.-C., et al. 2024. The structure of an amyloid precursor protein/talin complex indicates a mechanical basis of Alzheimer's disease. *Open Biology*. 14(11):240185. DOI: 10.1098/rsob.240185.

Endemann, D.H. & Schiffrin, E.L. 2004. Endothelial dysfunction. *Journal of the American Society of Nephrology: JASN*. 15(8):1983–1992. DOI: 10.1097/01.ASN.0000132474.50966.DA.

Engel, D.F., Grzyb, A.N., de Oliveira, J., Pötzsch, A., Walker, T.L., Brocardo, P.S., Kempermann, G. & de Bem, A.F. 2019. Impaired adult hippocampal neurogenesis in a mouse model of familial hypercholesterolemia: A role for the LDL receptor and cholesterol metabolism in adult neural precursor cells. *Molecular Metabolism*. 30:1–15. DOI: 10.1016/j.molmet.2019.09.002.

Estudillo, E., López-Ornelas, A., Rodríguez-Oviedo, A., de la Cruz, N.G., Vargas-Hernández, M.A. & Jiménez, A. 2023. Thinking outside the black box: are the brain endothelialcells the new main target in Alzheimer's disease? *Neural Regeneration Research*. 18(12):2592–2598. DOI: 10.4103/1673-5374.373672.

Fakruddin, M., Mannan, K.S.B., Chowdhury, A., Mazumdar, R.M., Hossain, Md.N., Islam, S. & Chowdhury, Md.A. 2013. Nucleic acid amplification: Alternative methods of polymerase chain reaction. *Journal of Pharmacy & Bioallied Sciences*. 5(4):245–252. DOI: 10.4103/0975-7406.120066.

Fan, Q., Yu, W., Senda, T., Yanagisawa, K. & Michikawa, M. 2001. Cholesterol-dependent modulation of tau phosphorylation in cultured neurons. *Journal of Neurochemistry*. 76(2):391–400. DOI: 10.1046/j.1471-4159.2001.00063.x.

Fang, Y.-C., Hsieh, Y.-C., Hu, C.-J. & Tu, Y.-K. 2023. Endothelial Dysfunction in Neurodegenerative Diseases. *International Journal of Molecular Sciences*. 24(3):2909. DOI: 10.3390/ijms24032909.

Farias, H.R., Ramos, J.M.O., Griesang, C.T., Santos, L., Junior, O.V.R., Souza, D.G., Ferreira, F.S., Somacal, S., et al. 2024. LDL Exposure Disrupts Mitochondrial Function and Dynamics in a Hippocampal Neuronal Cell Line. *Molecular Neurobiology*. (September, 20). DOI: 10.1007/s12035-024-04476-y.

farnesol (CHEBI:28600). n.d. Available: https://www.ebi.ac.uk/chebi/searchId.do?chebiId=CHEBI:28600 [2024, November 27].

Fearon, I. 2006. OxLDL enhances L-type Ca2+ currents via lysophosphatidylcholine-induced mitochondrial reactive oxygen species (ROS) production. *Cardiovascular Research*. 69(4):855–864. DOI: 10.1016/j.cardiores.2005.11.019.

Feles, S., Overath, C., Reichardt, S., Diegeler, S., Schmitz, C., Kronenberg, J., Baumstark-Khan, C., Hemmersbach, R., et al. 2022. Streamlining Culture Conditions for the Neuroblastoma Cell Line SH-SY5Y: A Prerequisite for Functional Studies. *Methods and Protocols*. 5(4):58. DOI: 10.3390/mps5040058.

Feron, O., Dessy, C., Moniotte, S., Desager, J.P. & Balligand, J.L. 1999. Hypercholesterolemia decreases nitric oxide production by promoting the interaction of caveolin and endothelial nitric oxide synthase. *The Journal of Clinical Investigation*. 103(6):897–905. DOI: 10.1172/JCI4829.

Ferroni, P., Basili, S. & Davi, G. 2003. Platelet Activation, Inflammatory Mediators and Hypercholesterolemia. *Current Vascular Pharmacology*. 1(2):157–169. DOI: 10.2174/1570161033476772.

Filograna, R., Mennuni, M., Alsina, D. & Larsson, N.-G. 2021. Mitochondrial DNA copy number in human disease: the more the better? *FEBS Letters*. 595(8):976–1002. DOI: 10.1002/1873-3468.14021.

Fletcher, D.A. & Mullins, R.D. 2010. Cell mechanics and the cytoskeleton. *Nature*. 463(7280):485–492. DOI: 10.1038/nature08908.

Fong, L.K., Yang, M.M., dos Santos Chaves, R., Reyna, S.M., Langness, V.F., Woodruff, G., Roberts, E.A., Young, J.E., et al. 2018. Full-length amyloid precursor protein regulates lipoprotein metabolism and amyloid-β clearance in human astrocytes. *Journal of Biological Chemistry*. 293(29):11341–11357. DOI: 10.1074/jbc.RA117.000441.

Fontana, I.C., Zimmer, A.R., Rocha, A.S., Gosmann, G., Souza, D.O., Lourenco, M.V., Ferreira, S.T. & Zimmer, E.R. 2020. Amyloid-β oligomers in cellular models of Alzheimer's disease. *Journal of Neurochemistry*. 155(4):348–369. DOI: 10.1111/jnc.15030.

Forster, J.I., Köglsberger, S., Trefois, C., Boyd, O., Baumuratov, A.S., Buck, L., Balling, R. & Antony, P.M.A. 2016. Characterization of Differentiated SH-SY5Y as Neuronal Screening Model Reveals Increased Oxidative Vulnerability. *SLAS Discovery*. 21(5):496–509. DOI: 10.1177/1087057115625190.

Fort, A.G., Murray, J.W., Dandachi, N., Davidson, M.W., Dermietzel, R., Wolkoff, A.W. & Spray, D.C. 2011. In Vitro Motility of Liver Connexin Vesicles along Microtubules Utilizes Kinesin Motors. *Journal of Biological Chemistry*. 286(26):22875–22885. DOI: 10.1074/jbc.M111.219709.

Frame, N.M. & Gursky, O. 2017. Structure of serum amyloid A suggests a mechanism for selective lipoprotein binding and functions: SAA as a hub in macromolecular interaction networks. *Amyloid*. 24(sup1):13–14. DOI: 10.1080/13506129.2016.1270930.

Franco-Cea, A., Ellis, S.J., Fairchild, M.J., Yuan, L., Cheung, T.Y.S. & Tanentzapf, G. 2010. Distinct developmental roles for direct and indirect talin-mediated linkage to actin. *Developmental Biology*. 345(1):64–77. DOI: 10.1016/j.ydbio.2010.06.027.

Frears, E.R., Stephens, D.J., Walters, C.E., Davies, H. & Austen, B.M. 1999. The role of cholesterol in the biosynthesis of beta-amyloid. *Neuroreport*. 10(8):1699–1705. DOI: 10.1097/00001756-199906030-00014.

Frederick, K. & Ciborowski, P. 2016. 9 - SWATH-MS: Data Acquisition and Analysis. In *Proteomic Profiling and Analytical Chemistry (Second Edition)*. P. Ciborowski & J. Silberring, Eds. Boston: Elsevier. 161–173. DOI: 10.1016/B978-0-444-63688-1.00009-4.

Fukai, T. 2002. Extracellular superoxide dismutase and cardiovascular disease. *Cardiovascular Research*. 55(2):239–249. DOI: 10.1016/S0008-6363(02)00328-0.

Fukai, T., Galis, Z.S., Meng, X.P., Parthasarathy, S. & Harrison, D.G. 1998. Vascular expression of extracellular superoxide dismutase in atherosclerosis. *Journal of Clinical Investigation*. 101(10):2101–2111. DOI: 10.1172/JCI2105.

Fukushima, N., Furuta, D., Hidaka, Y., Moriyama, R. & Tsujiuchi, T. 2009. Post-translational modifications of tubulin in the nervous system. *Journal of Neurochemistry*. 109(3):683–693. DOI: 10.1111/j.1471-4159.2009.06013.x.

Gamba, P., Testa, G., Gargiulo, S., Staurenghi, E., Poli, G. & Leonarduzzi, G. 2015. Oxidized cholesterol as the driving force behind the development of Alzheimer's disease. *Frontiers in Aging Neuroscience*. 7:119. DOI: 10.3389/fnagi.2015.00119.

Ganjali, S., Keshavarz, R., Hosseini, S., Mansouri, A., Mannarino, M.R., Pirro, M., Jamialahmadi, T. & Sahebkar, A. 2021. Evaluation of Oxidative Stress Status in Familial Hypercholesterolemia. *Journal of Clinical Medicine*. 10(24):5867. DOI: 10.3390/jcm10245867.

Gao, H.-M., Zhou, H. & Hong, J.-S. 2012. NADPH oxidases: novel therapeutic targets for neurodegenerative diseases. *Trends in Pharmacological Sciences*. 33(6):295–303. DOI: 10.1016/j.tips.2012.03.008.

Gaugler, J., James, B., Johnson, T., Reimer, J. & Wueve, J. 2021. Alzheimer's disease facts and figures. *Alzheimer's & Dementia*. 17(3):327–406. DOI: 10.1002/alz.12328.

Goicoechea, L., Conde de la Rosa, L., Torres, S., García-Ruiz, C. & Fernández-Checa, J.C. 2023. Mitochondrial cholesterol: Metabolism and impact on redox biology and disease. *Redox Biology*. 61:102643. DOI: 10.1016/j.redox.2023.102643.

Goldstein, J.L. & Brown, M.S. 2009. History of Discovery: The LDL Receptor. *Arteriosclerosis, thrombosis, and vascular biology*. 29(4):431–438. DOI: 10.1161/ATVBAHA.108.179564.

Goldstein, M.R. & Mascitelli, L. 2013. Do statins cause diabetes? *Current Diabetes Reports*. 13(3):381–390. DOI: 10.1007/s11892-013-0368-x.

Gong, C.-X. & Iqbal, K. 2008. Hyperphosphorylation of Microtubule-Associated Protein Tau: A Promising Therapeutic Target for Alzheimer Disease. *Current medicinal chemistry*. 15(23):2321–2328.

Gong, C.X., Shaikh, S., Wang, J.Z., Zaidi, T., Grundke-Iqbal, I. & Iqbal, K. 1995. Phosphatase activity toward abnormally phosphorylated tau: decrease in Alzheimer disease brain. *Journal of Neurochemistry*. 65(2):732–738. DOI: 10.1046/j.1471-4159.1995.65020732.x.

Good, D.J., Polverini, P.J., Rastinejad, F., Le Beau, M.M., Lemons, R.S., Frazier, W.A. & Bouck, N.P. 1990. A tumor suppressor-dependent inhibitor of angiogenesis is immunologically and functionally indistinguishable from a fragment of thrombospondin. *Proceedings of the National Academy of Sciences*. 87(17):6624–6628. DOI: 10.1073/pnas.87.17.6624.

Goodenough, D.A. & Paul, D.L. 2009. Gap Junctions. *Cold Spring Harbor Perspectives in Biology*. 1(1):a002576. DOI: 10.1101/cshperspect.a002576.

Grantham, J. 2020. The Molecular Chaperone CCT/TRiC: An Essential Component of Proteostasis and a Potential Modulator of Protein Aggregation. *Frontiers in Genetics*. 11. DOI: 10.3389/fgene.2020.00172.

Green, P.S., Mendez, A.J., Jacob, J.S., Crowley, J.R., Growdon, W., Hyman, B.T. & Heinecke, J.W. 2004. Neuronal expression of myeloperoxidase is increased in Alzheimer's disease. *Journal of Neurochemistry*. 90(3):724–733. DOI: 10.1111/j.1471-4159.2004.02527.x.

Gu, L. & Guo, Z. 2013. Alzheimer's Aβ42 and Aβ40 peptides form interlaced amyloid fibrils. *Journal of Neurochemistry*. 126(3):305–311. DOI: 10.1111/jnc.12202.

Guerra-De-Blas, P.D.C., Bobadilla-Del-Valle, M., Sada-Ovalle, I., Estrada-García, I., Torres-González, P., López-Saavedra, A., Guzmán-Beltrán, S., Ponce-de-León, A., et al. 2019. Simvastatin Enhances the Immune Response Against Mycobacterium tuberculosis. *Frontiers in Microbiology*. 10:2097. DOI: 10.3389/fmicb.2019.02097.

Gui, Y., Zheng, H. & Cao, R.Y. 2022. Foam Cells in Atherosclerosis: Novel Insights Into Its Origins, Consequences, and Molecular Mechanisms. *Frontiers in Cardiovascular Medicine*. 9. DOI: 10.3389/fcvm.2022.845942.

Gülden, M., Jess, A., Kammann, J., Maser, E. & Seibert, H. 2010. Cytotoxic potency of H2O2 in cell cultures: Impact of cell concentration and exposure time. *Free Radical Biology and Medicine*. 49(8):1298–1305. DOI: 10.1016/j.freeradbiomed.2010.07.015.

Gunning, P., O'neill, G. & Hardeman, E. 2008. Tropomyosin-Based Regulation of the Actin Cytoskeleton in Time and Space. *Physiological Reviews*. 88(1):1–35. DOI: 10.1152/physrev.00001.2007.

Guo, B., Huang, Y., Gao, Q. & Zhou, Q. 2020. Stabilization of microtubules improves cognitive functions and axonal transport of mitochondria in Alzheimer's disease model mice. *Neurobiology of Aging*. 96:223–232. DOI: 10.1016/j.neurobiolaging.2020.09.011.

Guo, J., Chen, S., Zhang, Y., Liu, J., Jiang, L., Hu, L., Yao, K., Yu, Y., et al. 2024. Cholesterol metabolism: physiological regulation and diseases. *MedComm*. 5(2):e476. DOI: 10.1002/mco2.476.

Guo, N., Krutzsch, H.C., Inman, J.K. & Roberts, D.D. 1997. Thrombospondin 1 and Type I Repeat Peptides of Thrombospondin 1 Specifically Induce Apoptosis of Endothelial Cells1. *Cancer Research*. 57(9):1735–1742.

Guo, Q., Feng, X. & Zhou, Y. 2020. PCSK9 Variants in Familial Hypercholesterolemia: A Comprehensive Synopsis. *Frontiers in Genetics*. 11:1020. DOI: 10.3389/fgene.2020.01020.

Gutierrez, L.S. & Gutierrez, J. 2021. Thrombospondin 1 in Metabolic Diseases. *Frontiers in Endocrinology*. 12. DOI: 10.3389/fendo.2021.638536.

Guven, K., Gunning, P. & Fath, T. 2011. TPM3 and TPM4 gene products segregate to the postsynaptic region of central nervous system synapses. *BioArchitecture*. 1(6):284–289. DOI: 10.4161/bioa.1.6.19336.

Hamazaki, H. 1995. Amyloid P component promotes aggregation of Alzheimer's beta-amyloid peptide. *Biochemical and Biophysical Research Communications*. 211(2):349–353. DOI: 10.1006/bbrc.1995.1819.

Han, Y. & Kim, S.J. 2018. Simvastatin-dependent actin cytoskeleton rearrangement regulates differentiation via the extracellular signal-regulated kinase-1/2 and p38 kinase pathways in rabbit articular chondrocytes. *European Journal of Pharmacology*. 834:197–205. DOI: 10.1016/j.ejphar.2018.07.016.

Han, X.-J., Hu, Y.-Y., Yang, Z.-J., Jiang, L.-P., Shi, S.-L., Li, Y.-R., Guo, M.-Y., Wu, H.-L., et al. 2017. Amyloid β-42 induces neuronal apoptosis by targeting mitochondria. *Molecular Medicine Reports*. 16(4):4521–4528. DOI: 10.3892/mmr.2017.7203.

Hansen, K.B., Yi, F., Perszyk, R., Menniti, F.S. & Traynelis, S.F. 2017. NMDA receptors in the central nervous system. *Methods in molecular biology (Clifton, N.J.)*. 1677:1–80. DOI: 10.1007/978-1-4939-7321-7_1.

Haque, R.U. & Levey, A.I. 2019. Alzheimer's disease: A clinical perspective and future nonhuman primate research opportunities. *Proceedings of the National Academy of Sciences*. 116(52):26224–26229. DOI: 10.1073/pnas.1912954116.

Hedman, A.C., Smith, J.M. & Sacks, D.B. 2015. The biology of IQGAP proteins: beyond the cytoskeleton. *EMBO reports*. 16(4):427–446. DOI: 10.15252/embr.201439834.

Heneka, M.T., Golenbock, D.T. & Latz, E. 2015. Innate immunity in Alzheimer's disease. *Nature Immunology*. 16(3):229–236. DOI: 10.1038/ni.3102.

Heneka, M.T., Carson, M.J., El Khoury, J., Landreth, G.E., Brosseron, F., Feinstein, D.L., Jacobs, A.H., Wyss-Coray, T., et al. 2015. Neuroinflammation in Alzheimer's Disease. *The Lancet. Neurology*. 14(4):388–405. DOI: 10.1016/S1474-4422(15)70016-5.

Herman, M.A. & Samuel, V.T. 2016. The sweet path to metabolic demise: fructose and lipid synthesis. *Trends in endocrinology and metabolism: TEM*. 27(10):719–730. DOI: 10.1016/j.tem.2016.06.005.

Herrmann, H., Bär, H., Kreplak, L., Strelkov, S.V. & Aebi, U. 2007. Intermediate filaments: from cell architecture to nanomechanics. *Nature Reviews Molecular Cell Biology*. 8(7):562–573. DOI: 10.1038/nrm2197.

Hiyoshi, H., Yanagimachi, M., Ito, M., Yasuda, N., Okada, T., Ikuta, H., Shinmyo, D., Tanaka, K., et al. 2003. Squalene synthase inhibitors suppress triglyceride biosynthesis through the farnesol pathway in rat hepatocytes Published, JLR Papers in Press, October 16, 2002. DOI 10.1194/jlr.M200316-JLR200. *Journal of Lipid Research*. 44:128–135. DOI: 10.1194/JLR.M200316-JLR200.

Hohmann, T. & Dehghani, F. 2019. The Cytoskeleton—A Complex Interacting Meshwork. *Cells*. 8(4):362. DOI: 10.3390/cells8040362.

Hornby, J.M., Kebaara, B.W. & Nickerson, K.W. 2003. Farnesol Biosynthesis in Candida albicans: Cellular Response to Sterol Inhibition by Zaragozic Acid B. *Antimicrobial Agents and Chemotherapy*. 47(7):2366–2369. DOI: 10.1128/AAC.47.7.2366-2369.2003.

Hu, X., Crick, S.L., Bu, G., Frieden, C., Pappu, R. & Lee, J. 2009. Amyloid seeds formed by cellular uptake, concentration, and aggregation of the amyloid-beta peptide. *Proceedings of the National Academy of Sciences*. 106:20324–20329. DOI: 10.1073/pnas.0911281106.

Huang, L.-K., Kuan, Y.-C., Lin, H.-W. & Hu, C.-J. 2023. Clinical trials of new drugs for Alzheimer disease: a 2020–2023 update. *Journal of Biomedical Science*. 30:83. DOI: 10.1186/s12929-023-00976-6.

Huang, X., Su, Y., Wang, N., Li, H., Li, Z., Yin, G., Chen, H., Niu, J., et al. 2021. Astroglial Connexins in Neurodegenerative Diseases. *Frontiers in Molecular Neuroscience*. 14. DOI: 10.3389/fnmol.2021.657514.

Hughes, C.G., Pandharipande, P.P., Thompson, J.L., Chandrasekhar, R., Ware, L.B., Ely, E.W. & Girard, T.D. 2016. Endothelial Activation and Blood-Brain Barrier Injury as Risk Factors for Delirium in Critically Ill Patients. *Critical care medicine*. 44(9):e809–e817. DOI: 10.1097/CCM.0000000000001739.

Hutter-Paier, B., Huttunen, H.J., Puglielli, L., Eckman, C.B., Kim, D.Y., Hofmeister, A., Moir, R.D., Domnitz, S.B., et al. 2004. The ACAT Inhibitor CP-113,818 Markedly Reduces Amyloid Pathology in a Mouse Model of Alzheimer's Disease. *Neuron*. 44(2):227–238. DOI: 10.1016/j.neuron.2004.08.043.

Huttunen, H.J. & Kovacs, D.M. 2008. ACAT as a Drug Target for Alzheimer's Disease. *Neuro-Degenerative Diseases*. 5(3–4):212–214. DOI: 10.1159/000113705.

Huttunen, H.J., Peach, C., Bhattacharyya, R., Barren, C., Pettingell, W., Hutter-Paier, B., Windisch, M., Berezovska, O., et al. 2009. Inhibition of acyl-coenzyme A: cholesterol acyl transferase modulates amyloid precursor protein trafficking in the early secretory pathway. *The FASEB Journal*. 23(11):3819–3828. DOI: 10.1096/fj.09-134999.

Iashchishyn, I.A., Sulskis, D., Nguyen Ngoc, M., Smirnovas, V. & Morozova-Roche, L.A. 2017. Finke–Watzky Two-Step Nucleation–Autocatalysis Model of S100A9 Amyloid Formation: Protein Misfolding as "Nucleation" Event. *ACS Chemical Neuroscience*. 8(10):2152–2158. DOI: 10.1021/acschemneuro.7b00251.

IGHG4 immunoglobulin heavy constant gamma 4 (G4m marker) [Homo sapiens (human)] - Gene - NCBI. n.d. Available: https://www.ncbi.nlm.nih.gov/gene?Db=gene&Cmd=DetailsSearch&Term=3503 [2025, February 12].

Islam, M.M., Hlushchenko, I. & Pfisterer, S.G. 2022. Low-Density Lipoprotein Internalization, Degradation and Receptor Recycling Along Membrane Contact Sites. *Frontiers in Cell and Developmental Biology*. 10. Available: https://www.frontiersin.org/article/10.3389/fcell.2022.826379 [2022, June 30].

Jang, B.G., Yun, S.-M., Ahn, K., Song, J.H., Jo, S.A., Kim, Y.-Y., Kim, D.K., Park, M.H., et al. 2010. Plasma carbonic anhydrase II protein is elevated in Alzheimer's disease. *Journal of Alzheimer's disease: JAD*. 21(3):939–945. DOI: 10.3233/JAD-2010-100384.

Jayaraman, S., Haupt, C. & Gursky, O. 2016. Paradoxical effects of SAA on lipoprotein oxidation suggest a new antioxidant function for SAA[S]. *Journal of Lipid Research*. 57(12):2138–2149. DOI: 10.1194/jlr.M071191.

Jeng, J., Yeh, T., Lee, J., Lin, S., Fong, T. & Hsieh, R. 2008. Maintenance of mitochondrial DNA copy number and expression are essential for preservation of mitochondrial function and cell growth. *Journal of Cellular Biochemistry*. 103(2):347–357. DOI: 10.1002/jcb.21625.

Jeon, S.-M. 2016. Regulation and function of AMPK in physiology and diseases. *Experimental & Molecular Medicine*. 48(7):e245–e245. DOI: 10.1038/emm.2016.81.

Jin, M., Liu, C., Han, W. & Cong, Y. 2019. TRiC/CCT Chaperonin: Structure and Function. *Sub-Cellular Biochemistry*. 93:625–654. DOI: 10.1007/978-3-030-28151-9_19.

Jin, U., Park, S.J. & Park, S.M. 2019. Cholesterol Metabolism in the Brain and Its Association with Parkinson's Disease. *Experimental Neurobiology*. 28(5):554–567. DOI: 10.5607/en.2019.28.5.554.

Jumeau, C., Awad, F., Assrawi, E., Cobret, L., Duquesnoy, P., Giurgea, I., Valeyre, D., Grateau, G., et al. 2019. Expression of SAA1, SAA2 and SAA4 genes in human primary monocytes and monocyte-derived macrophages. *PloS One*. 14(5):e0217005. DOI: 10.1371/journal.pone.0217005.

Kamalaldinezabadi, S.S., Watzlawik, J.O., Rosenberry, T.L., Paravastu, A.K. & Stagg, S.M. 2024. DOI: 10.1101/2024.07.30.605873.

Kamenetz, F., Tomita, T., Hsieh, H., Seabrook, G., Borchelt, D., Iwatsubo, T., Sisodia, S. & Malinow, R. 2003. APP Processing and Synaptic Function. *Neuron*. 37(6):925–937. DOI: 10.1016/S0896-6273(03)00124-7.

Kang, S., Byun, J., Son, S.M. & Mook-Jung, I. 2018. Thrombospondin-1 protects against Aβ-induced mitochondrial fragmentation and dysfunction in hippocampal cells. *Cell Death Discovery*. 4(1):1–12. DOI: 10.1038/s41420-017-0023-4.

van der Kant, R., Langness, V.F., Herrera, C.M., Williams, D.A., Fong, L.K., Leestemaker, Y., Steenvoorden, E., Rynearson, K.D., et al. 2019. Cholesterol Metabolism Is a Druggable Axis that Independently Regulates Tau and Amyloid-β in iPSC-Derived Alzheimer's Disease Neurons. *Cell Stem Cell*. 24(3):363-375.e9. DOI: 10.1016/j.stem.2018.12.013.

Karp, N.A. & Lilley, K.S. 2007. Design and analysis issues in quantitative proteomics studies. *Proteomics*. 7 Suppl 1:42–50. DOI: 10.1002/pmic.200700683.

Keen, J.H. & Jakoby, W.B. 1978. Glutathione transferases. Catalysis of nucleophilic reactions of glutathione. *The Journal of Biological Chemistry*. 253(16):5654–5657.

Kerr, A.G., Tam, L.C.S., Hale, A.B., Cioroch, M., Douglas, G., Agkatsev, S., Hibbitt, O., Mason, J., et al. 2017. A Genomic DNA Reporter Screen Identifies Squalene Synthase Inhibitors That Act Cooperatively with Statins to Upregulate the Low-Density Lipoprotein Receptor. *Journal of Pharmacology and Experimental Therapeutics*. 361(3):417–428. DOI: 10.1124/jpet.116.239574.

Khan, M.G. 2006. Diabetes and Cardiovascular Disease. In *Encyclopedia of Heart Diseases*. M.G. Khan, Ed. Burlington: Academic Press. 293–306. DOI: 10.1016/B978-012406061-6/50051-5.

Khan, R. & Sultana, S. 2011. Farnesol attenuates 1,2-dimethylhydrazine induced oxidative stress, inflammation and apoptotic responses in the colon of Wistar rats. *Chemico-Biological Interactions*. 192(3):193–200. DOI: 10.1016/j.cbi.2011.03.009.

Khan, A.A., Alsahli, M.A. & Rahmani, A.H. 2018. Myeloperoxidase as an Active Disease Biomarker: Recent Biochemical and Pathological Perspectives. *Medical Sciences*. 6(2):33. DOI: 10.3390/medsci6020033.

Khan, S.R., Yaqub, A., Wolters, F.J., Ikram, M.K., Dalm, V.A.S.H., Chaker, L. & Ikram, M.A. 2021. The association of serum immunoglobulins with cognition and dementia: The Rotterdam Study. *Alzheimer's & Dementia*. 17(S5):e053612. DOI: 10.1002/alz.053612.

Khoo, L.H.B., Thiam, C.H., Soh, S.Y. & Angeli, V. 2015. Splenic extrafollicular reactions and BM plasma cells sustain IgM response associated with hypercholesterolemia. *European Journal of Immunology*. 45(5):1300–1312. DOI: 10.1002/eji.201344347.

Kiener, P.A., Davis, P.M., Murray, J.L., Youssef, S., Rankin, B.M. & Kowala, M. 2001. Stimulation of inflammatory responses in vitro and in vivo by lipophilic HMG-CoA reductase inhibitors. *International Immunopharmacology*. 1(1):105–118. DOI: 10.1016/S0162-3109(00)00272-1.

Kierans, S.J. & Taylor, C.T. 2024. Glycolysis: A multifaceted metabolic pathway and signaling hub. *Journal of Biological Chemistry*. 300(11):107906. DOI: 10.1016/j.jbc.2024.107906.

Kim, J., Castellano, J.M., Jiang, H., Basak, J.M., Parsadanian, M., Pham, V., Mason, S.M., Paul, S.M., et al. 2009. Overexpression of Low Density Lipoprotein Receptor in the Brain Markedly Inhibits Amyloid Deposition and Increases Extracellular Aβ Clearance. *Neuron*. 64(5):632–644. DOI: 10.1016/j.neuron.2009.11.013.

Kim, S.Y., Moon, J.H., Lee, H.G., Kim, S.U. & Lee, Y.B. 2007. ATP released from β-amyloid-stimulated microglia induces reactive oxygen species production in an autocrine fashion. *Experimental & Molecular Medicine*. 39(6):820–827. DOI: 10.1038/emm.2007.89.

Kliment, C.R., Tobolewski, J.M., Manni, M.L., Tan, R.J., Enghild, J. & Oury, T.D. 2008. Extracellular Superoxide Dismutase Protects Against Matrix Degradation of Heparan Sulfate in the Lung. *Antioxidants & Redox Signaling*. 10(2):261–268. DOI: 10.1089/ars.2007.1906.

Kochumon, S., Hasan, A., Al-Rashed, F., Sindhu, S., Thomas, R., Jacob, T., Al-Sayyar, A., Arefanian, H., et al. 2022. Increased Adipose Tissue Expression of IL-23 Associates with Inflammatory Markers in People with High LDL Cholesterol. *Cells*. 11(19):3072. DOI: 10.3390/cells11193072.

Kojro, E., Füger, P., Prinzen, C., Kanarek, A.M., Rat, D., Endres, K., Fahrenholz, F. & Postina, R. 2010. Statins and the squalene synthase inhibitor zaragozic acid stimulate the non-amyloidogenic pathway of amyloid-beta protein precursor processing by suppression of cholesterol synthesis. *Journal of Alzheimer's disease: JAD*. 20(4):1215–1231. DOI: 10.3233/JAD-2010-091621.

Kontush, A. 2006. Lipid peroxidation and Alzheimer's disease: Key role of Amyloid-β. *Oléagineux, Corps gras, Lipides*. 13(1):46–53. DOI: 10.1051/ocl.2006.2222.

Köpke, E., Tung, Y.C., Shaikh, S., Alonso, A.C., Iqbal, K. & Grundke-Iqbal, I. 1993. Microtubule-associated protein tau. Abnormal phosphorylation of a non-paired helical filament pool in Alzheimer disease. *Journal of Biological Chemistry*. 268(32):24374–24384. DOI: 10.1016/S0021-9258(20)80536-5.

Koriyama, Y., Furukawa, A., Muramatsu, M., Takino, J. & Takeuchi, M. 2015. Glyceraldehyde caused Alzheimer's disease-like alterations in diagnostic marker levels in SH-SY5Y human neuroblastoma cells. *Scientific Reports*. 5(1):13313. DOI: 10.1038/srep13313.

Koushki, K., Shahbaz, S.K., Mashayekhi, K., Sadeghi, M., Zayeri, Z.D., Taba, M.Y., Banach, M., Al-Rasadi, K., et al. 2021. Anti-inflammatory Action of Statins in Cardiovascular Disease: the Role of Inflammasome and Toll-Like Receptor Pathways. *Clinical Reviews in Allergy & Immunology*. 60(2):175–199. DOI: 10.1007/s12016-020-08791-9.

Krabbe, G., Halle, A., Matyash, V., Rinnenthal, J.L., Eom, G.D., Bernhardt, U., Miller, K.R., Prokop, S., et al. 2013. Functional Impairment of Microglia Coincides with Beta-Amyloid Deposition in Mice with Alzheimer-Like Pathology. *PLoS ONE*. 8(4):e60921. DOI: 10.1371/journal.pone.0060921.

Kril, J.J., Patel, S., Harding, A.J. & Halliday, G.M. 2002. Neuron loss from the hippocampus of Alzheimer's disease exceeds extracellular neurofibrillary tangle formation. *Acta Neuropathologica*. 103(4):370–376. DOI: 10.1007/s00401-001-0477-5.

Krishtal, J., Bragina, O., Metsla, K., Palumaa, P. & Tõugu, V. 2015. Toxicity of amyloid beta 1-40 and 1-42 on SH-SY5Y cell line. *SpringerPlus*. 4(Suppl 1):P19. DOI: 10.1186/2193-1801-4-S1-P19.

Krishtal, J., Bragina, O., Metsla, K., Palumaa, P. & Tõugu, V. 2017. In situ fibrillizing amyloid-beta 1-42 induces neurite degeneration and apoptosis of differentiated SH-SY5Y cells. *PLOS ONE*. 12(10):e0186636. DOI: 10.1371/journal.pone.0186636.

Kumar, R.A., Pilz, D.T., Babatz, T.D., Cushion, T.D., Harvey, K., Topf, M., Yates, L., Robb, S., et al. 2010. TUBA1A mutations cause wide spectrum lissencephaly (smooth brain) and suggest that multiple neuronal migration pathways converge on alpha tubulins. *Human Molecular Genetics*. 19(14):2817–2827. DOI: 10.1093/hmg/ddq182.

Kurvits, L., Reimann, E., Kadastik-Eerme, L., Truu, L., Kingo, K., Erm, T., Kõks, S., Taba, P., et al. 2019. Serum Amyloid Alpha Is Downregulated in Peripheral Tissues of Parkinson's Disease Patients. *Frontiers in Neuroscience*. 13. DOI: 10.3389/fnins.2019.00013.

Lakka Klement, G., Shai, E. & Varon, D. 2013. Chapter 24 - The Role of Platelets in Angiogenesis. In *Platelets (Third Edition)*. A.D. Michelson, Ed. Academic Press. 487–502. DOI: 10.1016/B978-0-12-387837-3.00024-9.

Landmesser, U., Bahlmann, F., Mueller, M., Spiekermann, S., Kirchhoff, N., Schulz, S., Manes, C., Fischer, D., et al. 2005. Simvastatin Versus Ezetimibe: Pleiotropic and Lipid-Lowering Effects on Endothelial Function in Humans. *Circulation*. 111(18):2356–2363. DOI: 10.1161/01.CIR.0000164260.82417.3F.

Larvie, M., Shoup, T., Chang, W.-C., Chigweshe, L., Hartshorn, K., White, M.R., Stahl, G.L., Elmaleh, D.R., et al. 2012. Mannose-Binding Lectin Binds to Amyloid Protein and Modulates Inflammation. *Journal of Biomedicine and Biotechnology*. 2012:1–12. DOI: 10.1155/2012/929803.

Lee, C., Liu, C., Hsieh, R. & Wei, Y. 2005. Oxidative Stress-Induced Depolymerization of Microtubules and Alteration of Mitochondrial Mass in Human Cells. *Annals of the New York Academy of Sciences*. 1042(1):246–254. DOI: 10.1196/annals.1338.027.

Lee, H.C., Yin, P.H., Lu, C.Y., Chi, C.W. & Wei, Y.H. 2000. Increase of mitochondria and mitochondrial DNA in response to oxidative stress in human cells. *Biochemical Journal*. 348(Pt 2):425–432.

Lemon, N., Canepa, E., Ilies, M.A. & Fossati, S. 2021. Carbonic Anhydrases as Potential Targets Against Neurovascular Unit Dysfunction in Alzheimer's Disease and Stroke. *Frontiers in Aging Neuroscience*. 13. DOI: 10.3389/fnagi.2021.772278.

Li, H.-H., Lin, C.-L. & Huang, C.-N. 2018. Neuroprotective effects of statins against amyloid β-induced neurotoxicity. *Neural Regeneration Research*. 13(2):198–206. DOI: 10.4103/1673-5374.226379.

Li, M.-Z., Zheng, L.-J., Shen, J., Li, X.-Y., Zhang, Q., Bai, X., Wang, Q.-S. & Ji, J.-G. 2018. SIRT1 facilitates amyloid beta peptide degradation by upregulating lysosome number in primary astrocytes. *Neural Regeneration Research*. 13(11):2005–2013. DOI: 10.4103/1673-5374.239449.

Li, N.-M., Liu, K.-F., Qiu, Y.-J., Zhang, H.-H., Nakanishi, H. & Qing, H. 2019. Mutations of beta-amyloid precursor protein alter the consequence of Alzheimer's disease pathogenesis. *Neural Regeneration Research*. 14(4):658. DOI: 10.4103/1673-5374.247469.

Li, P., Marshall, L., Oh, G., Jakubowski, J.L., Groot, D., He, Y., Wang, T., Petronis, A., et al. 2019. Epigenetic dysregulation of enhancers in neurons is associated with Alzheimer's disease pathology and cognitive symptoms. *Nature Communications*. 10(1):2246. DOI: 10.1038/s41467-019-10101-7.

Li, Y., Xie, Z., Luo, X., Wang, X., Wang, Y., Guo, M., Zhou, Z., Sun, R., et al. 2023. Farnesol Exerts Protective Effects against Chronic Sleep Deprivation-Induced Cognitive Impairment via Activation SIRT1/Nrf2 Pathway in the Hippocampi of Adult Mice. *Molecular Nutrition & Food Research*. 67(11):2200735. DOI: 10.1002/mnfr.202200735.

Liddell, J.R., Hoepken, H.H., Crack, P.J., Robinson, S.R. & Dringen, R. 2006. Glutathione peroxidase 1 and glutathione are required to protect mouse astrocytes from iron-mediated hydrogen peroxide toxicity. *Journal of Neuroscience Research*. 84(3):578–586. DOI: 10.1002/jnr.20957.

Lin, A., Liu, J., Gong, P., Chen, Y., Zhang, H., Zhang, Y. & Yu, Y. 2020. Serum amyloid A inhibits astrocyte migration via activating p38 MAPK. *Journal of Neuroinflammation*. 17(1):254. DOI: 10.1186/s12974-020-01924-z.

Lin, C.-L., Cheng, Y.-S., Li, H.-H., Chiu, P.-Y., Chang, Y.-T., Ho, Y.-J. & Lai, T.-J. 2016. Amyloid-β suppresses AMP-activated protein kinase (AMPK) signaling and contributes to α-synuclein-induced cytotoxicity. *Experimental Neurology*. 275:84–98. DOI: 10.1016/j.expneurol.2015.10.009.

Liste-Calleja, L., Lecina, M., Lopez-Repullo, J., Albiol, J., Solà, C. & Cairó, J.J. 2015. Lactate and glucose concomitant consumption as a self-regulated pH detoxification mechanism in HEK293 cell cultures. *Applied Microbiology and Biotechnology*. 99(23):9951–9960. DOI: 10.1007/s00253-015-6855-z.

Liu, K. & Czaja, M.J. 2013. Regulation of lipid stores and metabolism by lipophagy. *Cell Death & Differentiation*. 20(1):3–11. DOI: 10.1038/cdd.2012.63.

Liu, C.-S., Tsai, C.-S., Kuo, C.-L., Chen, H.-W., Lii, C.-K., Ma, Y.-S. & Wei, Y.-H. 2003. Oxidative stress-related alteration of the copy number of mitochondrial DNA in human leukocytes. *Free Radical Research*. 37(12):1307–1317. DOI: 10.1080/10715760310001621342.

Liu, H.-R., Tao, L., Gao, E., Qu, Y., Lau, W.B., Lopez, B.L., Christopher, T.A., Koch, W., et al. 2008. Rosiglitazone inhibits hypercholesterolaemia-induced myeloperoxidase upregulation--a novel mechanism for the cardioprotective effects of PPAR agonists. *Cardiovascular Research*. 81(2):344–352. DOI: 10.1093/cvr/cvn308.

Liu, S., Zhang, R., Zhang, L., Yang, A., Guo, Y., Jiang, L., Wang, H., Xu, S., et al. 2024. Oxidative stress suppresses PHB2 -mediated mitophagy in β-cells *via* the Nrf2/ PHB2 pathway. *Journal of Diabetes Investigation*. 15(5):559–571. DOI: 10.1111/jdi.14147.

Liu, X., Blazejewski, S.M., Bennison, S.A. & Toyo-oka, K. 2021. Glutathione S-transferase Pi (Gstp) proteins regulate neuritogenesis in the developing cerebral cortex. *Human Molecular Genetics*. 30(1):30–45. DOI: 10.1093/hmg/ddab003.

Liu, X., Sun, X., Zhang, Y., Jiang, W., Lai, M., Wiggins, K.L., Raffield, L.M., Bielak, L.F., et al. 2023. Association Between Whole Blood–Derived Mitochondrial DNA Copy Number, Low-Density Lipoprotein Cholesterol, and Cardiovascular Disease Risk. *Journal of the American Heart Association*. 12(20):e029090. DOI: 10.1161/JAHA.122.029090.

Livingston, G., Huntley, J., Sommerlad, A., Ames, D., Ballard, C., Banerjee, S., Brayne, C., Burns, A., et al. 2020. Dementia prevention, intervention, and care: 2020 report of the Lancet Commission. *Lancet (London, England)*. 396(10248):413–446. DOI: 10.1016/S0140-6736(20)30367-6.

Loers, G., Bork, U. & Schachner, M. 2024. Functional Relationships between L1CAM, LC3, ATG12, and Aβ. *International Journal of Molecular Sciences*. 25(19):10829. DOI: 10.3390/ijms251910829.

Long, J.M., Coble, D.W., Xiong, C., Schindler, S.E., Perrin, R.J., Gordon, B.A., Benzinger, T.L.S., Grant, E., et al. 2022. Preclinical Alzheimer's disease biomarkers accurately predict cognitive and neuropathological outcomes. *Brain: A Journal of Neurology*. 145(12):4506–4518. DOI: 10.1093/brain/awac250.

Lopez, A., Siddiqi, F.H., Villeneuve, J., Ureshino, R.P., Jeon, H.-Y., Koulousakis, P., Keeling, S., McEwan, W.A., et al. 2024. Carbonic anhydrase inhibition ameliorates tau toxicity via enhanced tau secretion. *Nature Chemical Biology*. (October, 31):1–11. DOI: 10.1038/s41589-024-01762-7.

Lovell, M.A., Xie, C. & Markesbery, W.R. 1998. Decreased glutathione transferase activity in brain and ventricular fluid in Alzheimer's disease. *Neurology*. 51(6):1562–1566. DOI: 10.1212/WNL.51.6.1562.

de Macedo-Silva, S.T., Visbal, G., Souza, G.F., dos Santos, M.R., Cämmerer, S.B., de Souza, W. & Rodrigues, J.C.F. 2022. Benzylamines as highly potent inhibitors of the sterol biosynthesis pathway in Leishmania amazonensis leading to oxidative stress and ultrastructural alterations. *Scientific Reports*. 12(1):11313. DOI: 10.1038/s41598-022-15449-3.

Madison, B.B. 2016. Srebp2: A master regulator of sterol and fatty acid synthesis1. *Journal of Lipid Research*. 57(3):333–335. DOI: 10.1194/jlr.C066712.

Manzoor, M.F., Arif, Z., Kabir, A., Mehmood, I., Munir, D., Razzaq, A., Ali, A., Goksen, G., et al. 2022. Oxidative stress and metabolic diseases: Relevance and therapeutic strategies. *Frontiers in Nutrition*. 9:994309. DOI: 10.3389/fnut.2022.994309.

Marais, A.D., Firth, J.C. & Blom, D.J. 2004. Familial hypercholesterolemia in South Africa. *Seminars in Vascular Medicine*. 4(1):93–95. DOI: 10.1055/s-2004-822991.

Marcoff, L. & Thompson, P.D. 2007. The Role of Coenzyme Q10 in Statin-Associated Myopathy. *Journal of the American College of Cardiology*. 49(23):2231–2237. DOI: 10.1016/j.jacc.2007.02.049.

Martinez-Hervas, S. & Ascaso, J.F. 2019. Hypercholesterolemia. In *Encyclopedia of Endocrine Diseases (Second Edition)*. I. Huhtaniemi & L. Martini, Eds. Oxford: Academic Press. 320–326. DOI: 10.1016/B978-0-12-801238-3.65340-0.

Massaad, C.A. & Klann, E. 2011. Reactive Oxygen Species in the Regulation of Synaptic Plasticity and Memory. *Antioxidants & Redox Signaling*. 14(10):2013. DOI: 10.1089/ars.2010.3208.

Mazidi, M., Dehghan, A., Banach, M., & on behalf of the Lipid and Blood Pressure Meta-Analysis Collaboration (LBPMC) Group and the International Lipid Expert Panel (ILEP). 2021. Genetically

Higher Level of Mannose Has No Impact on Cardiometabolic Risk Factors: Insight from Mendelian Randomization. *Nutrients*. 13(8):2563. DOI: 10.3390/nu13082563.

Meneghetti Da Rosa, J., Lidani, K.C.F., Andrade, F.A., Sena, L., Nisihara, R., Ambrosio, A.R. & Messias-Reason, I.J. 2024. Mannose Binding Lectin and C3 Serum Levels in Coronary Artery Disease: A Cross-Sectional Study. *Immunological Investigations*. 53(5):752–765. DOI: 10.1080/08820139.2024.2337023.

Metaxas, A. & Kempf, S.J. 2016. Neurofibrillary tangles in Alzheimer's disease: elucidation of the molecular mechanism by immunohistochemistry and tau protein phospho-proteomics. *Neural Regeneration Research*. 11(10):1579–1581. DOI: 10.4103/1673-5374.193234.

Michelucci, A., Heurtaux, T., Grandbarbe, L., Morga, E. & Heuschling, P. 2009. Characterization of the microglial phenotype under specific pro-inflammatory and anti-inflammatory conditions: Effects of oligomeric and fibrillar amyloid-β. *Journal of Neuroimmunology*. 210(1–2):3–12. DOI: 10.1016/j.jneuroim.2009.02.003.

Miller, Y.I., Altamentova, S.M. & Shaklai, N. 1997. Oxidation of low-density lipoprotein by hemoglobin stems from a heme-initiated globin radical: antioxidant role of haptoglobin. *Biochemistry*. 36(40):12189–12198. DOI: 10.1021/bi970258a.

Min, S.-W., Cho, S.-H., Zhou, Y., Schroeder, S., Haroutunian, V., Seeley, W.W., Huang, E.J., Shen, Y., et al. 2010. Acetylation of Tau Inhibits Its Degradation and Contributes to Tauopathy. *Neuron*. 67(6):953–966. DOI: 10.1016/j.neuron.2010.08.044.

Min, S.-W., Sohn, P.D., Li, Y., Devidze, N., Johnson, J.R., Krogan, N.J., Masliah, E., Mok, S.-A., et al. 2018. SIRT1 Deacetylates Tau and Reduces Pathogenic Tau Spread in a Mouse Model of Tauopathy. *The Journal of Neuroscience*. 38(15):3680–3688. DOI: 10.1523/JNEUROSCI.2369-17.2018.

Miralles, F. & Visa, N. 2006. Actin in transcription and transcription regulation. *Current Opinion in Cell Biology*. 18(3):261–266. DOI: 10.1016/j.ceb.2006.04.009.

Mitra, S., Prasad, P. & Chakraborty, S. 2018. A Unified View of Assessing the Pro-oxidant versus Antioxidant Nature of Amyloid Beta Conformers. *ChemBioChem*. 19(22):2360–2371. DOI: 10.1002/cbic.201800446.

Mollazadeh, H., Carbone, F., Montecucco, F., Pirro, M. & Sahebkar, A. 2018. Oxidative burden in familial hypercholesterolemia. *Journal of Cellular Physiology*. 233(8):5716–5725. DOI: 10.1002/jcp.26466.

Mollazadeh, H., Tavana, E., Fanni, G., Bo, S., Banach, M., Pirro, M., von Haehling, S., Jamialahmadi, T., et al. 2021. Effects of statins on mitochondrial pathways. *Journal of Cachexia, Sarcopenia and Muscle*. 12(2):237–251. DOI: 10.1002/jcsm.12654.

Monye, I. & Adelowo, A.B. 2020. Strengthening immunity through healthy lifestyle practices: Recommendations for lifestyle interventions in the management of COVID-19. *Lifestyle Medicine*. 1(1):e7. DOI: 10.1002/lim2.7.

Mor, F., Izak, M. & Cohen, I.R. 2005. Identification of Aldolase as a Target Antigen in Alzheimer's Disease. *The Journal of Immunology*. 175(5):3439–3445. DOI: 10.4049/jimmunol.175.5.3439.

Mueller, R.L., Combs, B., Alhadidy, M.M., Brady, S.T., Morfini, G.A. & Kanaan, N.M. 2021. Tau: A Signaling Hub Protein. *Frontiers in Molecular Neuroscience*. 14. Available: https://www.frontiersin.org/articles/10.3389/fnmol.2021.647054 [2023, March 07].

Murphy, C., Dyer, A.H., Lawlor, B., Kennelly, S.P., & for the NILVAD study group. 2023. What is the impact of ongoing statin use on cognitive decline and dementia progression in older adults with mild-moderate Alzheimer disease? *PLOS ONE*. 18(5):e0285529. DOI: 10.1371/journal.pone.0285529.

Nakase, T. & Naus, C.C.G. 2004. Gap junctions and neurological disorders of the central nervous system. *Biochimica et Biophysica Acta (BBA) - Biomembranes*. 1662(1):149–158. DOI: 10.1016/j.bbamem.2004.01.009.

Nauta, A.J., Raaschou-Jensen, N., Roos, A., Daha, M.R., Madsen, H.O., Borrias-Essers, M.C., Ryder, L.P., Koch, C., et al. 2003. Mannose-binding lectin engagement with late apoptotic and necrotic cells. *European Journal of Immunology*. 33(10):2853–2863. DOI: 10.1002/eji.200323888.

Nayernia, Z., Jaquet, V. & Krause, K.-H. 2014. New Insights on NOX Enzymes in the Central Nervous System. *Antioxidants & Redox Signaling*. 20(17):2815–2837. DOI: 10.1089/ars.2013.5703.

Nguyen, A.D., Itoh, S., Jeney, V., Yanagisawa, H., Fujimoto, M., Ushio-Fukai, M. & Fukai, T. 2004. Fibulin-5 Is a Novel Binding Protein for Extracellular Superoxide Dismutase. *Circulation Research*. 95(11):1067–1074. DOI: 10.1161/01.RES.0000149568.85071.FB.

Nichols, E., Steinmetz, J.D., Vollset, S.E., Fukutaki, K., Chalek, J., Abd-Allah, F., Abdoli, A., Abualhasan, A., et al. 2022. Estimation of the global prevalence of dementia in 2019 and forecasted prevalence in 2050: an analysis for the Global Burden of Disease Study 2019. *The Lancet Public Health*. 7(2):e105–e125. DOI: 10.1016/S2468-2667(21)00249-8.

Nulton-Persson, A.C. & Szweda, L. 2001. Modulation of Mitochondrial Function by Hydrogen Peroxide. *The Journal of Biological Chemistry*. 276:23357–23361. DOI: 10.1074/jbc.M100320200.

O'Brien, R.J. & Wong, P.C. 2011. Amyloid Precursor Protein Processing and Alzheimer's Disease. *Annual review of neuroscience*. 34:185. DOI: 10.1146/annurev-neuro-061010-113613.

Obulesu, T., Mathew, S., Lakshmanan, P.T., Krishna, G., Lakra, W.S. & Anandan, R. 2014. Salubrious Effects of Dietary Supplementation of Squalene and n-3 Polyunsaturated Fatty Acid Concentrate on Mitochondrial Function in Young and Aged Rats. *Fishery technology*. 51. Available: https://consensus.app/papers/salubrious-effects-of-dietary-supplementation-of-obulesu-mathew/d241b17f8dcc52309fa2ee7640e1aac9/ [2025, February 01].

Occhipinti, R. & Boron, W.F. 2019. Role of Carbonic Anhydrases and Inhibitors in Acid–Base Physiology: Insights from Mathematical Modeling. *International Journal of Molecular Sciences*. 20(15):3841. DOI: 10.3390/ijms20153841.

O'Donnell, R.W., Johnson, D.K., Ziegler, L.M., DiMattina, A.J., Stone, R.I. & Holland, J.A. 2003. Endothelial NADPH Oxidase: Mechanism of Activation by Low-Density Lipoprotein. *Endothelium*. 10(6):291–297. DOI: 10.1080/10623320390272280.

de Oliveira, J., Hort, M.A., Moreira, E.L.G., Glaser, V., Ribeiro-do-Valle, R.M., Prediger, R.D., Farina, M., Latini, A., et al. 2011. Positive correlation between elevated plasma cholesterol levels and cognitive

impairments in LDL receptor knockout mice: relevance of cortico-cerebral mitochondrial dysfunction and oxidative stress. *Neuroscience*. 197:99–106. DOI: 10.1016/j.neuroscience.2011.09.009.

de Oliveira, J., Engel, D.F., de Paula, G.C., Dos Santos, D.B., Lopes, J.B., Farina, M., Moreira, E.L.G. & de Bem, A.F. 2020. High Cholesterol Diet Exacerbates Blood-Brain Barrier Disruption in LDLr-/- Mice: Impact on Cognitive Function. *Journal of Alzheimer's disease: JAD*. 78(1):97–115. DOI: 10.3233/JAD-200541.

Ono, S. & Ono, K. 2002. Tropomyosin inhibits ADF/cofilin-dependent actin filament dynamics. *The Journal of Cell Biology*. 156(6):1065–1076. DOI: 10.1083/jcb.200110013.

Pająk, B., Kania, E. & Orzechowski, A. 2016. Killing Me Softly: Connotations to Unfolded Protein Response and Oxidative Stress in Alzheimer's Disease. *Oxidative Medicine and Cellular Longevity*. 2016:1–17. DOI: 10.1155/2016/1805304.

Pan, S., Aebersold, R., Chen, R., Rush, J., Goodlett, D.R., McIntosh, M.W., Zhang, J. & Brentnall, T.A. 2009. Mass spectrometry based targeted protein quantification: methods and applications. *Journal of proteome research*. 8(2):787–797. DOI: 10.1021/pr800538n.

Park, J.-C., Noh, J., Jang, S., Kim, K.H., Choi, H., Lee, D., Kim, J., Chung, J., et al. 2022. Association of B cell profile and receptor repertoire with the progression of Alzheimer's disease. *Cell Reports*. 40(12):111391. DOI: 10.1016/j.celrep.2022.111391.

Parmar, H.S., Houdek, Z., Pesta, M., Vaclava, C., Dvorak, P. & Hatina, J. 2017. Protective Effect of Aspirin Against Oligomeric Aβ42 Induced Mitochondrial Alterations and Neurotoxicity in Differentiated EC P19 Neuronal Cells. *Current Alzheimer Research*. 14(8):810–819. DOI: 10.2174/1567205014666170203104757.

Patte-Mensah, C., Meyer, L., Schaeffer, V., Eckert, A. & Mensah-Nyagan, A.G. 2012. Transfection of Human Neuroblastoma Cells with Alzheimer's Disease Brain Hallmarks as a Promising Strategy to Investigate the Role of Neurosteroidogenesis in Neuroprotection. *Genetically Modified Organisms and Genetic Engineering in Research and Therapy*. 3:50–59. DOI: 10.1159/000339189.

Pavel, M., Imarisio, S., Menzies, F.M., Jimenez-Sanchez, M., Siddiqi, F.H., Wu, X., Renna, M., O'Kane, C.J., et al. 2016. CCT complex restricts neuropathogenic protein aggregation via autophagy. *Nature Communications*. 7:13821. DOI: 10.1038/ncomms13821.

Pedreño, J., Hurt-Camejo, E., Wiklund, O., Badimón, L. & Masana, L. 2001. Low-density lipoprotein (LDL) binds to a G-protein coupled receptor in human platelets. Evidence that the proaggregatory effect induced by LDL is modulated by down-regulation of binding sites and desensitization of its mediated signaling. *Atherosclerosis*. 155(1):99–112. DOI: 10.1016/s0021-9150(00)00545-1.

Pelucchi, S., Stringhi, R. & Marcello, E. 2020. Dendritic Spines in Alzheimer's Disease: How the Actin Cytoskeleton Contributes to Synaptic Failure. *International Journal of Molecular Sciences*. 21(3):908. DOI: 10.3390/ijms21030908.

Penzes, P. & VanLeeuwen, J.-E. 2011. Impaired regulation of synaptic actin cytoskeleton in Alzheimer's disease. *Brain research reviews*. 67(1–2):184. DOI: 10.1016/j.brainresrev.2011.01.003.

Perez-Nievas, B.G. & Serrano-Pozo, A. 2018. Deciphering the Astrocyte Reaction in Alzheimer's Disease. *Frontiers in Aging Neuroscience*. 10. DOI: 10.3389/fnagi.2018.00114.

Peterson, E., Shippee, E., Brinton, M.A. & Kaur, P. 2019. Biochemical characterization of the mouse ABCF3 protein, a partner of the flavivirus-resistance protein OAS1B. *The Journal of Biological Chemistry*. 294(41):14937–14952. DOI: 10.1074/jbc.RA119.008477.

Pfrieger, F.W. & Ungerer, N. 2011. Cholesterol metabolism in neurons and astrocytes. *Progress in Lipid Research*. 50(4):357–371. DOI: 10.1016/j.plipres.2011.06.002.

Philbert, S.A., Xu, J., Unwin, R.D., Dowsey, A.W. & Cooper, G.J.S. 2021. Widespread severe cerebral elevations of haptoglobin and haemopexin in sporadic Alzheimer's disease: Evidence for a pervasive microvasculopathy. *Biochemical and Biophysical Research Communications*. 555:89–94. DOI: 10.1016/j.bbrc.2021.02.107.

Piccoli, C., Quarato, G., D'Aprile, A., Montemurno, E., Scrima, R., Ripoli, M., Gomaraschi, M., Cirillo, P., et al. 2011. Native LDL-induced oxidative stress in human proximal tubular cells: multiple players involved. *Journal of Cellular and Molecular Medicine*. 15(2):375–395. DOI: 10.1111/j.1582-4934.2009.00946.x.

Pineda, J.A., Aono, M., Sheng, H., Lynch, J., Wellons, J.C., Laskowitz, D.T., Pearlstein, R.D., Bowler, R., et al. 2001. Extracellular Superoxide Dismutase Overexpression Improves Behavioral Outcome from Closed Head Injury in the Mouse. *Journal of Neurotrauma*. 18(6):625–634. DOI: 10.1089/089771501750291864.

Poljsak, B., Šuput, D. & Milisav, I. 2013. Achieving the Balance between ROS and Antioxidants: When to Use the Synthetic Antioxidants. *Oxidative Medicine and Cellular Longevity*. 2013:956792. DOI: 10.1155/2013/956792.

Porrello, E., Uberti, D., Prasad, K. & Uberti, D.L. 2007. Over-expression of amyloid precursor protein in HEK cells alters p53 conformational state and protects against doxorubicin. *Journal of Neurochemistry*. (January, 1). Available: https://www.academia.edu/18700373/Over_expression_of_amyloid_precursor_protein_in_HEK_cells_alters_p53_conformational_state_and_protects_against_doxorubicin [2022, June 02].

Puglielli, L., Konopka, G., Pack-Chung, E., Ingano, L.A.M., Berezovska, O., Hyman, B.T., Chang, T.Y., Tanzi, R.E., et al. 2001. Acyl-coenzyme A: cholesterol acyltransferase modulates the generation of the amyloid β-peptide. *Nature Cell Biology*. 3(10):905–912. DOI: 10.1038/ncb1001-905.

Puntoni, M., Sbrana, F., Bigazzi, F., Minichilli, F., Ferdeghini, E. & Sampietro, T. 2011. Myeloperoxidase modulation by LDL apheresis in Familial Hypercholesterolemia. *Lipids in Health and Disease*. 10:185. DOI: 10.1186/1476-511X-10-185.

Purves, D., Augustine, G.J., Fitzpatrick, D., Katz, L.C., LaMantia, A.-S., McNamara, J.O. & Williams, S.M. 2001. Electrical Synapses. In *Neuroscience. 2nd edition*. Sinauer Associates. Available: https://www.ncbi.nlm.nih.gov/books/NBK11164/ [2024, December 08].

Quinzii, C.M. & Hirano, M. 2010. Coenzyme Q and Mitochondrial Disease. *Developmental disabilities research reviews*. 16(2):183–188. DOI: 10.1002/ddrr.108.

Rajkumar, A.S., Muley, A., Chatterjee, S. & Jaffar Ali, B.M. 2010. Probing the effect of elevated cholesterol on the mechanical properties of membrane-cytoskeleton by optical tweezers. K. Dholakia & G.C. Spalding, Eds. San Diego, California. 77621K. DOI: 10.1117/12.860464.

Rampersad, S.N. 2012. Multiple Applications of Alamar Blue as an Indicator of Metabolic Function and Cellular Health in Cell Viability Bioassays. *Sensors (Basel, Switzerland)*. 12(9):12347–12360. DOI: 10.3390/s120912347.

Rather, M.A., Khan, A., Alshahrani, S., Rashid, H., Qadri, M., Rashid, S., Alsaffar, R.M., Kamal, M.A., et al. 2021. Inflammation and Alzheimer's Disease: Mechanisms and Therapeutic Implications by Natural Products. *Mediators of Inflammation*. 2021:9982954. DOI: 10.1155/2021/9982954.

Rauchmann, B., Toth, H., Guersel, S.Ü., Schirge, P., Schweiger, M., Brendel, M., Franzmeier, N., Lamby, N., et al. 2023. Blood-brain barrier disruption measured by dynamic contrast-enhanced MRI in Alzheimer's disease. *Alzheimer's & Dementia*. 19(S10):e081842. DOI: 10.1002/alz.081842.

Read, T.-A., Cisterna, B.A., Skruber, K., Ahmadieh, S., Liu, T.M., Vitriol, J.A., Shi, Y., Black, J.B., et al. 2024. The actin binding protein profilin 1 localizes inside mitochondria and is critical for their function. *EMBO reports*. 25(8):3240–3262. DOI: 10.1038/s44319-024-00209-3.

Reddy, P.H. 2013. Amyloid beta-induced glycogen synthase kinase 3β phosphorylated VDAC1 in Alzheimer's disease: Implications for synaptic dysfunction and neuronal damage. *Biochimica et Biophysica Acta (BBA) - Molecular Basis of Disease*. 1832(12):1913–1921. DOI: 10.1016/j.bbadis.2013.06.012.

Refinetti, P., Warren, D., Morgenthaler, S. & Ekstrøm, P.O. 2017. Quantifying mitochondrial DNA copy number using robust regression to interpret real time PCR results. *BMC Research Notes*. 10(1):593. DOI: 10.1186/s13104-017-2913-1.

Refolo, L.M., Pappolla, M.A., Malester, B., LaFrancois, J., Bryant-Thomas, T., Wang, R., Tint, G.S., Sambamurti, K., et al. 2000. Hypercholesterolemia Accelerates the Alzheimer's Amyloid Pathology in a Transgenic Mouse Model. *Neurobiology of Disease*. 7(4):321–331. DOI: 10.1006/nbdi.2000.0304.

Reitz, C. 2012. Dyslipidemia and Dementia: Current Epidemiology, Genetic Evidence, and Mechanisms Behind the Associations. *Journal of Alzheimer's Disease*. 30(s2):S127–S145. DOI: 10.3233/JAD-2011-110599.

Ren, J.-G., Li, Z. & Sacks, D.B. 2007. IQGAP1 modulates activation of B-Raf. *Proceedings of the National Academy of Sciences*. 104(25):10465–10469. DOI: 10.1073/pnas.0611308104.

Ren, X., Jemth, P., Board, P.G., Luo, G., Mannervik, B., Liu, J., Zhang, K. & Shen, J. 2002. A Semisynthetic Glutathione Peroxidase with High Catalytic Efficiency. *Chemistry & Biology*. 9(7):789–794. DOI: 10.1016/S1074-5521(02)00167-9.

Reveille, J.D. & Bruce, G.S. 2004. 4 - MHC CLASS II AND NON-MHC GENES IN THE PATHOGENESIS OF SYSTEMIC LUPUS ERYTHEMATOSUS. In *Systemic Lupus Erythematosus (Fourth Edition)*. R.G. Lahita, Ed. San Diego: Academic Press. 109–151. DOI: 10.1016/B978-012433901-9/50007-7.

Rezakhani, L., Salimi, Z., Zarei, F., Moradpour, F., Khazaei, M.R., Khazaei, M. & Pourjalili, M. 2023. Protective Effects of Statins against Alzheimer Disease. *The Ewha Medical Journal*. 46(4):e17. DOI: 10.12771/emj.2023.e17.

Riddell, D.R., Christie, G., Hussain, I. & Dingwall, C. 2001. Compartmentalization of beta-secretase (Asp2) into low-buoyant density, noncaveolar lipid rafts. *Current biology: CB*. 11(16):1288–1293. DOI: 10.1016/s0960-9822(01)00394-3.

Rifkind, J.M., Mohanty, J.G. & Nagababu, E. 2015. The pathophysiology of extracellular hemoglobin associated with enhanced oxidative reactions. *Frontiers in Physiology*. 5. DOI: 10.3389/fphys.2014.00500.

Risher, W.C., Kim, N., Koh, S., Choi, J.-E., Mitev, P., Spence, E.F., Pilaz, L.-J., Wang, D., et al. 2018. Thrombospondin receptor α2δ-1 promotes synaptogenesis and spinogenesis via postsynaptic Rac1. *Journal of Cell Biology*. 217(10):3747–3765. DOI: 10.1083/jcb.201802057.

Rodriguez, M.Z., Tatulian, S. & Teter, K. 2024. Abstract 2390 Peptide-based Inhibitors of Amyloid Beta Oligomerization and Toxicity. *Journal of Biological Chemistry*. 300(3):107084. DOI: 10.1016/j.jbc.2024.107084.

Rogers, G.W., Nadanaciva, S., Swiss, R., Divakaruni, A.S. & Will, Y. 2014. Assessment of Fatty Acid Beta Oxidation in Cells and Isolated Mitochondria. *Current Protocols in Toxicology*. 60(1). DOI: 10.1002/0471140856.tx2503s60.

Roy, M., Li, Z. & Sacks, D.B. 2005. IQGAP1 Is a Scaffold for Mitogen-Activated Protein Kinase Signaling. *Molecular and Cellular Biology*. 25(18):7940–7952. DOI: 10.1128/MCB.25.18.7940-7952.2005.

Ruggiero, C. & Lalli, E. 2021. Targeting the cytoskeleton against metastatic dissemination. *Cancer and Metastasis Reviews*. 40(1):89–140. DOI: 10.1007/s10555-020-09936-0.

Rutkowsky, J.M., Lee, L.L., Puchowicz, M., Golub, M.S., Befroy, D.E., Wilson, D.W., Anderson, S., Cline, G., et al. 2018. Reduced cognitive function, increased blood-brain-barrier transport and inflammatory responses, and altered brain metabolites in LDLr -/-and C57BL/6 mice fed a western diet. *PLOS ONE*. 13(2):e0191909. DOI: 10.1371/journal.pone.0191909.

Sadeghi, M., Khayati, S., Dehnavi, S., Almahmeed, W., Sukhorukovi, V.N. & Sahebkar, A. 2024. Regulatory impact of statins on macrophage polarization: mechanistic and therapeutic implications. *Journal of Pharmacy and Pharmacology*. 76(7):763–775. DOI: 10.1093/jpp/rgae024.

Salim, S. 2017. Oxidative Stress and the Central Nervous System. *The Journal of Pharmacology and Experimental Therapeutics*. 360(1):201. DOI: 10.1124/jpet.116.237503.

Salminen, A. & Kaarniranta, K. 2012. AMP-activated protein kinase (AMPK) controls the aging process via an integrated signaling network. *Ageing Research Reviews*. 11(2):230–241. DOI: 10.1016/j.arr.2011.12.005.

Salminen, A., Kaarniranta, K., Haapasalo, A., Soininen, H. & Hiltunen, M. 2011. AMP-activated protein kinase: a potential player in Alzheimer's disease. *Journal of Neurochemistry*. 118(4):460–474. DOI: 10.1111/j.1471-4159.2011.07331.x.

Sanjurjo, L., Castelblanco, E., Julve, J., Villalmanzo, N., Téllez, É., Ramirez-Morros, A., Alonso, N., Mauricio, D., et al. 2023. Contribution of Elevated Glucose and Oxidized LDL to Macrophage Inflammation: A Role for PRAS40/Akt-Dependent Shedding of Soluble CD14. *Antioxidants*. 12(5):1083. DOI: 10.3390/antiox12051083.

Santhanasabapathy, R., Vasudevan, S., Anupriya, K., Pabitha, R. & Sudhandiran, G. 2015. Farnesol quells oxidative stress, reactive gliosis and inflammation during acrylamide-induced neurotoxicity: Behavioral and biochemical evidence. *Neuroscience*. 308:212–227. DOI: 10.1016/j.neuroscience.2015.08.067.

Saraste, A. & Pulkki, K. 2000. Morphologic and biochemical hallmarks of apoptosis. *Cardiovascular Research*. 45(3):528–537. DOI: 10.1016/s0008-6363(99)00384-3.

Sarkar, P. & Chattopadhyay, A. 2023. Statin-induced increase in actin polymerization modulates GPCR dynamics and compartmentalization. *Biophysical Journal*. 122(11):1938–1955. DOI: 10.1016/j.bpj.2022.08.039.

Sarkar, P., Kumar, G.A., Shrivastava, S. & Chattopadhyay, A. 2022. Chronic cholesterol depletion increases F-actin levels and induces cytoskeletal reorganization via a dual mechanism. *Journal of Lipid Research*. 63(5):100206. DOI: 10.1016/j.jlr.2022.100206.

Sarkar, S., Pandey, A., Kumar Yadav, S., Haris Siddiqui, M., Pant, A.B. & Yadav, S. 2025. Differentiated and mature neurons are more responsive to neurotoxicant exposure at both transcriptional and translational levels. *Neuroscience*. 564:110–125. DOI: 10.1016/j.neuroscience.2024.11.017.

Schilling, T. & Eder, C. 2011. Amyloid-β-induced reactive oxygen species production and priming are differentially regulated by ion channels in microglia. *Journal of Cellular Physiology*. 226(12):3295–3302. DOI: 10.1002/jcp.22675.

Schmidt, S.I., Blaabjerg, M., Freude, K. & Meyer, M. 2022. RhoA Signaling in Neurodegenerative Diseases. *Cells*. 11(9):1520. DOI: 10.3390/cells11091520.

Schroer, A.B., Ventura, P.B., Sucharov, J., Misra, R., Chui, M.K.K., Bieri, G., Horowitz, A.M., Smith, L.K., et al. 2023. Platelet factors attenuate inflammation and rescue cognition in ageing. *Nature*. 620(7976):1071–1079. DOI: 10.1038/s41586-023-06436-3.

Schutt, C.E., Karlén, M. & Karlsson, R. 2022. A structural model of the profilin–formin pacemaker system for actin filament elongation. *Scientific Reports*. 12(1):20515. DOI: 10.1038/s41598-022-25011-w.

Schweinhuber, S.K., Meßerschmidt, T., Hänsch, R., Korte, M. & Rothkegel, M. 2015. Profilin Isoforms Modulate Astrocytic Morphology and the Motility of Astrocytic Processes. *PLOS ONE*. 10(1):e0117244. DOI: 10.1371/journal.pone.0117244.

Searle, A., Gómez-Rosso, L., Meroño, T., Salomon, C., Durán-Sandoval, D., Giunta, G., Grant, C., Calvo, C., et al. 2011. High LDL levels are associated with increased lipoprotein-associated phospholipase A2 activity on nitric oxide synthesis and reactive oxygen species formation in human endothelial cells. *Clinical Biochemistry*. 44(2–3):171–177. DOI: 10.1016/j.clinbiochem.2010.10.004.

Segeritz, C.-P. & Vallier, L. 2017. Cell Culture. *Basic Science Methods for Clinical Researchers*. 151–172. DOI: 10.1016/B978-0-12-803077-6.00009-6.

Seino, S., Kimoto, T., Yoshida, H., Tanji, K., Matsumiya, T., Hayakari, R., Seya, K., Kawaguchi, S., et al. 2018. Gnetin C, a resveratrol dimer, reduces amyloid-β 1–42 (Aβ42) production and ameliorates Aβ42-lowered cell viability in cultured SH-SY5Y human neuroblastoma **cells** . *Biomedical Research*. 39(3):105–115. DOI: 10.2220/biomedres.39.105.

Sen, S., Lagas, S., Roy, A. & Kumar, H. 2022. Cytoskeleton saga: Its regulation in normal physiology and modulation in neurodegenerative disorders. *European Journal of Pharmacology*. 925:175001. DOI: 10.1016/j.ejphar.2022.175001.

Seo, E., Kang, H., Choi, H., Choi, W. & Jun, H.-S. 2019. Reactive oxygen species-induced changes in glucose and lipid metabolism contribute to the accumulation of cholesterol in the liver during aging. *Aging Cell*. 18(2):e12895. DOI: 10.1111/acel.12895.

Shah, K. & Lahiri, D.K. 2014. Cdk5 activity in the brain – multiple paths of regulation. *Journal of Cell Science*. 127(11):2391–2400. DOI: 10.1242/jcs.147553.

Shapira, K.E., Shapira, G., Schmukler, E., Pasmanik-Chor, M., Shomron, N., Pinkas-Kramarski, R., Henis, Y.I. & Ehrlich, M. 2021. Autophagy is induced and modulated by cholesterol depletion through transcription of autophagy-related genes and attenuation of flux. *Cell Death Discovery*. 7(1):1–11. DOI: 10.1038/s41420-021-00718-3.

Shi, Y., Andhey, P.S., Ising, C., Wang, K., Snipes, L.L., Boyer, K., Lawson, S., Yamada, K., et al. 2021. Overexpressing low-density lipoprotein receptor reduces tau-associated neurodegeneration in relation to apoE-linked mechanisms. *Neuron*. 109(15):2413-2426.e7. DOI: 10.1016/j.neuron.2021.05.034.

Shupp, A., Casimiro, M.C. & Pestell, R.G. 2017. Biological functions of CDK5 and potential CDK5 targeted clinical treatments. *Oncotarget*. 8(10):17373–17382. DOI: 10.18632/oncotarget.14538.

Sidiropoulou, G.A., Metaxas, A. & Kourti, M. 2023. Natural antioxidants that act against Alzheimer's disease through modulation of the NRF2 pathway: a focus on their molecular mechanisms of action. *Frontiers in Endocrinology*. 14. DOI: 10.3389/fendo.2023.1217730.

Sies, H. 2017. Hydrogen peroxide as a central redox signaling molecule in physiological oxidative stress: Oxidative eustress. *Redox Biology*. 11:613–619. DOI: 10.1016/j.redox.2016.12.035.

Silva Ramos, E., Motori, E., Brüser, C., Kühl, I., Yeroslaviz, A., Ruzzenente, B., Kauppila, J.H.K., Busch, J.D., et al. 2019. Mitochondrial fusion is required for regulation of mitochondrial DNA replication. *PLOS Genetics*. 15(6):e1008085. DOI: 10.1371/journal.pgen.1008085.

Šimić, G., Babić Leko, M., Wray, S., Harrington, C., Delalle, I., Jovanov-Milošević, N., Bažadona, D., Buée, L., et al. 2016. Tau Protein Hyperphosphorylation and Aggregation in Alzheimer's Disease and Other Tauopathies, and Possible Neuroprotective Strategies. *Biomolecules*. 6(1):6. DOI: 10.3390/biom6010006.

Singh, R.R., Mohammad, J., Orr, M. & Reindl, K.M. 2020. Glutathione S-Transferase pi-1 Knockdown Reduces Pancreatic Ductal Adenocarcinoma Growth by Activating Oxidative Stress Response Pathways. *Cancers*. 12(6):1501. DOI: 10.3390/cancers12061501.

Sinha, M., Bhowmick, P., Banerjee, A. & Chakrabarti, S. 2013. Antioxidant role of amyloid β protein in cell-free and biological systems: implication for the pathogenesis of Alzheimerdisease. *Free Radical Biology and Medicine*. 56:184–192. DOI: 10.1016/j.freeradbiomed.2012.09.036.

Sjöberg, A.P., Trouw, L.A., McGrath, F.D.G., Hack, C.E. & Blom, A.M. 2006. Regulation of complement activation by C-reactive protein: targeting of the inhibitory activity of C4b-binding protein. *Journal of Immunology (Baltimore, Md.: 1950)*. 176(12):7612–7620. DOI: 10.4049/jimmunol.176.12.7612.

Son, S.M., Nam, D.W., Cha, M.-Y., Kim, K.H., Byun, J., Ryu, H. & Mook-Jung, I. 2015. Thrombospondin-1 prevents amyloid beta-mediated synaptic pathology in Alzheimer's disease. *Neurobiology of Aging*. 36(12):3214–3227. DOI: 10.1016/j.neurobiolaging.2015.09.005.

Song, I.-U., Kim, Y.-D., Chung, S.-W. & Cho, H.-J. 2015. Association between serum haptoglobin and the pathogenesis of Alzheimer's disease. *Internal Medicine (Tokyo, Japan)*. 54(5):453–457. DOI: 10.2169/internalmedicine.54.2876.

Spuch, C., Ortolano, S. & Navarro, C. 2012. New Insights in the Amyloid-Beta Interaction with Mitochondria. *Journal of Aging Research*. 2012(1):324968. DOI: 10.1155/2012/324968.

Stahmann, N., Woods, A., Carling, D. & Heller, R. 2006. Thrombin Activates AMP-Activated Protein Kinase in Endothelial Cells via a Pathway Involving Ca^{2+} /Calmodulin-Dependent Protein Kinase Kinase β. *Molecular and Cellular Biology*. 26(16):5933–5945. DOI: 10.1128/MCB.00383-06.

Staines, A.G., Sindelar, P., Coughtrie, M.W.H. & Burchell, B. 2004. Farnesol is glucuronidated in human liver, kidney and intestine in vitro, and is a novel substrate for UGT2B7 and UGT1A1. *Biochemical Journal*. 384(Pt 3):637–645. DOI: 10.1042/BJ20040997.

Stringer, H.A.J., Sohi, G.K., Maguire, J.A. & Côté, H.C.F. 2013. Decreased skeletal muscle mitochondrial DNA in patients with statin-induced myopathy. *Journal of the Neurological Sciences*. 325(1–2):142–147. DOI: 10.1016/j.jns.2012.12.023.

Suica, V.-I., Uyy, E., Boteanu, R.M., Ivan, L. & Antohe, F. 2015. Alteration of actin dependent signaling pathways associated with membrane microdomains in hyperlipidemia. *Proteome Science*. 13(1):30. DOI: 10.1186/s12953-015-0087-0.

Sun, H., Chen, D.-W., Ma, Y.-Y., Liu, B., Wang, J., Lai, Y.-J., Zeng, G.-H., Shen, Y.-Y., et al. 2025. Decreased serum PF4 levels correlate with cognitive decline and CSF biomarkers in Alzheimer's disease in a Chinese cohort. *Experimental Gerontology*. 201:112689. DOI: 10.1016/j.exger.2025.112689.

Sun, K.-H., Chang, K.-H., Clawson, S., Ghosh, S., Mirzaei, H., Regnier, F. & Shah, K. 2011. Glutathione-S-transferase P1 is a critical regulator of Cdk5 kinase activity. *Journal of Neurochemistry*. 118(5):902–914. DOI: 10.1111/j.1471-4159.2011.07343.x.

Sun, X., Chen, W.-D. & Wang, Y.-D. 2015. β-Amyloid: The Key Peptide in the Pathogenesis of Alzheimer's Disease. *Frontiers in Pharmacology*. 6. Available: https://www.frontiersin.org/article/10.3389/fphar.2015.00221 [2022, June 05].

Sytnyk, V., Leshchyns'ka, I. & Schachner, M. 2017. Neural Cell Adhesion Molecules of the Immunoglobulin Superfamily Regulate Synapse Formation, Maintenance, and Function. *Trends in Neurosciences*. 40(5):295–308. DOI: 10.1016/j.tins.2017.03.003.

Szklarczyk, D., Gable, A.L., Lyon, D., Junge, A., Wyder, S., Huerta-Cepas, J., Simonovic, M., Doncheva, N.T., et al. 2019. STRING v11: protein–protein association networks with increased coverage, supporting functional discovery in genome-wide experimental datasets. *Nucleic Acids Research*. 47(Database issue):D607–D613. DOI: 10.1093/nar/gky1131.

Tall, A.R. & Yvan-Charvet, L. 2015a. Cholesterol, inflammation and innate immunity. *Nature Reviews Immunology*. 15(2):104–116. DOI: 10.1038/nri3793.

Tall, A.R. & Yvan-Charvet, L. 2015b. Cholesterol, inflammation and innate immunity. *Nature reviews. Immunology*. 15(2):104. DOI: 10.1038/nri3793.

Tanzi, R.E. 2012. The Genetics of Alzheimer Disease. *Cold Spring Harbor Perspectives in Medicine*. 2(10):a006296. DOI: 10.1101/cshperspect.a006296.

Taraboletti, G., Roberts, D.D. & Liotta, L.A. 1987. Thrombospondin-induced tumor cell migration: haptotaxis and chemotaxis are mediated by different molecular domains. *The Journal of cell biology*. 105(5):2409–2415. DOI: 10.1083/jcb.105.5.2409.

Tavridou, A., Megaritis, G., Kourounakis, A.P., Charalambous, A. & Manolopoulos, V.G. 2007. EP2306 and EP2302, Two Novel Squalene Synthase Inhibitors, Stimulate Endothelial Nitric Oxide Synthase Expression in Cultured Endothelial Cells. *Endothelium*. 14(4–5):239–243. DOI: 10.1080/10623320701547216.

Tennent, G.A., Lovat, L.B. & Pepys, M.B. 1995. Serum amyloid P component prevents proteolysis of the amyloid fibrils of Alzheimer disease and systemic amyloidosis. *Proceedings of the National Academy of Sciences of the United States of America*. 92(10):4299–4303. DOI: 10.1073/pnas.92.10.4299.

Terzioglu-Usak, S., Negis, Y., Karabulut, D.S., Zaim, M. & Isik, S. 2017. Cellular Model of Alzheimer's Disease: Aβ1-42 Peptide Induces Amyloid Deposition and a Decrease in Topo Isomerase IIβ and Nurr1 Expression. *Current Alzheimer Research*. 14(6):636–644. DOI: 10.2174/1567205014666170117103217.

Thirumangalakudi, L., Prakasam, A., Zhang, R., Bimonte-Nelson, H., Sambamurti, K., Kindy, M.S. & Bhat, N.R. 2008. High cholesterol-induced neuroinflammation and amyloid precursor protein processing correlate with loss of working memory in mice. *Journal of Neurochemistry*. 106(1):475–485. DOI: 10.1111/j.1471-4159.2008.05415.x.

Thornton, C., Bright, N.J., Sastre, M., Muckett, P.J. & Carling, D. 2011. AMP-activated protein kinase (AMPK) is a tau kinase, activated in response to amyloid β-peptide exposure. *The Biochemical Journal*. 434(3):503–512. DOI: 10.1042/BJ20101485.

van Tits, L., de Graaf, J., Hak-Lemmers, H., Bredie, S., Demacker, P., Holvoet, P. & Stalenhoef, A. 2003. Increased Levels of Low-Density Lipoprotein Oxidation in Patients with Familial Hypercholesterolemia and in End-Stage Renal Disease Patients on Hemodialysis. *Laboratory Investigation*. 83(1):13–21. DOI: 10.1097/01.LAB.0000048633.76607.E0.

Tucker, B., Ephraums, J., King, T.W., Abburi, K., Rye, K.-A. & Cochran, B.J. 2023. Impact of Impaired Cholesterol Homeostasis on Neutrophils in Atherosclerosis. *Arteriosclerosis, Thrombosis, and Vascular Biology*. 43(5):618–627. DOI: 10.1161/ATVBAHA.123.316246.

Tzikas, S., Schlak, D., Sopova, K., Gatsiou, A., Stakos, D., Stamatelopoulos, K., Stellos, K. & Laske, C. 2014. Increased myeloperoxidase plasma levels in patients with Alzheimer's disease. *Journal of Alzheimer's disease: JAD*. 39(3):557–564. DOI: 10.3233/JAD-131469.

Ugawa, T., Kakuta, H., Moritani, H., Matsuda, K., Ishihara, T., Yamaguchi, M., Naganuma, S., Iizumi, Y., et al. 2000. YM-53601, a novel squalene synthase inhibitor, reduces plasma cholesterol and triglyceride levels in several animal species. *British Journal of Pharmacology*. 131(1):63–70. DOI: 10.1038/sj.bjp.0703545.

Van Der Veen, B.S., De Winther, M.P.J. & Heeringa, P. 2009. Myeloperoxidase: Molecular Mechanisms of Action and Their Relevance to Human Health and Disease. *Antioxidants & Redox Signaling*. 11(11):2899–2937. DOI: 10.1089/ars.2009.2538.

Van Der Zwan, L.P., Scheffer, P.G. & Teerlink, T. 2010. Reduction of Myeloperoxidase Activity by Melatonin and Pycnogenol May Contribute to their Blood Pressure Lowering Effect. *Hypertension*. 56(3). DOI: 10.1161/HYPERTENSIONAHA.110.158170.

Vankoningsloo, S., Piens, M., Lecocq, C., Gilson, A., De Pauw, A., Renard, P., Demazy, C., Houbion, A., et al. 2005. Mitochondrial dysfunction induces triglyceride accumulation in 3T3-L1 cells: role of fatty acid β-oxidation and glucose. *Journal of Lipid Research*. 46(6):1133–1149. DOI: 10.1194/jlr.M400464-JLR200.

Varma, V.R., Büşra Lüleci, H., Oommen, A.M., Varma, S., Blackshear, C.T., Griswold, M.E., An, Y., Roberts, J.A., et al. 2021. Abnormal brain cholesterol homeostasis in Alzheimer's disease—a targeted metabolomic and transcriptomic study. *npj Aging and Mechanisms of Disease*. 7(1):1–14. DOI: 10.1038/s41514-021-00064-9.

Veerhuis, R. 2011. Histological and direct evidence for the role of complement in the neuroinflammation of AD. *Current Alzheimer Research*. 8(1):34–58. DOI: 10.2174/156720511794604589.

Volkman, R., Ben-Zur, T., Kahana, A., Garty, B.Z. & Offen, D. 2019. Myeloperoxidase Deficiency Inhibits Cognitive Decline in the 5XFAD Mouse Model of Alzheimer's Disease. *Frontiers in Neuroscience*. 13. DOI: 10.3389/fnins.2019.00990.

Wang, C., Iashchishyn, I.A., Pansieri, J., Nyström, S., Klementieva, O., Kara, J., Horvath, I., Moskalenko, R., et al. 2018. S100A9-Driven Amyloid-Neuroinflammatory Cascade in Traumatic Brain Injury as a Precursor State for Alzheimer's Disease. *Scientific Reports*. 8(1):12836. DOI: 10.1038/s41598-018-31141-x.

Wang, C., Klechikov, A.G., Gharibyan, A.L., Wärmländer, S.K.T.S., Jarvet, J., Zhao, L., Jia, X., Shankar, S.K., et al. 2014. The role of pro-inflammatory S100A9 in Alzheimer's disease amyloid-neuroinflammatory cascade. *Acta Neuropathologica*. 127(4):507–522. DOI: 10.1007/s00401-013-1208-4.

Wang, H., Kulas, J.A., Wang, C., Holtzman, D.M., Ferris, H.A. & Hansen, S.B. 2021. Regulation of beta-amyloid production in neurons by astrocyte-derived cholesterol. *Proceedings of the National Academy of Sciences*. 118(33):e2102191118. DOI: 10.1073/pnas.2102191118.

Wang, Q. & Zou, M.-H. 2018. Measurement of Reactive Oxygen Species (ROS) and Mitochondrial ROS in AMPK Knockout Mice Blood Vessels. In *AMPK*. V. 1732. D. Neumann & B. Viollet, Eds. (Methods in Molecular Biology). New York, NY: Springer New York. 507–517. DOI: 10.1007/978-1-4939-7598-3_32.

Wang, S., Song, R., Wang, Z., Jing, Z., Wang, S. & Ma, J. 2018. S100A8/A9 in Inflammation. *Frontiers in Immunology*. 9. DOI: 10.3389/fimmu.2018.01298.

Wang, T. 2015. Glutathione S-transferases variants as risk factors in Alzheimer's disease. *Neurological Sciences: Official Journal of the Italian Neurological Society and of the Italian Society of Clinical Neurophysiology*. 36(10):1785–1792. DOI: 10.1007/s10072-015-2245-7.

Wang, X., Wang, W., Li, L., Perry, G., Lee, H. & Zhu, X. 2014. Oxidative stress and mitochondrial dysfunction in Alzheimer's disease. *Biochimica et Biophysica Acta (BBA) - Molecular Basis of Disease*. 1842(8):1240–1247. DOI: 10.1016/j.bbadis.2013.10.015.

Wang, Y., Huang, H., Weng, H., Jia, C., Liao, B., Long, Y., Yu, F. & Nie, Y. 2024. Talin mechanotransduction in disease. *The International Journal of Biochemistry & Cell Biology*. 166:106490. DOI: 10.1016/j.biocel.2023.106490.

Ward, N.C., Watts, G.F. & Eckel, R.H. 2019. Statin Toxicity. *Circulation Research*. 124(2):328–350. DOI: 10.1161/CIRCRESAHA.118.312782.

Wasko, B.M., Wiemer, D.F., Smits, J.P., Tong, H. & Hohl, R.J. 2010. Identification and characterization of novel bisphosphonate inhibitors of squalene synthase. *The FASEB Journal*. 24. DOI: 10.1096/fasebj.24.1_supplement.681.15.

Watanabe, T., Wang, S. & Kaibuchi, K. 2015. IQGAPs as Key Regulators of Actin-cytoskeleton Dynamics. *Cell Structure and Function*. 40(2):69–77. DOI: 10.1247/csf.15003.

Wong, Y.Y., Xiong, L.Y., Mori-Fegan, D.K., Noor, S., Chenoweth, M.J., Mirza, S.S., Masellis, M., Black, S.E., et al. 2023. Relationships between polymorphisms in keratin genes and Alzheimer's disease phenotypes. *Alzheimer's & Dementia*. 19(S12):e074162. DOI: 10.1002/alz.074162.

Woods, A., Dickerson, K., Heath, R., Hong, S.-P., Momcilovic, M., Johnstone, S.R., Carlson, M. & Carling, D. 2005. Ca2+/calmodulin-dependent protein kinase kinase-β acts upstream of AMP-activated protein kinase in mammalian cells. *Cell Metabolism*. 2(1):21–33. DOI: 10.1016/j.cmet.2005.06.005.

World Health Organisation. 2023. *Dementia*. Available: https://www.who.int/news-room/fact-sheets/detail/dementia [2024, December 23].

Wu, D. & Meydani, S.N. 2008. Age-associated changes in immune and inflammatory responses: impact of vitamin E intervention. *Journal of Leukocyte Biology*. 84(4):900–914. DOI: 10.1189/jlb.0108023.

Wu, S.-B. & Wei, Y.-H. 2012. AMPK-mediated increase of glycolysis as an adaptive response to oxidative stress in human cells: implication of the cell survival in mitochondrial diseases. *Biochimica et biophysica acta*. 1822 2:233–47. DOI: 10.1016/j.bbadis.2011.09.014.

Wu, M., Zhai, Y., Liang, X., Chen, W., Lin, R., Ma, L., Huang, Y., Zhao, D., et al. 2022. Connecting the Dots Between Hypercholesterolemia and Alzheimer's Disease: A Potential Mechanism Based on 27-Hydroxycholesterol. *Frontiers in Neuroscience*. 16. Available: https://www.frontiersin.org/articles/10.3389/fnins.2022.842814 [2023, June 07].

Wurz, A.I., Schulz, A.M., O'Bryant, C.T., Sharp, J.F. & Hughes, R.M. 2022. Cytoskeletal dysregulation and neurodegenerative disease: Formation, monitoring, and inhibition of cofilin-actin rods. *Frontiers in Cellular Neuroscience*. 16:982074. DOI: 10.3389/fncel.2022.982074.

Xi, D., Zhao, J., Guo, K., Hu, L., Chen, H., Fu, W., Lai, W. & Guo, Z. 2018. Serum amyloid P component therapeutically attenuates atherosclerosis in mice via its effects on macrophages. *Theranostics*. 8(12):3214–3223. DOI: 10.7150/thno.22704.

Yan, H., He, L., Lv, D., Yang, J. & Yuan, Z. 2024. The Role of the Dysregulated JNK Signaling Pathway in the Pathogenesis of Human Diseases and Its Potential Therapeutic Strategies: A Comprehensive Review. *Biomolecules*. 14(2):243. DOI: 10.3390/biom14020243.

Yang, D., Han, Y., Zhang, J., Chopp, M. & Seyfried, D.M. 2012. Statins enhance expression of growth factors and activate the PI3K/Akt-mediated signaling pathway after experimental intracerebral hemorrhage. 2012. DOI: 10.4236/wjns.2012.22011.

Yang, L., Jiang, Y., Shi, L., Zhong, D., Li, Y., Li, J. & Jin, R. 2020. AMPK: Potential Therapeutic Target for Alzheimer's Disease. *Current Protein & Peptide Science*. 21(1):66–77. DOI: 10.2174/1389203720666190819142746.

Yang, R., Wei, L., Fu, Q.-Q., Wang, H., You, H. & Yu, H.-R. 2016. SOD3 Ameliorates H2O2-Induced Oxidative Damage in SH-SY5Y Cells by Inhibiting the Mitochondrial Pathway. *Neurochemical Research*. 41(7):1818–1830. DOI: 10.1007/s11064-016-1897-x.

Yang, R., Wei, L., Fu, Q.-Q., You, H. & Yu, H.-R. 2017. SOD3 Ameliorates Aβ25–35-Induced Oxidative Damage in SH-SY5Y Cells by Inhibiting the Mitochondrial Pathway. *Cellular and Molecular Neurobiology*. 37(3):513–525. DOI: 10.1007/s10571-016-0390-z.

Yao, H., Arunachalam, G., Hwang, J., Chung, S., Sundar, I.K., Kinnula, V.L., Crapo, J.D. & Rahman, I. 2010. Extracellular superoxide dismutase protects against pulmonary emphysema by attenuating oxidative fragmentation of ECM. *Proceedings of the National Academy of Sciences*. 107(35):15571–15576. DOI: 10.1073/pnas.1007625107.

Yao, Y., Muench, M., Alle, T., Zhang, B., Lucero, B., Perez-Tremble, R., McGrosso, D., Newman, M., et al. 2024. A small-molecule microtubule-stabilizing agent safely reduces Aβ plaque and tau pathology in transgenic mouse models of Alzheimer's disease. *Alzheimer's & Dementia: The Journal of the Alzheimer's Association*. 20(7):4540–4558. DOI: 10.1002/alz.13875.

Yarza, R., Vela, S., Solas, M. & Ramirez, M.J. 2016. c-Jun N-terminal Kinase (JNK) Signaling as a Therapeutic Target for Alzheimer's Disease. *Frontiers in Pharmacology*. 6:321. DOI: 10.3389/fphar.2015.00321.

Ye, Z., Lu, Y. & Wu, T. 2020. The impact of ATP-binding cassette transporters on metabolic diseases. *Nutrition & Metabolism*. 17:61. DOI: 10.1186/s12986-020-00478-4.

Youngblom, E., Pariani, M. & Knowles, J.W. 1993. Familial Hypercholesterolemia. In *GeneReviews*®. M.P. Adam, G.M. Mirzaa, R.A. Pagon, S.E. Wallace, L.J. Bean, K.W. Gripp, & A. Amemiya, Eds. Seattle (WA): University of Washington, Seattle. Available: http://www.ncbi.nlm.nih.gov/books/NBK174884/ [2022, June 05].

Yu, G. & He, Q.-Y. 2016. ReactomePA: an R/Bioconductor package for reactome pathway analysis and visualization. *Molecular BioSystems*. 12(2):477–479. DOI: 10.1039/C5MB00663E.

Zachariae, E.D.F., Hu, L. & Petersen, S.V. 2020. Extracellular superoxide dismutase (SOD3): An antioxidant or prooxidant in the extracellular space? In *Oxidative Stress*. Elsevier. 183–215. DOI: 10.1016/B978-0-12-818606-0.00012-2.

Zambón, D., Quintana, M., Mata, P., Alonso, R., Benavent, J., Cruz-Sánchez, F., Gich, J., Pocoví, M., et al. 2010. Higher Incidence of Mild Cognitive Impairment in Familial Hypercholesterolemia. *The American Journal of Medicine*. 123(3):267–274. DOI: 10.1016/j.amjmed.2009.08.015.

Zhang, F., Su, B., Wang, C., Siedlak, S.L., Mondragon-Rodriguez, S., Lee, H., Wang, X., Perry, G., et al. 2015. Posttranslational modifications of α-tubulin in alzheimer disease. *Translational Neurodegeneration*. 4:9. DOI: 10.1186/s40035-015-0030-4.

Zhang, J. & Liu, Q. 2015. Cholesterol metabolism and homeostasis in the brain. *Protein & Cell*. 6(4):254–264. DOI: 10.1007/s13238-014-0131-3.

Zhang, X., Wen, J. & Zhang, Z. 2018. Statins use and risk of dementia: A dose-response meta analysis. *Medicine*. 97(30):e11304. DOI: 10.1097/MD.0000000000011304.

Zhao, L.N., Zhang, T., Zhang, C., Wang, C., Morozova-Roche, L.A., Chew, L.Y. & Mu, Y. 2013. S100A9 induces aggregation-prone conformation in Abeta peptides: a combined experimental and simulation study. *RSC Advances*. 3(46):24081. DOI: 10.1039/c3ra43665a.

Zhao, Z., Yan, J., Huang, L. & Yang, X. 2024. Phytochemicals targeting Alzheimer's disease via the AMP-activated protein kinase pathway, effects, and mechanisms of action. *Biomedicine & Pharmacotherapy*. 173:116373. DOI: 10.1016/j.biopha.2024.116373.

Zheng, J. & Lu, C. 2020. Oxidized LDL Causes Endothelial Apoptosis by Inhibiting Mitochondrial Fusion and Mitochondria Autophagy. *Frontiers in Cell and Developmental Biology*. 8. Available: https://www.frontiersin.org/article/10.3389/fcell.2020.600950 [2022, June 06].

Zheng, P., Ding, Y., Lu, F., Liu, N., Wu, H., Bian, Z., Chen, X. & Yang, D. 2021. Atorvastatin reverses high cholesterol-induced cardiac remodelling and regulates mitochondrial quality-control in a cholesterol-independent manner: An experimental study. *Clinical and Experimental Pharmacology and Physiology*. 48(8):1150–1161. DOI: 10.1111/1440-1681.13507.

Zhou, X., Paulsson, G., Stemme, S. & Hansson, G.K. 1998. Hypercholesterolemia is associated with a T helper (Th) 1/Th2 switch of the autoimmune response in atherosclerotic apo E-knockout mice. *Journal of Clinical Investigation*. 101(8):1717–1725. DOI: 10.1172/JCI1216.

Zhou, Z., Chan, C.H., Ma, Q., Xu, X., Xiao, Z. & Tan, E.-K. 2011. The roles of amyloid precursor protein (APP) in neurogenesis, implications to pathogenesis and therapy of Alzheimer disease (AD). *Cell Adhesion & Migration*. 5(4):280–292. DOI: 10.4161/cam.5.4.16986.

Zhu, X., Kong, X., Zang, L., Sun, N., Yu, Q. & Han, L. 2022. Reactive oxygen species-mediated oxidative stress accelerates glycolysis via activation of the CaMKKβ/AMPK pathway in the yak longissimus dorsi postmortem. *Journal of the science of food and agriculture*. 103 2:514–523. DOI: 10.1002/jsfa.12161.

Zou, Y., Chen, C., Fike, J.R. & Huang, T. 2009. A new mouse model for temporal- and tissue-specific control of extracellular superoxide dismutase. *genesis*. 47(3):142–154. DOI: 10.1002/dvg.20470.

10. Appendix

10.1 - Supplementary Results

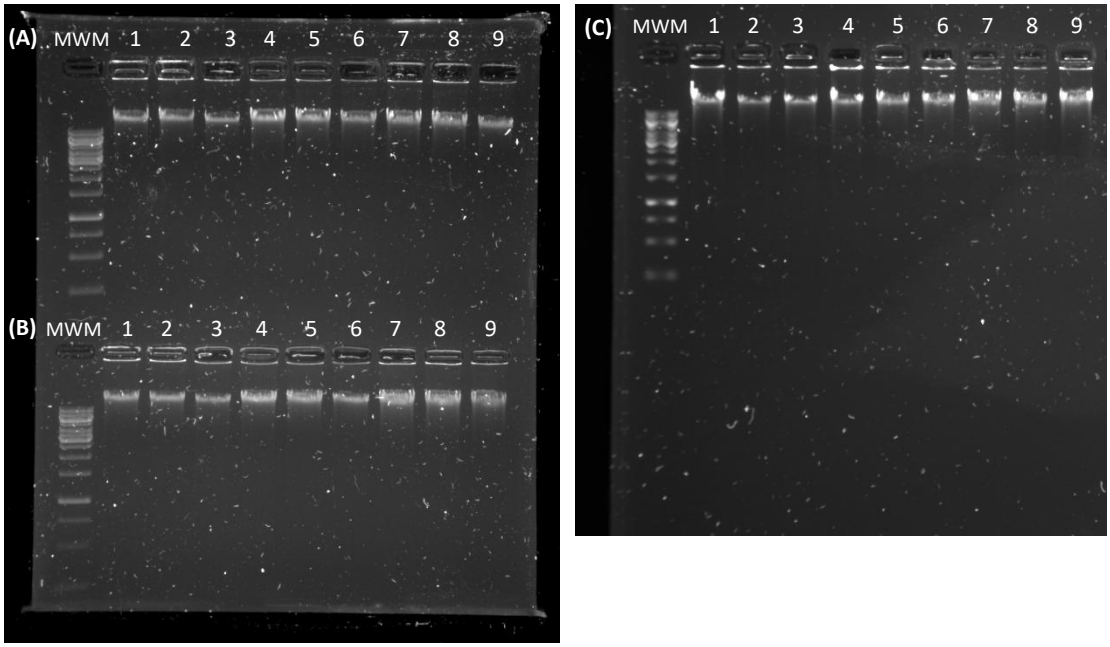


Figure S1: Agarose gel electrophoresis of extracted DNA from HEK293 cells after 48-hour treatment.

After DNA extraction from HEK293 cells, the DNA samples were run in a 1% agarose gel to evaluate DNA integrity. Each lane exhibited a distinct band with no smearing, indicating intact, non-degraded DNA was extracted. Approximately 100 ng of DNA was loaded per sample. (A) Biological repeat 1, (B) Biological repeat 2, (C) Biological repeat 3. Lanes: (1) untreated, (2) DMSO vehicle control, (3) 50 nM SSI, (4) 500 μM H_2O_2, (5) 1 μM Aβ42, (6) 150 μg/ml LDL (7) 500 μM H_2O_2 + 50 nM SSI, (8) 1 μM Aβ42 + 50 nM SSI, (9) 150 μg/ml LDL + 50 nM SSI. MWM: Molecular weight marker.

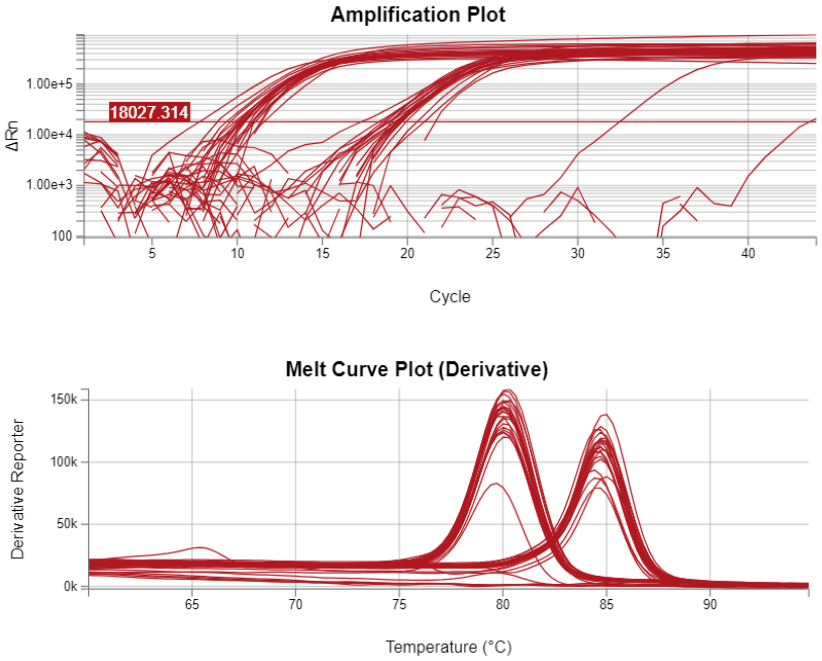
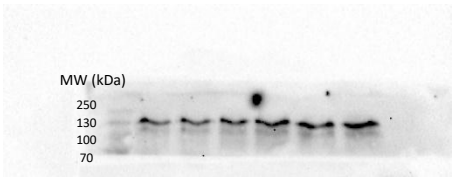


Figure S2: Amplification plot and Melt Curve analysis of the mtDNA and nuclear DNA sequences during qPCR.

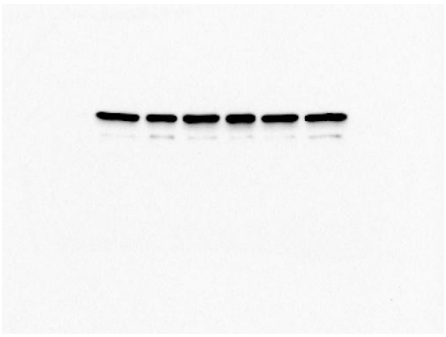
The amplification curves indicate that two distinct genomic products were amplified, the left for mtDNA and the right for the nuclear specific sequence. The corresponding qPCR melt curve plot exhibits two distinct peaks which indicate high specificity of the two primer sets for a single gene product each (mtDNA and nuclear DNA) and no presence of primer-dimer formation. The PCR was performed using DNA extracts from HEK293 cells after 48-hour treatments in the following groups: (1) untreated, (2) DMSO vehicle control, (3) 50 nM SSI, (4) 500 µM H_2O_2, (5) 1 µM Aβ42, (6) 150 µg/ml LDL (7) 500 µM H_2O_2 + 50 nM SSI, (8) 1 µM Aβ42 + 50 nM SSI, (9) 150 µg/ml LDL + 50 nM SSI.

(A) HEK293

(i)

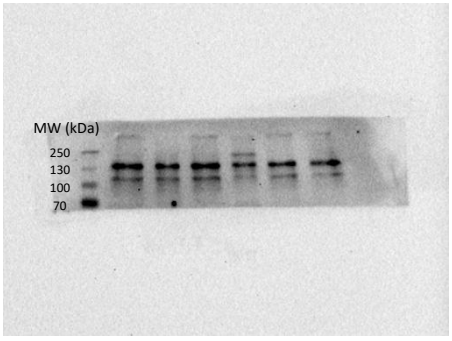


(ii)

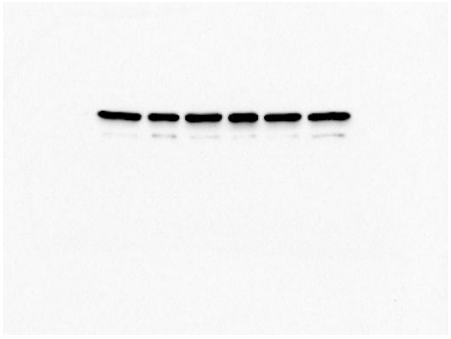


LDLR **β-actin**

(iii)

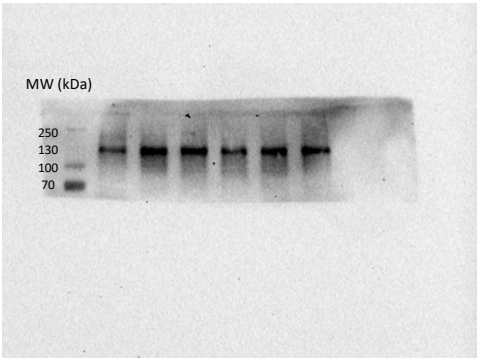


(iv)



(B) SH-SY5Y

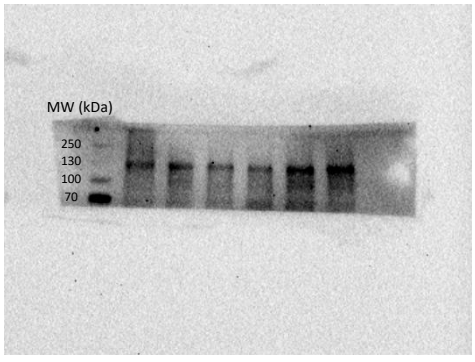
(i)



(ii)

LDLR **β-actin**

(iii)



(iv)

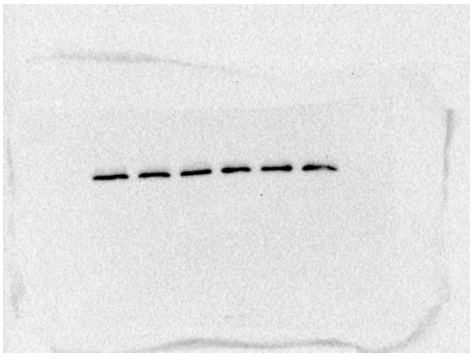


Figure S3: Representative non-truncated western blot images showing the detection of LDLR (left) and β-actin (right).

Western blotting was performed in replicate for **(A)** HEK293 and **(B)** SH-SY5Y cells following SSI treatment for 24 and 48 hours. Full-length replicate images for each cell line and time point are shown, indicating the molecular weight (MW) markers on the left side of the LDLR blots, to validate the band size of LDLR. The molecular weight marker indicates that the LDLR protein bands separated at approximately 130 kDa as expected. **(i)** LDLR bands after 24-hour SSI treatment, **(ii)** Corresponding β-actin (loading control) bands (24-hr SSI treatment), **(iii)** LDLR bands after 48-hour SSI treatment, **(iv)** Corresponding β-actin (loading control) bands (48-hr SSI treatment). The PageRuler Prestained Protein Ladder (Thermo Fisher Scientific, USA) was used as the molecular weight marker.

10.2 - Recipes

Table S1: 10× TBE Buffer Recipe (pH 8.3)

Reagent	Concentration
Tris	0.89 M (108 g)
Boric Acid	0.89 M (55 g)
0.5 M EDTA	0.02 M (40 ml)
dH_2O	Up to 1 L

Table S2: 2× Radioimmunoprecipitation assay (RIPA) Lysis Buffer

Reagent	Concentration
NaCl (58.44 g.mol)	0.3 M (1.7532 g)
Triton X-100	2% (2 ml)
Sodium deoxycholate	1% (1 g)
Sodium dodecyl sulfate	0.2% (2 ml of 10%)
500 mM Tris-HCl (pH 8.0)	0.1 M (20 ml)
500 mM EDTA (pH 8.0)	0.01 M (2 ml)

Table S3: 10× Electrophoresis Running Buffer (pH 8.3)

Reagent	Concentration
Tris	0.25 M (30 g)
Glycine	1.92 M (144 g)
Sodium dodecyl sulfate	0.035 M (10 g)
dH_2O	Up to 1 L

Table S4: 10× Transfer Buffer

Reagent	Concentration
Tris	0.25 M (30 g)
Glycine	1.92 M (144 g)
dH_2O	Up to 1 L

Table S5: SDS-PAGE Gel Recipe

Reagent	10% Separating Gel	5% Stacking Gel
30%/0.8% Acrylamide/bis (ml)	3.33	0.4
2× Resolving gel buffer (pH 8.8) (ml)	5	-
4× Stacking gel buffer (pH 6.8) (ml)	-	0.75
10% Ammonium persulfate (µl)	75	45
Tetramethylethylenediamine (TEMED) (µl)	7.5	4.5
dH_2O (ml)	1.59	1.83

10.3 - Ethics Clearance Form

UNIVERSITY OF THE WITWATERSRAND, JOHANNESBURG

R49 Dr E van der Merwe and Professor FJ Raal

HUMAN RESEARCH ETHICS COMMITTEE (MEDICAL)
CLEARANCE CERTIFICATE NO. M210289

NAME: **(Principal Investigator)**	Dr E van der Merwe and Professor FJ Raal
DEPARTMENT:	School of Molecular and Cell Biology University
PROJECT TITLE:	*Hypercholesterolaemia and Alzheimer's Disease: investigating shared pathological pathways and molecular mechanisms*
DATE CONSIDERED:	Ad hoc
DECISION:	Approved unconditionally
CONDITIONS:	Sub-study under M210287 Prior condition satisfied on 2021/01/31
NOTE:	If contact information regarding student study participants is required, please contact the Registrar's office - <Nicoleen.Potgieter@wits.ac.za>
SUPERVISOR:	Not applicable
APPROVED BY:	Dr CB Penny, Chairperson, HREC (Medical)
DATE OF APPROVAL:	2021/03/25

This Clearance Certificate is valid for 5 years from the date of approval. An extension may be applied for.

DECLARATION OF INVESTIGATORS

To be completed in duplicate and **ONE COPY** returned to the Research Office secretariat on the 3rd floor, Phillip Tobias Building, Parktown, University of the Witwatersrand, Johannesburg.

I/we fully understand the conditions under which I am/we are authorized to carry out the above-mentioned research and I/we undertake to ensure compliance with these conditions. Should any departure be contemplated from the research protocol as approved, I/we undertake to submit details to the Committee. **I agree to submit a yearly progress report**. When a funder requires annual re-certification, the application date will be one year after the date when the study was initially reviewed. In this case, the study was initially reviewed in **February** and therefore reports and re-certification will be due in the month of **February** each year. Unreported changes to the study may invalidate the clearance given by the HREC (Medical).

Signature of Principal Investigator _____ Date _____